ENERGY SYSTEMS RESEARCH UNIT
AEROSPACE AND MECHANICAL ENGINEERING DEPARTMENT
UNIVERSITY OF LIÈGE

Investigation of a heat pump reversible into an organic Rankine cycle and its application in the building sector

in Partial Fulfilment of the Requirements for the Degree of
Doctor of Applied Sciences

Presented to the Faculty of Applied Science
of the University of Liège (Belgium) by
Olivier Dumont

Liège, September 2017

Abstract

This thesis studies the concept of reversible heat pump / organic Rankine cycle (HP/ORC) and its application in the building sector. Chapter one describes this HP/ORC system and its possible applications. A tool based on operating maps is developed to determine the feasibility of such a system depending on the operating conditions of a given application.

In Chapter two, the reversibility of volumetric machines is studied based on a theoretical comparison followed by experimental results collected on four different compressor/expander technologies. The comparison shows which technology should be used depending on the characteristics of an application.

In Chapter three, the design and sizing methodology to optimize the performance of the reversible heat pump /organic Rankine cycle is described. This design and sizing optimisation is performed in the case of the residential application: the reversible HP/ORC system is coupled with a large solar absorber in a building to provide a polyvalent machine able to produce heat or electricity depending on the needs of the building. Steady-state models are then used to predict the annual performance of the system integrated in a building.

As the theoretical results are promising in the case of the residential application, a test-rig is built and an experimental campaign is performed in both HP and ORC modes (Chapter four). A global methodology to improve the quality of experimental data is proposed based on two different mathematical tools. The method combines the reconciliation method and the Gaussian Processes sensitivity analysis. A model is calibrated based on experimentation to characterize the performance of the HP/ORC unit with an optimal control and with a wide range of inputs.

Chapter five studies the reversible unit in the case of the building application based on advanced dynamic models. The global model combines validated sub-models: the reversible unit, the solar roof, the thermal energy storage, the horizontal ground heat exchanger and the building. An optimal control strategy is developed and presented. A parametric study is performed to observe the performance of the system in a wide range of typologies. The influence of different lights and appliances profiles, building envelopes, integration of batteries, roof tilt angles, locations, storage sizes is developed. Furthermore, a technical and economic comparison with one of the most mature technologies to get a positive energy building, namely photovoltaics panels combined with a heat pump in a passive house, is performed.

Acknowledgments

I would like to thank Professor Vincent Lemort for his trust and his support during the whole period of this work. I wish to thank him for the numerous moments spent working together on practical and theoretical issues as well as for countless valuable discussions.

Thank you to the members of the Thesis Committee, for their valuable comments and constructive criticism.

A large part of this work would not have been possible without the trust of colleagues from foreign universities, namely Carolina Carmo, Andreas Brummer, Kristian Harley and their respective teams. They allowed me to gain valuable experience and know-how and warmly welcomed me to stay in their labs.

Special thanks go to all the members of the Thermodynamics Laboratory for their help and availability, but above all for their friendship and the great moments spent together during these four years.

Furthermore, I want to thank my friends for their support and encouragements throughout my studies.

Table of contents

Nomenclature

A	Area [m^2]
b	Solubility coefficient [-]
C	Exchanger calibration parameter [-]
C_m	Correlation coefficient [-]
c	Constant losses [-]
Cp	specific heat capacity at constant pressure [J/K.Kg]
d	Diameter [m]
DD	Discharge depth [-]
err	Error
F	Factor
FF	Filling factor [-]
f	Fanning friction factor [-]
G	Mass velocity [kg/s]
h	Specific enthalpy [J/(kg.K]
H	Height
i	Indice
I	Solar irradiance [W/m^2]
K	Constant
L	Length [m]
M	Mass [kg]
$\dot{m}$	Mass flow rate [kg/s]
n	Number of points
Np	Number of plates
Nu	Nusselt [-]
Pr	Prandtl [-]
P	Pressure [bar]
Price	Price [eur]
q	Quartile
Q	Thermal energy [kWh]

$\dot{Q}$	Thermal power [W]
R	Revenue [eur]
r	Discount rate [%]
R^2	Coefficient of determination
Re	Reynolds [-]
Res	Residue [W]
rv	Volume ratio [-]
s	Entropy [J/(Kg.K)]
S	Speed [m/s]
t	Temperature [°C]
T	Time [s]
U	Heat exchange coefficient [W/(m^2.K)]
v	Specific volume [m^3/kg]
V	Volume [m^3]
$\dot{V}$	Volumetric flow rate [m^3/s]
w	Weighting coeficient [-]
W	Energy [W.h]
Wi	Width [m]
$\dot{W}$	Power [W]
x	Input
X	Fraction
y	Output

Greek symbols

α	Proportional loss coefficient [-]
Δ	Difference [-]
η	Efficiency [-]
ε	Effectiveness [-]
ζ	Torque [N.m]
ϰ	Time constant [s]
ρ	Density [kg/m^3]

σ	Standard deviation [-]
φ	Minimization function
x	Oil fraction [%]
Ψ	Kinetic energy factor [m^3/s]
ψ	Constraint
Φ	Filling factor [-]
ς	Liquid fraction of refrigerant in the liquid phase [-]
ω_0	Parameter [-]
γ_S	Self production rate [-]
γ_D	Self consumption rate [-]

Subscripts and superscripts

abs	absorber
amb	ambient
bat	battery
C	compactness
cmp	compressor
cd	condenser
cons	consumption
cst	constant0
in	internal
is	isentropic
ev	evaporator
ex	exhaust
exp	expander
glazing	glazing
global	global
gw	glycol water
h	hydraulic
in	internal
inj	injected

l	liquid
leak	leakage
m	mean
max	maximum
meas	measured
mec	mechanical
min	minimum
net	net
nom	nominal
oh	over-heating
oil	oil
overall	overall
p	plate
pp	pump
pred	predicted
prod	Produced
r	refrigerant
ref	reference
s	swept
sat	saturation
sc	sub-cooler
sf	secondary fluid
sh	shaft
sto	storage
su	supply
th	theoretical
tot	total
tp	two-phase
us	used
v	vapour
var	variable

vol	volumetric
w	water
wf	working fluid

Acronyms

BH	Borehole
CFD	Computational Fluid dynamics
COP	Coefficient Of Performance
DH	Direct heating
DHW	Domestic Hot water
DNI	Direct Normal Irradiation [W/m^2]
FF	Filling factor
FH	Floor Heating
FM	Fully mixed
GP	Gaussian Process
HD	Heat demand
HGHE	Horizontal Ground Heat Exchanger
HP	Heat Pump
Hp	High pressure
Lp	Low pressure
HVAC	Heat and Ventilation Air Conditioning
ICE	Internal Combustion Engine
ITE	Information Technology Equipment
L&A	Light and applicances
LMTD	Logarithmic mean temperature difference
MAE	Mean average error
MAPE	Mean Average Percentage Error
MB	Moving boundary
MN	Multi Node
NPSH	Net Positive Suction Head [m]
ORC	Organic Rankine Cycle

ODE	Ordinary Differential Equation
PB	Pay-Back
PDE	Partial Derivative Equation
PEB	Positive Energy Building
PF	Plug flow
PTES	Pumped Thermal Energy Storage
PV	Photovoltaic Panel
RM	Reconciliation method
RMSE	Root Mean Square Error
TES	Thermal Energy Storage
VR	Volume ratio
XHR	Waste Heat recovery
ZN	Zonal

Publications

Dumont, O., Dickes, R., Lemort, V., 2017. Extrapolability and limitations of a semi-empirical model for the simulation of volumetric expanders, Energy Procedia 129:315-322DOI10.1016/j.egypro.2017.09.198

Dumont, O., Dickes, R., Lemort, V., 2016. Experimental investigation of four volumetric expanders, 2017Energy Procedia 129:859-866, DOI10.1016/j.egypro.2017.09.206

Quoilin, S., Dumont,O . Dickes, R., Lemort, V., 2017. Evaluating the quality of steady-state multivariate experimental data relative to various ORC experimental setups 2017, Energy Procedia 129:915-922 DOI10.1016/j.egypro.2017.09.107

Dumont, O., Carmo, C., Fontaine, V., Quoilin, S., Randhaxe, F., Lemort, V., Elmegaard, B, Nielsen,M.P., 2016. Performance of a reversible heat pump/organic Rankine cycle unit coupled with a passive house to get a positive energy building 2016Journal of Building Performance Simulation, DOI10.1080/19401493.2016.1265010.

Dumont, O., Carmo, V., Quoilin, S., Lemort, V., 2016. Economic assessment of electric energy storage for load shifting in positive energy building , International Journal of Energy and Environmental Engineering DOI10.1007/s40095-016-0224-2.

Carmo, C, Dumont, O., Nielsen, M.P., Lemort, V., 2016. Energy performance and economic evaluation of a heat pump/organic Rankine cycle with sensible storage. Conference: ECOS 2016.

Dumont, O., Carmo, C., Georges, E., Balderama, S., Quoilin, S., Lemort, V., 2016. Economic assessment of energy storage for load shifting in Positive Energy Building , Conference: ECOS 2016

Dumont, O., Carmo, V., Georges, Dickes, R., Quoilin, S., Lemort, V., 2016. Hot water tanks : How to select the optimal modelling approach? , 2016 Conference: CLIMA 2016, At Aalborg

Dumont, O., Quoilin, S., Lemort, V., 2016. Importance of the reconciliation method to handle experimental data in refrigeration and power cycle: application to a reversible heat pump/organic Rankine cycle unit integrated in a positive energy building, International Journal of Energy and Environmental Engineering 7(2) DOI10.1007/s40095-016-0206-4

Dumont, O., Carmo, C., Randhaxe, F., Quoilin, S., Lemort, V., 2015. Performance Comparison of Two Types of Technologies Associated with a Positive Energy Building: a Reversible Heat Pump/ORC Unit and a Heat Pump Coupled with PV Panels, DOI10.18086/swc.2015.04.13 Conference: SWC 2015/ ISES Conference, At Daegu, Korea

Oudkerk, J-F, Dumont, O., Dickes, R., Lemort, V., 2015. Experimental performance of a piston expander in a small- scale organic Rankine cycle, British Food Journal 90(1)DOI10.1088/1757-899X/90/1/012066

Quoilin, S., Dumont, O., Harley, K., Lemort, V., 2015. Design, Modeling, and Performance Optimization of a Reversible Heat Pump/Organic Rankine Cycle System for Domestic Application, Journal of Engineering for Gas Turbines and Power 138(1) DOI10.1115/1.4031004

Dumont, O., Quoilin, S., Lemort, V., 2015. Importance of the reconciliation method to handle experimental data: application to a reversible heat pump / organic Rankine cycle unit integrated in a positive energy building Conference: ECOS 2015, At Pau, France

Dumont, O., Quoilin, S., Lemort, V., 2015. Experimental investigation of a reversible heat pump / organic Rankine cycle unit designed to be coupled with a passive house (Net Zero Energy Building), International Journal of Refrigeration 54, DOI10.1016/j.ijrefrig.2015.03.008

Dumont, O., Carmo, C., Randhaxe, F., Quoilin, S., Lemort, V., 2014. Simulation of a passive house coupled with a heat pump/organic Rankine cycle reversible unit, Conference: Proceedings of the 9th International Conference on System Simulation in Buildings (SSB2014), At Liège, Belgium

Dumont, O., Quoilin, S., Lemort, V., 2014. Design, Modeling and Experimentation of a Reversible HP-ORC Prototype, DOI10.1115/GT2014-26854

Dumont, O., Quoilin, S., Lemort, V., 2014. Experimental investigation of a scroll unit used as a compressor and as an expander in a reversible Heat Pump/ORC unit, Conference: 2014 Purdue Conferences : Herrick Conferences

Chapter I:

Introduction

"Man is the most insane species.
He worships an invisible God and
destroys a visible Nature. Unaware
that this Nature he's destroying
is this God he's worshiping."
Hubert Reeves

Abstract

This chapter presents the context which lead to the interest in technologies decreasing the CO_2 emissions. It also presents the concept of reversible heat pump/organic Rankine cycle and different applications leading to the decrease of CO_2 emissions. Finally, a simple tool is developed to analyse the technical feasibility of a given application. Using this methodology, the residential building with solar panel is identified as one of the most interesting applications.

1 CONTEXT

By 2030, greenhouse gases emissions must be reduced by 40% as compared to the levels of 1990, according to European objectives (European Commission, 2012). This goal will be achieved both through an increase in the proportion of renewable energy from 9% to 27%, and an increase in energy system efficiency. According to the EU 2050 Roadmap (European Climate Foundation, 2010), greenhouse gases emissions could be cut by 80% in 2050. This pathway involves several modifications of the current energy system. First, a decrease in the energy intensity of buildings (decrease of 950 TWh/year by 2050) and industry (decrease of 450 TWh/year). Also, a shift from fossil fuels towards electricity, e.g. for transportation and space heating should be done. Clean power must be generated by a massive shift towards renewable energies, among which 25% of wind energy, 19% of photovoltaics panels, 5% of concentrated solar power, 12% of biomass, 2% of geothermal, 12% of large hydro (European Climate Foundation, 2010). A reinforcement of the grid capacity and inter-regional transmission lines to absorb daily and seasonal fluctuations must be achieved. In this context it is paramount to develop systems that can reach those standards.

Heat pump (HP) can be considered as a mature technology nowadays. In contrast with other heating technologies - which transform chemical energy into thermal energy - HPs are non-combustion technologies. In practice, they transfer free thermal energy at low temperature contained in the air, water and/or ground and use electricity – or mechanical energy-, to

deliver heat (higher heat production than electrical consumption). In this way, they reduce emissions and improve energy efficiency in heating and cooling buildings. It is estimated that in the European Union, a reduction of 54% of CO_2 emissions could be achieved with the introduction of heat pumps into the building sector (Bettgenhäuser et al., 2013). Basically, a heat pump absorbs heat from a cold heat source and releases it to a warmer heat sink. The basic schematic representation of a heat pump is shown in Figure 1a.

The heat pump comprises four major components: a condenser, an evaporator, a compressor and an expansion valve. First, the compressor increases the pressure and temperature of the working fluid. The working fluid in vapour state is then cooled down, condensed and sub-cooled in the condenser, releasing heat to a heat sink. The working fluid then flows into the expansion valve, which decreases its pressure from the condensing pressure down to the evaporating pressure. The working fluid is then evaporated and eventually superheated in the evaporator, absorbing heat from the heat source (Figure 1). For the use of heat pumps in buildings, the heat source is typically outside air or water (coming for instance from a geothermal borehole field). The heat sink is the heating network of the building: hot water network supplying radiators or hot air to be pulsed into the rooms.

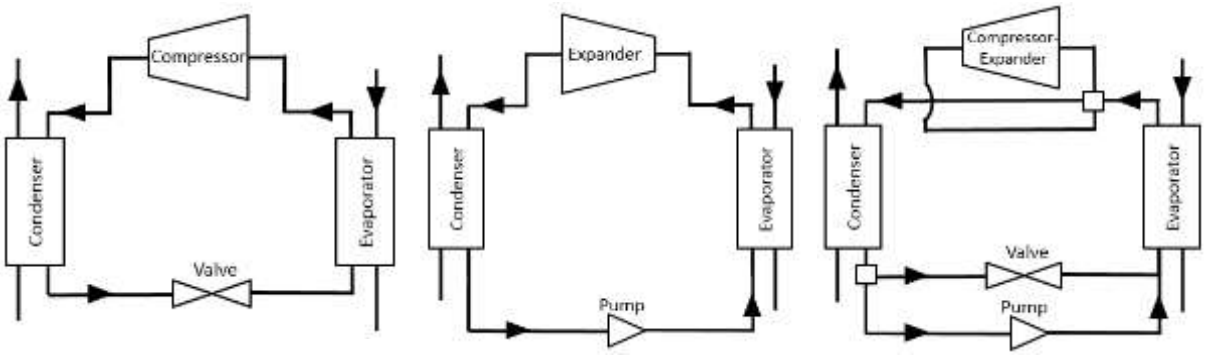

(a) (b) (c)

Figure 1: Layout of a heat pump (a), organic Rankine cycle power system (b) and example of reversible HP/ORC unit (c)

In recent years, another technology, the ORC (organic Rankine cycle) power system, has become increasingly popular (Figure 2). Commercial applications have been in operation since the 70's, but are mainly limited to medium-scale units (several hundreds kW). While the heat pump describes a refrigeration cycle, the organic Rankine cycle system describes a power cycle: heat from a low temperature heat source (typically below 250°C) is converted into useful work (Quoilin, 2011). The schematic representation of an ORC system is shown in Figure 2b. The system comprises four main components: condenser, evaporator, expander and pump. First, the pump imposes a given refrigerant flow that increases the pressure of the working fluid. Then, it passes through an evaporator, where the fluid is vaporized using the thermal energy from the heat source. Following that, the working fluid flows into an expander where the useful work is produced (Figure 1). At the end, the working fluid is then sent back to the pump after being condensed using the low temperature of the cold source.

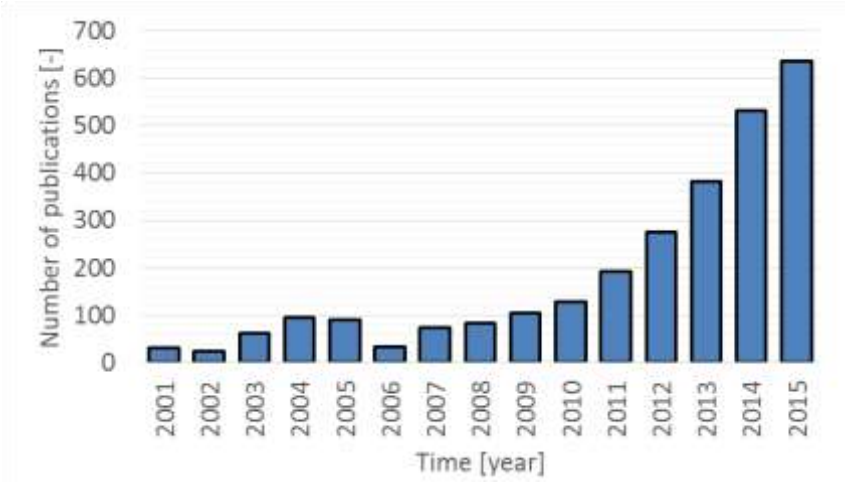

Figure 2: Number of publications related to ORC systems (source: advanced search in ScienceDirect with 'ORC')

2 CONCEPT OF REVERSIBLE HP/ORC UNIT

It is interesting to note that low-capacity ORC power systems units are similar to HP systems in many aspects: volumetric machines are preferred to turbomachines because of their lower rotating speed (Persson, 1990), plate heat exchangers are the most cost-effective type of heat exchangers and common working fluids included HVAC-like refrigerants. Based on this observation, this thesis aims at investigating an innovative combined system able to operate either in heat pump or ORC mode. The proposed system takes advantage of the similarity between the heat pump and the ORC: by adding a pump and a four way valve (to allow switching between the inlet and outlet of the compressor) to a classical heat pump, the system can be inverted and work in ORC mode (Figure 1). The scheme is an example of configuration but the different layouts will be discussed more in details in Chapter 3. The main advantage of this system is to provide the additional capability of producing electrical power to a heat pump with few additional costs.

Very few literature can be found on the reversible[1] HP/ORC system. In 2005, it is mentioned that the heat pump of a vehicle could be used to recover energy based on waste heat from cooling engine through the reversibility of the heat pump in an organic Rankine cycle (Inaba et al., 2005). In 2006, a patent has been put regarding the energy optimisation in automotive application. More precisely, a reversible HP/ORC unit could provide power trough waste heat from cooling engine and/or exhaust gases (Girard, 2006). The first theoretical investigation on such a reversible HP/ORC system in the building sector has been introduced in 2011 (Schimpf et al., 2011). The system investigated is a residential water-to-water heat pump connected to a small area of solar collector (12 m^2) and a vertical ground heat exchanger. The goal is to provide electricity in summer months by means of the ORC mode

[1] The word « reversible » in this thesis should be understood as « system that can be inverted » and not as a thermodynamic reversible process.

and heating from the heat pump in winter months. The vertical ground heat exchanger is used to cool the condenser of the ORC system. In 2013, a patent for such a residential application is approved (Innogie Aps, 2013). In this application, the evaporator of the ORC is coupled to an innovative large solar roof collector and the condenser of the ORC is cooled by a horizontal ground heat exchanger. From author's knowledge, no report of an existing experimental HP/ORC reversible facility exists.

Based on this state of the art, the concept of reversible HP/ORC unit is far from being mature. Other technologies that presents the same "reversibility" are thermoelectricity and fuel cells. The three technologies (reversible HP/ORC system, fuel cell and thermoelectricity) have been compared (Carmo et al., 2016). The authors concluded that all these technologies cannot be considered as mature and their investment cost is currently too high for investors.

Several applications are possible for the reversible HP/ORC but the technical feasibility should be assessed depending on its specifications. The next section (section 3) tries to present typical possible applications (as examples) and gives a methodology to roughly estimate their technical feasibility.

3 APPLICATIONS AND FEASIBILITY STUDY

3.1 Operating MAPS

The goal of this section is to define a simple tool and operating maps to determine if an existing heat pump is suitable or not to become reversible in ORC mode depending on the operating parameters of a given application. The model is based on six different inputs (Figure 3):

- the working fluid,
- the heat pump thermal capacity,
- the temperature levels (evaporation and condensation) of the heat pump and of the ORC.

It should be noted that it is possible, alternatively, to set a minimum ORC efficiency and to evaluate the minimum ORC evaporation temperature.

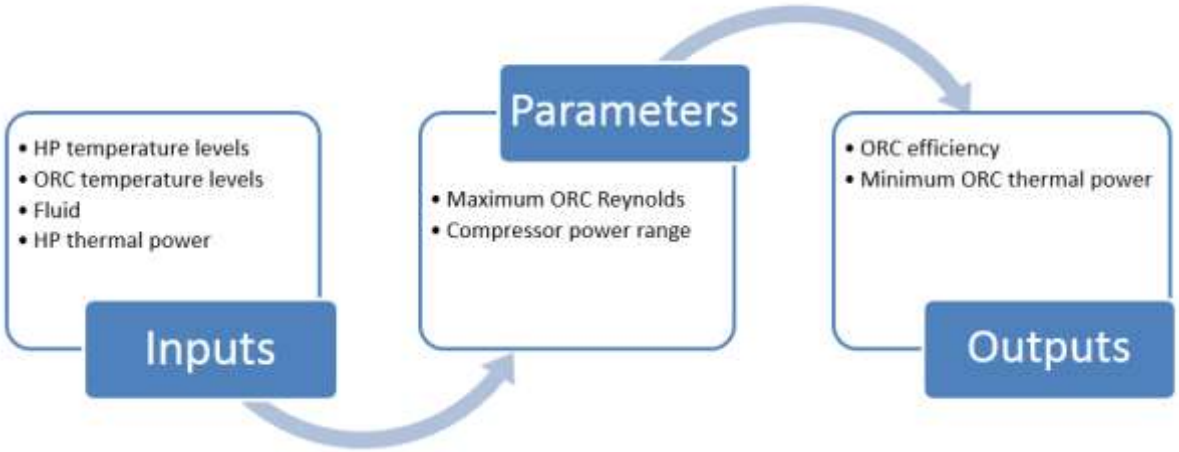

Figure 3: Model to determine if a heat pump is suitable for reversible application

Three main factors are considered to decide whether the reversibility of the heat pump could be achieved.

1. The electrical power (or efficiency) produced by the ORC should be positive. This minimum efficiency requires a minimum evaporation temperature threshold for the ORC for a given heat pump nominal conditions. To predict the efficiency, the model is based on the following hypotheses:
    a. Compressor nominal isentropic efficiency of 75%.
    b. Super-heating and sub-cooling degrees in heat pump and ORC modes of 5K.
    c. Maximum expander isentropic efficiency of 75%.
    d. Constant pump isentropic efficiency of 50%.

    Only the sub-critical ORC is studied in this work but other architectures are promising (wet expansion (Fischer, 2011; Schutster et al., 2010; Smith, 2012) and trans-critical cycles (Lecompte et al., 2015; Zhang et al., 2011) for examples). However, the high required flows (inducing large components) for the wet expansion and the high cost (due to the large operating pressure and temperature) are relatively restrictive for small scale reversible HP/ORC applications (Dumont et al., 2018).

Table 1 : Advantages and disadvantages for each architecture of ORC power system.

	Sub-critical	Wet expansion	Trans-critical
Advantages	- Mature - Low investment - Low pressure	- High exergy efficiency - Good match with heat source profile	- High exergy efficiency - Good match with heat source profile
Disadvantages	- Low exergy efficiency	- Expander must tolerate wet expansion - High flows - Larger piping, exchangers and expander	-High pressure - Large volume ratio's (several stages of expansion necessary) - Higher investments

For given heat pump nominal conditions (condensation pressure, evaporation pressure, fluid and thermal capacity), it is possible to evaluate the optimal compressor volume ratio. It is always supposed that the compressor is sized following the heat pump requirements in terms of volume ratio. However, it is possible to obtain higher global performance of the reversible HP/ORC system by optimizing the compressor/expander geometry based on both the HP and ORC conditions and the fraction of operating time of each mode (see Chapter 3).

The compressor, used as an expander, is supposed to present an efficiency varying in function of the ORC operating conditions. To this end, the expansion modelling is divided into two parts to account for over and under-expansion losses (Eq. 1). First, an isentropic expansion ($\dot{W}_{exp,1}$) is described (Eq. 2) followed by a constant machine volume expansion ($\dot{W}_{exp,2}$ – Eq. 3). The isentropic power is evaluated with the isentropic exhaust enthalpy calculated with the exhaust pressure and the supply entropy (Eq. 4).

$$\varepsilon_{exp,is} = \frac{\dot{W}_{exp,1} + \dot{W}_{exp,2}}{\dot{W}_{exp,is}} \quad (1)$$

$$\dot{W}_{exp,1} = \dot{m}(h_{exp,su} - h_{exp,in}) \quad (2)$$

$$\dot{W}_{exp,2} = \dot{V}_{in}(P_{exp,in} - P_{exp,ex}) \quad (3)$$

$$\dot{W}_{exp,is} = \dot{m}(h_{exp,su} - h_{exp,ex,is}) \quad (4)$$

Assuming a given condensation temperature of the ORC system, the minimum evaporation temperature to get a given efficiency can be determined. Figure 4 shows the minimum ORC system evaporation temperature for a given heat pump (evaporation and condensation temperatures and refrigerant R245fa) and for a given ORC condensation temperature (60°C) in order to obtain a 5% ORC efficiency. In this figure, it should be noted that a heat pump with a high lift (difference between condensation and evaporation temperature) leads to a high minimum ORC temperature. This is because a high HP lift leads to a high pressure and volume ratio of the compressor. Therefore, the expander requires a relatively high pressure ratio in ORC mode to avoid large over-expansion losses.

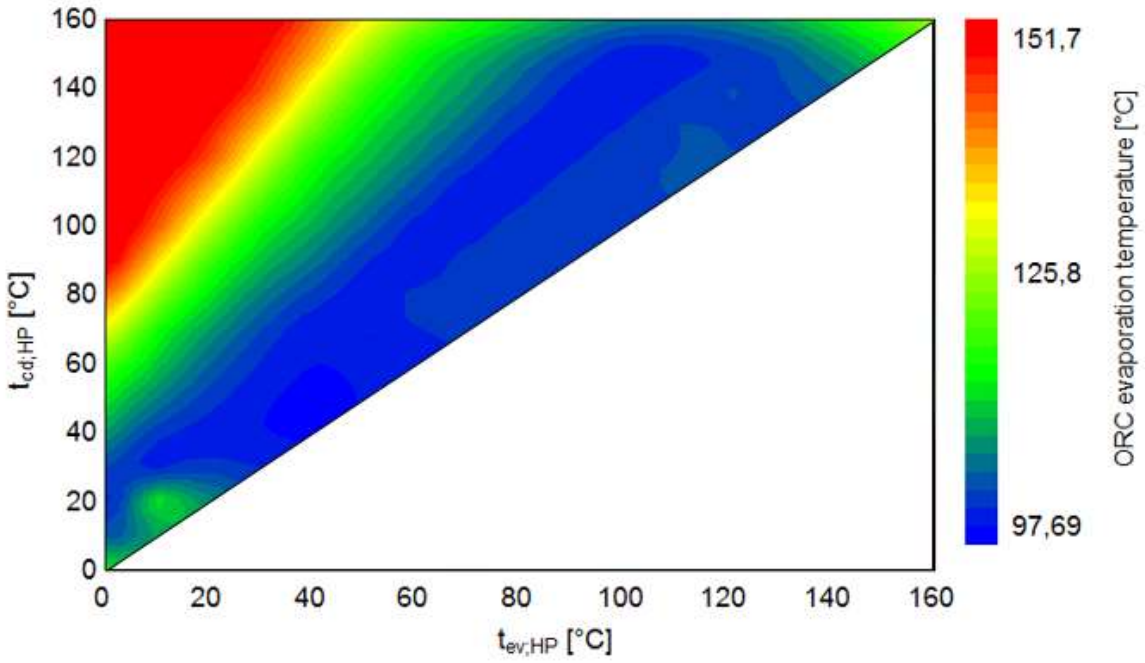

Figure 4: Minimum ORC evaporation temperature based on the heat pump temperature levels. The working fluid is R245fa, the condensation temperature is 60°C and the ORC efficiency is set to 5%.

2. A compressor presents a given nominal power. Working out of these conditions will lead to poor performance. The mechanical power produced by the ORC should therefore be relatively close to the one consumed by the compressor in heat pump. Combining the equations of the COP of a heat pump (Eq. 5) and the efficiency of an ORC (Eq. 6) leads to an equation giving the minimum ratio between the evaporator thermal powers in ORC and HP modes (Eq. 7). As an example, with a typical COP equal to 4 and an ORC efficiency of 10%, the ORC requires 2.5 more thermal power than the heat pump at the evaporator.

$$COP_{HP} = \frac{\dot{Q}_{ev,HP}}{\dot{W}_{cmp}} \quad (5)$$

$$\eta_{ORC} = \frac{\dot{W}_{exp}}{\dot{Q}_{ev,ORC}} \quad (6)$$

$$\frac{\dot{Q}_{ev,ORC}}{\dot{Q}_{ev,HP}} = \frac{1}{\eta_{ORC}.COP_{HP}} \quad (7)$$

As an example, the minimum thermal power ratio between ORC and heat pump is depicted in Figure 5. Here, the working fluid is R245fa, the condensation temperature is 30°C and the ORC efficiency is set to 5%. In this figure, it should be noted that a heat pump with a high lift (difference between condensation and evaporation temperatures) leads to a high thermal power ratio between ORC and heat pump.

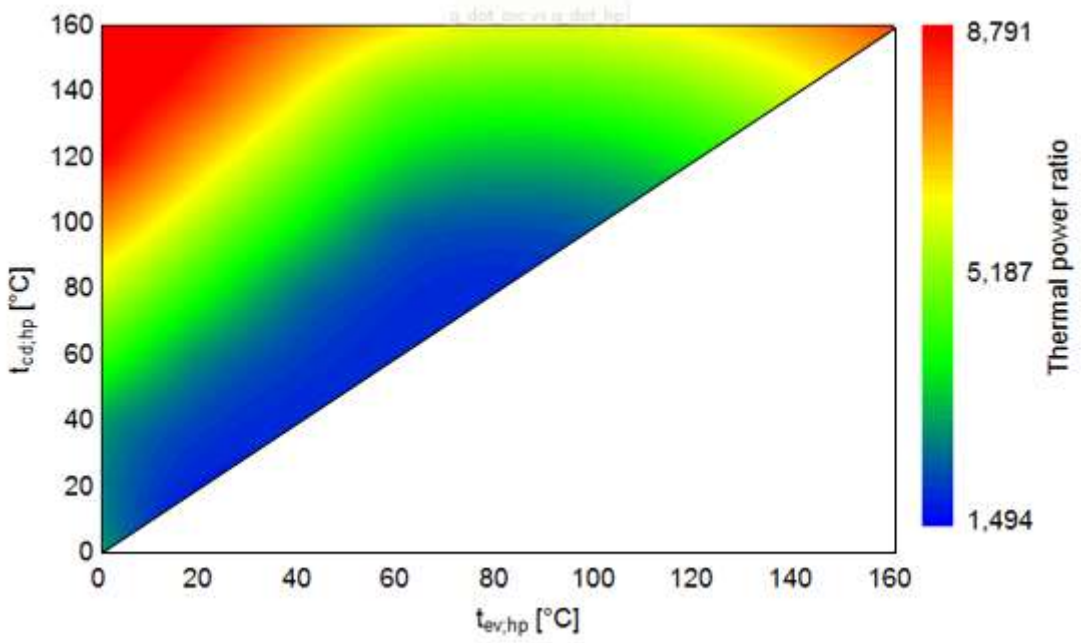

Figure 5: Miminum thermal power ratio between ORC and heat pump . The working fluid is R245fa, the condensation temperature is 30°C and the ORC efficiency is set to 5%.

3. Finally, a third criterion is an upper limit on the ORC thermal power. Practically, it is not possible for a system to work efficiently whatever the thermal power. First, the flow should be limited to avoid too large pressure drop in the pipes and in the heat exchangers. Secondly, positive displacement machines can only absorb a limited flow rate. Finally, Reynolds numbers should be of the same order of magnitude to keep decent heat exchange coefficient in the exchangers. For these reasons, a lumped approach to take these effects into account is to limit the Reynolds number of the ORC system (at the expander outlet) in the order of magnitude of the heat pump

system (at the compressor inlet). These two locations are chosen because they correspond to the higher pressure losses locations. This proposed constraint based on the Reynolds number is not validated but should play an important role to avoid a huge mismatch between ORC and HP working conditions. Of course, this approach is only used for the pre-selection of a given application but more accurate models are required to assess the performance of the system accurately (see Chapter three). As an example, this limitation is detailed in Figure 6 where the maximum thermal power ratio between ORC and heat pump is given for different evaporation and condensation temperatures of a given heat pump. In this example, the working fluid is R245fa, the condensation temperature is 30°C and the Reynolds number in ORC mode is limited to three times the Reynolds number in heat pump mode.

4.

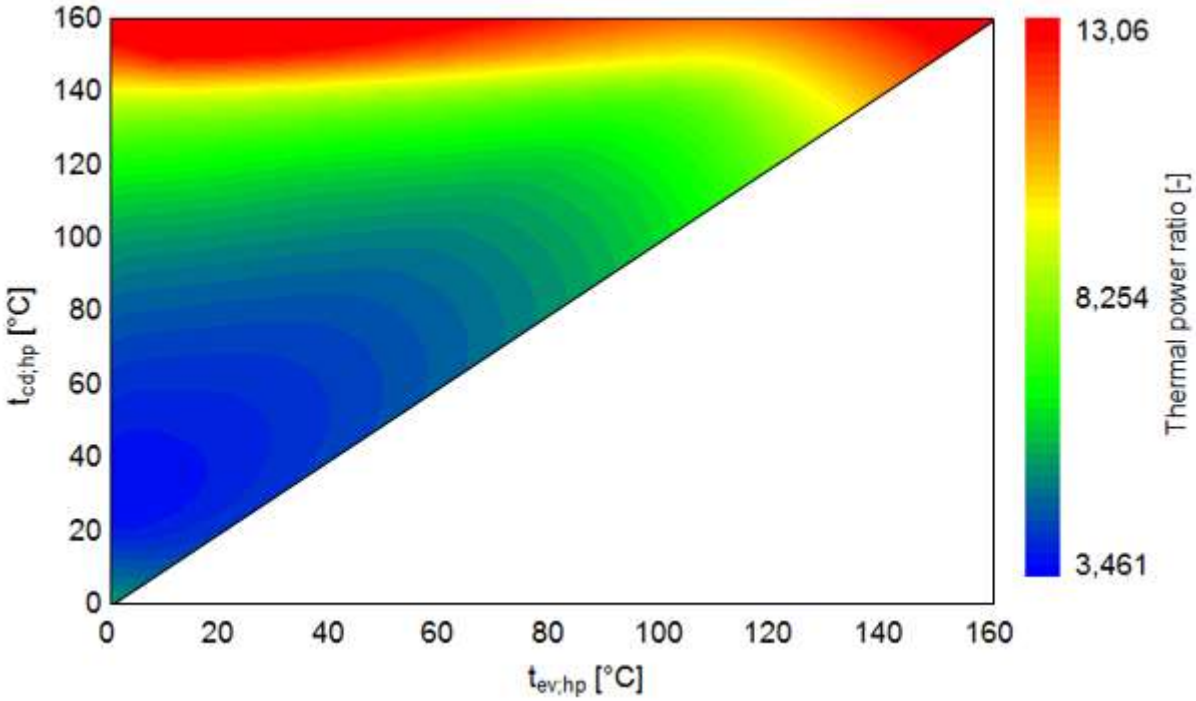

Figure 6 : Maximum thermal ratio between ORC and heat pump. The working fluid is R245fa, the condensation temperature is 30°C and the ORC efficiency is set to 5%.

After the introduction of the three constraints (positive ORC efficiency, Reynolds limitation and volumetric machine power range), the methodology to evaluate the technical feasibility of a given heat pump to become reversible is summarized in Figure 7:

1. Definition of the heat pump parameters for the application in terms of temperature levels, thermal power and compressor efficiency.
2. Sizing of the heat pump based on the inputs to determine the compressor volume ratio, the mass flow and the compressor power.
3. Definition of the ORC parameters in terms of Reynolds factor, power factor and temperature levels of the application.

4. Determination of the outputs: ORC efficiency, minimal and maximal thermal power.

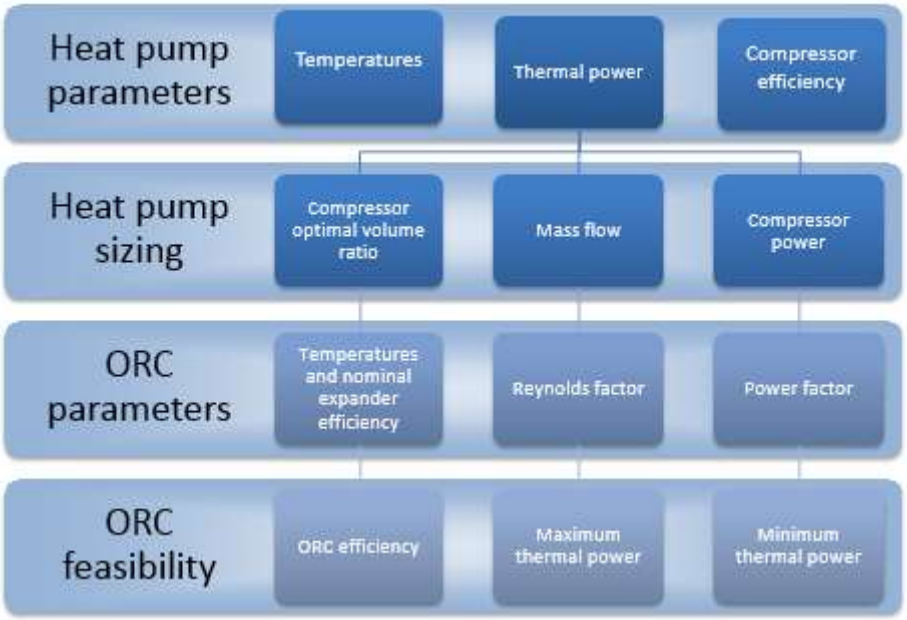

Figure 7 : Methodology to evaluate the technical feasibility of a reversible HP/ORC system.

Other criteria could be raised but are more subject to specific applications (temperature or pressure limitations, weight or space constraints, fraction of the time where the heat pump is used, oil lubrication, etc.). This methodology will be applied in section 3.2 to evaluate the viability of different applications.

3.2 LISTING OF APPLICATIONS

In this section, a few applications where a reversible HP/ORC could be used are briefly described. A given application can have different inputs in terms of thermal power and temperature levels. This would lead to different results but the focus of this section is to compare a variety of applications with typical inputs. More accurate modelling should be performed for a specific study case to evaluate the performance accurately. This calculation is detailed in the case of the residential heat pump application in Chapters 3 and Chapter 5.

3.2.1 Internal combustion engine in industrial applications

In industrial applications, heat is required in a lot of processes (dryer, steamer, etc) In some context, it is interesting to upgrade a waste heat flux at low temperature to a higher temperature with a heat pump for a given process. This allows the efficiency of the industrial plant to be increased. Internal combustion engines (ICE) are widely used in combined heat and power generation due to their heat recovery potential mainly contained in exhaust gases and cooling water. However, the low temperature of the cooling water circuit does not

always allow its use, thermal energy often being rejected to the ambient. Yet, from about 90°C of cooling water waste heat, a heat pump can provide useful heat for processes up to 140°C. A reversible HP/ORC system in this context could use the cooling water of the engine as the heat source when the heat pump is not working (Peris et al., 2016). The condenser is water cooled and the cooling circuit is connected to a dry air cooler. The inputs on the nominal point for this application are described in Table 2.

3.2.2 Residential heat pump with solar panels (or biomass boiler)

The integration of a heat pump and solar thermal panels in a residential building is a promising way to increase energy efficiency and to increase the share of renewable energy in the building sector (Bettgenhauser et al., 2013; IEA, 2012). However, large amounts of thermal energy produced by the solar thermal panels are not used, particularly in summer when the building solar gains are high and the heat demand of the building is low. An elegant way to improve the global system efficiency is to produce electricity through a reversible HP/ORC system with the surplus heat provided by the solar roof. This system is therefore flexible with three operating modes. The heat pump is activated to supply the heat requirements of the building in the case of low solar radiation. The direct heating mode (solar thermal energy to thermal storage for domestic hot water and floor heating) is activated as soon as the solar roof temperature is higher than the storage temperature. Finally, when the storage has reached its high temperature set-point, the ORC mode is activated to produce electricity (Dumont et al., 2015). The condenser in ORC mode could be cooled either by a horizontal ground heat exchanger (HGHE) or by an air-cooled condenser. A more detailed investigation of this application will be presented in Chapter 3 (modelling), Chapter 4 (experimental investigation) and in Chapter 5 (dynamic modelling and study of influence). Instead of using solar panels, the system could integrate a combined heat and power (CHP) biomass boiler. The inputs on the nominal point for these applications in the case of the biomass CHP and the solar heat pump are described in Table 2.

3.2.3 Air-conditioning unit with solar panels (or biomass boiler)

In temperate climates, the cooling demand of new residential buildings is much higher than the heating requirements. The same concept as the residential heat pump combined with solar panels (described in section 3.2.2) could be applied with an air-conditioning unit.

3.2.4 Data center air conditioning

The purpose of data center cooling technology is to maintain environmental conditions suitable for information technology equipment (ITE) operation. Achieving this goal requires removing the heat produced by the ITE and transferring that heat to some heat sink. In 2020, data centers will represent 6% of the greenhouse gas emissions in the world (Sigma, 2015). Those data centers should be installed in northern countries with cold climates in a way to decrease their large cooling demand. However, when the outdoor temperature is close or

higher than the maximum acceptable temperature inside the data center ([21°C-27°C]), an air conditioning system is necessary. A reversible air conditioning/ORC system could use the thermal energy produced by ITE to produce electricity when the outdoor temperature is low. The inputs on the nominal point for this application are described in Table 2.

3.2.5 Car (or truck) air conditioning with heat recovery on exhaust gases or cooling engine

Valorisation of the waste heat in mobile internal combustion engines (car, truck, tractor…) is paramount to reach the norms in terms of CO_2 emissions (European Union, 2014). ORC (and Rankine cycle) systems have been studied intensively during this last decade to recover the heat from the cooling engine or from the exhaust gas (Legros, 2014). This waste heat, converted in mechanical work through an ORC, can be directly injected to power the wheels or to charge the battery trough an alternator. Therefore, the heat pump of the vehicle could be used in ORC mode to recover the waste heat. The nominal point for car (gasoline) and truck application using cooling engine or exhaust gases are described in Table 2. The condenser could be an air-cooled condenser in the front of the vehicle (such as the one used for the cooling engine). The lower limit of exhaust gas temperature is 120°C to avoid acid condensation.

3.2.6 Refrigeration truck (or boat)

Air conditioning systems used for refrigeration trucks or boats are only used to reach a given cold environment temperature for the medium transported. In 2012, the number of refrigeration trucks is 1.2 million worldwide and the average CO2 annual emissions are estimated at 50 tons (Liu et al., 2012). Those trucks could convert the cooling engine or exhaust gas thermal energy into mechanical energy trough the reversibility of the air conditioning system. The condenser of such an ORC system on a truck could be air-cooled. In the case of a boat, the seawater could be used in open loop to cool the ORC condenser. A case study involving a reversible air conditioning /ORC system on a truck is detailed in Table 2. The boat application is not studied here because of the very large range of different boat typologies and sizes but the same methodology could be applied to a specific given case to determine the feasibility of the reversible application.

3.2.7 Waste heat energy district heating

A large amount of waste heat is produced in industrial applications and power generation. This thermal energy can be used in a district heating network. Because of the possible temperature fluctuations of the low temperature waste heat energy, a heat pump can be used to reach a given temperature set-point for the district heating network. This heat pump is not run continuously and could provide electricity by reverting its cycle using the heat flux from the waste heat. The considered nominal point for this application in the case of the biomass CHP and the solar heat pump are described in Table 2.

3.2.8 DX Free cooling

Usually free cooling systems that are designed for specific applications are used in commercial buildings and require the use of a water/glycol solution, oversized circulation pumps, reduced energy efficiency outside the free-cooling operating period and increased investment cost. Carrier (Carrier, 2008) proposes a refrigeration cycle without compressors where only a circulation mini-pump and the fans ensure water cooling (Figure 8).

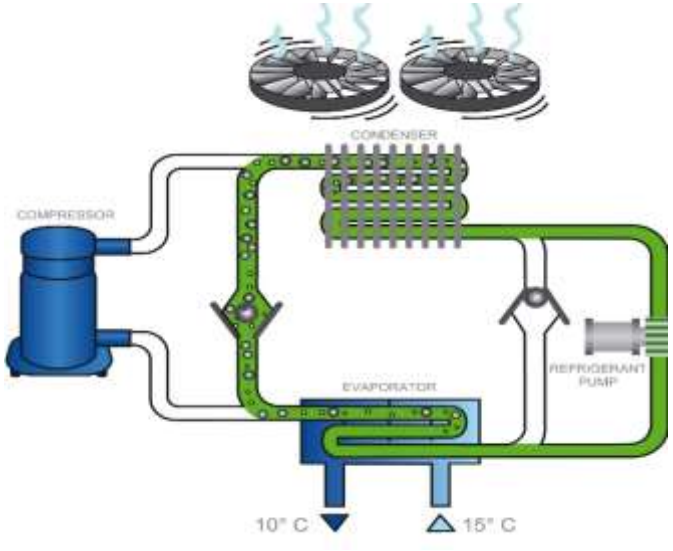

Figure 8 : Free cooling DX (CIAT, 2015)

In the evaporator, the water circulating in the building releases its heat to the refrigerant that evaporates. These vapours join the condenser directly without passing through the compressor. In this heat exchanger the liquid refrigerant releases its heat to the cold outside air and returns from the vapour state to the liquid state. A circulation mini-pump ensures the return of the liquid refrigerant to the evaporator and allows the refrigeration cycle to repeat. A COP of 24 can be reached for a lift of 10 K (Carrier, 2008). This system is not fully a reversible HP/ORC system but presents a lot of similarities. It would just require an expansion machine instead of an expansion valve to produce energy.

3.2.9 Pumped thermal energy storage (PTES)

Electrical energy storage becomes paramount with the increase of renewable energy share in the energy system. In the last years, a new technology has been investigated: the pumped thermal energy storage. During charge, PTES makes use of a high temperature ratio heat pump to convert electrical energy into thermal energy which is stored as ‘sensible heat’ in two thermal reservoirs, one hot and one cold (Figure 9). When required, the thermal energy is then converted back into electricity by effectively operating the heat pump backwards as a heat engine. (Mercangoz et al., 2012; Steinmann, 2014; White et al., 2013). This application could use a reversible HP/ORC system with the same machine for expansion and compression of the working fluid.

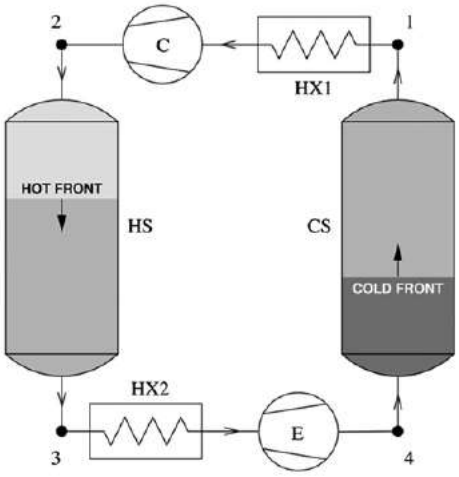

Figure 9: Pumped thermal energy storage (White et al., 2013)

This system could also be exploited with a waste heat flux. In this way, the heat pump is able to work with a higher cold source temperature (the temperature of the waste heat flux) and operates with a higher COP than a conventional pumped thermal energy storage (Frate et al., 2017).

3.3 DISCUSSION

Various applications where a heat pump could be inverted in an ORC have been presented here above. However some applications are technically more interesting than the others. A comparison is performed in terms of ORC efficiency, operating time and compatibility. The first criterion is chosen because the temperature levels of heat pump and ORC could be inappropriate and lead to very low ORC efficiency (temperature and/or volume ratio of the compressor non-adapted). The operating time criterion refers to the fraction of time when the heat pump is not used and when the ORC could be run. Finally, the compatibility refers to the thermal power of the heat pump and the required power of the ORC. In section 3.1, it has been shown that there is a minimum and maximum thermal power ratio between the ORC system and the heat pump. This analysis limits the Reynolds number of the ORC at three times the one in heat pump mode and limits the electrical power of the expander at half of that of the compressor (as an example). No cost or limit on the volume ratio of the machine are considered. The inputs for each application in terms of temperature levels and thermal power of the heat pump and fluid are listed in Table 2. In this table, $\dot{Q}_{HP}$ represents the thermal power at the condenser of the heat pump. The temperature levels (condensation and evaporation) are usually not know a priori (dependence of the temperature glide, the fluid…) but are roughly estimated in this study to obtain a first approximation of the performance.

Table 2 : Inputs of the selected applications with optimal fluid

Application	$\dot{Q}_{HP}$ [kW]	$t_{HP,cd}$[°C]	$t_{HP,ev}$[°C]	$t_{ORC,cd}$[°C]	$t_{ORC,ev}$[°C]	Fluid
Datacenter air conditioning	118	30	15	-15	27	R134a
ICE in industrial application	145	120	90	30	90	R245fa
Residential heat pump + solar panel	15	60	15	30	100	R245fa
Residential air conditioning + solar panel	17	35	15	30	100	R245fa
Residential air conditioning + biomass	17	35	15	30	144	R245fa
Refrigeration truck (exhaust gas)	9	30	-15	50	144	R245fa
Refrigeration truck (cooling engine)	9	30	-15	50	110	R245fa
Car (exhaust gas)	15	60	5	50	144	R245fa
Car (cooling engine)	15	60	5	50	110	R245fa
Truck (exhaust gas)	15	60	5	50	144	R245fa
Truck (cooling engine)	15	60	5	50	110	R245fa
WHR + disctrict heating	100	65	15	30	65	R134a

Two typical fluids have been tested (R245fa, R134a) and the results are extensively described in Annex (Table 4). Those two fluids have been chosen because R134a (resp. R245fa) is widespread in heat pumps and ORC systems (for the temperature levels encountered). Table 3 presents a summary of performance and limitations of each study case with the optimal working fluid (which is the fluid giving the highest efficiency). In this table, η_{ORC} is the efficiency of the ORC system, $\dot{Q}_{min}$(resp. $\dot{Q}_{max}$) is the minimum (resp. maximum) thermal power required at the evaporator of the ORC system, VR is the machine volume ratio and $\varepsilon_{exp,is}$ is the isentropic efficiency of the expander in ORC mode.

Table 3 : Performance and limitation of each study case with the optimal working fluid.

Application	η_{ORC}[-]	$\dot{Q}_{min}$[kW]	$\dot{Q}_{max}$[kW]	VR_{HP} [-]	$\varepsilon_{exp,is}$ [-]
Data center air conditioning	0.037	103.3	472.9	1.533	0.56
ICE in industrial application	0.048	174.1	812.6	2.034	0.57
Residential heat pump + solar panel	0.075	18.93	83.45	4.271	0.70
Residential air conditioning + solar panel	0.048	14.7	87.36	2.005	0.53
Residential air conditioning + biomass	0.046	15.35	119.2	2.005	0.37
Exhaust gas (Refrigeration truck)	0.090	10.15	61.26	6.034	0.70
Cooling Engine (Refrigeration truck)	0.063	14.4	47.52	6.034	0.73
Exhaust gas (car)	0.091	19.56	106.3	6.295	0.7
Cooling Engine (car)	0.062	28.42	82.43	6.295	0.73
Exhaust gas (Truck)	0.091	19.56	106.3	6.295	0.7
Cooling Engine (Truck)	0.062	28.42	82.43	6.295	0.73
WHR + disctrict heating	0.033	344.4	453.7	3.703	0.673

Following the results from Table 3, each application can be compared based on the ORC efficiency, operating time and compatibility. To facilitate the analysis, a ranking between zero and five is given for each criterion and application. The ORC system efficiency is normalized based on a maximum efficiency of 10% (=5) (Figure 10).

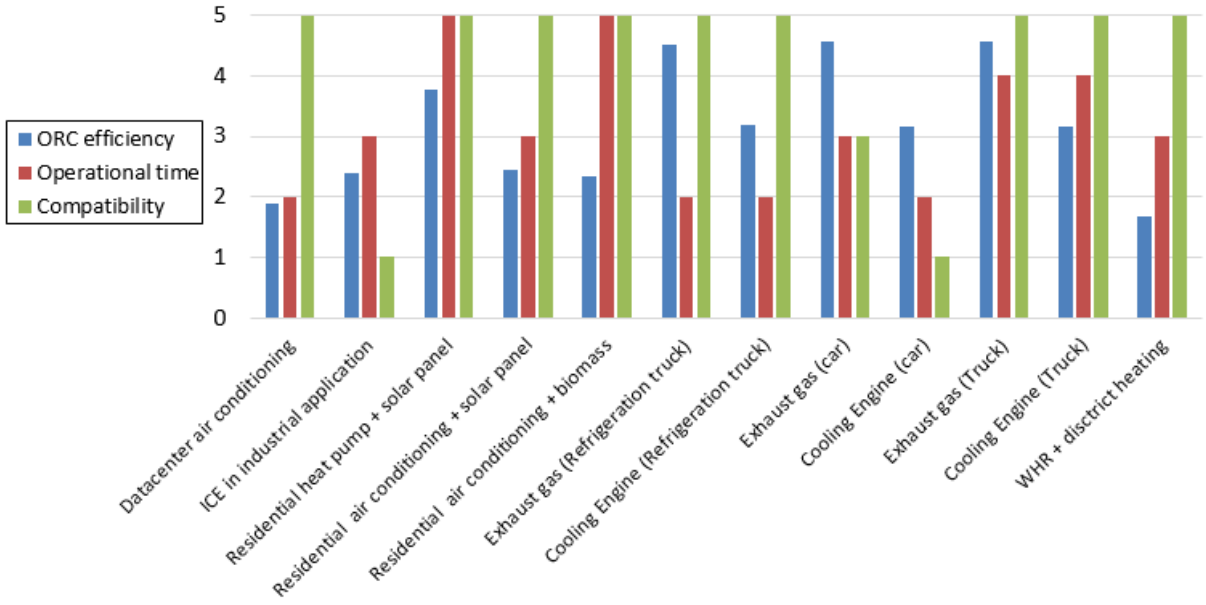

Figure 10: Performance criteria in terms of ORC efficiency, operating time and compatibility for each application.

First, the data center is interesting in terms of thermal power compatibility because the available thermal energy at the evaporator is equal to 118 kW and fits in the minimum and maximum imposed criteria. But, this system can only produce a decent level of electrical production when the outdoor temperature is very cold (-15°C), leading to a relatively low operating time (depending on the climate). The low temperature difference between evaporation and condensation temperature leads to a low-pressure ratio around the expander. This creates over-expansion that leads to a lower expander efficiency (see Table 3).

The internal combustion engine in industrial application presents a decent ORC efficiency of 4.8 %. The operating time is very dependent on the study case, which is the reason to use an average value of 3. Unfortunately, the minimum required thermal power at the ORC evaporator is 1.2 times higher than the actual one. The expander production is indeed much lower than the compressor consumption. To overcome this issue, it is possible to couple two electric machines (one motor for the compressor and one generator for the expander) to the reversible volumetric machine in a way to get decent efficiency in expander mode.

The residential heat pump combined with solar thermal panels is very interesting with a high efficiency and a high operating time because the heat pump and the ORC system are not operated during the same periods. Also, the ORC evaporator thermal power should be comprised between 18.93 kW and 83.45 kW for compatibility reasons. This corresponds to a minimum solar thermal roof area of 35 m^2 in nominal conditions in mid-Europe (chap 3). In hot climates, a residential air conditioning system also presents a nice opportunity to be used in ORC mode. However, the operating time of the ORC system is limited because the air conditioning system often operates when the ORC could produce electricity. The combination of an air conditioning system with a biomass CHP system would lead to a higher operating time.

The refrigeration truck application is promising with high ORC efficiencies (more than 9% when coupled with exhaust gas). Also, the available thermal power (around 150 kW at the exhaust gases on a high load nominal point) is compatible with the requirement of the reversible HP/ORC system. Nevertheless, depending on the refrigeration needs of the application, the operating time of the ORC could be relatively low.

The reversibility of a heat pump in ORC for a passenger car could present decent efficiencies with cooling engine and/or exhaust gas. Unfortunately, the necessity to have the same order of magnitude for the electrical power of the compressor and the expander leads to a high minimum thermal energy (19.56 kW) necessary at the evaporator of the ORC system. This value could be reached with the exhaust gases on a passenger car but only during high load and a relatively small fraction of time.

The integration of a reversible HP/ORC system on a truck for air-conditioning is one of the most attractive applications because it presents relatively high ORC efficiency (like the passenger car) and presents a high operating time (except in the case of severe climates). The advantage compared to the car application is that the minimum thermal power

necessary at the exhaust gas (19.56 kW) or at the cooling engine (28.42 kW) fits with the actual heat rejection of a truck (respectively 150 kW and 75 kW).

Finally, the waste heat recovery district heating application presents a nice compatibility and an operating time depending on the waste heat fluctuations. However, the ORC efficiency is rather low in the studied configuration but is depending on the waste heat temperature.

4 OBJECTIVES AND ORGANISATION OF THE MANUSCRIPT

Based on the novelty of the reversible HP/ORC unit and the very low number of references relative to this topic in literature, this thesis tries to give answer to the following questions:

- Which applications are interesting for a given HP/ORC unit?
- Which technology of volumetric machine is the most adapted for a given application?
- Which layout and architecture should be used depending on the application?
- How to optimally size a reversible HP/ORC unit?
- How to predict realistic performance in a given study-case?

This thesis tries to answer those questions by developing modelization tools and generalised methodologies.

This thesis studies the concept of reversible heat pump/organic Rankine cycle (HP/ORC) and its application in the building sector. **Chapter 1** includes the introduction and describes this system and its possible applications. A tool based on operating maps is developed to examine the feasibility of such a system depending of the operating conditions of a given application.

In **Chapter 2**, the reversibility of reversible volumetric machines is studied based on a theoretical comparison followed by experimental results performed on four different compressor/expander technologies. A semi-empirical model is calibrated for each technology and allows to extrapolate the performance outside of the experimental data range. The comparison shows which technology should be used depending on the application.

In **Chapter 3**, the design and sizing methodology to optimize the performance of the reversible heat pump organic Rankine cycle is described. This design and sizing optimisation methodology is performed in the case of the residential application: the reversible HP/ORC system is coupled with a large solar absorber in a building to provide a polyvalent machine able to produce heat or electricity depending on the needs of the building. Steady-state models are then used to predict the performance of the system integrated into a building.

As the theoretical results are promising in the case of the residential application, a test-rig is mounted and an experimental campaign is performed in both HP and ORC modes (**Chapter 4**). A global methodology to improve the quality of experimental data is proposed based on mathematical tools. The method combines a reconciliation method, a Gaussian Processes, a

sensitivity analysis and takes into account the solubility of refrigerant within lubricating oil. A model is calibrated based on experimentation in order to characterize the performance of the HP/ORC unit with an optimal control.

Chapter 5 studies the reversible unit in the case of the building application based on advanced dynamic models. The global model combines validated sub-models: the reversible HP/ORC unit, the solar roof, the thermal energy storage, the horizontal ground heat exchanger and the building. An optimal strategy control is developed and presented. A parametric study is performed to observe the performance of the system in a wide range of typologies. The influence of different lights and appliances profiles, building envelope characteristics, integration of batteries, roof tilt angle, location, storage size is developed. Furthermore, a technical and economic comparison with a mature technology to get a positive energy building, photovoltaics panels combined with a heat pump in a passive house, is performed.

5 CONCLUSION

This chapter presents the context and the concept of the reversible HP/ORC unit. Moreover, a methodology, based on practical limitations to modify a heat pump into a reversible HP/ORC unit is developed. It helps to identify which applications could be the most interesting for a heat pump to become a reversible HP/ORC unit. This preliminary study shows that a residential building with a solar roof and the truck application for air-conditioning are the most promising ones (with efficiencies of 7.5% and 9% respectively). More advanced modelling should be considered to determine accurately the energy performance and the economic interest in a specific given case. An example of optimal sizing and modelling is provided with the residential building coupled with solar roof in this thesis. (Chapter 3). Also, a dynamic simulation including models validated on real components (Chapter 4) and a realistic control strategy can provide accurate performance of such a system. An example of such a modelling approach is given in chapter 5.

6 APPENDICES

Table 4 : Results of the study cases with several fluids

Application	Fluid	η_{ORC}[-]	$\dot{Q}_{min}$[kW]	$\dot{Q}_{max}$[kW]	VR [-]	$\varepsilon_{exp,is}$ [-]
Car exhaust gas	R134a	0.03293	58.19	71.1	4.467	0.03293
Car (Cooling Engine)	R134a	0.03293	58.19	71.1	4.467	0.03293
Truck (Exhaust gas)	R134a	0.03293	58.19	71.1	4.467	0.03293
Truck (Cooling Engine)	R134a	0.03293	58.19	71.1	4.467	0.03293
Refrigeration truck (Exhaust gas)	R134a	0.03694	25.76	38.88	4.129	0.03694
Refrigeration truck (Cooling Engine)	R134a	0.03694	25.76	38.88	4.129	0.03694
Data center air conditioning	R134a	0.03781	103.3	472.9	1.533	0.03781
Residential building	R134a	0.06883	22.3	80.63	3.289	0.06883
Residential air conditioning	R134a	0.04649	16.15	81.97	1.754	0.04649
Biomass building + air conditioning	R134a	0.04649	16.15	81.97	1.754	0.04649
Waste heat recovery + district heating	R134a	0.03344	344.4	453.7	3.703	0.03344
Car exhaust gas	R245fa	0.09148	19.56	106.3	6.295	0.09148
Car exhaust gas	R245fa	0.09148	19.56	106.3	6.295	0.09148
Car (Cooling Engine)	R245fa	0.06297	28.42	82.43	6.295	0.06297
Truck (Exhaust gas)	R245fa	0.09148	19.56	106.3	6.295	0.09148
Truck (Cooling Engine)	R245fa	0.06297	28.42	82.43	6.295	0.06297
Refrigeration truck (Exhaust gas)	R245fa	0.09043	10.15	61.26	6.034	0.09043
Refrigeration truck (Cooling Engine)	R245fa	0.06373	14.4	47.52	6.034	0.06373
Data center air conditioning	R245fa	0.03741	100.3	466	1.7	0.03741
ICE in industrial application	R245fa	0.04801	174.1	812.6	2.034	0.04801
Residential building	R245fa	0.07551	18.93	83.45	4.271	0.07551
Residential air conditioning	R245fa	0.04888	14.7	87.36	2.005	0.04888
Biomass building + air conditioning	R245fa	0.04683	15.35	119.2	2.005	0.04683
Waste heat recovery + district heating	R245fa	0.03109	342	450.3	4.911	0.03109
Car exhaust gas	R245fa	0.03293	58.19	71.1	4.467	0.03293

References

- Alexander W., Parks G., Markides C., 2013. Thermodynamic analysis of pumped thermal electricity storage Applied Thermal Engineering 53, 291-298.

- Baek, J. S., Groll, E. A., Lawless, P.B., 2005. Piston-cylinder work producing expansion device in a transcritical carbon dioxide cycle. Part I: experimental investigation, International Journal of Refrigeration 28, 141–151.

- Bettgenh€auser, K., Offermann, M., Boermans, T., Bosquet, M., Gr€ozinger, J., von Manteuffel, B., Surmeli, N., 2013. Heat Pump Implementation Scenarios until 2030: an Analysis of the Technology's Potential in the Building Sector of Austria, Belgium, Germany, Spain, France, Italy, Sweden and the United Kingdom. Ecofys. Report, Project number: BUIDE12080.

- Carmo, C., Dumont, O., Nielsen, M., Elmegaard, B., 2016. Assessment of Emerging Renewable Energy-based Cogeneration Systems, CLIMA conference 2016, Aalborg.

- for nZEB Residential Buildings

- Carrier, 2008. DX free cooling, available at http://www.climamarket.bg/wp-content/uploads/Brochure-Carrier-30XARBRQ.pdf.

- CIAT, 2015. http://www.ciat.cz/chillery/free-cooling consulted the 14/07/2015.

- Dumont, O., Quoilin, S., Lemort, V. 2015. Experimental investigation of a reversible heat pump / organic Rankine cycle unit designed to be coupled with a passive house (Net Zero Energy Building), International Journal of Refrigeration, http://dx.doi.org/10.1016/j.ijrefrig.2015.03.008.

- Dumont, O., Dickes, R., De Rosa, M., Douglas, R., Lemort, V., 2018. Technical and economic optimization of subcritical, wet expansion and transcritical Organic Rankine Cycle (ORC) systems coupled with a biogas power plant, Energy Conversion and Management – Journal, in press.

- European Climate Foundation, 2010. EU Roadmap 2050. Retrieved from http://www.roadmap2050.eu.

- European Union, 2014. Reducing CO2 emissions from passenger cars. Available: http://ec.europa.eu/clima/policies/transport/vehicles/cars/index_en.htm#top-page

- Fischer, J., 2011. Comparison of trilateral cycles and organic Rankine cycles. Energy 36,6208–6219.

- Frate, G., Antonelli, M., Desideri, U., 2017. Pumped Thermal Electricity Storage: an interesting technology for power-to-heat applications, proceedings of ECOS 2017 conference, San diego, USA.

- Girard O., 2006. Système et procédé de gestion d'énergie d'un véhicule. French patent FR29132117.

- Innogie ApS, 2013. Thermal solar absorber system generating heat and electricity, United States Patent Application Publication, US 2013/025778 A1.

- Inaba, I., Shinichi, H., Shigeru, H., Tadashi, H., 2005. Waste heat collecting system having Rankine cycle and heating cycle. US patent 6,928,820.

- Lai, N.A., Fischer, J., 2012. Efficiencies of power flash cycles. Energy 44, 1017–1027.

- Lecompte S., Huisseune H., Van der Broek M., Vanslambrouck B., De Paepe M., 2015. Review of organic Rankine cycle (ORC) architectures for waste heat recovery, Renew Sustain Energy Rev. 47:448-461.

- Legros, A., Guillaume, L., Diny, M., Hamid, Z., Lemort, V., 2014. Comparison and impact of waste heat recovery technologies on 7 passenger car fuel consumption on a normalized driving cycle, Energies 2014, 7, 1-x manuscripts; doi:10.3390/en70x000x.

- Liu, M. Saman, W., Bruno, F., 2012. Development of a novel refrigeration system for refrigerated trucks incorporating phase change material, Applied Energy 92, 336–342.

- Mercangöz, M., Hemrle, J., Kaufmann, L., Z'Graggen, A., Christian, 2012. Energy 45, 407-415.

- Peris B., Dumont O., Quoilin S., Navarro-Esbría, J., 2016. Internal combustion engines cooling water valorization through invertible HTHP/ORC systems, Symposium waste heat valorization in industrial processes, Kortrijk, Belgium.

- Persson, J. G., 1990. Performance Mapping Versus Design Parameters for Screw Compressors and Other Displacement Compressor Types, Screw Machine '90: Screw

Compressors, Screw Loader, Screw Motors: Conference Dortmund, Dusseldorf, Germany, Oct. 2–3, VDI-Berichte 859, pp. 15–31.

- Quoilin, S, 2011. Sustainable energy conversion through the use of organic Rankine cycles for waste heat Recovery and Solar Applications. PhD thesis, Liege (Belgium).

- Schimpf, S., K. Uitz, and R. Span, 2011. Simulation of a solar assisted combined heat pump-organic Rankine cycle system. Proceedings of World renewable Energy Congress, 2011, Sweden.

- Smith, I.K., 1993. Development of the trilateral flash cycle system Part1: Fundamental considerations. Proc. Inst. Mech. Eng. Part A J. Power Energy, 207, 179–194.

- Schuster A., Karellas S., Aumann R., 2010. Efficiency optimization potential in supercritical Organic Rankine Cycles. Energy, 35:1033-1039.

- Steinmann, W.D., 2014. The CHEST (Compressed Heat Energy STorage) concept for facility scale thermo mechanical energy storage, Energy 69, 543-552.

- Zhang, S., Wang, H., Guo, T., 2011. Performance comparison and parametric optimization of subcritical Organic Rankine Cycle (ORC) and transcritical power cycle system for low-temperature geothermal power generation. Appl. Energy, 88, 2740–2754.

Chapter II:

Investigation of reversible volumetric machines

"I can't change the direction of the wind, but I can adjust my sails to always reach my destination."
Jimmy Dean

Abstract

At small scale, volumetric machine can be considered as mature in compressor mode but not in expander mode. Therefore, an experimental investigation is performed on different volumetric machine in an ORC test rig. Based on the experimental results and the extrapolation trough a semi-empirical model, some guidelines are drawn to identify which technology is optimal for a given study case.

1 INTRODUCTION

The most important component in a reversible HP/ORC is the machine able to work as a compressor and as an expander. The compressor technology can be seen as mature and no major novelties are expected in the future. Most of the manufacturers provide curves of performance for their machines. Small and mid–size heat pumps (<350 kW) are using almost exclusively three types of compressors: reciprocating, screw and scroll (rotary vane compressor are occasionally also used for power below 50 kW) (Butrymowicz et al., 2005*)*.

The knowledge about compressor being well established, this chapter focuses on expander performance, characteristics and the possibility to be run in compressor. A lot of developments have been done recently in small-scale expanders but no technology has reached maturity yet. Many theoretical investigations have demonstrated the considerable influence of the expander efficiency over the global performance of ORC systems (Ziviani et al., 2013, Qiu et al., 2011 among others). No single expander technology has been identified to be the optimal one, particularly for mid- and small-scale systems (Qiu et al., 2011). The optimal technology depends on a large number of parameters: working conditions,

compactness, cost, and availability among others. It is therefore important to evaluate and compare the performance of different expander technologies in order to select the optimal candidate for a given application. Operating maps (Appendices - Figure 24) help to select the fluid and expander technology based on the evaporation and condensation temperatures and on practical and theoretical considerations (Quoilin et al., 2012). These operating maps are established with a global basic approach, including only under and over-expansion losses and a volume flow coefficient based on compressor data. So, based on literature, very few works are done to characterise the performance of each technology accurately. Therefore, a comparison between the experimental performances of different volumetric expander machines is made in this chapter. Volumetric machines are often chosen for small-scale applications because of the low rotational speed, the low flow rate for a relatively high pressure difference and compatibility with two-phase conditions, which may appear at the end of the expansion in some operating conditions (Qiu et al., 2011). The four machines, namely a modified hermetic scroll compressor running at constant speed, a variable speed modified scroll compressor, a variable speed twin-screw expander and an swash-plate piston expander working at variable speed (Oudkerk et al., 2015), are tested in a same micro-scale ORC system using R245fa as working fluid (Dickes et al., 2014). After a brief comparison of the technologies based on a literature review, the experimental setup and the four expanders are described in details. The experimental performance of the machines is then compared in terms of isentropic efficiency and filling factor. Also, semi-empirical models are calibrated[1] to identify the main losses of each expander and a performance extrapolation in optimal operating conditions is assessed. Finally, an operating map is drawn based on these models to select the optimal expander depending on the temperature levels of the ORC. Also, a general conclusion to select the optimal machine depending on the flexibility, the compactness, the efficiency, the power range and the ability to handle high pressure and temperature of a given application is proposed.

2 STATE OF THE ART

2.1 PISTON MACHINES

In a piston compressor, the intake gas enters the suction manifold, then flows into the compression cylinder where it is compressed under the action of a piston driven in a reciprocating motion via a crankshaft, and is then discharged (Figure 1 – Axial piston and crank train). In a piston expander, at position where the cylinder volume is minimum and equal to the clearance volume V_0 (Top Dead Center position), the piston starts its downward stroke. Since the supply port is opened, the fluid at the supply pressure enters the cylinder. The admission process extends until the supply valve closes. Then, the expansion phase starts. After that, the exhaust port opens and the discharge process is initiated. Finally, the mass trapped inside the cylinder behaves as a closed system and as the piston continues its

[1] By calibration of the model, it is implied that some defined calibration parameters are tuned to get a model prediction as close as possible of the measurements.

upward movement, the pressure is increased to the internal pressure of the expander. This trapped mass is in connection with the intake fluid when the supply port opens in the next cycle.

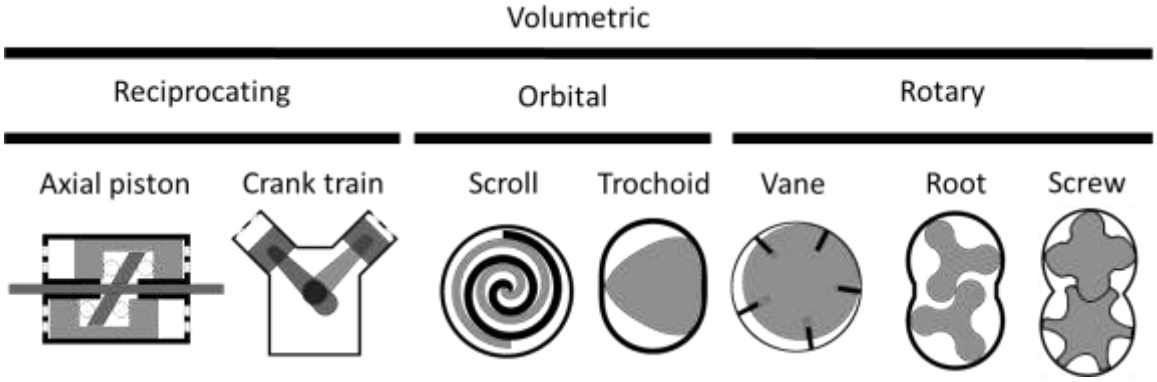

Figure 1 : Different expander technologies (Lemort and Legros, 2016)

A piston compressor can work as an expander by adjusting the inlet and outlet valves (or cylinder openings) for the intake and outtake of fluid. Piston expanders are currently used for niche-market applications: small-scale CHP and waste heat recovery on internal combustion engines (Seher et al., 2012; Endo et al., 2012). This type of expander is suited for low displacement and power applications. It presents the advantage to be able to work with high inlet temperatures, inlet pressures and pressure ratio (Appendices - Figure 1). In 2005, the COP of an air-conditioning system has been increased by 10% by replacing the expansion valve with a piston expander despite its low isentropic efficiency of 11% (Baek et al., 2005). In 2012, a 7 kW reciprocating expander reached 70% adiabatic efficiency in a Rankine cycle (Glavatskaya et al., 2012). In 2013, a 3 kWe oil-free single cylinder piston expander is tested with an adiabatic efficiency of 47% with water (Daccord et al., 2013). Figure 2 shows the evolution of the maximal isentropic effectiveness achieved by the other piston expanders found in literature.

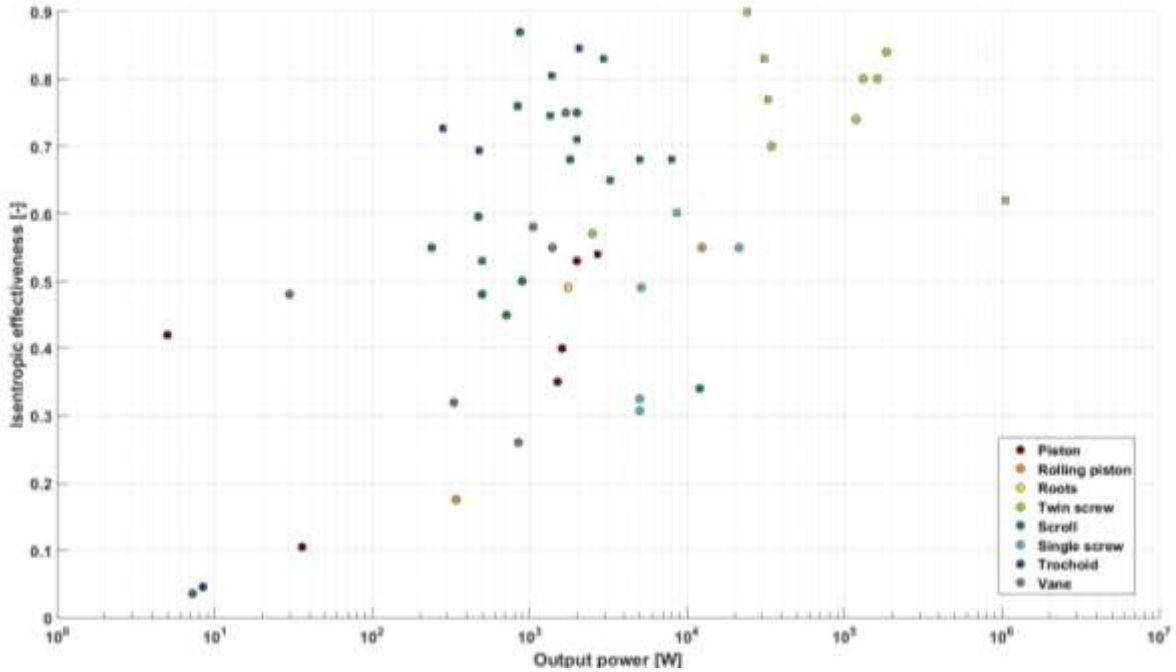

Figure 2: Evolution of the maximal measured isentropic effectiveness with the maximal measured output power for 67 machines described in the literature (circles denote mechanical power/isentropic effectiveness and squares electrical power/isentropic effectiveness) (Lemort and Legros, 2016).

2.2 SCROLL MACHINES

A scroll compressor compresses pockets of fluid between two interleaving scrolls. In a scroll expander, the suction chamber (located in the centre of the machine) is communicating with the supply. From the position where the suction chamber is at its minimal volume ("clearance volume"), its volume increases over one entire shaft revolution. The suction chamber divides itself into two expansion chambers and form two different expansion paths. The volume of the expansion chamber increases, so that the fluid pressure decreases from the supply pressure to the internal expander pressure. Finally, when the expansion chambers open up to the exhaust line, the expansion chambers become the discharge chambers (Figure 3).

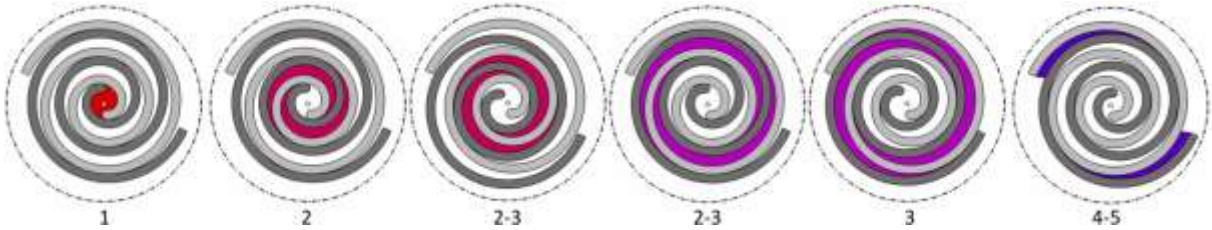

Figure 3 : Scroll expander (Lemort and Legros, 2016)

A scroll compressor is easily modified in a scroll expander by removing the check valve and if necessary a system to push the floating seal upwards (Dumont et al., 2014).

Scroll expander benefits from few rotating parts and rather constant filling factor. It presents a limited expansion pressure ratio since the volume ratio is limited to 5 (Appendices - Table 7). The use of two scroll in series allows to overcome this issue. First, record of scroll expander use appeared in 1994 (Zanelli et al., 1994). Many sources (Zanelli et al., 1994; Kane et al., 2003; Mathias et al., 2009,; Lemort et al., 2012 and Braco et al., 2013) show that the best isentropic efficiencies are always above 65% whatever the fluid (R245fa, R123, R134a). Also, scroll expanders present the best performance for low power applications with a maximum measured isentropic efficiency of 87% (Harada, 2010). Figure 2 shows the evolution of the maximal isentropic efficiency achieved by the other scroll expanders described in literature.

2.3 SCREW MACHINES

Screw compressors use two meshing helical screws to compress the gas. Currently, most of the screw expanders are twin-screw machines, the use of single-screw expanders is seldom. A twin-screw expander is made up of two helically toothed rotors that delimit a series of working chambers with the casing (Figure 4). The same chamber becomes successively a suction chamber, an expansion chamber and finally a discharge chamber. The supply port allows for the filling of the chamber with the high-pressure fluid. Expansion starts when the chamber ceases to be in communication with the supply port. The chamber reaches the discharge port as soon as its volume is maximum. The volume then decreases until the chamber disappears.

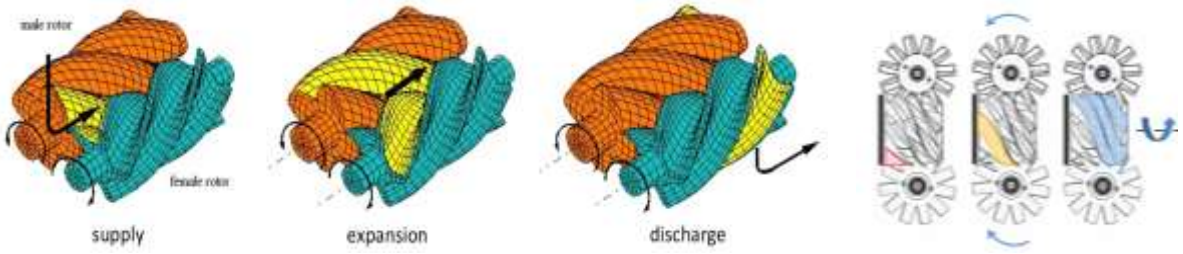

(a) (b)

Figure 4 : Twin-screw expander (a) and single-screw expander (b) (Brummer et al., 2012; Ziviani et al., 2014).

The screw compressor requires no particular modification to work as an expander. Screw expanders presents advantages such as high allowed rotational speed, compactness and wet expansion handling among others (Appendices - Table 7). In 2000, a 20 kW - twin screw expander reached 70% adiabatic isentropic efficiency with fluid R113 to replace a throttle valve in a chiller (Brasz et al., 2000). In 2011, an adiabatic efficiency of 59% is reached with air in a 5kW single screw expander. In 2014, a 50 kW twin screw showed an isentropic efficiency of 72.4% with R245fa (Hsu et al., 2014). In 2015, a 5 kW single screw expander has been tested with R123 with a maximum isentropic efficiency of 49.5 % (Xia et al., 2015). In

2017, a 4 kW twin screw was tested with R245fa and it was proven that the efficiency could reach up to 70% (Nikolov et al., 2017).

A single-screw expander (Figure 4b) is made up of a central rotor with helical grooves meshing with two toothed gate rotors. This meshing delimits a working chamber on each side of the rotor, resulting in symmetrical and simultaneous evolution of the fluid with respect to the central rotor rotation axis. According to He et al. (2013), single-screw expanders could cover powers ranging from 1 kW to 200 kW. Volume ratios of 7 could be achieved with such machines. A single screw expander with heated compressed air as the working fluid produced up to 4 kW with an inlet temperature of 80°C (Wang et al., 2011). In 2014, a 10 kW single screw is tested with refrigerants SES36 and R245fa and presented a maximum isentropic efficiency of 65% (Desideri et al., 2014). A 10 kW single screw expander is tested with refrigerant R123 and shows efficiency up to 58% (Zhang et al., 2014). Figure 2 shows the evolution of the maximal isentropic effectiveness achieved by the other screw expanders found in literature.

2.4 OTHER MACHINES

2.4.1 Vane expanders

A vane expander consists in a cylindrical housing (stator) in which a cylindrical rotor is in motion (Figure 1). Slots are spread out all over the rotor and allow the insertion of vanes that are pushed out by a spring or similar mechanisms. The chamber in communication with the admission port is referred as the suction chamber. When that chamber is no longer in contact with the suction port, the expansion process begins and ends when the chamber faces the exhaust port, becoming then a discharge chamber. Temperature limits are not so often reported in literature. However, Badr et al. (1985) report a maximal allowable operating temperature of 140°C and a maximal rotational speed of 4000 rpm. Built-in volume ratios encountered in practice are in the range of 2.0 to 8.5 (Badr et al., 1985).

2.4.2 Roots expanders

Roots expanders are not encountered frequently. Roots blower has either cycloidal rotors or a geometry close to a screw expander (Figure 1). The inlet and outlet are set in a perpendicular direction of the axis of the rotor so that their built-in volume ratio is always close to 1. The fluid enters the machine into the suction chamber and then, is trapped between the housing and the rotors. When the chamber enters in contact with the exhaust port, the fluid is released to the exhaust line. Roots expander show power ranging from 1 to 30 kW with maximal rotational speed around 20000 rpm.

Other technology such as trochoidal (Figure 1), or spool expanders could be used but are not considered here because of the lack of maturity and literature.

2.5 OPERATING POWER RANGE

The three most-widespread compressor types for small and mid-scale heat pumps (<350 kW) are the reciprocating, the scroll and the screw). Among them, scroll and screw compressors have been increasing their market share during the last decade. Reciprocating compressors are still used because of their low cost and because they were well established in the market in the past. However, this type of compressor is slowly replaced by rotary compressors. Reciprocating compressor represents less than 15% of the Asian market and their sales value in the European Union fell from 31% in 1999 to 27 % in 2000 (Kreider, 2000). Screw compressors are mainly used in the range 100-1000 kW.

For expanders, Lemort and Legros (2016) compared the ranges of power produced by major technologies of expanders (based on the analysis of reported performance of 67 machines published in technical literature) (Figure 5). Screw expanders typically produce the largest powers, with high effectiveness. Over the range 100 W - 10 kW, scroll machines show the best performance. Piston and vane expanders cover the same range of powers, but with lower performance. Single-screw expanders produce lower powers than twin-screw expanders and with lower effectiveness (Lemort and Legros, 2016).

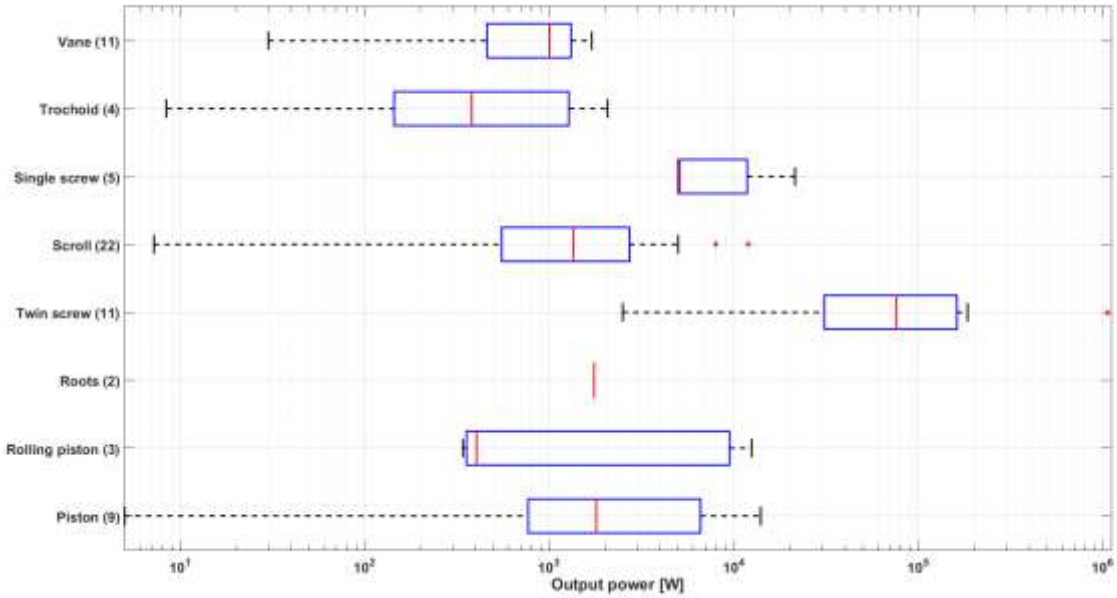

Figure 5: Ranges of power produced by major technologies of expanders (based on the analysis of reported performance of 67 machines published in technical literature) (Lemort, 2016). The left and right extremities of the box respectively indicate the first and third quartiles q1 and q3. The red band inside the box indicates the median. The whiskers correspond to the lowest and highest data still within respectively q1-1.5*(q3-q1) and q3+1.5*(q3-q1). The red points indicate the outliers.

A comparison of the power ranges (in compressor and expander modes) of the most widespread technologies in heat pumps (scroll, piston and screw) is presented in Figure 6.

The compressor data comes from the main manufacturers of the market while the expander data comes from Lemort and Legros (2016).

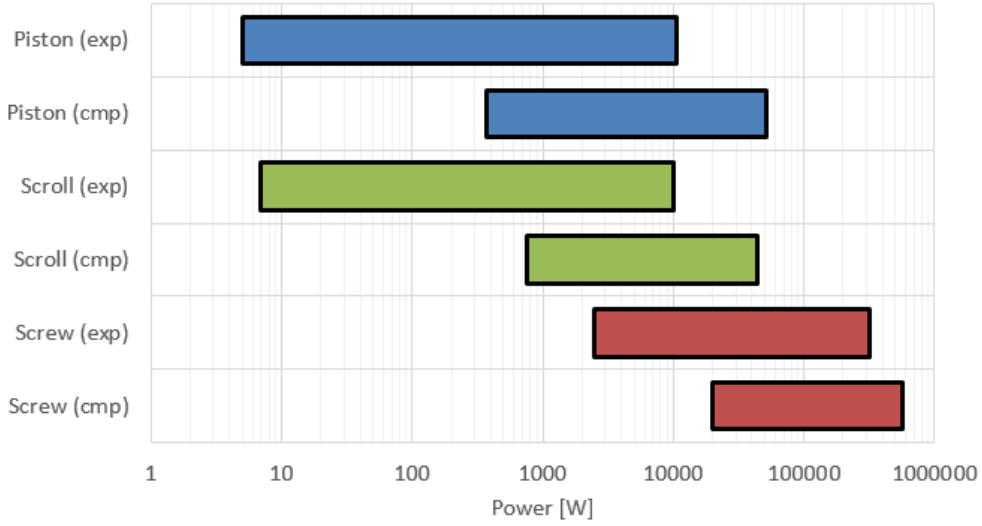

Figure 6 : Range of power for scroll, piston and screw expanders in compressor and expander.

The first observation is that the scroll and the piston machines compete in the same range of power as expander and as compressor. Screw machine being adapted for larger ranges of power. Also, for the three types of technologies, the expanders covers smaller values of power for multiple reasons:

- For a given indicated power, a given expander produces less mechanical power than what the compressor consumes because losses are subtracted from the indicated power in the case of an expander and added to the indicated power in the case of a compressor. Moreover, the electric machine is oversized (and therefore less efficient) in generator mode for the same indicated power (Oudkerk et al., 2013).
- Because the volumetric efficiency is always lower than one, the compressor consumes more energy because of the leakages while an expander produces less energy when increasing the leakages.
- Also, the expander technologies at small- and mid-scale are less mature than for the compressor leading to lower isentropic efficiency and lower power production.

3 EXPERIMENTAL SET-UP

3.1 TEST-RIG

The test-rig used to characterize the expanders performance is depicted in Figure 7. It is constructed using standard mass-manufactured components from the HVAC industry. The working fluid is R245fa and the test bench consists of a brazed plate evaporator, a shell and

tube water-cooled condenser, a brazed plate recuperator, a gear pump and a liquid receiver. A 150 kW electric boiler is used as heat source and it is controlled to adjust the temperature at the expander inlet. The evaporating pressure in the ORC is regulated by means of the pump mass flow rate and the condensing pressure is adjusted with the water flow in the condenser. Oil (5% mass fraction) is added to the refrigerant to lubricate the expanders. This value is a minimum to avoid usury and to obtain decent filling factors of the volumetric machine. A higher mass oil mass fraction lead to a significant decrease of the ORC performance due to higher required working fluid flow and deterioration of the heat transfer in the exchangers (Daccord et al., 2017). In this test-rig, the oil flow is ensured trough an optimal sizing of the piping. The diameter of the piping is sized to obtain the minimum required speed (0.5m/s for liquid and 10m/s for vapour) of fluid at part load. For small-scale ORC power systems, this method of lubrication is usually preferred to an additional oil separator which requires an oil tank, a liquid level sensor, an additional pump…

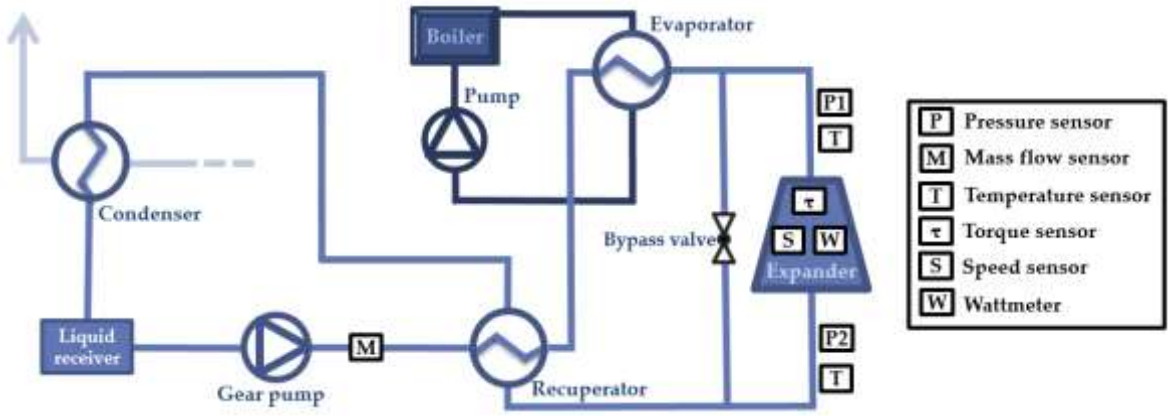

Figure 7: Hydraulic scheme of the test-rig

Pressures and temperatures at key locations of the cycle are measured by different sensors. The working fluid mass flow rate is acquired with a Coriolis flow meter at the pump outlet. The power output of the piston expander is measured with a torque and a speed meter whereas the scroll expanders are equipped with a wattmeter. Main characteristics of the different sensors of the plant are summarized in Table 7 (Appendices).

3.2 EXPANDER CHARACTERISTICS

3.2.1 Constant speed scroll compressor

The scroll machine investigated is a lubricated hermetic scroll compressor (Emerson ZR34K3E – designed to work with fluid R134a) modified to run in reverse as an expander (Dumont et al., 2014). More details about the modifications are provided in Chapter four. It is directly connected to the grid resulting in a constant shaft speed (~3000 RPM) whatever the operating conditions (Dickes et al., 2014). Its main characteristics are summarized in Table 1 and the electrical power output is measured with a wattmeter. The mechanical

power generation is calculated using the electromechanical efficiency of the generator as provided by the manufacturer.

3.2.2 Piston expander

The piston expander tested is a swash-plate piston expander characterized by a total cylinder volume of 195 cm³ (Table 1). Lubrication is performed by an external circuit with oil injection at main friction points. The admission and exhaust processes are achieved by means of a valve-less system that induces symmetric opening and closing of the cylinders' volumes. The expander is connected to an asynchronous electrical motor and a four-quadrant variable-frequency drive is used to control the shaft speed (Oudkerk et al., 2015). Unlike the scroll expander, the mechanical power of the piston machine is directly measured by means of a torque and a speed meters. It has been sized for ethanol/water mixture applications. This is not the last version of the prototype conceived by the industrial partner: a more efficient machine already exists and should be tested in future works.

3.2.3 Screw expander

A twin-screw expander is tested. The sizing methodology for this screw expander is presented by Brümmer (2012). The design of the screw expander is oriented towards an unsynchronized, liquid injection machine with the rotors and bearings being lubricated by the working fluid and the injected liquid. It presents a swept volume of 19.96 cm^3 and a built-in volume ratio of 2.5 (Table 1). The nominal supply pressure (12 bar) is relatively low compared to the two other expanders. The speed is controlled by an Eddy current brake. A magnetic coupling ensures the transmission of the torque between the expander and the shaft (Nikolov and Brummer, 2017).

3.2.4 Variable speed scroll compressor

It is designed for vehicle air-conditioning system with fluid R134a. Its volume ratio is close to the constant speed scroll but the swept volume is lower (12.74 cm^3) as presented in Table 1.

Besides the standard criteria summarized Table 1, two additional terms are used to compare the four expander technologies. First, the *compactness factor* $F_{C,1}$ (Eq. 1) is defined as the ratio of the nominal mechanical power ($\dot{W}_{shaft,,nom}$) and the total volume of the expansion and mechanical parts (without the shaft, the generator and the casing). As shown in Table 2, the screw expander is more compact than the other technologies (21 $W.cm^{-3}$). The constant speed modified compressor presents a low compactness factor probably because it has been built for stationary application where compactness is less important than other criteria. Also, the piston compactness factor is low mainly because the chambers are compressing vapour half of the time contrarily to the afore-mentioned technologies. The sizing factor criteria, which is defined in Equation 2, illustrates the volume importance of the expansion parts compared to the global system necessary to spin the shaft. Nevertheless, these values are

given as an order of magnitude and should be taken with care since different machine with different level of maturity are compared.

$$F_{C,1} = \frac{\dot{W}_{mec,nom}}{V_{exp} + V_{mec}} \quad (1)$$

$$F_{C,2} = \frac{V_{exp}}{V_{exp} + V_{mec}} \quad (2)$$

Table 1 : Expander characteristics. The typical length is two times the length of the stroke in the case of the piston expander, the eccentricity for the scroll expanders and the diameter of the male rotor for the screw expander. The nominal linear speed is the product of the nominal speed and the typical length.

Parameter	**Scroll expanders (cst speed/var speed)**		**Screw expander**	**Piston expander**
Swept volume [cm^3]	20.2	12.74	19.96	195
Volume ratio [-]	2.2	2.19	2.5	4.74
Maximum inlet temperature [°C]	140	130	140	250
Maximum inlet pressure [bar]	28	25	16	40
Rotational speed range [RPM]	3000	[800-8000]	20000	[1000-4000]
Typical length [mm]	2.57	2.34	48.44	31X2
Nominal linear speed [$m.s^{-1}$] (nominal rotational speed [RPM])	0.806 (3000)	1.46 (6000)	60.8 (12000)	12.9 (2000)
Compactness factor [$W.cm^{-3}$]	1.099	3.39	21	1.2
Sizing factor [-]	0.569	0.74	0.53	0.5
Nominal shaft power [W]	2277	2000	2000	4000-15000

3.3 IMPORTANT NOTE ABOUT THE COMPARISON OF PERFORMANCE

Generally, a perfectly fair comparison between different types of expanders is not possible for different reasons:

- It is not possible to test expanders with exactly the same level of maturity. In this case, the scroll compressors, modified in expanders, have been produced in large series for many years and have reached commercial maturity compared to the piston and screw expanders, which are prototypes and that could see their performance and commercial maturity slightly increased in the future.

- Not a single expander in this experimental investigation has been sized for the test-rig. This means that limitations in the test-rig in terms of mass flow rate, pressure and temperature affect the performance of the expanders (not necessarily in the same way for each one).

- Furthermore, the fluids considered during the sizing of those expanders are not the one used in the ORC test bench (R245fa).

- Nominal working conditions in terms of pressure and temperature are different for each technology (higher pressure and temperature for the piston for example).

- Finally, scroll compressors are not designed for expansion. This leads to an eventual lack of lubrication in the bearings, pressure drop through the inlet valve and higher internal leakage or wear due to different operating conditions.

Nevertheless, the choice of an expander technology remains difficult nowadays and only very few objective comparisons exist in literature. Some precautions are used to tackle the aforementioned arguments. In this study, the same test-rig with the same organic fluid is used, only the expander is replaced meaning that temperature, pressure and flow limitations are the same for each machine. Following that, semi-empirical models are calibrated to evaluate the performance in optimal conditions not reachable on the test-rig (chapter 5). This allows for a comparison of the expanders without the limitations of the test-rig.

4 EXPERIMENTAL RESULTS

4.1 OPERATING CONDITIONS

The range of operating conditions and the maximum performance of the expanders are given in Table 2. Since the speed of the piston expander can be decreased with the variable frequency drive, higher evaporating pressures are achieved (up to 30.2 bar) compared to the constant-speed scroll expander, which remains at constant speed (20 bar maximum). In consequence, even if the piston expander demonstrates a lower isentropic efficiency (Eq. 3), it can be used in operating conditions with higher pressure ratios leading to higher power output. The screw expander allows a wide range of rotational speeds but is limited to a

supply temperature of 130°C. Its maximum isentropic efficiency is close to the one of the piston expander.

Table 2: Range of operating conditions and performance

Parameter	Scroll (cst speed/var speed)		Piston	Screw
Supply pressure [bar]	14.5-19.8	5.7-14.7	17.7-30.2	6.4-11.0
Exhaust pressure [bar]	4.3-11.4	4.3-11.1	1.75-4.01	1.6-6.1
Pressure ratio [-]	1.8-3.37	1.4-7.4	6.2-10.6	1.9-4.17
Flow [kg.s^{-1}]	0.77-0.127	0.014-0.07	0.0273-0.104	0.0290-0.137
Supply temperature [°C]	122-133	122-133	118-153	75-130
Exhaust temperature [°C]	85-107	47-97	60-89	50-120
Highest shaft power [W]	1706	1544	2700	1292
Max. shaft. isentropic efficiency [%]	81	76	53	53
Filling factor [-]	1.033-1.12	0.63-1.53	0.205-0.62	0.89-5.42
Rotational speed [RPM]	3000	1137-7920	1000-4000	500-12450
Maximum torque [N.m]	4.91	4.6	16.4	3.31

4.2 EFFICIENCY

The experimental comparison is performed in terms of filling factor (*FF*) and isentropic efficiency (η_{is}) evaluated over a wide range of working conditions (Eqs. 3-4).

$$FF = \frac{\dot{V}_{meas}}{\dot{V}_{th}} \quad 3$$

$$\varepsilon_s = \frac{\dot{W}_{sh}}{\dot{m}_{wf}\left(h_{exp,su} - h_{exp,ex,is}\right)} \quad 4$$

$\dot{V}_{meas}$ is the volumetric flow rate, $\dot{V}_{th}$ is the theoretical volumetric flow rate defined at the supply of the machine (without taking recompressed mass from the clearance volume in the case of the piston machine), $\dot{W}_{sh}$ is the shaft power generated at the shaft, $\dot{m}_r$ is the

refrigerant mass flow rate, $h_{exp,su}$ is the expander supply enthalpy and $h_{exp,ex,is}$ is the expander exhaust isentropic enthalpy. The shaft power of the scroll machines is evaluated trough the asynchronous motor efficiency curve.

4.2.1 Isentropic efficiency

The experimental isentropic efficiency calculated for the four machines in function of the pressure ratio is depicted in Figure 8. Only a small range of pressure ratio is achievable for the scroll expander because of its constant spindle speed and experimental limitations on the test rig. The piston expander is able to work on a much larger range and with pressure ratios up to 10.6. The trend is the same for each machine: at low pressure ratio, the efficiency is rather low mainly because of over-expansion losses and at high pressure, a decrease is observed because of under-expansion phenomenon.

Because of the test rig limitations (low maximum refrigerant flow rate and high pressure drops in the pipes), the optimum working conditions are not reached for each expander. As it is presented in Section 5, it is proposed to use calibrated semi-empirical models to evaluate the optimum efficiency versus the pressure ratio to get a comparison insensitive to test-rig limitations.

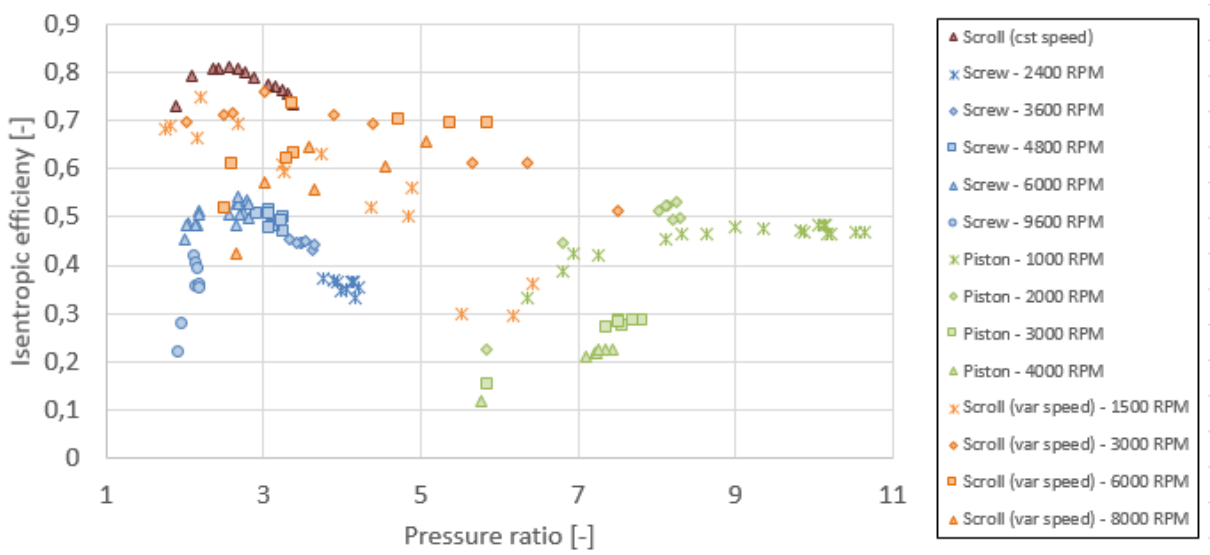

Figure 8: Isentropic efficiency versus pressure ratio

4.2.2 Filling factor

The filling factors measured for each expander are plotted versus the pressure ratio in Figure 9. The constant speed scroll filling factor is rather constant with values between 1.033 and 1.12. For the piston expander, the filling factor decreases when increasing the rotational speed and when decreasing the pressure ratio mainly because of leakages. The screw filling factor is very dependent of the rotational speed and becomes lower than one for values

higher than 10 000 RPM. This is explained by a decrease in the density of the working fluid because of the supply pressure drop before expansion.

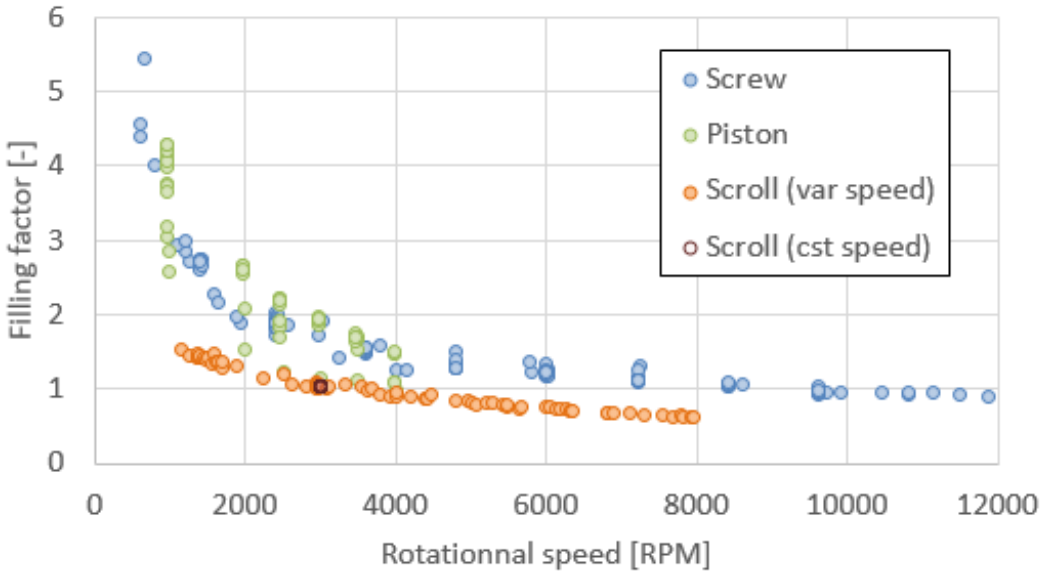

Figure 9: Filling factor versus shaft speed

5 SEMI EMPIRICAL MODEL

5.1 NOTION OF SEMI-EMPIRICAL MODELLING

Components in a thermal system can be simulated following various modelling approaches which could be classified in three groups: black-box (empirical) models, grey-box (semi-empirical) models and white-box (deterministic) models. Black-box models are referring to empirical modelling methods which do not describe the physics of the processes. In the case of an expander, for example, such models would characterize the machine performance through its isentropic and volumetric efficiencies by means of constant empirical values or polynomial regressions. Although fast to implement, to calibrate and to simulate, black-box models do not ensure reliable predictions in extrapolated conditions (Dickes et al., 2017). On the other hand, white-box models implement equations describing all the physical and the chemical phenomena in the system. Although more accurate, deterministic models are often computational intensive and, consequently, too slow for system-level simulations. Examples of deterministic models for volumetric expanders can be found in (Bell, 2011; Legros et al., 2013). Semi-empirical models are a compromise between the two aforementioned methods. They rely on a limited number of physically meaningful equations which describe the most influent phenomena in the system. They offer a good trade-off between simulation speed, calibration efforts, modelling accuracy and extrapolation capabilities. Semi-empirical models have extensively been used for the sizing and the modelling of heat exchangers,

compressors, expanders and pumps (Lemort, 2008; Quoilin, 2011; Lemort et al., 2013; Declaye, 2015; Dumont et al., 2015; Quoilin et al., 2015).

5.2 SEMI-EMPIRICAL MODEL FOR VOLUMETRIC EXPANDERS.

In this work, the semi-empirical model investigated to simulate volumetric expanders is an extended version of the model proposed by Lemort et al. (2013). One advantage of this approach is its common framework to simulate different types of technologies (scroll, screw, piston, vane…) (Lemort et al., 2013). Besides of under- and over-expansion losses (due to the fixed built-in volumetric ratio of the machine), the model can account for pressure drops and heat transfers at the inlet and outlet ports of the machine, internal leakages, mechanical losses, heat losses to the environment and recompression phenomena. Depending on the case study, the level of details of the model may be adjusted by adding or removing some parameters. As depicted in Figure 10, the expansion process of the fluid is divided into successive steps i.e. a supply pressure drop (su ➔ su_1), a supply heat transfer (su1 ➔su2), a two-stage expansion (su_2 ➔ ex_2), an exhaust heat transfer (ex_3 ➔ ex_2), an exhaust pressure drop (ex_2 ➔ ex_1), an internal leakages flow (su_2 ➔ ex_1 in black) and a recompression flow (ex_1➔su_2 in green). The supply and exhaust pressure drops are modelled as an isentropic flow through a converging nozzles, whose diameters d_{su} and d_{ex} respectively, are parameters to be identified. The three heat transfer (supply, exhaust and ambient) are characterized with nominal heat transfer coefficients i.e. $AU_{su,nom}$, $AU_{ex,nom}$ *and* AU_{amb}. Leakages are lumped into one parameter as an isentropic flow through a simply convergent nozzle whose diameter, d_{leak}, is another parameter to identify. Mechanical losses are computed with a constant term (α) and a loss proportional to the shaft speed (by means of a losses torque c_{loss}). Finally, in the case of piston expanders, the recompression losses due to the fluid trapped inside the clearance volume (V_0) is modelled by means of two-stage compression as proposed by (Oudkerk, 2016). For further information regarding the governing equations of this model, refer to (Lemort, 2008).

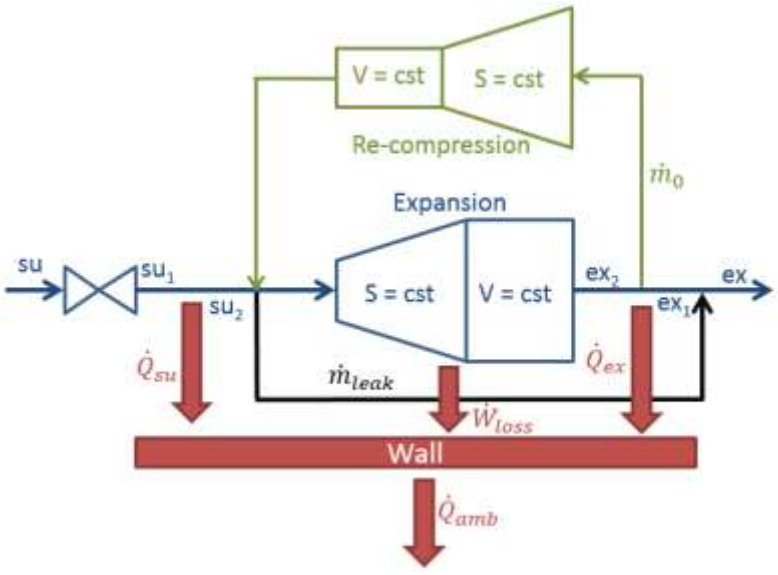

Figure 10: Schematic representation of the overall expander model (the green part – re-compression- is only used in the case of the piston expander).

Ultimately, the modelling of most volumetric expanders can be summarized by the proper identification of 7 parameters (if neglecting outlet pressure drop). Based on these parameters and five independent inputs (the machine rotational speed, the fluid inlet and outlet pressures, the fluid supply enthalpy and the ambient temperature), the model computes the fluid outlet enthalpy, the shaft power and the fluid mass flow rate (as summarized in Table 3). It should be noted that sometimes the volume ratio is not known is therefore also becomes a calibration parameter. The parameters calibration can be performed using experimental measurements or manufacturer data, as well as simulation results from deterministic models. To this end, an optimization algorithm is used to calibrate the parameters *x* so as to minimize a global error residual *f* as given in Eq. 4. This equation is arbitrary (some weights are introduced for the three terms sometimes (Ziviani et al., 2016).

$$\min_x f = \sqrt{\sum_i \left(\left(\frac{\dot{m}_{meas,i} - \dot{m}_{pred,i}}{\dot{m}_{meas,i}} \right)^2 + \left(\frac{T_{meas,i} - T_{pred,i}}{\max(T_{meas}) - \min(T_{meas})} \right)^2 + \left(\frac{\dot{W}_{sh,meas,i} - \dot{W}_{sh,pred,i}}{\dot{W}_{sh,meas,i}} \right)^2 \right)} \quad 5$$

Table 3: Inputs, calibration parameters and outputs of the semi-empirical model

Inputs	Calibration parameters	Nom.	Outputs
Built-in volume ratio	Supply nozzle equivalent diameter	d_{su}	Shaft power [W]
Swept volume	Supply heat transfer coefficient	AU_{su}	Mass flow rate [kg/s]
Inlet temperature	Exhaust heat transfer coefficient	AU_{ex}	Outlet temperature [°C]
Inlet pressure	Ambient heat transfer coefficient	AU_{amb}	
Outlet pressure	Equivalent leakage area	A_{leak}	
Rotational speed	Proportional mechanical losses	C_{loss}	
Ambient temperature	Constant mechanical losses	α	
Clearance volume			

5.3 EXTRAPOLATION

In practice, the reference database used for the parameters calibration (e.g. the measurements gathered on a test rig) does not necessarily cover the entire range of conditions onto which the model will be evaluated. For example, practical limitations of a test-rig may not allow to experimentally investigate the highest expander rotational speeds or the highest cycle pressure ratios. Therefore, the capability of the semi-empirical model to behave well in extrapolated conditions (i.e. in conditions out of its calibration domain) must be assessed to ensure reliable simulation predictions. This section is dedicated to this topic and describes a methodology to investigate the extrapolability of the expander semi-

empirical model. The following analysis is performed in Matlab and the expander model can be downloaded in the open-access ORCmKit library (Dickes et al., 2016).

Such a work has been done previously for compressors in 2015 (Cheung et al., 2015) but the research is very limited for the case of expanders. In a previous paper, some authors investigated the extrapolation capability of various modelling approaches for the off-design simulation of ORC systems (Dickes et al., 2017). This analysis was performed for different system components, including a scroll expander and the semi-empirical model for volumetric machines investigated here. The extrapolability of the model was assessed by means of a cross-validation method in which the points used for the model evaluation (i.e. the test set) were defined outside of the training set (i.e. the reference points used for the model calibration). By means of a method extensively described in (Dickes et al., 2017), the reference database was first plotted as a point cloud in function of the pressure ratio and the expander speed and then divided into two subgroups of equal size: an internal training dataset (used to calibrate the models) and an external testing dataset (used to cross-validate the models outside of the calibration domain). The results showed that the semi-empirical model is much more robust in extrapolation than polynomial regressions or constant-parameter models. The Mean Absolute Percent Error in extrapolation was equal to 5.52 for the expander power prediction and 1.6 for the mass flow rate (Fig. 2).

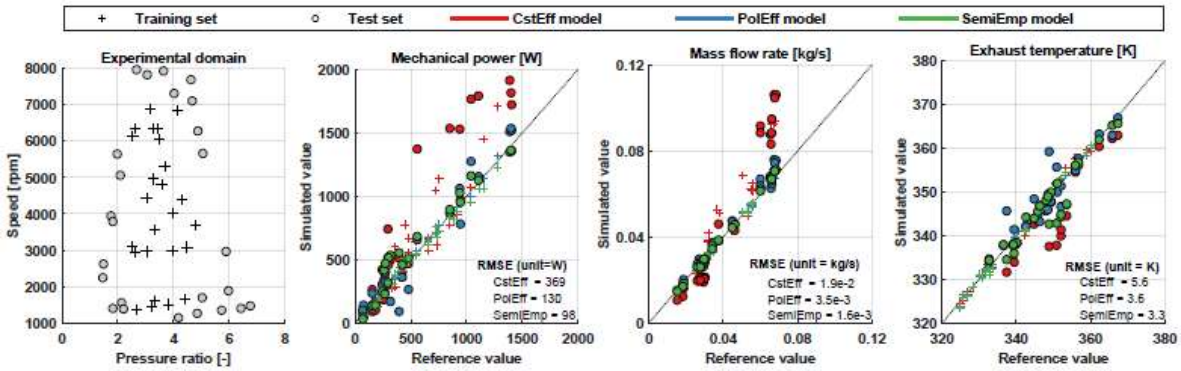

Fig. 2: Investigation of the extrapolation capability of various modelling approaches for the off-design simulation of ORC systems (Dickes et al., 2016). RMSE is the Root Mean Square Error.

An issue with this approach is that it does not investigate the extrapolation conditions as generally met in practice. As presented here above, the method proposed in Dickes et al., 2017 uses as training set the points located in the “middle” of the database and assess the extrapolation performance of the model with the outermost points. In practice, however, a common problem with the experimental datasets is the absence of high rotational speeds and pressure ratios measurements while low values for these two parameters are easily obtainable. Therefore, in this work, it is proposed to study the extrapolation performance of the expander semi-empirical model by using points with low pressure ratios and shaft speed as the training set and the rest of the reference database as test set.

To perform this work, an experimental database gathered on a 2 kWe ORC system is used as case study (see (Dickes et al., 2014) for further details on the test rig). The ORC unit includes a variable speed hermetic scroll expander and employs R245fa as working fluid. The expander swept volume is 12.74 cm^3 and its volume ratio is 2.19. The methodology employed to characterize the extrapolation performance is as follows:

1. First, the experimental points in the database are sorted in function of their pressure ratio (resp. rotational speed).
2. Secondly, the selection of a training set is established with the points of the dataset are corresponding to a fraction of the pressure ratio (or rotational speed) range. It is accounted that the lowest pressure ratio (resp. rotational speed) corresponds to 0% and the highest to 100%. The training set is always composed of a minimum of 9 points to insure the acceptability of the calibration algorithm.
3. Then, the semi-empirical model is calibrated using points from the training set only (i.e. the points with a pressure ratio, or rotational speeds, lower than the specified threshold). The initial guess value for the parameters calibration is set equal to the optimal calibration with the full set of data.
4. Finally, the semi-empirical model is evaluated on the entire database and the Mean Average Error is computed for each of the three model outputs y_i (i.e. the mechanical power, the fluid mass flow rate and the exhaust temperature) with Eq. 5:

$$MAE = \frac{\sum_{i=1}^{N} |\bar{y}_i - y_i|}{N} \qquad 6$$

where *N* is the total number of points, $\bar{y}_i$ is the reference output and y_i is the model output. The MAE is meaningful when we compare it to the actual value of the outputs. For this purpose, the mean value of the shaft power and the mass flow rate are 597 W and 0.042 kg/s respectively. The outlet temperature varies between 49°C and 95°C. The optimization algorithm used is the Patternsearch in Matlab. The comparison of different algorithm is out of the scope of this study.

The methodology described in the previous section is first applied for 5 different calibration ranges (20%, 40%, 60%, 80% and 100%) in terms of pressure ratio. The evolution of the MAEs committed on the exhaust temperature, the shaft power and the mass flow rate predictions is depicted in Figure 11. The analysis is performed using three different set of guess values for the parameters calibration (i.e. xguess = xopt, xguess = 300%.xopt and xguess = 600%.xopt). From this graph, it can be seen that the mean average errors are very large only when the initial guesses are poorly chosen for the parameters calibration (i.e. xguess = 600%.xopt) and when the calibration range covers solely over-expanded operating conditions (i.e. the maximum isentropic efficiency is not reached). Except for this particular

situation, the extrapolation capability of the semi-empirical model appears to be very good and the MAEs are kept low even with narrow calibration ranges.

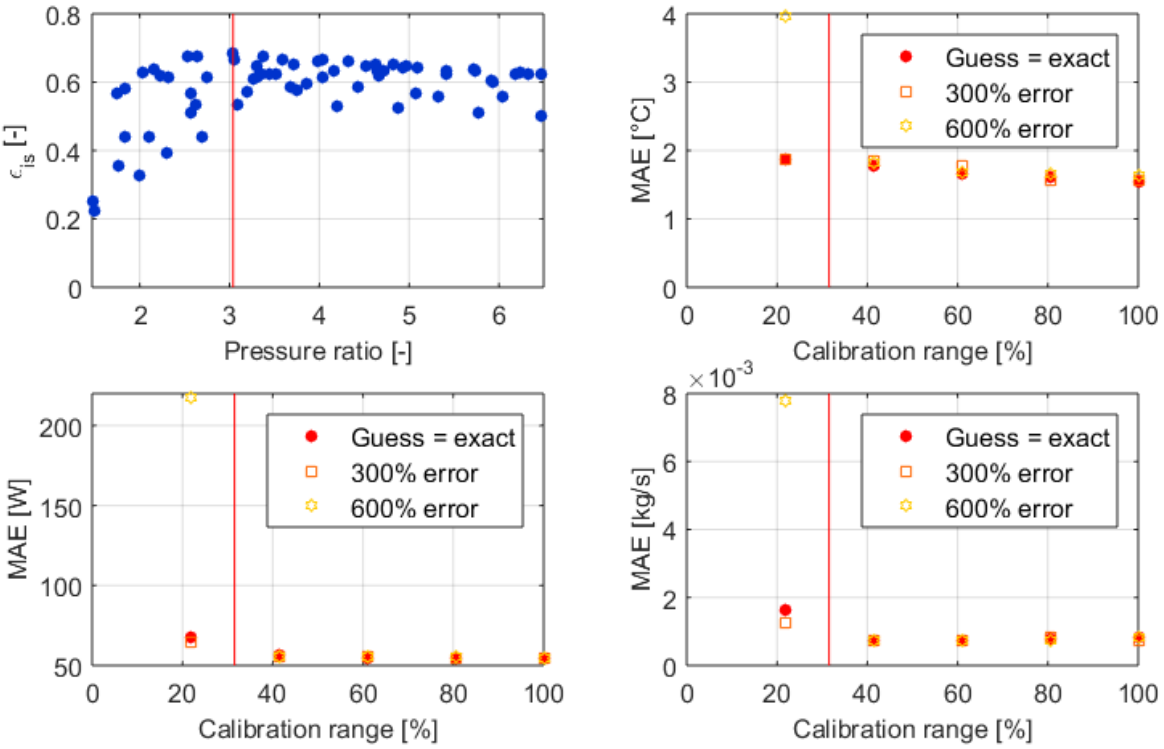

Figure 11 : Isentropic efficiency of the expander dataset as a function of the pressure ratio (a). Mean average error in extrapolation in function of the calibration range for the exhaust temperature (b), shaft power (a) and mass flow rate (d).

Figure 12 depicts the evolution of the calibrated parameters in function of the pressure ratio calibration range (in the case of well-posed guesses, i.e. $x_{guess} = x_{opt}$). These results correspond to the red points in Figure 11. It can be seen that the parameters converge to

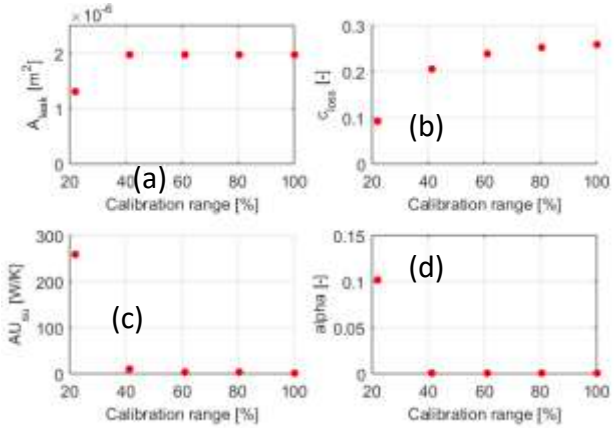

Figure 12 : Calibrated parameters with different calibration ranges. (a) Leakage area, (b) proportional mechanical losses, (c) supply heat transfer coefficient and (d) constant mechanical losses.

Several local minima exists due to the large number of calibration parameters and sometimes, a combination of "wrong" parameters can lead to decent accuracy of the model outputs (there is not a global minimum for (1) but instead several local minima). In Figure 12, it is shown that the MAEs are low (i.e. the model predicts well in extrapolation) even with 22% of the calibration range of pressure ratio. However, the parameters can have very different values from the optimal ones (100% range).

The same analysis is then applied for 5 different rotational speed calibration ranges (20%, 40%, 60%, 80% and 100%). The evolution of the MAE evaluated on the three model outputs is shown in Figure 13. Like before, the study is performed with three different guess values for performing the parameters calibration. The observations are similar for the rotational speed (Fig. 5) and for the pressure ratio (Fig. 3)): A too large error on the initial guess and a too small calibration range (<27%) leads to large MAE. But contrarily to the pressure ratio results, it appears that sometimes the MAE of a given output is smaller with a guess presenting a higher error. This is explained by the fact the only the sum of the square of the errors are minimized (1).

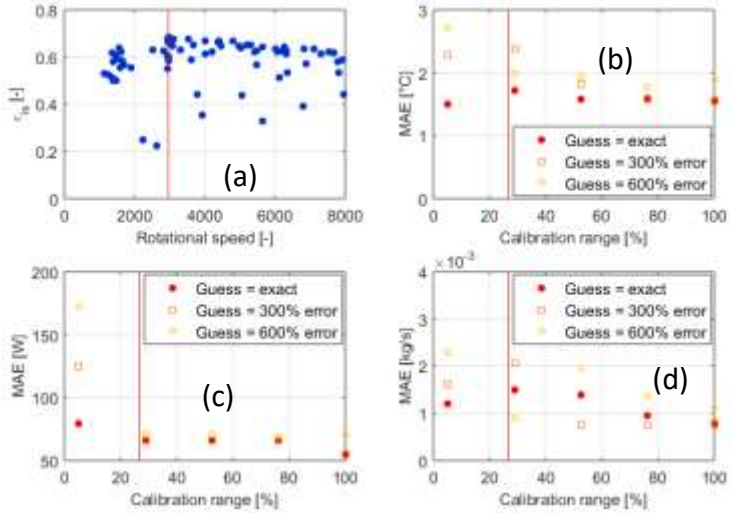

Figure 13 : Isentropic efficiency of the expander dataset as a function of the rotational speed (a). Mean average error in extrapolation in function of the calibration range for the exhaust temperature (b), shaft power (a) and mass flow rate (d).

Based on the results in section 3, it is possible to draw several guidelines to properly calibrate and use the semi-empirical model for volumetric expanders:

1. When calibrating the model with experimental measurements, it is recommended to experimentally explore the widest range of conditions to better assess the machine performance and to limit the extrapolation of the model in unseen conditions. At minimum, the training set should include over-expanded and under-expanded operating conditions so as to contain the machine maximum isentropic efficiency.

2. The selection of an accurate initial guess for the parameters calibration is mandatory if the training set misses points with high pressure ratios. If the training set includes points with both over-expanded and under-expander conditions, this constraint may be relaxed (i.e. a good estimate of the parameters values is not crucial).

3. Despite of the longer computational time, the parameters calibration should be performed with a derivative-free optimization algorithm in order to be less sensible to the parameters initial guesses and the presence of local minima in the residual function (1).

The best way to get reliable initial guesses for the parameters calibration is probably to perform a review of literature with experiments using the same technology of volumetric machine and fluid. However it is possible to approximate some parameters easily (neglecting supply and exhaust heat transfers, supply and exhaust pressure drops):

- The ambient heat transfer coefficient can be evaluated using an energy balance on the volumetric machine.

- The equivalent leakage area can be deduced from a flow conservation: the measured volumetric flow rate equals the leakage volumetric flow rate plus the theoretical volumetric flow of the machine.

- The mechanical loss coefficient(s) can be approximated assuming a given percentage of the isentropic power (e.g. 15%).

A wide range of other cases should be tested following this methodology to generalize the results. The results could indeed be influenced by:

- The model itself: the semi-empirical model of an expander can presents various level of details. Some take into account (or not), an exhaust pressure drop, different laws of mechanical losses… and fifer in their modelling (Ayachi et al., 2016; Ziviani et al., 2016)
- The considered volumetric machine: other power ranges, technologies, fluids and losses trends.
- The form of the objective function (1).

5.4 CALIBRATION OF THE MODEL BASED ON THE EXPERIMENTAL CAMPAIGNS.

Now that the extrapolability has been validated within a given range, the models can be calibrated following section 5.2. A comparison of the calibrated parameters is drawn in Table 4. The screw expander presents a higher diameter of equivalent converging nozzle, meaning a lower pressure drop in the same conditions. Ambient losses presents the same order of magnitude for the four expanders (except for the variable speed scroll) while the mechanical losses are significantly higher in the piston machine (Table 4).

Table 4: Calibrated parameters of the semi empirical model calibrated based on measurements

Parameter	Scroll (Copeland/Valeo)		Piston	Screw
d_{su} [mm]	5.9	3.2	3	10
AU_{su} [W/K]	35.1	35.1	20	36
AU_{ex} [W/K]	23.9	23.8	18	34
AU_{amb}[W/K]	5.78	1	5.5	4
$\dot{m}_{nom}$ [kg.s^{-1}]	0.106	0.068	0.107	0.127
A_{leak} [m^2]	1.02e-6+1. 28e-8*$P_{exp,su\ [bar]}$	1.6e-6	1.1e-6	2.6^{e}-6
τ [N.m]	0.88	0.01	(see Oudkerk, 2016)	0.8
V_0 [cm^3]	-		6.5	

The quality of prediction of semi-empirical models is evaluated through the coefficient of determination (Equation 7). $x_{meas,i}$, is the measured variable, $x_{pred,i}$ is the outputs calculated with the semi-empirical model $\overline{x_{meas}}$ the mean value of the measured variable.

$$R^2 = 1 - \frac{\sum\left(x_{meas,i} - x_{pred,i}\right)^2}{\sum\left(x_{meas,i} - \overline{x_{meas}}\right)^2} \qquad 7$$

Table 5 presents the determination coefficient for output prediction of each semi-empirical model. The values observed for the determination coefficient show a good agreement between model and measurements. Figure 18 to Figure 23 (appendices) present a comparison between model prediction and measurements.

Table 5: Determination coefficient for the output prediction of each semi-empirical model

R^2 [%]	Scroll (Copeland/Valeo)		Piston	Screw
Shaft power [W]	98	93	90	95
Mass flow [$g.s^{-1}$]	98	98	96	97
Exhaust temperature [°C]	87	94	94	98

5.5 OPTIMUM EFFICIENCY PREDICTION

In this section, the semi-empirical models are used to extrapolate the performance of each expander in optimum conditions (Figure 14). For each simulation a constant 5K overheating and an ambient temperature of 25°C are imposed. For each curve, the constant shaft speed is adjusted to get the maximum of isentropic efficiency for each supply pressure. A wide range of pressure ratios is computed by adjusting the exhaust pressure. Isentropic efficiencies are evaluated for typical operating supply pressures in Figure 14. In this figure, the efficiency observed in the case of high supply pressure is almost always higher because in this case the flow is higher, leading to higher power and so to lower influence of constant losses. Here, the constant-speed scroll expander is disadvantaged because of its constant rotational speed but still presents the highest isentropic efficiency. Compared to section 4, conclusions are essentially the same except that the limitations of the test-rig do not influence the curves anymore. The screw expander efficiency simulated in optimal conditions is significantly higher than the one measured on the test-rig. During experimentation, the isentropic efficiency is dropping sharply when increasing the pressure ratio because the mass flow delivered by the pump is lower due to internal leakages in the pump (Figure 8). Furthermore, the model predicts a decrease of the efficiency of the piston expander with high pressure ratio (mainly because of mechanical losses) which was not observable during the tests because of pressure drops in the pipes of the test-rig (at the inlet and the outlet of the expander).

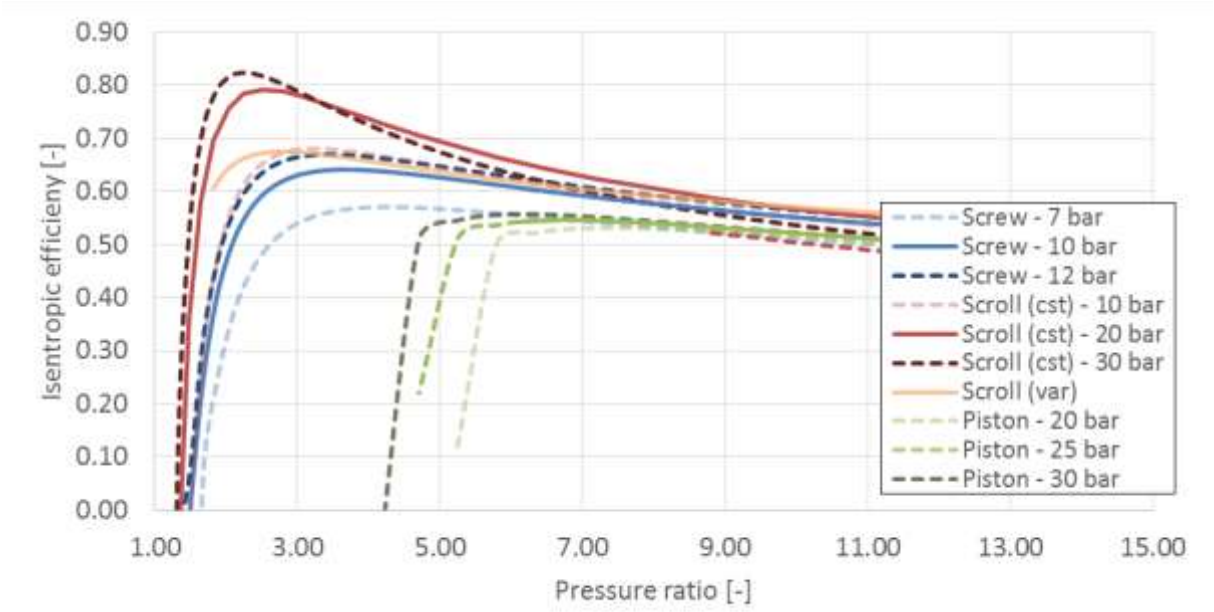

Figure 14: Predicted isentropic efficiency with semi-empirical models.

5.6 OPERATING MAP

A former investigation (Quoilin et al., 2012) proposed operating map to select a fluid and an expander technology. These maps were drawn based on three practical considerations (Figure 24):

- The upper left curve is defined by the limitation regarding under-expansion losses by fixing the minimum expansion isentropic efficiency at 0.9.
- The downright curve is defined by the maximum flow rate that can be absorbed. The maximum volume coefficient (Quoilin et al., 2012) is fixed at 0.5 (following compressor data).
- Finally, the critical temperature of the fluid defines the upper line.

A similar approach is conducted to derive operating maps for each expander tested with refrigerant R245fa (Figure 15). The calibrated models (section 3.3) allows to define operating maps depending on the supply temperature of the fluid at the inlet of the expander (5K overheating) and on the condensation temperature. Contrarily to the work done by Quoilin et al. (2012), all the losses (pressure drops, internal leakages, mechanical losses, under and over-expansion, heat exchanges) are taken into account to evaluate zones where the isentropic efficiency is above 10% (Figure 15). For example, if a 30°C condensation temperature is considered, it means that the variable-speed scroll needs a temperature at the supply of the expander at least of 45°C to get an expander isentropic efficiency of 10%. The screw and constant-speed scroll would require 55°C at the inlet and the piston 87°C.

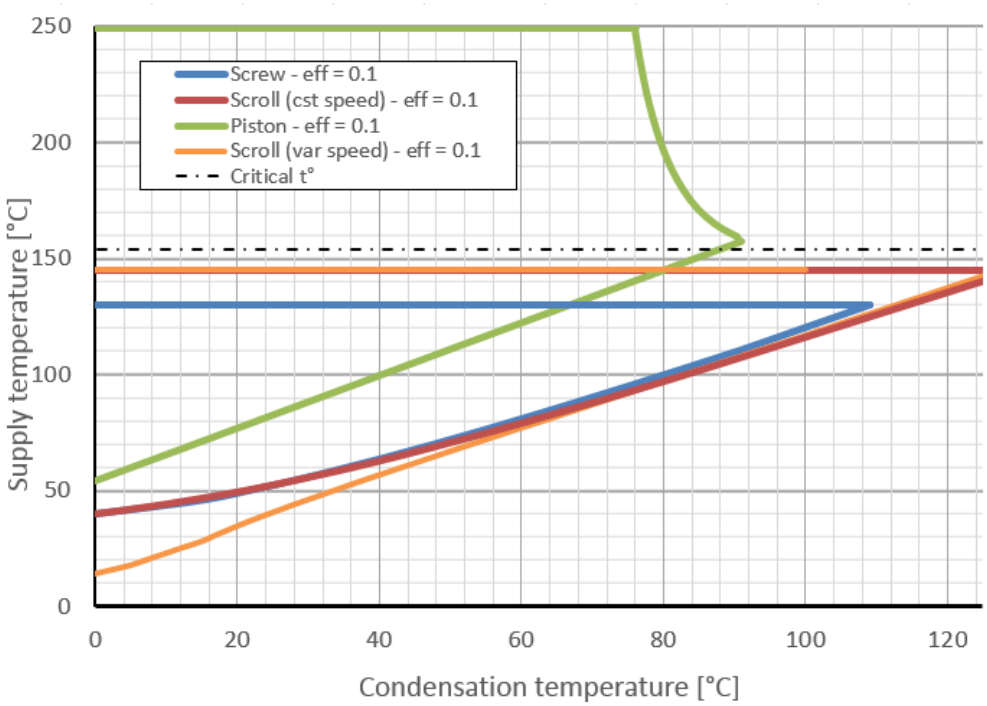

Figure 15 : Operating map for the different prototypes tested with fluid R245fa evaluated for isentropic efficiencies equal to 10%.

This delimitates two curves resulting of a combination of the aforementioned losses (but mainly under- and over-expansion losses). Also, the horizontal line (high inlet temperature) is fixed by the temperature limitation of the expander (Figure 15). The black dotted horizontal line represents the critical temperature of the refrigerant. The hypothesis used to draw this map are, an optimal rotational speed and a 5 K constant over-heating. The over-heating is changed only if the critical temperature is reached. In this case, the pressure is imposed as the one corresponding to the critical temperature only for the piston expander. This operating map has been drawn for several typical isentropic efficiencies for each expander on a four-quadrant graph (Figure 16).

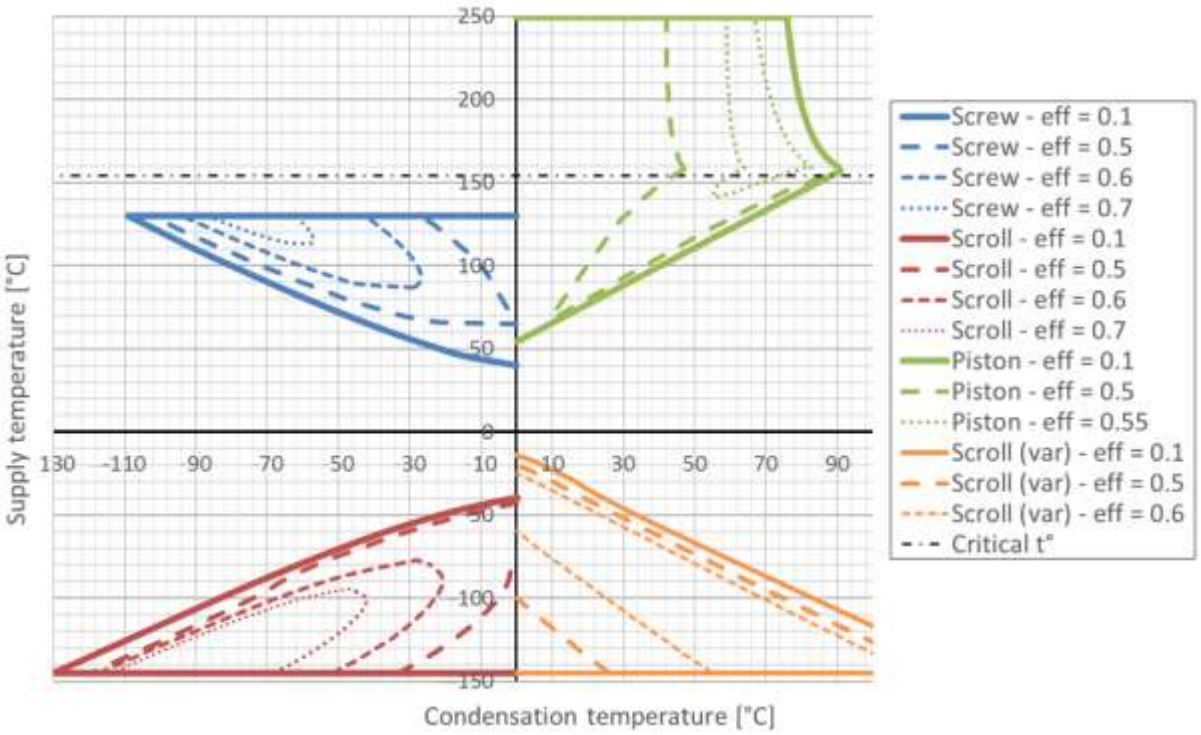

Figure 16: Operating map for the different prototypes tested with fluid R245fa evaluated for several isentropic efficiencies.

The scroll and screw expanders' maps are rather close. Whatever the isentropic efficiency considered, the screw map is slightly narrower because of its inlet temperature limitation and, more generally, its lower isentropic efficiency. The piston shows less possibility to work at low inlet temperature as expected but shows the widest running area because of the high allowed temperature and its high volume ratio. It is obvious that fluids such as water/ethanol mixture or ethanol would extend this area for the piston expander because of higher critical temperature.

6 CONCLUSION

Three different technologies of volumetric expanders, namely scroll, screw and piston machines, are tested experimentally in a small-scale ORC test rig using R245fa as working fluid. Experimental measurements over a wide range of operating conditions are used to assess the performance in terms of filling factor and isentropic efficiency. The data set is used afterwards to calibrate semi-empirical models in order to extrapolate the expander performance. This allows comparing efficiencies in optimal conditions not reachable on the test-rig and to draw an operating map. The scroll expander shows the largest isentropic efficiency (81% against 53% for the piston and the screw expanders).

It is very important to remind that these results are done in the case of small-capacity expanders (< 5kW) with different maturities of development for each of them and with a single fluid (R245fa). Conclusions may vary in the case of other expander power ranges.

Besides the limitations on the power output range, other technical limitations must be taken into consideration such as maximal allowable operating pressure and temperature, ability to operate without lubricating oil, and maximal achievable built-in volume ratio, costs, compactness.

The piston expander can be run with much higher pressure and temperature and it therefore allows higher shaft power production to be reached. The piston expander therefore achieves higher pressure ratios (even if two scroll expanders could be used in series to tackle this issue). In this case, the flexibility of the constant-speed scroll is limited since its speed is constant but allows the presence of a liquid phase. For the piston, the flexibility is also limited but for the opposite reasons (variable speed but limited wet expansion). Furthermore, the compactness is the best for the screw expander and slightly lower for the piston and scroll expander. In conclusion, the selection of a volumetric expander depends on the requirements of the dedicated application: Is the efficiency, the working conditions, the flexibility or the compactness that is the most important? A comparison in terms of compactness, efficiency, working conditions (extreme conditions) and flexibility (adaptability to working conditions like wet expansion, and wide range of rotational speeds) is performed in Table 6. An economic comparison is not performed since it essentially depends on the maturity of the machine. A mass production could decrease the price of a prototype to a level comparable with cheapest technologies…

Table 6: Comparison of expander advantages and disadvantages

Expander	Power	High Pressure and temperature	Wet expansion	compactness	flexibility	Efficiency
Piston	<<	+	+	+	+	+
Screw	>>	-	+++	++	+++	+
Scroll	<<	-	+++	+	++	++

As a consequence, the choice of the expander technology has to be conducted in parallel with the selection of the ORC architecture, range of power, operating conditions and working fluid of the selected application.

In conclusion, because the choice of the reversible volumetric machine has a considerable influence on the performance of a reversible HP/ORC unit, it was necessary to define some general guidelines in order to select the optimal technology depending on the characteristics of a given study-case. These considerations will be useful for the selection of the volumetric machine in Chapter three (Sizing) and Chapter four (experimentation).

An interesting perspective is the extrapolation of the semi-empirical model to different size/power of volumetric machine. Lemort (2008) proposes some laws to scale the semi-empirical parameters but these remain not validated. This emphasizes the necessity to perform more experimental studies on volumetric expanders with a wide range of size and power.

7 APPENDICES

Table 7**:** characteristics of piston, scroll and screw expanders

Parameter	**Scroll**	**Piston**	**Screw**
Displacement [l/s]	0.76-?	[1.25:75]	[25-1100]
Cm3	1-283		
Power [kW]	[0.5-45] (Emerson, 2015)	-	[20-1000]
Rotational speed [RPM]	10000 (Sanden, 2015)	-	21000 (Ng et al., 1990)
Built-in volume ratio	[1.5-4.2] (Kane, 2009)	[6-15]	[?-8] (Yanagisawa, 2012)
Maximum pressure [bar]	-	70 (Seher, 2012)	
Max. temperature [°C]	215 (Lemort et al., 2006)	380 (Seher, 2012)	
Pressure ratio	15 (Lemort, 2006)	-	
Two-phase flow	yes	no	yes
Isentropic efficiency [%]	87 (Harada, 2010)	70bof (Glavatskaya, 2012)	84 (Ng et al., 1990)
Number of rotating parts	low		

Table 8: Sensors characteristics

Sensor	Type	Range	Accuracy
Expander supply pressure - P1	Keller PA-21Y	[0-40] bar	0.4 bar
Expander exhaust pressure - P2	Keller PA-21Y	[0-20] bar	0.2 bar
Mass flow rate - M	Krohne optimass 7000	[10-140] $g.s^{-1}$	0.2 %
Torque/rotational speed meter – τ	ETH messtechnic DRFL II	[0:20] $N.m^{-1}$	0.02 $N.m^{-1}$
Wattmeter – W (scroll)	Gossen A2000	[0-2000] W	0.5 %

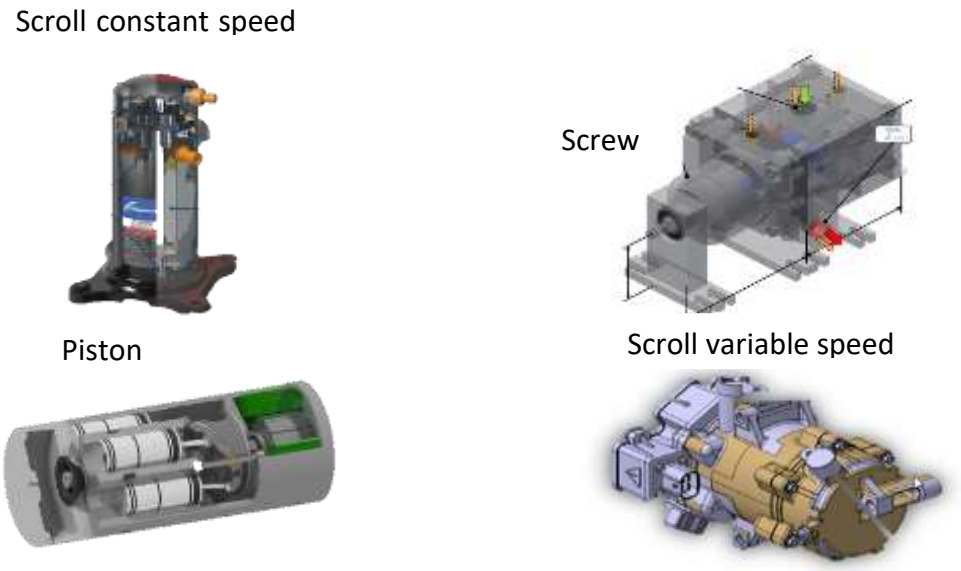

Figure 17: Schematic representation of each expander.

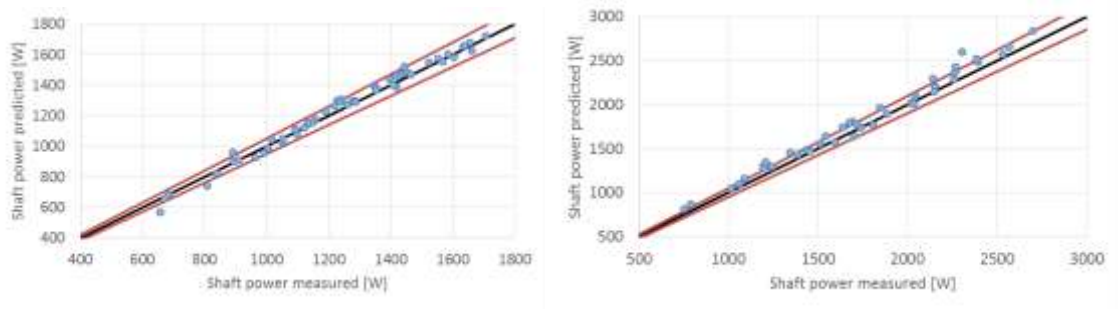

Figure 18: Comparison of the shaft power between model predictions and measurements (5% error bars). Left: Scroll expander, right – Piston expander.

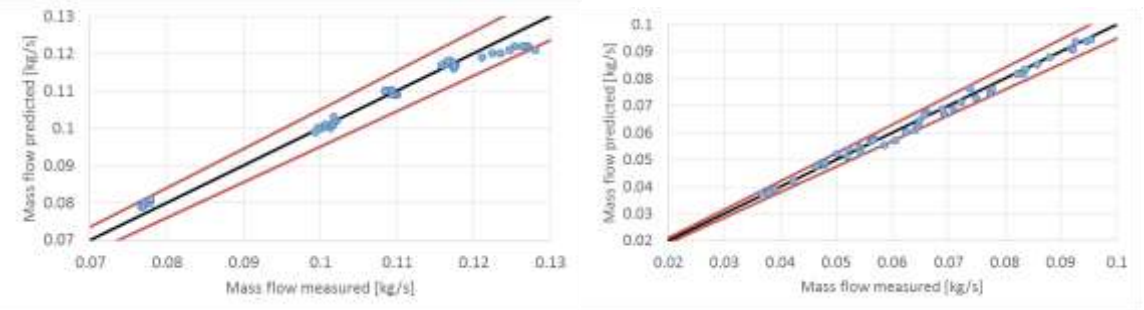

Figure 19: Comparison of the mass flow between model predictions and measurements (5% error bars). Left: Scroll expander, right – Piston expander.

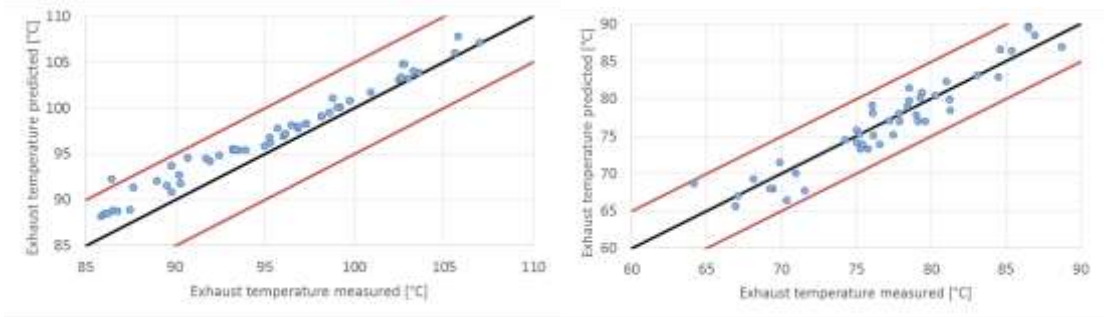

Figure 20: Comparison of the exhaust temperature between model predictions and measurements (5K error bars). Left: Scroll expander, right – Piston expander.

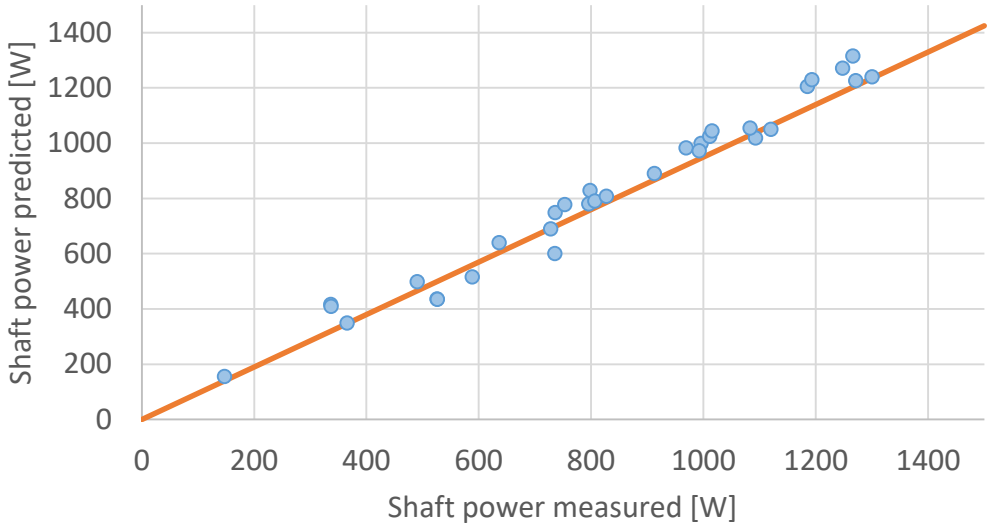

Figure 21: Comparison of the shaft power between model predictions and measurements (Screw – 5% error bars).

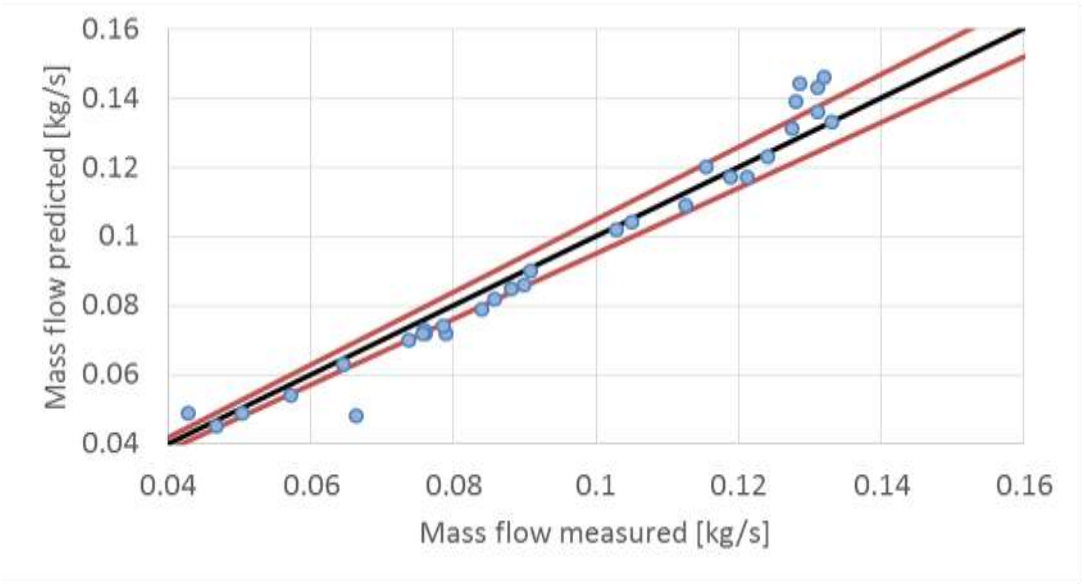

Figure 22: Comparison of the mass flow between model predictions and measurements (Screw – 5% error bars).

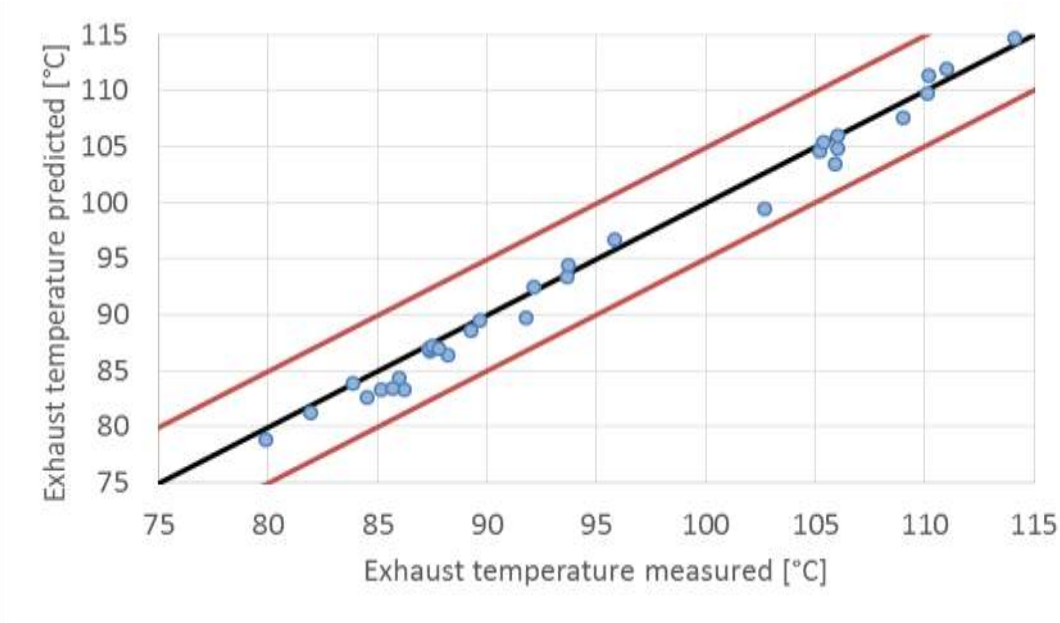

Figure 23: Comparison of the exhaust temperature between model predictions and measurements (Screw - 5K error bars).

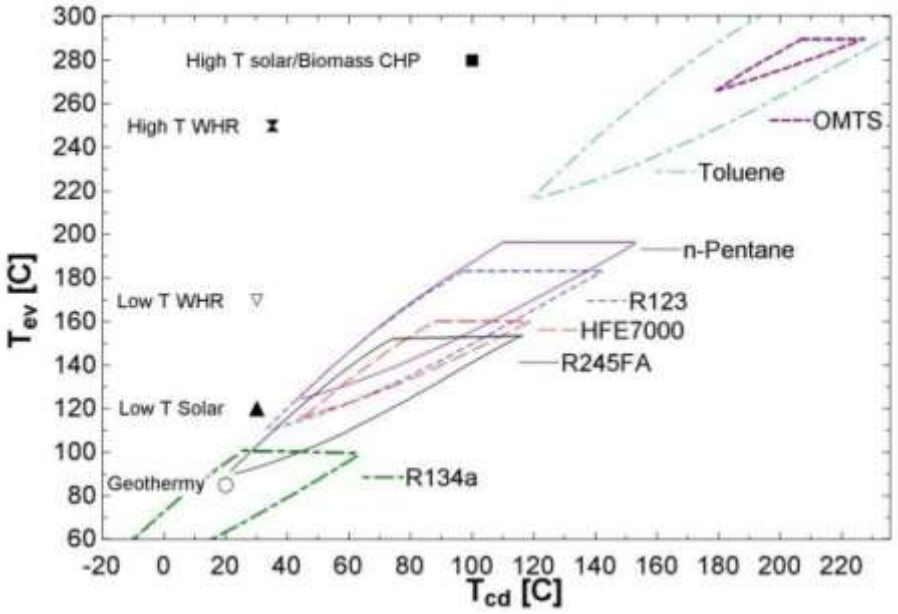

Figure 24: Scroll expander operating map (Quoilin et al., 2012).

References

- Ayachi, F., Ksayer, B., Neveu, P., Zoughaib, A., 2016. Experimental investigation and modeling of a hermetic scroll expander, Applied Energy Volume 181, Pages 256–267, http://doi.org/10.1016/j.apenergy.2016.08.030.

- Badr, O., O'Callaghan, P.W., Probert S., 1985. Multi-vane Expanders: Geometry and Vane Kinematics. Applied Energy 19, 159-182.

- Baek, J. S., Groll, E. A., Lawless, P.B., 2005. Piston-cylinder work producing expansion device in a transcritical carbon dioxide cycle. Part I: experimental investigation, International Journal of Refrigeration 28, 141–151.

- Bell, I., PhD thesis, 2011. Theoretical and Experimental Analysis of Liquid Flooded Compression in Scroll Compressors, Purdue.

- Bracco, R., Clemente, S., Micheli, D, Reini, M., 2013. Experimental tests and modelization of a domestic-scale ORC (organic Rankine cycle), Energy 58, 107-116.

- Brasz, J., Smith, I., Stosic, N., 2000.Development of a twin Screw expressor as a throttle valve replacement for water-cooled chillers, proceedings of the International Compressor Engineering Conference, Purdue.

- Brummer, A., 2012. Energy efficiency – waste heat utilization with screw expanders, Pumps, compressors and process components.

- Butrymowicz D., Crawford J., Godwin, D., Hickman, K., Keller, F., Onishi, 2005. H, IPCC/TEAP Special Report: Safeguarding the Ozone Layer and the Global Climate System, Residential and Commercial Air Conditioning and Heating.

- Cheung, H., Bach, C., 2015. Prediction of uncertainty of 10-coefficient compressor maps for extreme operating conditions, IOP Conference Series: Materials Science and Engineering, Vol.90.

- Daccord, R., Kientz, T., Mélis, J., Darmedru, A., Brisseau, N., 2013. Automotive heat recovery with piston expanders and wet fluids, proceedings of the ASME ORC 2013 conference.

- Daccord, R., Melis, J., Darmedru, A., 2017. Impact of water and oil contents in ethanol applied to ORC for exhaust heat recovery in heavy duty trucks, 4th Engine ORC Consortium Workshop November 15 - 17, Detroit, Michigan.

- Declaye, S., PhD thesis, 2015. Improving the performance of μ-ORC systems, Liège.

- Desideri, A., Van den Broek, M., Gusev, S., Lemort, V., Quoilin, V., 2014. Experimental campaign and modeling of a low capacity waste heat recovery system based on a single screw expander, proceedings of Purdue conference 2014.

- Dickes, R., Dumont, O., Declaye, S., Quoilin, S., Bell, I., Lemort, V., 2014. Experimental investigation of an ORC system for a micro-solar power plant, proceedings of the 22nd International Compressor Engineering Conference at Purdue.

- Dickes, R., Dumont, O., Daccord, R., Quoilin, S., Lemort V., 2017. Modelling of organic Rankine cycle power systems in off-design conditions: an experimentally-validated comparative study, Energy, doi: 10.1016/j.energy.2017.01.130

- Dickes, R., Ziviani, D., Van den Broack, M., De paepe, M, Quoilin, S., Lemort, V., 2016. ORCmKit: an open-source library for organic Rankine cycle modelling and analysis, ECOS 2016 - 29th international conference on Efficiency, Cost, Optimisation, Simulation and Environmental Impact of Energy Systems.

- Dumont O., Quoilin, S., Lemort, V., 2014. Experimental investigation of a Scroll unit used as a compressor and as an expander in a Heat Pump/ ORC reversible unit. Purdue conference 2014. http://docs.lib.purdue.edu/iracc/1471/

- Dumont, O., Quoilin, S., Lemort, V., 2015. Experimental investigation of a reversible heat pump/organic Rankine cycle unit designed to be coupled with a passive house to get a Net zero Energy Building, international journal of refrigeration 54, 190-203.

- Eckard, S. E., Brooks, E. D., 1973. Design of reciprocating single cylinder expanders for steam, Report prepared for U.S. Environmental Protection Agency, Office of Air Pollution Control, Alternative Automotive Power Systems Division.

- Emerson website, 2015, consulted the 3th of March2015, http://www.emersonclimate.com/en-US/products/compressors/scroll_compressors.aspx

- Endo, T., Kawajiri, S., Kojima, Y., Takahashi, K., Baba, T., Ibaraki, S., Takahashi, T., Shinohara, M., 2007. Study on Maximizing Exergy in Automotive Engines, Society of Automotive Engineers, 2007-01-0257.

- Giuffrida, A., Improving the semi-empirical modelling of a single-screw expander for small organic Rankine cycles, 2017. Applied Energy Volume 193, Pages 356–368, http://doi.org/10.1016/j.apenergy.2017.02.015.

- Glavatskaya, Y., Podevin, P., Lemort, V., Shonda, O., Descombes, G., 2012. Reciprocating Expander for an exhaust heat recovery Rankine cycle for a passenger car application, Energies, 5, 1751-1765.

- Harada, K. J., 2010. Development of a small scale scroll expander, for the degree of Master of Science in Mechanical Engineering.

- He, W., Wu, Y., Peng, Y., Zhang, Y., Ma, C., Ma, G., 2013. Influence of intake pressure on the performance of single screw expander working with compressed air. Applied Thermal Engineering 51, 662e669.

- Hsu, S., Chiang, H., Yen, C., 2014. Experimental investigation of the performance of a hermetic screw expander organic Rankine cycle, Energies 2014, 7, 6172-6185.

- Kane, M., Larrain, D., Favrat, D., Allani, Y., 2003. Small hybrid solar power system, Energy 28, 1427-1443.

- Kane, M., Cretegny, D., Favrat, D., Maquet, J., 2009. Projet HTScroll, Nouveau système de cogénération à turbine spirale haute température, Rapport final, Département fédéral de l'environnement, des transports, de l'énergie et de la communication DETEC, Office fédéral de l'énergie OFEN.

- Kreider, Handbook of Heating, 2000. Ventilation, and Air Conditioning Handbook.

- Legros, A., Guillaume, L., Lemort, V., Diny, M., Bell, I., Quoilin, S., 2013. Investigation on a scroll expander for waste heat recovery on internal combustion engines, International conference on compressors and their systems, At London.

- Lemort, V., Teodorese, I. V., Lebrun, J., 2006, Experimental study of the integration of a scroll expander into a heat recovery rankine cycle, procceedings of the 18th International Compressor Engineering Conference.

- Lemort, V., PhD thesis, 2008. Contribution to the characterization of scroll machines in compressor and expander modes, Liege.

- Lemort, V., Declaye, S, Quoilin, S., 2012. Experimental characterization of a hermetic scroll expander for use in a micro-scale Rankine cycle, P. I. Mech. Eng. A-J., Pow. 226, 126-136.

- Lemort, V., Guillaume, L., Legros, A., Declaye, S., Quoilin, S., 2013. Comparison of piston, screw and scroll expanders for small scale Rankine application, Proceedings of the 3rd International Conference on Microgeneration and Related Technologies,

- Lemort, V., Legros, A., 2016. Organic Rankine cycle (ORC) power systems technologies and applications, Positive displacement expanders for Organic Rankine Cycle systems.

- Mathias, J. A., Johnston, J. J. R., Cao, J., Priedeman, D. K., Christensen, R. N., 2009. Experimental testing of Gerotor and scroll expanders used in, and Energetic and Exergetic modeling of an organic rankine cycle, J. Energy Resour. Tech. 131, 1-9.

- Mikielewicsz, D., Mikielewicz, J., Wajs, J., 2010. Experiences from operation of different expansion devices for application in domestic micro CHP, Archives of Thermodynamics 31, 4.

- McKay, R., 1984, International test and demonstration of a 1-MW wellhead generator: helical screw expander power plant, model 76-1, final report prepared for the U.S. department of energy, JPL, Publication 84-29, DOE/ET-37116-2.

- Molinaroli, L., Joppolo, C., De Antonellis, S., A semi-empirical model for hermetic rolling piston compressors, 2017. International Journal of Refrigeration, in press, http://doi.org/10.1016/j.ijrefrig.2017.04.015

- Ng, K. C., Bong, T. Y., and Lim., T. B., 1990. A Thermodynamic model for the analysis of screw expander performance, Heat Reovery Systems & CHP, 10, 2:119-133.

- Oudkerk J, Quoilin S, Declaye S, Guillaume L, Winandy E, Lemort V, 2013. Evaluation of the Energy Performance of an Organic Rankine Cycle-Based Micro Combined Heat and Power System Involving a Hermetic Scroll Expander. ASME. J. Eng. Gas Turbines Power, 135(4):042306-042306-10. doi:10.1115/1.4023116.

- Oudkerk, J.F., Dickes, R., Dumont, O., Lemort, V., 2015. Experimental performance of a piston expander in small-scale organic Rankine cycle, Proceedings of the International Conference on Compressors and their Systems.

- Oudkerk, J.F, PhD thesis, 2016. Contribution to the Characterization of Piston Expanders for Their Use in Small-scale Power Production Systems.

- Qiu, G., Liu, H., Riffat, S., 2011. Expanders for micro-CHP systems with organic Rankine cycle, Applied Thermal Engineering, 31, 3301-3307.

- Quoilin, S., PhD thesis, 2011. Sustainable energy conversion through the use of organic Rankine cycles for waste heat recovery and solar applications, (Liege).

- Quoilin S., S. Declaye, A. Legros, L. Guillaume, V. Lemort. 2012. Working Fluid Selection and Operating Maps for Organic Rankine Cycle Expansion Machines. Proceedings of the 21st International Compressor Engineering Conference at Purdue, West Lafayatte, USA.

- Quoilin, S., Dumont, O., Harley Hansen, K., Lemort, V., 2015. Design, Modeling, and Performance Optimization of a Reversible Heat Pump/Organic Rankine Cycle System for Domestic Application, J. Eng. Gas Turbines Power 138(1), 011701.

- Sanden website, 2015. http://www.sanden.com/scrollcompressors.html, consulted the 16th of april 2015.

- Seher D., Lengenfelder, T., Gerhardt, J., Eisenmenger, N., Hackner, M., Krinn, I., 2012. Waste Heat Recovery for Commercial Vehicles with a Rankine Process, Proceeding of the 21st Aachen Colloquium Automobile and Engine Technology 2012.

- Wang, W., Wu, Y., Maa, C., Liu, L., Yu, J., 2011. Preliminary experimental study of single screw expander prototype, Applied Thermal Engineering 31, 3684-3688.

- Wang, J., Zhanga, X., Zhanga, Y., Zhanga, Y., Wanga, W., 2014. Experimental study of single screw expander used in low medium temperature geothermal power system, Energy Procedia 61, 854 – 857, 6th International Conference on Applied Energy – ICAE2014.

- Wikipedia, 2016. https://en.wikipedia.org/wiki/Roots-type_supercharger, consulted the 19/07/2016.

- Xia, G-D., Zhang Y., Wu, Y., Ma, Y., Ji, W., Liu, S., Guo, H., 2015. Experimental study on the performance of single-screw expander with different inlet vapor dryness, Applied Thermal Engineering Volume 87, 5 August 2015, Pages 34–40.

- Yanagisawa, T., Fukuta, M., Ogi, Y., Hikichi, T., 2001. Performance of an oil-free scroll-type air expander, Proceedings of the ImechE Conference on compressors and their systems: 167-174.

- Zanelli, R., Favrat, D., 1994. Experimental investigation of a hermetic scroll expander-generator, Proceedings of the 12th Internnational Compressor Engineering Conference at Purdue: 459-464.

- Zhang, Y., Wu, Y., Xia, G., Ma, C., Ji, W., Liu, S., Yang, K., Yang, F., 2014. Development and experimental study on organic Rankine cycle system with single-screw expander for waste heat recovery from exhaust of diesel engine, Energy 77, 499-508.

- Ziviani, D., Beyene, A., Venturini, M., 2013, Design, Analysis and Optimization of a Micro-CHP System Based on Organic Rankine Cycle for Ultralow Grade Thermal Energy Recovery, J. Energy Resour. Technol. 136, 1.

- Ziviani, D., Sumanc, A., Lecomptea, S., De Paepe, M., van den Broek, M., Spinac, P.R., Pinellic, P., Venturinic, M., Beyened, A., 2014. Comparison of a single-screw and a scroll expander under part-load conditions for low-grade heat recovery ORC systems, 6th International Conference on Applied Energy – ICAE2014, Energy Procedia 61, 117 – 120.

- Ziviani D., Woodland, B., Georges, E., Groll, E., Braun, J., Horton, T., Van den Broek, M., De Paepe, M., 2016. Development and a Validation of a Charge Sensitive Organic Rankine Cycle (ORC) Simulation ToolEnergies, 9(6), 389; doi:10.3390/en9060389

Chapter III:

Design and sizing optimisation of a reversible HP/ORC system - case of a residential heat pump coupled with solar panels

"It's time for the human race to enter the solar system."
Dan Quayle

Abstract

This chapter helps the reader to select the optimal architecture and provides a methodology to optimally size a given reversible HP/ORC system. The methodology is applied to the residential building coupled with solar collectors. Once the system is sized, annual simulations can be performed. It proves that the technology can help to develop Positive Energy Building with a net electricity production of 2005 kWh a year while covering the heating requirements for the Domestic Hot Water and the Floor Heating.

1 INTRODUCTION

First, this chapter describes the different possible architectures for a reversible HP/ORC system and how to select the optimal one based on the characteristics of the application. In chapter one, for the sake of simplicity (given the large number of applications), the reversible HP/ORC unit has been sized only based on the heat pump nominal conditions (considering modification of existing ones). Practically, it is possible to optimize the sizing of each component to obtain the best trade-off between the performances in both modes (ORC and HP). The objective function could be related to the return on investments or on the net electrical production (ORC production minus heat pump consumption) for example. This chapter aims at developing a methodology to optimize the sizing of a given reversible

HP/ORC system. For each set of discrete parameters (working fluid selection for example), continuous sizing parameters (area of heat exchangers for example) are set to obtain the optimal performance with steady-state models. In this chapter, this methodology is described in detail in the case of the residential heat pump application with the selection of the optimal technology of components.

2 SELECTION OF THE SYSTEM ARCHITECTURE

Three main criterion are identified to select the architecture of a reversible HP/ORC system: the conventional or inverted cycle, the use of the ORC pump to act as an expansion valve or not and the use of one or two volumetric machines. This section describes those architectures with their benefits and disadvantages.

2.1 CONVENTIONAL OR INVERTED CYCLE

Two possibilities are identified for the global layout of a reversible HP/ORC system. In the conventional cycle (Table 1), both the evaporator and the condenser conserve their role in the operation modes (ORC and HP). The condenser is on the high pressure line in heat pump mode and on the low pressure line in ORC mode. A liquid receiver can eventually be installed at the condenser outlet to absorb the liquid level variations. If present, this receiver is used in both modes. A four-way valve is installed between the condenser, the evaporator and scroll machine to change the operation mode (compressor or expander). For this purpose, a classical four-way valve typically used in reversible heat pumps (heat pump that can produce heating or cooling trough the same heat exchanger) is one of the possible solutions (see section 6). The four-way valve produces a small heat exchange between high and low pressure working fluid and also a pressure drop that can lead to a reduction of the performance. In the inverted cycle, each heat exchanger plays the role of the condenser or of the evaporator depending on the operation mode (Table 1). The exchanger on the left is always located in the high pressure line and the right one on the low pressure line. Because of this, the properties of the fluid are closer in HP and ORC mode than with the conventional cycle in each exchanger. It leads to a lower operating range for the pressure sensors and thus, to a higher accuracy of measurement. The liquid receiver, not mandatory but commonly used before the pump in an ORC system to adjust the refrigerant level, cannot work without an additional valve in this configuration.

Table 1 : Comparison of the two different architecture for a reversible HP/ORC reversible system. The refrigerant lines without any flow are dashed.

	Conventional cycle	**Inverted cycle**
Heat pump	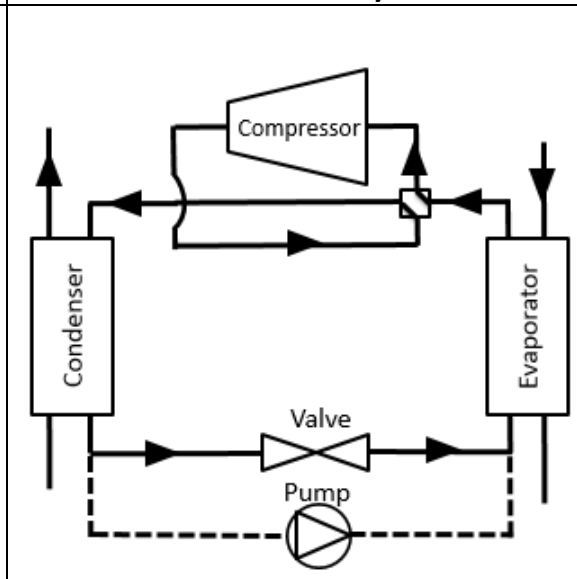	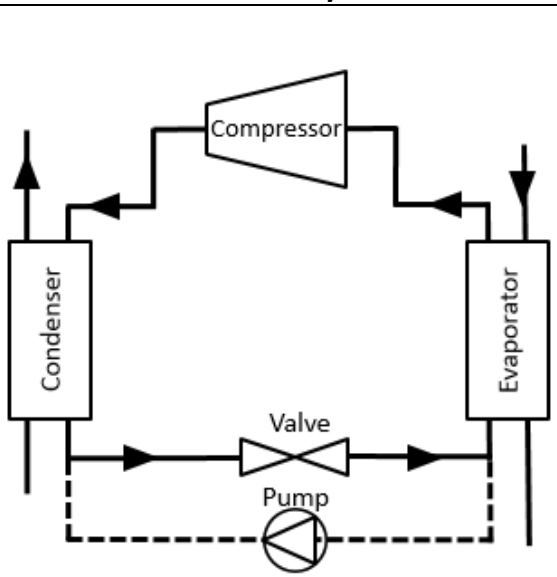
organic Rankine cycle	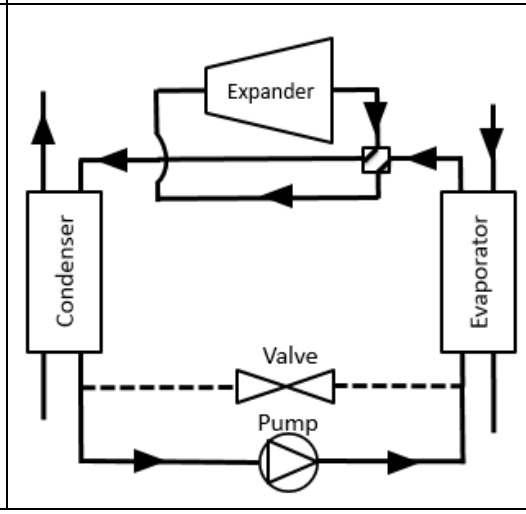	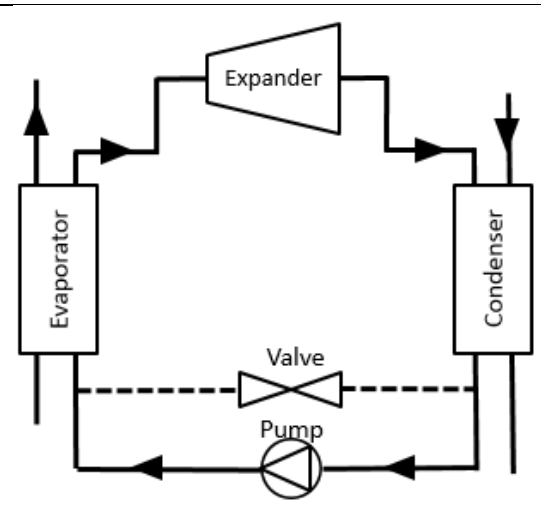

Depending on the operating mode, the working fluid circulates clockwise (ORC mode) or counter-clockwise (HP mode). If a flow-meter is used on the working fluid loop, it will therefore need the bi-flow functionality. Also, because the working fluid flow is inverted, it will lead to parallel flow evaporator and condenser (lower performance). Additionally, three way valves can be used on the secondary fluid side to obtain a counter-flow heat exchanger. A comparison of both systems is performed in Table 2.

Table 2 : Advantages and drawbacks between conventional and inverted cycles

Criterion	Conventional	Inverted
Heat exchangers conserve their role	yes	no
High pressure = left side, low pressure = right side	no	yes
Bi flow flow-meter (if working fluid mass flow-rate measurement)	no	yes
Pressure sensor range/accuracy	lower	higher
Addition of a four-way valve	yes	no
Secondary fluid direction inversion	no	yes
Integration of liquid receiver to optimize the working fluid charge.	easier	harder
Comparable properties of working fluid in heat exchangers	no	yes

2.2 ONE REVERSIBLE VOLUMETRIC MACHINE OR ONE COMPRESSOR AND ONE EXPANDER

The selection of the optimal volumetric machine type, based on experimentation, state of the art and modelling is extensively presented in Chapter two. The use of only one volumetric machine to work as a compressor or as an expander is interesting because of the reduced number of components and hence the lower cost, the simplicity and the compactness. But, two volumetric machines (one for compression and one for expansion) could also be suitable depending on the application because:

- The isentropic efficiency of a dedicated expander (or compressor) is intrinsically slightly higher than the efficiency of a reversible compressor/expander machine.
- It allows to increase the efficiency in both modes by adapting the compressor and expander swept volume and volume ratio to get a better match with the requirements of an application.

However, a two-volumetric machine architecture can involve oil return or charge transfer issues. When one of the two machines is operating, the working fluid condenses in the second and colder one. This modifies the total refrigerant charge traveling in the cycle and can cause negative effects such as pump cavitation. Also, the mixture of working fluid and lubricating oil can be entrained outside of the compressor shell. If the oil return is not sufficient, lubrication problem can occur in the volumetric machine.

Table 3 : Advantages and drawbacks between one or two volumetric machines

Criterion	One machine	Two machines
Efficiency	lower	higher
Compactness	yes	no
Simplicity	yes	no
Costs	low	high
Charge and lubricant issues	lower	higher

2.3 PUMP AS EXPANSION VALVE

The way to achieve a reversible HP/ORC system with the lowest number of components is to use the pump of the ORC system as an expansion valve in the heat pump mode. This results in lower costs, simpler architecture and furthermore, energy could be recovered by the expander in heat pump mode. Recovering the energy during an expansion process is not a new idea and has been investigated by several authors. In 2000, a 20 kW - twin screw expander reach 70% adiabatic isentropic efficiency with fluid R113 to replace a throttle valve in a chiller (Brasz et al., 2000). Similarly, in 2005, the COP of an air-conditioning system has been increased by 10% by replacing the expansion valve with a piston expander despite the low isentropic efficiency of 11% (Baek et al., 2005).

2.4 DISCUSSION

In conclusion, not a given architecture performs better than another. Each one presents advantages and disadvantages. Depending on the application, the efficiency can be the highest priority leading to more expensive systems or the priority could be the simplest system to reach maturity in a short time. If low cost and the simplicity of the system are major concerns, it is probably better to go for a conventional cycle with one reversible volumetric machine and an additional expansion valve. On the contrary, a system requiring a high efficiency should probably use the inverted cycle with a pump as expansion valve. Using two volumetric machines would probably be profitable only in the case where there is a huge mismatch between the HP and ORC mode (thermal compatibility – see Chapter one).

2.5 OTHER CONFIGURATIONS

Other considerations could be discussed but are not detailed here because it depends on the given application:

- The use of one generator (sized for ORC mode) and one engine (sized for HP mode) connected together to the same compressor/expander. This allows having high electro-mechanical efficiency when having very different powers consumed by the heat pump and produced by the ORC system. This has been considered in Peris et al. (2015) for example.
- One large (2/3 of the total nominal power) and one small (1/3 of the total nominal power) volumetric reversible machine could be used in applications with variable heat demand and/or variable ORC heat source to adapt the system and obtain high part-load efficiencies.
- The use of a recuperator (internal heat exchanger) could also improve the efficiency in some applications despite of the simplicity and cost.

3 Optimal sizing methodology

3.1 INTRODUCTION

In chapter one, for the sake of simplicity (given the large number of applications), the reversible HP/ORC unit has been sized only based on the heat pump nominal conditions (considering modification of existing ones). Practically, it is possible to optimize the sizing of each component to obtain the best trade-off between the performances in both modes (ORC and HP). The objective function could be related to the return on investments or on the net electrical production (ORC production minus heat pump consumption) for example. This section aims at developing a methodology to optimize the sizing of a given reversible HP/ORC system.

The accurate modelling of a given application of a reversible HP/ORC system, would require dynamic models of all the components (except if the application presents constant stable operating conditions) included in the application, e.g., to identify the start-up and shutdown times. In addition, a control strategy should be defined, and the operation of the system simulated for an entire year. This approach, although more accurate, is not suitable for a sizing/optimization problem in which the model is intended to be run multiple times and with a variety of system layouts and components. The main limitation is the large computational cost of the optimization process, dynamic models being usually significantly more computationally expensive than steady-state models (Quoilin et al., 2016). Chapter 5 studies such a complex dynamic model with the only purpose of simulation and not optimization.

3.2 METHODOLOGY

The proposed approach relies on steady-state models, which are run in quasi-steady state for each time-step of the year. Properly sizing the system in order to optimize its performance on a yearly basis is a complex task because the optimal size of the components differs depending on the variability of the inputs (season, atmospheric conditions, etc.). In the same manner, the optimal working fluid can change depending on the operating mode (HP or ORC) and on the heat source and heat sink temperature levels. The optimal size of the components must therefore be determined by performing yearly simulations. In this model, the optimization parameters are of two types:

- Continuous parameters: exchanger length and width, pump swept volume, pipe diameters, ect.
- Discrete parameters: working fluid selection, architecture (recuperator or not, conventional or inverted cycle for example)

Such an optimization problem is computationally intensive and the number of design parameters is too high for a multivariate optimization based on yearly simulations. Therefore, the following optimization methodology is proposed (inspired from Quoilin et al., 2016):

1) Set the discrete variables to one of the possible combinations.
2) Optimally size the continuous variables on the nominal point (of the mode presenting the highest interest in the considered application). The objective function is the net output power or the return on investment for example. This optimisation can be constrained depending on the application (maximum pressure or temperature of a given component for example). The variables taken into account in this step are intrinsic variables of the HP/ORC unit and are independent of the system boundary conditions. The influence of the external conditions on the system is considered in step 4.
3) For each time-step (typically one hour), the optimal system part-load performance in the HP and ORC modes (optimisation of the pump speed, compressor speed, expander speed, fan speed for example) must be computed. This calculation is performed with components optimally sized in step 2.
4) Optimal allocation of each operating mode over the load duration curve, i.e. defining a control logic that selects the optimal mode to be operated at each time step. Usually, the heat pump mode is more important to fulfil the heat requirements than the ORC mode but this depends on the application.

Steps two to four are repeated for each combination of the discrete variables (Figure 2). A decision is finally based on the optimized variable (return on investments, net electrical production, etc.) and on the suitability of this solution.

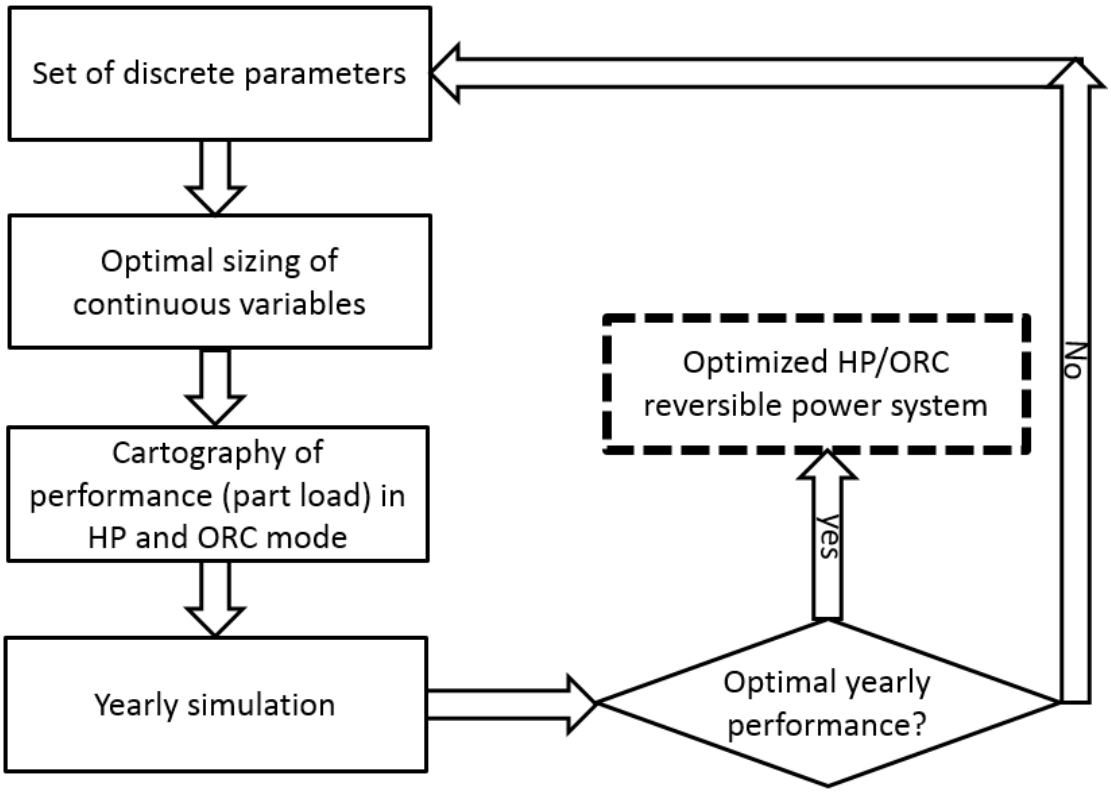

Figure 1 : Flowchart of the optimization process for a HP/ORC reversible system.

4 CASE STUDY - REVERSIBLE HP/ORC SYSTEM FOR DOMESTIC APPLICATION COUPLED WITH A SOLAR ROOF

4.1 INTRODUCTION

4.1.1 Context

Following the introduction to the global methodology to optimize a given HP/ORC reversible system, a case study is presented including the nominal conditions, the modelling, the architecture selection, the technological choices and the optimization. This methodology is applied in the case of a residential building coupled with a solar thermal roof. As shown in Chapter one, in this application, the operational time of the ORC system is high because the ORC mode and the HP mode do not operate during the same periods. The efficiency of the ORC is relatively high compared to other applications (see Chapter one) and the compatibility in terms of thermal energy provided by the solar roof fits the feasibility criterion described in Chapter one.

The building sector is one of the key economic sectors that present a high potential for energy consumption and greenhouse gases emission reduction. Households account for 27% of the final energy consumption (European Commission, 2012) and therefore can constitute an important part of the solution. Various technologies and concepts are being investigated, developed and implemented in the building sector. Net Zero Energy Buildings (Marszal et al., 2010) are expected to gain a significant importance: by 2019, all new buildings in the European Union should present a renewable energy production higher than their primary energy consumption on a yearly basis (European Commission, 2013). This definition should be clarified in the next years with a lower time basis to ensure an optimal matching between consumption and production. Net Zero Energy Buildings and, by extension, Positive Energy Buildings (PEB) will therefore play a major role in the future. Positive Energy Buildings offer different advantages: relatively high independence from energy prices, lower long-term running costs and zero fossil- fuel consumption among others. Amongst the different available energy sources, solar energy is pointed as a very interesting choice for PEB because it is free, 100% renewable and available in abundance. Among others, HPs are a promising technology for providing energy-efficient space and sanitary hot water. According to Bettgenhauser et al. (2013), HP technology could contribute for up to 54% of CO_2 emissions reductions in the buildings sector (both residential and non-residential) in the European Union by 2030. For these reasons and also because of the promising results announced in Chapter one (high operating time, relatively high efficiency and compatibility in terms of thermal energies of this application), the coupling of a reversible HP/ORC unit to a passive house to get a PEB is investigated (Figure 2).

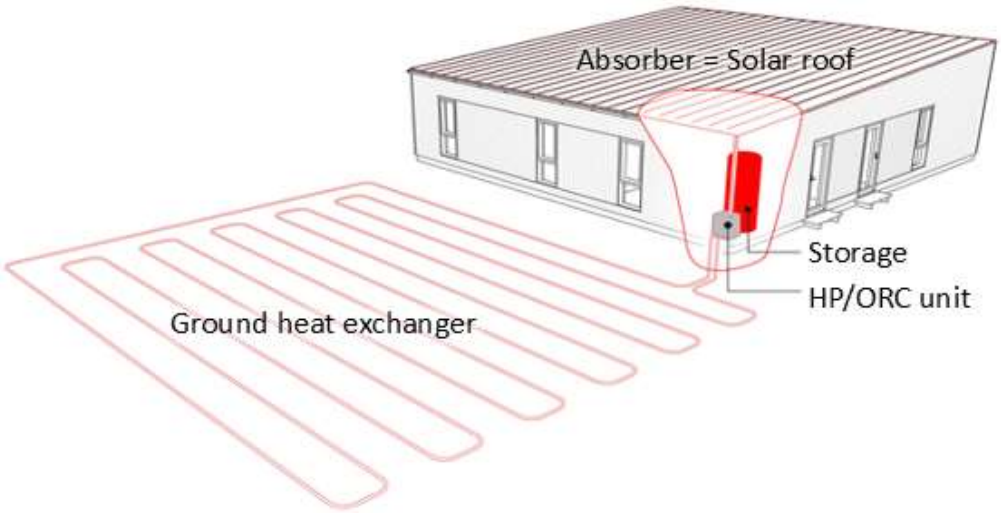

Figure 2: The reversible HP/ORC unit integrated in the house (Dumont et al., 2015).

This reversible unit coupled to a large solar thermal roof and a ground heat exchanger constitutes a combined system able to provide electricity and heat to the household with passive house characteristics. The system can operate in three modes: the direct heating (DH) mode uses the heat collected from the roof to supply the thermal energy in a hot water tank which supplies the floor heating (FH) and Domestic Hot Water (DHW). In case of unfavourable meteorological conditions, the heat pump mode (HP) allows to charge the hot water tank efficiently. On the other hand, in case of solar energy availability, the latter is collected and used to cover the heat demand. Finally, a large quantity of heat is generated by the roof during mid-season and summer periods. This surplus heat can be converted into electricity by means of the ORC. The ground heat exchanger is used to cool the condenser of the ORC system (Dumont et al., 2015). Figure 3 summarizes the control strategy of the system.

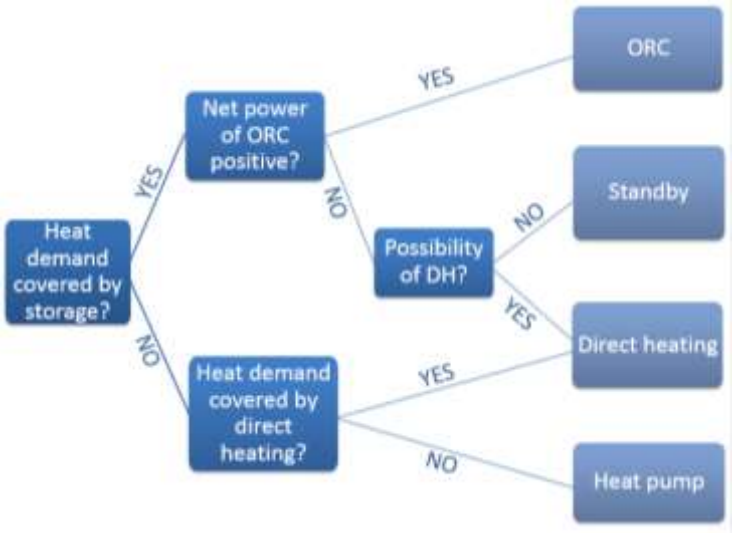

Figure 3 : Control flowchart for the residential application of the reversible HP/ORC system (Dumont et al., 2015)

The first investigation on such a system has been introduced in 2011 (Schimpf et al., 2011). A thermo-economical tool was developed but only a small area of collector (12 m^2) and a vertical ground heat exchanger was considered. In 2013, the patent "thermal solar absorber system generating heat and electricity" from the Danish company Innogie is accepted (Innogie, 2013). The project of this company is the one studied in this chapter. It consists in a residential building (136 m^2) located in Herning (Denmark) coupled with a 300 m long horizontal ground heat exchanger, 1000 litres heat storage and 138.8 m^2 solar roof. The studied solar roof presents a structure similar to a flat plate collector (Figure 4). More details about this roof are provided in Chapter five although the aim of this thesis is not to focus on the solar roof component in the present thesis.

Figure 4 : Solar roof picture (Innogie, 2014)

4.1.2 Architecture and operating modes

This small-scale reversible HP/ORC system needs to be competitive with other competing technologies (heat pump coupled with PV panels for example). This is the reason why the costs have to be minimal and the architecture of the system should therefore be as simple as possible. For this purpose, the conventional cycle with one volumetric machine acting as compressor and expander, no recuperator and an additional pump is chosen (see section 2). Based on this architecture, the hydraulic scheme of the system can be drawn and is presented in Figure 5.

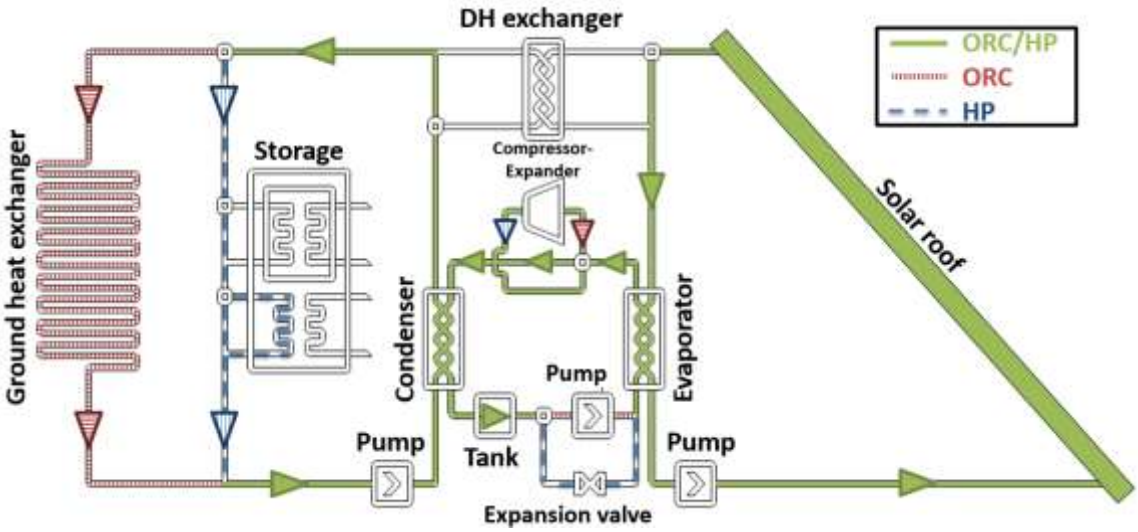

Figure 5: Scheme of the global system showing the three operating modes.

The different operating modes are described hereunder.

4.1.2.1 Organic Rankine cycle

This mode converts the thermal energy absorbed by the solar collector on the roof into electricity. The ORC mode (Figure 5) is run when the meteorological conditions are sufficient to get a positive net electrical production and the heat demand of the house can be covered by thermal energy in the storage volume (Figure 5). The pump increases the pressure of the working fluid, which then passes through an evaporator, where the fluid is vaporized absorbing the thermal energy from the solar roof. Following that, the working fluid flows into the expander (modified compressor) where electricity is produced. Thermal energy is then transferred from the working fluid into the ground heat exchanger, and the fluid is condensed. In addition to these components, a liquid receiver (tank) is used to handle the variation of the refrigerant charge and a four-way valve allows switching between the inlet and outlet of the compressor (see section 6).

4.1.2.2 Direct heating mode (DH)

In this mode, heat absorbed by the solar roof is directed to the storage through an intermediate heat exchanger. The direct heating mode is used to heat the storage at times when the storage temperature is not sufficient to cover the heat demand of the house, as long as there is enough incident solar energy to raise the temperature of the storage.

4.1.2.3 Heat pump mode (HP)

When direct heating is not sufficient to fulfill the heat demand of the house, the heat pump mode is activated to increase the storage temperature (Figure 5). First, the compressor increases the pressure and temperature of the working fluid to release its heat into the storage through the condenser. The refrigerant then flows into the expansion valve and is further evaporated at a low temperature by absorbing the thermal energy from the roof.

4.2 COMPONENT SELECTION/TECHNOLOGY

The heat exchangers need to be efficient, cheap and operate at pressure level usually encountered in typical ORC installations (~ 30 bars). Plate heat exchangers are probably the technology that meets all these criteria. This type of heat exchanger is therefore used for the condenser, the evaporator and the direct heating exchanger.

Three technologies of reversible volumetric machine have been intensively studied and compared in Chapter two. It has been shown that screw expander could work with a low power output but the efficiency is not as high as for larger machines (Nikolov et al., 2017). On the contrary, the piston and the scroll machines present an adequate power range. In comparison with the scroll expander, the piston presents the ability to work with high temperature and pressure which is not useful in this application. The scroll technology is the chosen technology because:

- It presents the best efficiency in this range of power (see Chapter 2).
- It has proven to operate efficiently both as a compressor and as an expander in laboratory tests (Zanelli et al., 1994 ; Quoilin, 2011).

- It shows a good flexibility and robustness in terms of liquid flooded expansion (see Chapter 2).

Very few manufacturers deliver scroll expanders. An off-the-shelf scroll compressor is therefore chosen and modified to work as an expander (Chapter four). The pressure limitation of typical scroll compressors (32 bars) should not decrease significantly the performance of the ORC since the temperature considered in this application is low (flat plate solar collector). It means that in this work, the volume ratio of the expander, the swept volume and the maximum pressure are imposed. It would also be possible to add those variable to the optimizer to design an optimized expander. However, this solution is rejected because of the cost related to such a prototype. An investigation of the volume ratio influence is shown in section 4.4.2.

A volumetric pump is preferred to a centrifugal one because it works efficiently with the high pressure difference and the low volumetric flow rate. Among volumetric pumps, a plunger pump is chosen because of its perfect tightness to avoid working fluid leakage, its constant volumetric efficiency and relatively high isentropic efficiency (see Chapter four).

4.3 NOMINAL CONDITIONS

As a reminder, the study case is a prototype of Positive Energy Building located in Herning, Denmark. In this chapter, section 4.3 to 4.5 are inspired from Quoilin et al. (2016). The ORC operating mode is the one involving the highest heat flow through the system (more than 50 kWth), and is thus the one selected for the sizing of the system components. A nominal sizing point is defined with the following parameters, representative of average mid-season operating conditions (Table 4):

- The evaporating temperature is set to 90°C, which approximately corresponds to the maximum allowable pressure at the inlet of the expander with refrigerant R134a.
- For the cooling water, an inlet temperature of 15°C and an outlet temperature of 20°C are assumed.
- The heat source temperature glide, i.e., the difference between the inlet and outlet glycol water temperature on the absorber, is set to 25K. Actually, a smaller temperature difference would require an unusually large glycol water flow rate, causing significant pressure drops.
- The pinch points (the smallest temperature difference between the working fluid and secondary fluid at the same position in the exchanger) are set to 5K for the evaporator and 7.5K for the condenser (Quoilin et al., 2011).
- The superheating and sub-cooling in the evaporator and the condenser are set to 10K and 2K, respectively.

Once the continuous optimization parameters are set (see section 3.2), they can also be input into the heat pump model to assess its performance in nominal operating conditions. To that aim, two different nominal operating points are defined:

- Evaporation temperature: -11°C or 15°C.
- The condensing temperature is fixed to 60°C in order to get a water temperature around 55°C in the heat storage.
- For hot water production, a temperature difference of 5K is assumed between the inlet and the outlet of the condenser.
- The superheating and sub-cooling of the evaporator and the condenser are set to 3K and 2K, respectively.

Table 4 : Nominal operating conditions in ORC and HP mode

Organic Rankine cycle		
Evaporation temperature	t_{ev} [°C]	90
Cooling water inlet/outlet temperature	$t_{w,su}/t_{w,ex}$ [°C]	15/20
Temperature glide on the heat transfer fluid	Δt_{gw} [K]	25
Pinch point on the evaporator	$pinch_{ev}$ [K]	5
Pinch point on the condenser	$pinch_{cd}$ [K]	7.5
Superheating (expander inlet)	Δt_{oh} [K]	10
Subooling (condenser outlet)	Δt_{sc} [K]	2
Ambient temperature	t_{amb} [°C]	25
Evaporator pressure drop	Δp_{ev} [mbar]	200
Condenser pressure drop	Δp_{cd} [mbar]	200
Heat pump		
Condensing temperature	t_{cd} [°C]	60
Temperature glide on the condenser	$\Delta t_{gw,cd}$ [K]	5
Superheating in the evaporator	Δt_{oh} [K]	3
Sub-cooling in the condenser	Δt_{sc} [K]	2
Glycol water flow rate	$\dot{V}_{gw,ev}$ [l/min]	0.2567
Evaporation temperature	t_{ev} [°C]	-11/15
Ambient temperature	t_{amb} [°C]	0/10

4.4 MODELLING

Each component is modelled following a semi-empirical approach. It allows a fast CPU-time for optimization purposes and decent extrapolation capabilities in a small scale ORC system for all the components (pump, condenser, evaporator an expander) (Dickes et al., 2016).

4.4.1 Heat exchangers

Both the evaporator and the condenser are plate heat exchangers in which the working fluid changes phase between three main states: vapour, two-phase and liquid. The plate heat exchangers are modelled by means of the ε-NTU (or LMTD methods) for counter-flow heat exchangers. They are subdivided into 3 zones, each of them being characterized by a heat transfer area *A* and a heat transfer coefficient *U*. Each heat transfer coefficient *U* is calculated by considering two convective heat transfer resistances in series (secondary fluid and refrigerant sides): $\frac{1}{U} = \frac{1}{u_f} + \frac{1}{u_{sf}}$. The conductive resistance of the wall (approximately $5 \cdot 10^{-5}\ m^2K/W$) is neglected because it appears to be negligible compared to that of the convection (with an order of magnitude of $\sim 2.5 \cdot 10^{-3}\ m^2K/W$ for single-phase fluids). The respective heat transfer area of each zone is obtained by imposing the total heat transfer area of the heat exchanger (Eq. 1).

$$A_l + A_{tp} + A_v = (N_p - 2) \cdot L \cdot Wi \qquad 1$$

where N_p is the number of plates, *L* is the plate length between inlet and outlet ports and *Wi* is the plate width between gaskets. The heat exchangers considered in the studied applications show relatively low pressure drops (typically not more than 200 mbar). Therefore, to facilitate the convergence of the numerical iteration process, these pressure drops are summed up and lumped into one single pressure drop located in the vapour line (Eq. 2)

$$\Delta p_{tot} = \Delta p_l + \Delta p_{tp} + \Delta p_v \qquad 2$$

The vapour line is selected because pressure drops across the liquid phase zone are relatively small in plate heat exchangers. In single-phase, the heat transfer coefficient and friction factors are calculated using the Thonon correlation (Thonon, 1995). Neglecting the port, manifold and acceleration pressure drops, the friction pressure drop is computed by Equation 3.

$$\Delta p = \frac{2 \cdot f \cdot v \cdot G^2}{d_h} \cdot L \qquad 3$$

f is the Fanning friction factor, *G* is the mass velocity, d_h is the hydraulic diameter (= 2·*b* for plates heat exchangers), v is the specific volume and *L* is the plate length.

The condensation heat transfer coefficient and pressure drop are calculated using the Kuo correlation (Kuo et al., 2005), and the evaporation heat transfer coefficient is calculated with the Hsieh correlation (Hsieh et al., 2002). Both correlations were established in the case of a vertical plate heat exchanger fed with R410a. In the two-phase flow region, the heat transfer and pressure drops are vapour-quality-dependent. However, in this model an average heat transfer coefficient is considered for simplicity. For this reason, the two-phase heat transfer correlations are integrated with respect to the vapour quality (Eq. 4).

$$\bar{h}_{tp} = \int_0^1 h_{tp} dx \qquad 4$$

x is the vapour quality. The pressure drop in the two-phase flow region strongly depends on the vapour quality. It is generally expressed by Eq. 5.

$$\frac{\Delta P_{tp}}{dL} = \frac{2 \cdot f_{tp} \bar{v} \cdot G^2}{D_h} \qquad 5$$

The Fanning friction factor f_{tp} depends on the vapor quality and $\bar{v} = x \cdot v_g + (1 - x) \cdot v_l$ (assuming that the two-phase flow is homogenous). The total pressure drop is thus obtained by numerically integrating the latter expression over the exchanger length and by assuming that the vapour quality evolves linearly in the heat exchanger along the axial coordinate (Eq. 6).

$$\Delta p_{tp} = \int_0^1 \frac{2 \cdot f_{tp} \bar{v} \cdot G^2}{D_h} dx \cdot L \qquad 6$$

When modelled using an a-causal modelling platform like the one adopted in this work, the described model can be used indifferently for sizing purposes or for simulation (part-load performance evaluation) purposes. In sizing mode, the inlet conditions, the pinch point and the pressure drop are imposed. The model calculates the required heat exchange area and the cross-sectional area to fulfil these conditions (i.e. the "total width" $(N_p - 2) \cdot W$). In simulation mode, the geometry of the heat exchanger (N_p and W) is imposed, the inlet

conditions are imposed, and the model recalculates the outlet conditions (Quoilin et al.; 2011).

4.4.2 Compressor/expander (Scroll)

The compressor is modelled using the EN 12900:2005 (E) European standard (European committee for standardisation, 2005). The empirical coefficients are provided from tests executed by the manufacturer, and the polynomials are expressed by Eq. 7 and Eq. 8.

$$\dot{W}_{cmp} = C_{i0} + C_{i1}.t_{ev} + C_{i2}.t_{cd} + C_{i3}.t_{ev}^2 + C_{i4}.t_{ev}.t_{cd} + C_{i5}.t_{cd}^2 + C_{i6}.t_{ev}^3 + C_{i7}.t_{cd}.t_{ev}^2 + C_{i8}.t_{ev}.t_{cd}^2 + C_{i9}.t_{cd}^3 \quad (7)$$

$$\dot{m}_{cmp} = C_{m0} + C_{m1}.t_{ev} + C_{m2}.t_{cd} + C_{m3}.t_{ev}^2 + C_{m4}.t_{ev}.t_{cd} + C_{m5}.t_{cd}^2 + C_{m6}.t_{ev}^3 + C_{m7}.t_{cd}.t_{ev}^2 + C_{m8}.t_{ev}.t_{cd}^2 + C_{m9}.t_{cd}^3 \quad (8)$$

C_{ix} & C_{mx} are coefficients related to each type of scroll compressor. The coefficients are provided on the manufacturer website (Emerson, 2015). Equation 7 estimates the power consumption of the compressor as a function of the evaporating temperature (t_{ev}) and the condensing temperature (t_{cd}), while Equation 8 estimates the refrigerant mass flow rate. This allows computing the outlet enthalpy (and thus temperature) by means of the following expression, valid in the hypothesis of hermetic and adiabatic compressors:

$$h_{ex,cmp} = h_{su,cmp} + \frac{\dot{W}_{cmp}}{\dot{m}_{cmp}} \quad (9)$$

While the performance of scroll machines in compressor mode is well-known due to their widespread use in the HVAC industry, this is not the case if the machine is used as an expander. In this work, the expander performance is based on a previous experimental campaign carried out at the Thermodynamics Laboratory of the University of Liege on a hermetic scroll expander. This machine, originally a scroll compressor, was adapted for reverse operation as an expander. Following this experimental campaign, a thermodynamic model of the expander was developed, calibrated and validated with the experimental data (Lemort et al.; 2011). This model is described in chapter 2. It accounts for the following types of losses: under and over-expansion losses, electromechanical losses, friction losses, internal leakage, suction pressure drop, internal heat transfers and ambient heat losses. The model requires only eight parameters (swept volume, build-in volume ratio, three heat transfer coefficients, friction torque, leakage area and pressure drop equivalent orifice area). Those eight parameters, defined for a specific type of expander and for a specific working fluid, are taken from Lemort et al. (2011) and detailed in Table 5.

Table 5 : Parameters of the expander model

Parameter	Value
Swept volume	$V_s\ [cm^3] = 22.4$
Internal built-in volume ratio	$r_{v_{in}} = 2.85$
Equivalent inlet pressure drop area	$A_{su}[mm^2] = 30$
Ambient losses conductance	$AU_{amb}[W/K]\ = 3.4$
Inlet heat conductance	$AU_{su}[W/K]\ = 30$
Outlet heat conductance	$AU_{ex}[W/K]\ = 30$
Equivalent leakage area	$A_{leak}[mm^2] = 0.68 - 0.116(10 - P_{su})$
Mechanical efficiency	$\eta_{mec} = 0.9$

For the requirements of this study, the expander model must be applicable to a range of different sizes (i.e. different swept volume), which is not the case for the model described in Lemort et al. (2011). In order to scale the model for different swept volumes, the model equivalent leakage areas have been "sized" as a function of the swept volume according to a methodology defined in Lemort (2009), namely with Eq. 10 and Eq. 11.

$$\frac{A_{leak}}{A_{leak,nom}} = \left(\frac{V_s}{V_{s,nom}}\right)^{2/3} \quad 10$$

$$\frac{A_{su}}{A_{su,nom}} = \left(\frac{\dot{V_s}}{V_{s,nom}}\right)^{2/3} \quad 11$$

The nominal values, indicated by the "nom" subscript, are taken from Table 5. As explained in the former section, it would also have been possible to optimize the volume ratio of the volumetric machine. The optimization is performed with the inputs from Table 4. The net electrical production of the ORC power unit and of the consumption of the heat pump are evaluated for different volume ratio's (Figure 6). It is shown that the optimal volume ratio for the ORC power system (3.75) is different from the optimum volume ratio for the heat pump (2.8). It means that in general, the solver should optimize the volume ratio by taking into account both performance of the heat pump and of the orc unit but also the total period while each mode is working. For example, if the ORC is working 90% of the time, it would make more sense to use the ORC optimal volume ratio. However, as explained in the former section, in this work, the volume ratio is imposed by the real off-the-shelf compressor because of its simplicity and low investment.

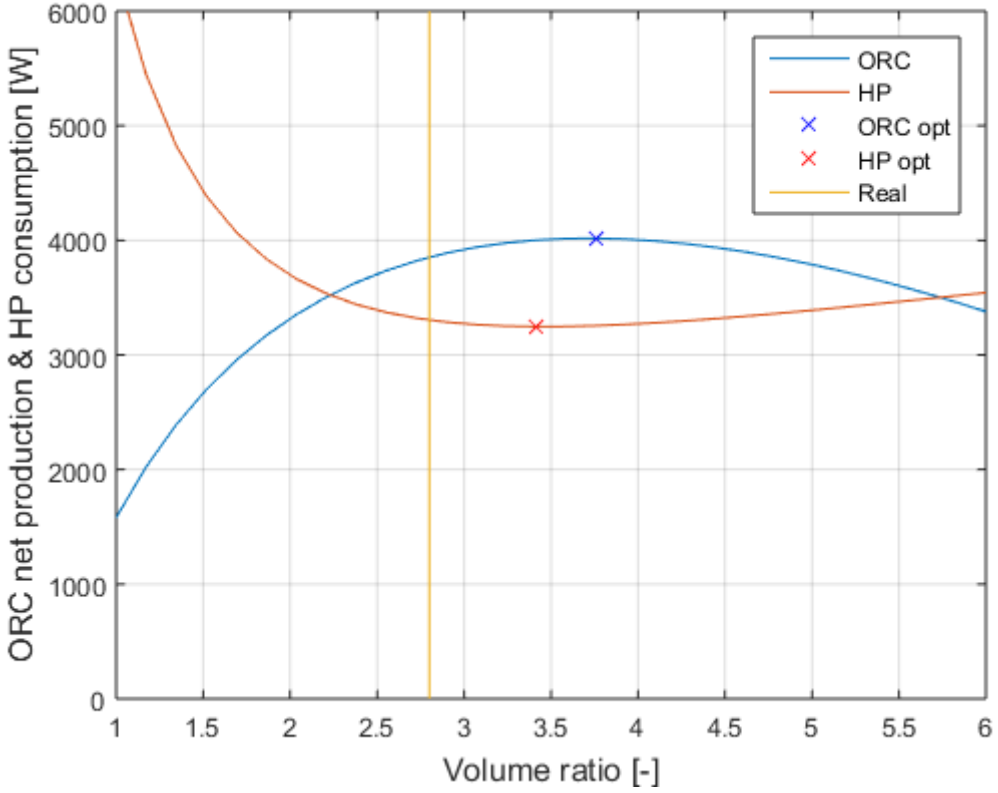

Figure 6 : Influence of the volume ratio optimization.

4.4.3 Pump

The volumetric pump is modelled using a constant parameter model. The isentropic efficiency (Eq. 12) is set to 0.5 and the volumetric efficiency is assumed equal to one (Eq. 16). Eq. 12 allows to compute the electrical consumption of the pump at part load while Eq. 13 allows to size the pump in terms of swept volume.

$$\varepsilon_{pp,s} = \frac{\dot{m}(h_{pp,ex,is} - h_{pp,su})}{\dot{W}_{el}} \quad 12$$

$$\varepsilon_{pp,vol} = \frac{\dot{V}_{pp,su}}{S_{pp} V_{pp,s}} \quad 13$$

Under the assumption of an adiabatic pump, the exhaust enthalpy is given by Eq. 17. This equation allows computing the exhaust temperature.

$$h_{ex,pp} = h_{su,pp} + \frac{\dot{W}_{pp,mec}}{\dot{m}_{wf}} \quad 14$$

4.4.4 Solar roof

The thermal energy from the solar roof is simulated with 3 inputs: the ambient temperature, the heat transfer fluid temperature and the solar irradiation. This expression is based on actual performance data for this type of absorber. The collector efficiency is obtained by fitting a linear curve to data provided by the manufacturer. It is expressed by Eq. 15 and Eq. 16.

$$\eta_{overall,abs} = \frac{\dot{Q}_{abs}}{A_{abs}.I} . \eta_{glazing} \quad 15$$

$$\dot{Q}_{abs} = A_{abs}.(-26{,}2 - 1.22\, t_{amb} - 1.783\, \Delta t_{abs} + 0{,}9034.I) \quad 16$$

$\dot{Q}_{abs}$ is the absorbed heat power, A_{abs} is the total absorber area (138.8 m²), $\eta_{glazing}$ is the optical efficiency (assumed to be 88%), t_{amb} is the ambient temperature, I is the current solar irradiation (in [W/m²]) and Δt_{abs} is the difference between the average temperature of the heat transfer fluid within the collector and the ambient temperature.

4.4.5 Storage and heat demand

To simplify the problem, the heat demand is assumed to be an input for each month of the year and the heat storage together with its control system are modelled by constant storage losses. The total (monthly) heat demand (space heating, domestic hot water and thermal storage ambient losses) must be fulfilled with one or a combination of both heating modes: direct heating and heat pump mode. The considered monthly heat demands are reported in Table 6.

Table 6 : Heat consumption & heat losses (monthly average)

Month	t_{amb} [°C]	Heat consumption [kWh]	Heat losses [kWh]	Heat required [kWh]
January	2	955	172	1127
February	2.4	896	159	1055
March	5.3	808	166	974
April	10	560	146	706
May	15.4	253	133	386
June	18.8	100	117	217
July	19.9	100	117	217
August	20.1	100	117	217
September	16.3	118	125	243
October	12.2	448	143	591
November	6.9	666	156	822
December	3.6	890	172	1062

The storage thermal losses are evaluated in [Wh/day] with respect to the ambient temperature, using the relationship from Kreider et al. (2009), Eq.17.

$$Q_{sto} = V_{sto} 4.2. V_{sto}^{-0,53}. (t_{sto} - t_{amb}) \quad 17$$

V_{sto} is the storage volume in liters, $T_{sto} = 55°C$ is the storage temperature, T_{amb} is the monthly average ambient temperature and C_r is a constant, dependent on the storage volume. For the present work, a large storage volume of 1000 l is assumed. The monthly heat losses are given in Table 6. The oversizing of the storage is necessary to fulfil the hypothesis of ideal switching between the different operating modes. In chapter five, detailed dynamic models of each component, together with the definition of a proper control strategy, will allow optimizing the size of the storage.

4.4.6 Reversible HP/ORC system

The model presented in this section is built as a sizing model, i.e. by imposing the operating conditions (Table 4) and recalculating the proper system geometry. From the nominal conditions, it is possible to evaluate the performance of the ORC and HP mode for a given

fluid and expander size (respectively R134a and 98.04 cm^3 in this example) as presented in Table 7. Figure 7 shows the T-s diagram for both modes on the nominal point.

Table 7 : Nominal operating conditions based on optimal sized parameters

Organic Rankine cycle			
Required minimum solar Irradiation	I [W/m²]	660.5	
Glycol water flow rate	$\dot{V}_{gw}$ [l/min]	0.2567	
Absorber temperature	T_{abs} [°C]	82.5/107.5	
Thermal power through the absorber	$\dot{Q}_{abs}$ [kW]	62.3	
Condensing temperature	t_{cd} [°C]	27.2	
Cooling water flow rate	$\dot{V}_w$ [l/s]	3.067	
Pump power consumption	$\dot{W}_{pp}$ [kWe]	1.252	
Power generation	$\dot{W}_{net}$ [kWe]	4.733	
Cycle first law efficiency	η_{ORC} [%]	7.6	
Expander nominal efficiency	$\varepsilon_{exp,is}$ [%]	68	
Absorber nominal efficiency	η_{abs} [%]	55.31	
Heat pump			
Required minimum solar irradiance	I [W/m²]	47.3	157.2
Absorber temperature	t_{abs} [°C]	-8.5/ -6.7	15.9/ 21.3
Thermal power through the absorber	$\dot{Q}_{abs}$ [kW]	4.5	13.2
Cooling water flow rate	$\dot{M}_w$ [kg/s]	0.40	0.66
Refrigerant flow rate	$\dot{M}_{ref}$ [kg/s]	0.041	0.104
Compressor consumption	$\dot{W}_{cmp}$ [kWe]	3.2	4.1
Thermal Power	$\dot{Q}_{cd}$ [kWe]	7.7	17.3
COP	COP [-]	2.4	4.2

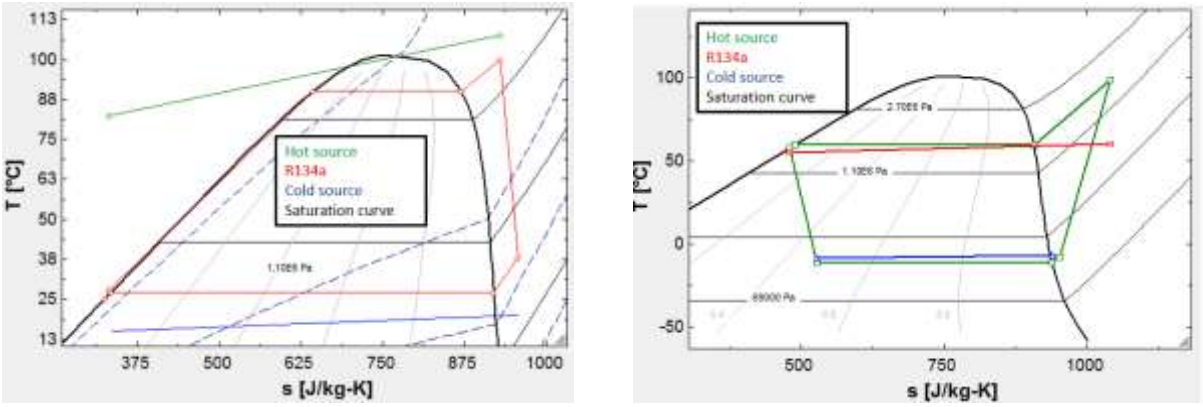

(a) (b)

Figure 7 : T-s diagram at the nominal conditions. a) ORC b) HP.

To perform a yearly simulation, the performance of the ORC/HP unit must be computed for a wide range of operating conditions. To compute part-load performance, the above-model is transformed into a simulation model by imposing the “optimized geometric parameters” from the nominal point. Sub-models are coupled together to obtain a global model to predict the part load performance of the heat pump (i.e. ORC). The operating conditions are recalculated by the model, except for the sub-cooling which is assumed to be maintained close to 2K. The pump shaft speed is adjusted to get a constant over-heating. The ground heat exchanger is supposed to be sized in a way that the return water temperature is constant (15°C) leading to a constant condensation temperature. Parametric studies are then performed by varying the externally-imposed boundary conditions, such as the absorber mean temperature. Figure 8 shows an example of the consumed thermal power and the net output power in ORC mode with R134a as working fluid and for 3 different expander sizes in off-design conditions.

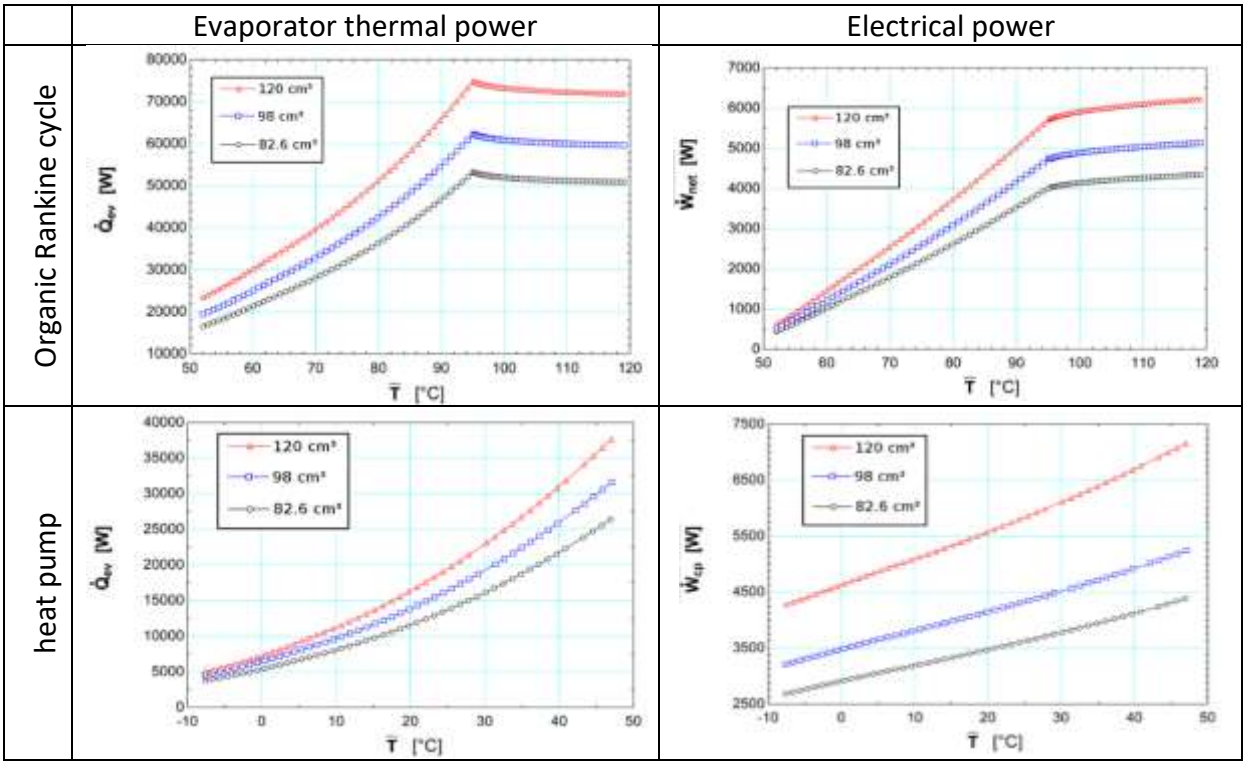

Figure 8 : Evaporator thermal power and electrical power as function of the mean absorber temperature for both the heat pump and organic Rankine cycle.

The discontinuity in both figures at 95°C is due to a constraint on the maximum inlet pressure of the scroll machine (max 32 bar): when this maximum is reached, the evaporation pressure cannot be increased anymore. However, some extra power can still be produced by increasing the superheating (the strategy adopted in this case). It should be noted that the nominal point is defined with a small degree of super-heating with a 32 bar evaporation pressure, i.e. at the discontinuity point. The nominal power is therefore lower than the maximum power of the ORC system, as found by the simulation. In the case of the HP mode, the relevant variables are the condensing/evaporating powers $\dot{Q}_{cd}/\dot{Q}_{ev}$ and the consumed compressor power $\dot{W}_{cmp}$. They are expressed as a function of the absorber mean temperature (Figure 8).

4.5 Evaluation of the Seasonal Performance

4.5.1 Optimization

The optimization function selected for this optimization is the net energy produced on a yearly basis (ORC production minus heat pump consumption). The total (monthly) heat demand (space heating, domestic hot water, and thermal storage ambient losses) must be fulfilled with one or a combination of both heating modes: direct heating and the HP mode. Switching between the three operating mode (HP, ORC, and direct heating) is performed in such a way that the net electricity production (resp. consumption) is maximized (resp.

minimized) throughout the month. Solar irradiation and ambient temperature are considered for each hour of each month and are computed using the Meteonorm database for the city of Herning, Denmark. The data are sorted with respect to the radiation to build a cumulated density function and the model is run for each (sorted) hour of the month. Running the model in this way allows the simulation to be easily balanced between the three operating modes, as shown in the three following subsections.

To simplify the problem, the heat demand is assumed to be an input for each month of the year and the heat storage together with its control system are modelled by constant storage losses (Table 6). Detailed models of these two components (storage and building) are therefore not required in this section. The main modelling assumptions and hypotheses can be summarized as follows:

- steady-state modelling with a 1 hour time resolution
- the chronology of time steps is neglected, as all hours in a month are simulated as a residual load curve
- optimal storage, supposed to balance the thermal energy between time slices (neglecting the dynamics)

The size of the scroll machine is taken as a discrete parameter because it is based on an off-the-shelf unit modified to run in the expander mode, and these units are only available in a finite number of sizes. Assuming a discrete number of possibilities moreover simplifies the optimization process by reducing the number of required simulations, as explained below. Following the methodology defined in section 3.2, the optimisation is performed to size the components and to predict the yearly performance of the system. In this case study, the continuous parameters are the evaporator length and total width, the pump swept volume and the condenser length and total width. The discrete parameters are the working fluid selection (either R124, R600, R152a, R600a, R134a, R245fa, R123 or R1234yf), and the displacement of the scroll machine (either 82.6, 98.04, or 119.96 cm^3).

4.5.2 Results

4.5.2.1 Monthly simulations: direct heating and ORC

During sunny months, when more heat than required is available through direct heating, the ORC mode is activated as long as the absorber temperature is sufficient to produce electricity. If electricity generation impedes achieving the heating requirement, the direct heating mode is activated in place of the ORC until those requirements are satisfied. This strategy is illustrated for the month of June in Figure 9. The red area is equal to the total electricity produced whereas the blue one is equal to the heating energy produced by direct heating: the ORC is activated during the 29 most irradiated hours. After that, the direct heating mode has to be activated to achieve the heat demand for the other hours of this month.

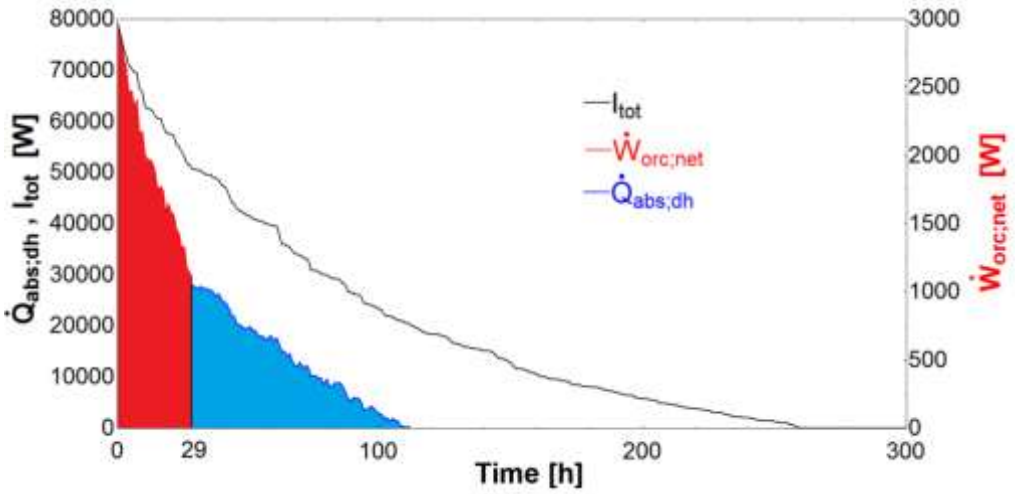

Figure 9 : Cumulated frequency curve of the incident irradiation, net power output and thermal power output by direct heating for the month of February (Quoilin et al., 2016).

4.5.2.2 Monthly simulations: direct heating and heat pump

During winter months, when heating requirements exceed the heat production capacity of direct heating, the heat pump must be activated. This is illustrated in Figure 10 for the month of December: the heat pump is started to provide heat to the user when the absorber is insufficient. Figure 10 shows that for the month of December, the direct heating mode is turned on during the 29 sunniest hours of the month. The heat pump is activated for 88 hours. It should be noted that the heat pump simulation is performed with the absorber as heat source, even when the geothermal heat exchanger is at a higher temperature. This conservative hypothesis is necessary because a dynamic model of the geothermal heat exchanger would have been required to compute its temperature, leading to a computationally intractable model for such a sizing problem.

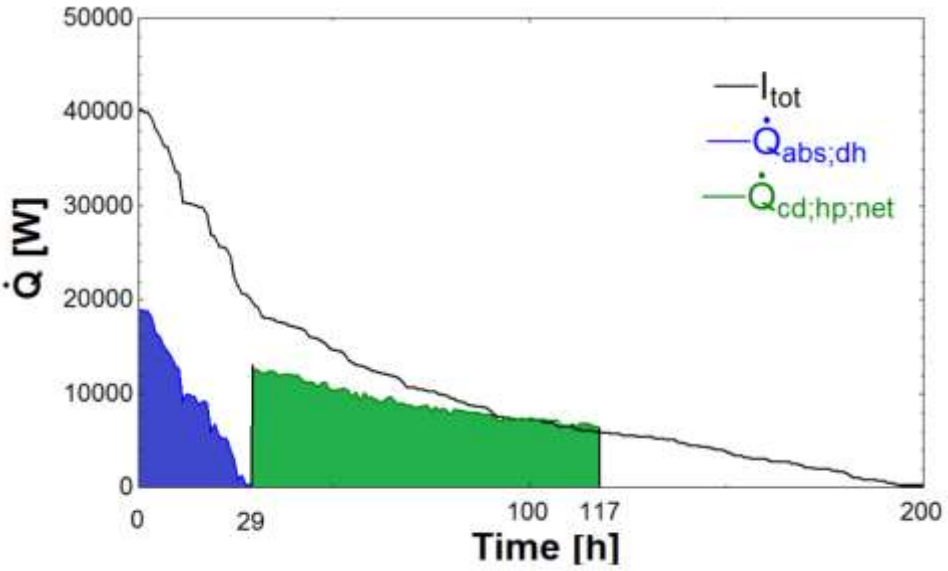

Figure 10 : Cumulated frequency curve of the incident irradiation, and thermal power output by direct heating and heat pump for the month of December (Quoilin et al., 2016).

4.5.2.3 Yearly simulations

Table 8 presents the optimized parameters based on the nominal point (Table 4) with R134a as working fluid and a swept volume of 98.04 cm^3 for the expander.

Table 8 : Optimal sizing and associated parameters (Quoilin et al., 2016).

Optimized geometric parameters		
Evaporator heat exchange area	A [m²]	4.73
Evaporator total width	$N_p \cdot Wi$ [m]	8.4
Condenser heat exchange area	A [m²]	9.96
Condenser total width	$N_p \cdot Wi$ [m]	14.2
Pump nominal flow rate	$\dot{M}_{pp}$ [kg/s]	0.299

Yearly simulation results with the selected optimal continuous parameters with refrigerant R134a are presented in Table 9. It can be noted that for most of the months, the maximum output power of the ORC unit has been reached at least once. The maximum net electricity generation corresponds to the month of July, and the total yearly output is 4030 kWh. The heat pump is activated during three months of the year. During all the other months, direct heating is sufficient to cover the heat demand. Over one year, the heat demand covered by

the heat pump is 1421 kWh, and the heat demand covered by direct heating is 6289 kWh. The average COP in heat pump mode is 2.7.

Table 9: Seasonal simulation of the system (Quoilin et al., 2016)

mode	**ORC**		**Heat pump**		**Direct Heating**
	Max. power output [kW]	W_{net} [kWh]	W_{cmp} [kWh]	Q_{cd} [kWh]	Q [kWh]
January	-	-	218.09	613.6	515.4
February	3.1	50.82	-	-	1077.6
March	5.13	193.1	-	-	979.2
April	5.13	519.9	-	-	720.5
Mai	5.13	759.7	-	-	392.3
June	5.13	708.9	-	-	225.3
July	5.13	798.7	-	-	225.3
August	5.13	626.9	-	-	220.2
September	4.95	302.1	-	-	249.5
October	3.7	79.1	-	-	602.4
November	-	-	3.82	12.5	815
December	-	-	305.4	795.6	266.5
TOTAL		4030.2	527.31	1421.7	6289.2

Table 10 illustrates the optimization process for the discrete parameters (working fluid, possible presence of a recuperator, expander size) through a few representative runs. The main performance indicator is the net yearly electricity production W_{net}, calculated as the difference between net ORC power generation and heat pump consumption.

Table 10 : Results of the seasonal simulations for a few selected cases (Quoilin et al., 2016)

	W_{net} [kWh]	Difference	Notes
Reference case	3496.27	0.00%	R134a, No recuperator, $V_{s,exp}$ = 98.04 cm³
Different fluids (with optimized components):			
R124	5079.42	45.28%	High ODP, high GWP, toxic, Flammable
R600	4239.98	21.27%	Flammable
R152a	3969.01	13.52%	Flammable
R600a	3814.85	9.11%	Flammable
R245fa	3349.76	-4.19%	High GWP
R123	3105.28	-11.18%	High ODP, high GWP, Toxic
Different architecture:			
With recuperator	3659.2	5.4%	Requires a modification of the cycle architecture (one additional heat exchanger)
Scroll control			
Variable speed scroll	3636.1	4%	Higher cost, additional control
Different compressor sizes:			
$V_{s,exp}$ = 82.6 cm³	3300.47	-5.6%	
$V_{s,exp}$ = 119.96 cm³	3376.07	-3.4%	

The reference case presented in Table 10 also happens to be the one selected at the end of the optimization process. It can be noted that the use of alternative working fluids such as R124, R600 or R152a can significantly increase the net electricity generation. However, these fluids were rejected because of their toxicity and/or flammability since the target unit has to be installed inside of a building and needs to comply with high safety standards. The simulation also shows that the use of a recuperator (whose effectiveness is set to 80%) can increase the electricity output by about 5%. The addition of a recuperator (an additional heat exchanger) would however also increase the cost of the unit. This solution has therefore been rejected as the recommended solution, in regard to the relatively low performance improvement for an additional cost.

In the presented ORC system, the scroll speed is constant (to reduce costs) and cannot be changed to optimize the net electrical production. However, it is possible to evaluate the gain in performance that could be reached by using an inverter (efficiency assumed equal to 97%) to control the expander speed. Simulations predict an increase of performance of 4% which is substantial but not sufficient to justify the additional costs and the more complex control.

An analysis of the scroll machine swept volume selection in expander mode indicates a trade-off:

- A too high swept volume does not allow power generation at times of low solar irradiation because the evaporation pressure is not sufficient to generate useful work in the expander (an expansion ratio higher than 2 or 3 is generally needed). In addition, the heat pump is oversized and therefore provides a lower performance and thus higher electricity consumption.
- A too low swept volume constraints power generation at times of high solar irradiation: the unit reaches its maximum power (because the maximum pressure is reached) and a part of the thermal energy is lost. This effect is partly counterbalanced by the fact that the heat pump operates with a more favourable compressor swept volume and therefore allows to reach a higher COP.

The final result of the optimization process therefore leads to the selection of R134a as working fluid, a system configuration with no recuperator is installed and the selected swept volume of the scroll machine is 98.04 cm^3.

5 CONCLUSION

This chapter tries to contribute to the conception of a reversible HP/ORC unit. First, the selection of the architecture and the technological choices are detailed. The design of such a system is a challenging task since trade-offs have to be found between the two operating modes. Thus, an optimization sizing methodology has been devised, which optimizes some continuous parameters on the basis of a nominal operating point, and some discrete parameters. The main goal of this methodology is to propose a realistic optimization without excessive computational effort, as it avoids running a detailed thermodynamic model over an entire year. The methodology is applied to an innovative reversible energy conversion system that can operate either as a heat pump or as an ORC unit. The system provides space and domestic hot water heating in the winter and electricity in the summer due to its coupling with a solar roof. The multiple simulations show the effect of the selected working fluid, the cycle configuration and the selected swept volume of the scroll machine on the system performance. The chosen configuration is selected not only because of the favourable performance indicators, but also for practical constraints such as the safety of the working fluid. The simulations show that the proposed system can produce up to 3500 kWh of electricity throughout the year, while also fulfilling thermal energy demand for space heating and domestic hot water. This promising performance lead to the interest to build a prototype to proof the technical feasibility of such a reversible HP/ORC (Chapter 5).

6 APPENDICES

The prototype needs to invert the supply and the exhaust of the compressor. A four way valve is used for this purpose.

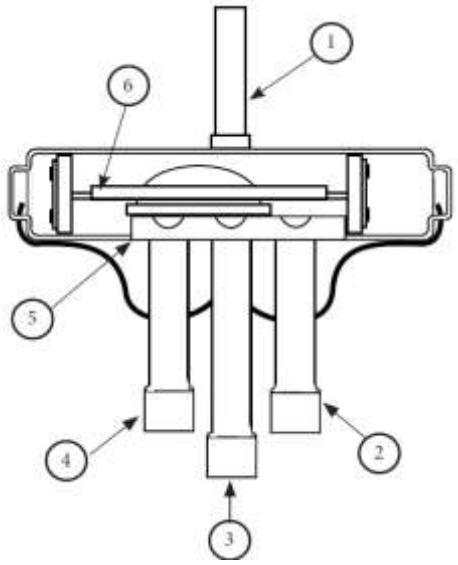

As usual, the compressor discharge is in 1 and the compressor suction is in 3. Normally, a 4 way valve invert the condenser and the evaporator (2 and 4). Here it was decided to always use the condenser with pipe number 2 and the evaporator with pipe number 4.

In heat pump mode, the coil is not energized (like the fig on the left). So everything is connected properly for the heat pump mode (compressor discharge (1) to the condenser (2) and evaporator (4) to compressor suction (3)). The flow goes from (1) to (2) and from (4) to (3).

In ORC mode, the compressor is started with the coil energized to place the piston chamber in its right position: it moves to the right. After that the cycle can be started in ORC mode: evaporator (4) connected to the compressor discharge = expander suction (1) and compressor suction = expander exhaust (3) to the condenser (2). The flow goes from (4) to (1) and from (3) to (2).

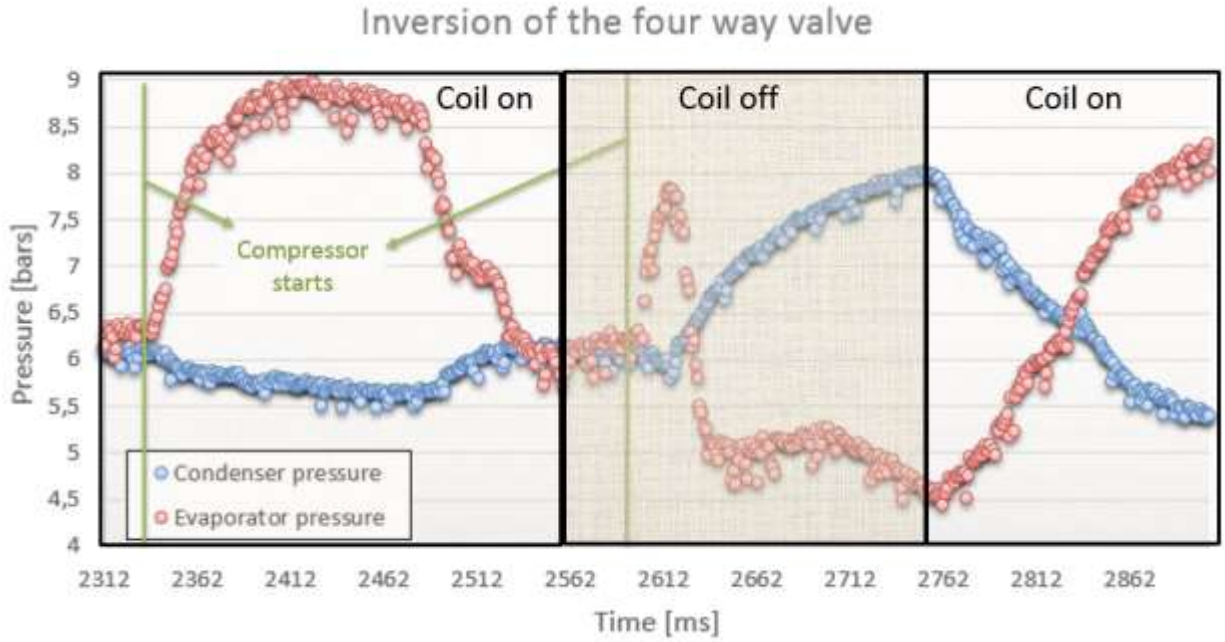

References

- Baek, J. S., Groll, E. A., Lawless, P.B., 2005. Piston-cylinder work producing expansion device in a transcritical carbon dioxide cycle. Part I: experimental investigation, International Journal of Refrigeration 28, 141–151.

- Bettgenhauser, K., Offermann, M., Boermans, T., Bosquet, M., Gr€ozinger, J., von Manteuffel, B., and Surmeli, N., 2013. Heat Pump Implementation Scenarios Until 2030: An Analysis of the Technology's Potential in the Building Sector of Austria, Belgium, Germany, Spain, France, Italy, Sweden and the United Kingdom, ECOFYS Germany GmbH, Koln, Germany, ECOFYS Report, Project No. BUIDE12080.

- Brasz, J., Smith, I., Stosic, N., 2000. Development of a twin Screw expressor as a throttle valve replacement for water-cooled chillers, proceedings of the International Compressor Engineering Conference, Purdue.

- Dickes, R., Dumont, O., Quoilin, S., Lemort, V., 2017. Modelling of organic Rankine cycle power systems in off-design conditions: an experimentally-validated comparative study, Energy, 10.1016/j.energy.2017.01.130.

- Dumont, O., Quoilin, S., Lemort, V., 2014. Experimental investigation of a Scroll unit used as a compressor and as an expander in a Heat Pump/ORC reversible unit, International Refrigeration and Air Conditioning Conference, Purdue, 2014.

- Dumont, O., Quoilin, S., Lemort, V., 2015. Experimental investigation of a reversible heat pump / organic Rankine cycle unit designed to be coupled with a passive house (Net Zero Energy Building), International Journal of Refrigeration, http://dx.doi.org/10.1016/j.ijrefrig.2015.03.008.

- Emerson Climate Technologies, 2015, "Selection Software", accessed April 15th, http://selectonline.emersonclimate.eu/

- European Comission, 2012. Energy markets in the European Union in 2011, ISBN: 978-92-79-25489-5, DOI: 10.2833/12806.

- European Commission, 2013. Progress by Member States towards Nearly Zero-Energy Buildings, COM (2013) 483

- European Committee for Standardization, 2005, "Refrigerant compressors - Rating conditions, tolerances and presentation of manufacturer's performance data", European Standard Ref. No. EN 12900:2005:E

- Hsieh, Y. Y., & Lin, T. F., 2002, "Saturated flow boiling heat transfer and pressure drop of refrigerant R-410A in a vertical plate heat exchanger," International Journal of Heat and Mass Transfer, **45**(5), pp. 1033-1044. doi:16/S0017-9310(01)00219-8

- Innogie ApS, 2013. Thermal solar absorber system generating heat and electricity, United States Patent Application Publication, US 2013/025778 A1.

- Kreider, Jan F., Peter Curtiss, and Ari Rabl, 2009, "Heating and Cooling of Buildings (2nd Edition)". McGraw-Hill, ISBN: 1-4398-1151-2.

- Kuo, W. S., Lie, Y. M., Hsieh, Y. Y., & Lin, T. F., 2005, Condensation heat transfer and pressure drop of refrigerant R-410A flow in a vertical plate heat exchanger, International Journal of Heat and Mass Transfer, **48**(25-26), pp. 5205-5220. doi:16/j.ijheatmasstransfer.2005.07.023

- Lemort V., 2009. Contribution to the characterization of scroll machines in compressor and expander modes, PhD Thesis, University of Liège, Liège.

- Lemort V., Declaye S., and Quoilin S., 2011. Experimental characterization of a hermetic scroll expander for use in a micro-scale Rankine cycle, Proceedings of the Institution of Mechanical Engineers, Part A: Journal of Power and Energy, **226**(1), pp. 126-136.

- Marszal, A. J., P. Heiselberg, J. S., Bourrelle, E. Musall, K. Voss, I. Sartori and A. Napolitano. 2011. Zero Energy Building – A review of definitions and calculation methodologies., Energy and Buildings, Volume 43, Issue 4, Pages 971-979, ISSN 0378-7788, Zero Energy Building – A review of definitions and calculation methodologies.

- Nikolov, A., Brümmer, A., 2017. Investigating a Small Oil-Flooded Twin-Screw Expander for Waste-Heat Utilisation in Organic Rankine Cycle Systems, energies, 10(7):869.

- Peris B., Dumont O., Quoilin S., Navarro-Esbría, J., 2016. Internal combustion engines cooling water valorization through invertible HTHP/ORC systems, 2016. Symposium waste heat valorization in industrial processes, Kortrijk, Belgium.

- Quoilin, S., 2011. Sustainable Energy Conversion Through the Use of Organic Rankine Cycles for Waste Heat Recovery and Solar Applications, Ph.D. thesis, University of Liège, Liège, Belgium.

- Quoilin, S., Dumont, O., Harley, K., Lemort, V., 2016. Design, Modeling, and Performance Optimization of a Reversible Heat Pump/Organic Rankine Cycle System for Domestic Application, Journal of Engineering for Gas Turbines and Power, 138, 011701-9, DOI: 10.1115/1.4031004.

- Schimpf, S., Uitz, K., Span, R., 2011. Simulation of a solar assisted combined heat pump-organic Rankine cycle system. In: Proceedings of World Renewable Energy Congress 2011 Sweden.

- Thonon B., 1995. Recent research and developments in plate heat exchangers, Fuel and Energy Abstracts, 36, DOI:10.1016/0140-6701(95)96878-G

- Zanelli, R., and Favrat, D., 1994, Experimental Investigation of a Hermetic Scroll Expander–Generator, 12th International Compressor Engineering Conference, West Lafayette, IN, July 19–22, pp. 459–464.

Chapter IV:

Experimental investigation of a reversible HP/ORC system: case of a residential heat pump combined with solar panels

"Only those who attempt the absurd will achieve the impossible."
Maurits Cornelis Escher

Abstract

A reversible HP/ORC test rig is mounted and tested in a wide range of operating conditions. The technical feasibility of the system is demonstrated. A cycle efficiency of 4.2% is achieved in ORC mode (with condensation and evaporation temperature respectively of 25°C and 88°C) and a COP of 3.1 is obtained in HP mode (with condensation and evaporation temperature respectively of 61°C and 21°C). A comparison between theoretical prediction and experimentation is proposed. Finally, a semi-empirical model allows to extrapolate the performance of the system in a wide range of conditions.

1 INTRODUCTION

Chapter three has demonstrated that the reversible HP/ORC system integrated into a residential building coupled with a solar roof is theoretically a promising way to obtain a Positive Energy Building (PEB). In this thesis, a PEB is defined as a building that produce more energy than it consumes on a yearly basis. As Steve Albini said: "*Doubt the conventional wisdom unless you can verify it with reason and experiment*." Thus, based on the optimal sizing performed in Chapter three, a prototype is built and tested to assess the real

performance of the system. Moreover, a global methodology to handle experimental data is developed. It allows to select the outliers that needs to be rejected, to assess the quality of the data and to improve its accuracy with mathematical tools (Gaussian Process (GP) and Reconciliation Method (RM)). The performance of the prototype is analysed and discussed. Also, a semi-empirical model is developed to predict the performance outside of the operational conditions achieved on the test-rig. This model is useful to run dynamic simulations with an optimized control (Chapter five).

2 EXPERIMENTAL SETUP

2.1 INTRODUCTION

The concept of a reversible HP/ORC system integrated into a residential building with a solar roof has already been described in detail in Chapter three. This section focuses on the layout and a complete description of the components and sensors of the test-rig. The components have been sized following the optimal sizing performed in Chapter three.

2.2 LAYOUT

In order to verify the promising simulation results described previously (Chapter 3), an experimental study is performed on a HP/ORC prototype working with refrigerant R134a (appendices: Figure 31). A scheme of the test rig is outlined in Figure 1 with the main elements shown: compressor, evaporator, condenser, pump and valves. The refrigerant loop (dark blue) also includes a liquid receiver for charge variations and a sub-cooler used to provide a sufficient degree of sub-cooling at the inlet of the pump. This loop also includes a four-way valve that allows for switching between ORC and HP modes and a bypass valve that is necessary to start the expander in ORC mode. The evaporator is supplied by a water loop (red) connected to an electrical boiler (150 kW). The condenser is cooled by tap water (light blue) to simulate the cold water flow in the storage or the ground heat exchanger, depending on the mode of operation. In this test-rig, the oil flow is ensured trough an optimal sizing of the piping. The diameter of the piping is sized to obtain the minimum required speed (0.5m/s for liquid and 10m/s for vapour) of fluid at part load. For small-scale ORC power systems, this method of lubrication is usually preferred to an additional oil separator which requires an oil tank, a liquid level sensor, an additional pump…

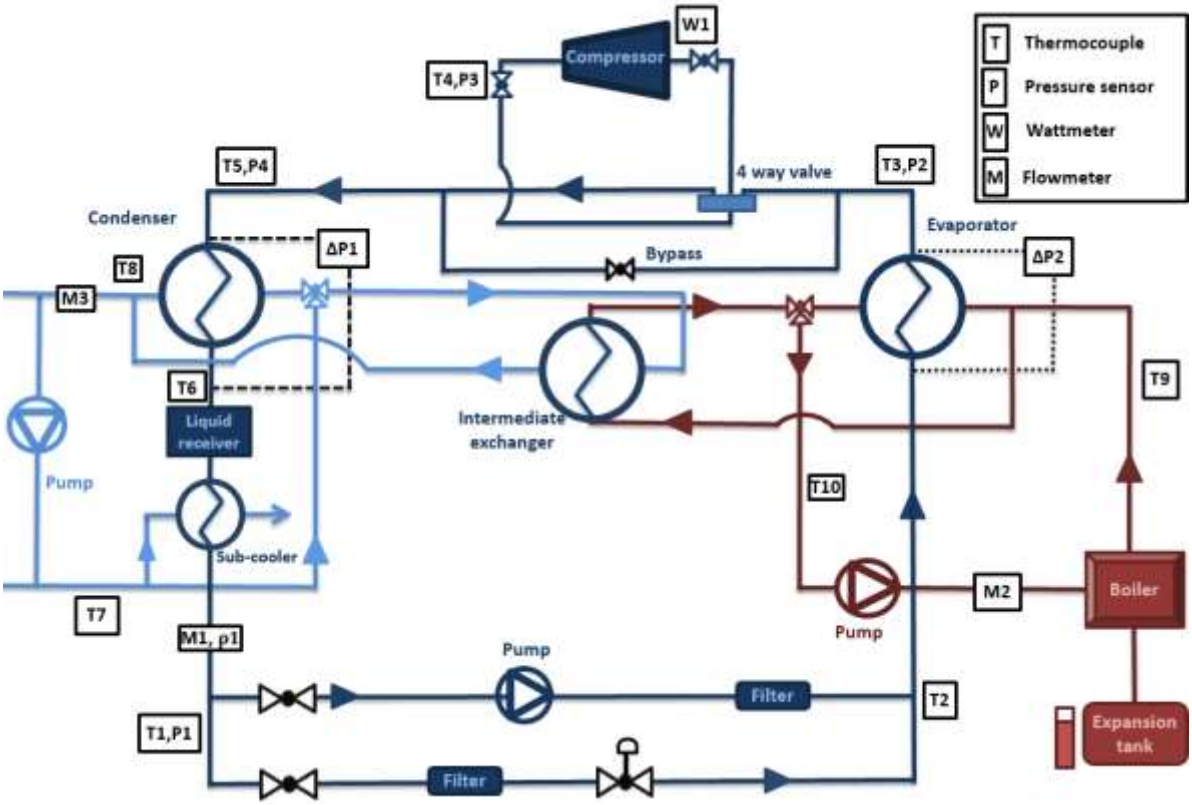

Figure 1: Detailed scheme of the experimental setup (dark blue = refrigerant loop, red = heating loop and light blue = cooling loop)

2.3 COMPONENTS

The design step and technological choices were based on Chapter three. The selected components will therefore only be briefly presented in this chapter.

To the author knowledge, it is the first time that an off-the-shelf HVAC scroll compressor has been used as a compressor and as an expander in the same application. The compressor has been modified following the methodology proposed by Quoilin (Quoilin, 2011). These modifications include the opening of the casing, the removal of the check valve and the addition of a spring below the floating seal (Figure 2).

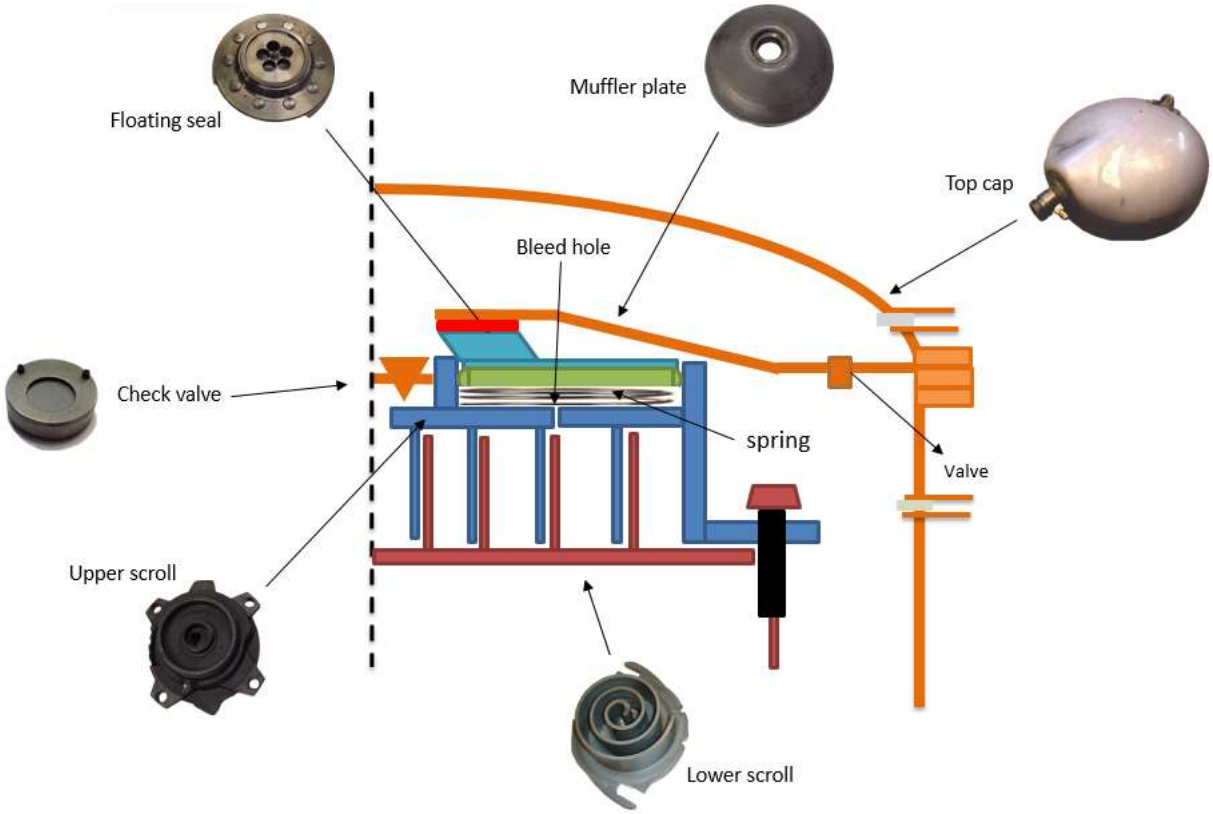

Figure 2 : Scroll compressor modified to work as an expander.

Plate-type heat exchangers are used for the evaporator and condenser (Table 1) they are selected for their compactness, efficiency and low cost. The pump is a volumetric plunger-type pump. The pump's rotational speed is controlled by an inverter (Table 1). An electronic expansion valve is chosen for its controllability compared to traditional expansion valves (Table 1).

Table 1: Technical data of the compressor, evaporator, condenser, pump and expansion valve

Component	Parameter	Value
Compressor	Displacement (compressor mode) [cm^3]	82.6
	Built-in volume ratio [-]	2.8
	Max pressure [bar]	32
	Motor power at max current [kW]	4
Evaporator	Exchange area [m^2]	4.08
	Max. pressure [bar]	32
	Max temperature [°C]	225
Condenser	Exchange area [m^2]	3.12
	Max. pressure [bar]	32
	Max temperature [°C]	225
Pump	Maximum flow [l/min]	15.1 (at 1725 RPM)
	Max. pressure [bar]	206
	Max temperature [°C]	121
	Motor [kW]	1.5
Expansion valve	Flow direction	Unidirectional
	Max. pressure [bar]	45
	Max temperature [°C]	100
	Nominal thermal heat at the condenser[kW]	13

2.4 SENSORS

This section summarizes the data acquisition system together with the technical data of the sensors. The pressure and flow sensors are described in Table 2. A Coriolis flowmeter is used to measure the refrigerant mass flow rate with high accuracy. The cold loop and hot loop water volumetric flow rates are measured manually with water counters. All temperatures are measured by T-type thermocouples. Their measuring range is between −200 °C and 350 °C, with a maximum error of ± 0.5 K. Watt-meters are used to measure the electrical power consumption of the pump and compressor.

Table 2: Sensors technical data (FS = full scale)

Sensors	Measured variable	Range	Accuracy [%FS]
Pressure	Condenser in and Condenser ex [bar]	[0:25]	0.5
	Evaporator ex [bar]	[0:40]	0.5
	Cold water and hot water [bar]	[0:6]	0.5
	Scroll suction port (compressor) [bar]	[0:20]	0.05
	Scroll ex (compressor) [bar]	[0:40]	0.3
	Δ condenser [bar]	[0:0.3]	0.5
	Δ evaporator [bar]	[0:0.15]	0.5
	Δ scroll [bar]	[0:20]	1
Flow	Refrigerant mass flow rate [kg/s]	[0:0.3]	0.2
	Cold water volume flow rate [m^3/h]	[0:3]	1
	Hot water volume flow rate [m^3/h]	[0:10]	1
Wattmeter	Pump consumption [W]	[-2000:2000]	0.5
	Compressor consumption /expander production [W]	[-6000:6000]	0.5

2.5 COSTS

Figure 3 presents the cost of the necessary components to build such a HP/ORC prototype, and excluding the costs of the high-accuracy data-acquisition equipment, which is necessary in a prototype unit, but not in the final application. Compared to a traditional heat pump, it can be noted that the additional cost is the pump (i.e. the only required additional main component to turn a heat pump into a HP/ORC unit) representing only 14% of the total unit cost. This statement suggests that HP/ORC units would present a relatively small additional cost compared to traditional heat pumps. It should also be noted that all these costs are prototyping costs and would be significantly lower in case of large-scale industrial production.

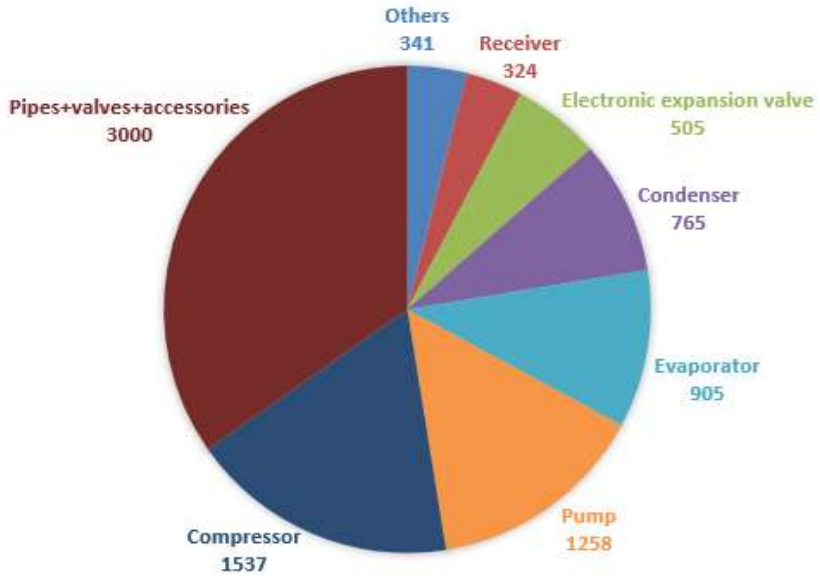

Figure 3: Price of the components of the reversible HP/ORC unit [€].

3 GLOBAL METHODOLOGY TO HANDLE EXPERIMENTAL DATA

3.1 INTRODUCTION

Measurements are always affected by random errors plus gross errors (error that cannot be explained with statistical distribution). Gross errors are outliers (process leaks and malfunction) or bias (systematical offset). These errors can lead to wrong analysis and understanding of the processes. Furthermore, the quality of the calibration of models is better when the errors are low. The use of reconciled values (see section 3.2) instead of raw data improves the accuracy of the prediction of the models. This is helpful in the context of this experimental campaign. The impact of the lubricating oil on the performance is significant in this experimental campaign (see section 4). For this reason, a brief description of the refrigerant-oil mixture and behaviour is proposed in annex (see section 7.1).

3.2 RECONCILIATION METHOD

This section presents the application of a mathematical tool called the reconciliation method (RM). The latter is recommended to obtain reliable information about the studied process but gross errors have to be identified and eliminated before the procedure. This technique has been used since 1961 in chemical engineering (Kuehn et al., 1967). In 1980, the reconciliation method was applied to adjust material balancing of mineral processed data - the process of separating commercially valuable minerals from their ores - (Hodouin et al., 1980). Later, Weiss and Romagnoli used this tool to better determine regeneration cycle time of a reactor in an industrial case study (Weiss et al., 1996). Heyen and Kalitventzeff developed a RM optimization to reduce energy use in production plants (Heyen et al., 1997). Placido and Loureiro studied the placement of new instruments in order to improve the estimation accuracy in ammonia plant units (Placido et al., 1998). Schladt and Hu developed

a rigorous model to estimate concentrations in a distillation column through the reconciliation method (Schladt, 2006). In 2008, Lid and Skogestad used the RM method to assess the optimal operation of a catalytic naphta reformer (Lid et al., 2008). Despite the proven performance of the method, few authors have used it in refrigeration systems. In 2007, Bruno et al., applied the method to a Hybrid solar/gas Single/Double effect absorption chiller (Bruno et al., 2007). In 2013, Martinez-Maradiaga et al. used the method for absorption refrigeration system to obtain performance calculations that are in agreement with the laws of conservation (Martinez-Maradiaga et al., 2013). In 2015, an optimization of redundant measurements location for thermal capacity of power unit steam boiler using data reconciliation method was performed (Szega, 2015). Finally, a data reconciliation based framework for integrated sensor and equipment performance monitoring in power plants is provided by (Jiang, 2014).

Some authors have predicted unmeasured values (flowrate, oil fraction etc.) simply by minimizing the sum of the residue of each component (Cuevas, 2006). A more complete and accurate method taking into account measurements redundancy and accuracy of sensors exists: the reconciliation method corrects each measurement as little as possible, taking its precision into account (assuming a Gaussian distribution around the measured value), in order to satisfy all constraints and to evaluate the most probable physical state conservation (Martinez-Maradiaga et al., 2013). Redundancy is obtained by having two sensors measuring the same variable and/or variable that can be obtained through balance equations (heat balance, residue, mass balance, thermodynamic state of equilibrium etc. This redundancy allows correcting measurements while non-redundant measurements will remain uncorrected. The RM method does not correct data to better fit a model but simply imposes constrains (physical laws) to improve the dataset intrinsic quality.

Reconciliation method should be used for multiple reasons. First, without this method, it is impossible to close energy and mass balances exactly, which is needed for predictive models. Also, it allows determining some unknowns that are not or that cannot be measured precisely (oil fraction, refrigerant mass flow rate etc.) Moreover, it fully exploits the collected measurements with redundancy. Finally, it allows to know which sensor should be checked or replaced if necessary.

Mathematically, the minimization of Eq. 1 allows to evaluate corrected (or reconciled) values (c_i) (and eventually additional unkowns) based on the measured values (u_i) and on their standard deviation (σ_i) while satisfying a certain number of constraints (Eq. 2).

$$\varphi(u_i) = \sum_{i=1}^{n} \frac{(u_i - c_i)^2}{\sigma_i^2} \quad (1)$$

$$\psi(c_i, z_k) \leq 0 \quad (2)$$

3.2.1 Validation of reconciliation

Data reconciliation is based on two main assumptions. On the one hand, most influent physical phenomena should be correctly described. This first assumption is reached using the validation of measurements. The validation of measurements is achieved by checking heat balances on the different components, cross-checking of pressures etc.

On the other hand, it assumes a Gaussian distribution of the errors. This needs to eliminate gross error (outliers). In this work, a Kriging method (or Gaussian process regression) is used in this aim (section 3.3). Other advanced methods exist to treat gross errors in data reconciliation: those proposed by Fair, Welsch, Hampel, Cauchy, logistic, Lorentzian and Quasi-Weighted Least Square, for example (Prata et al., 2010; Ozyurt et al., 2004; Zhang et al., 2010). Finally, to check the confidence of the corrected values, heat balances and residues should be verified a posteriori and the weighted deviation (w_i) should be evaluated (Eq. 3) to give the confidence level of the correction.

$$w_i = \frac{|u_i - c_i|}{\sigma_i} \qquad 3$$

The weight is a random variable following a χ-squared distribution with γ, the degree of freedom. The degree of freedom is equal to the number of reconciled variables minus the number of constraints (= the redundancy level). For example, the confidence level of the RM with a redundancy level of 5, a weight of 1.145 and 21 measured variables is 95%.

3.3 GAUSSIAN PROCESS

Gaussian processes, also known as Kriging regression, provide an automatic and robust framework to perform multivariate regressions and, thereby, constitutes an interesting tool to explore high-dimensional data (Rasmussen, 2006). Their Bayesian formulation allows predicting the variable of interest for new/unseen data points and provides coherent estimates of predictive uncertainty. The method reduces predictive confidence when extrapolating away from the data points: if the data density is locally high, the variance is small; on the opposite side, if the density is low, the variance is larger, leading to more distant confidence boundaries. Furthermore, the method is highly flexible and can accommodate a range of covariance structures, including non-linear relationships, and delivers state of the art prediction performance. It has been successfully applied to a variety of domains, including geostatistics, economics and cognitive neuroscience. It can be shown that Gaussian processes perform better than traditional linear regression in multiple ways. They are less subject to over-fitting and to the Runge phenomenon and exhibit a better behaviour outside of the fitting range. They build an underlying smooth representation of the data, which can then be compared to the actual distribution of the experimental data and provide a measure of the noise (Quoilin et al., 2016). The performance indicator selected for this work is the mean absolute error (MAE), computed with normalized values, Eq. 4.

$$MAE = \frac{1}{n}\sum_{i=1}^{n}|y_i - f(x_i)| \quad (4)$$

This method allows to:

- Evaluate the quality of the data with the MAE.
- Eliminate of the irrelevant measurements (outliers). An example is given in Figure 4 where the rejection criterion is based on a 1.96 standard deviation. Points 7 and 90 are therefore considered as outliers in this case.

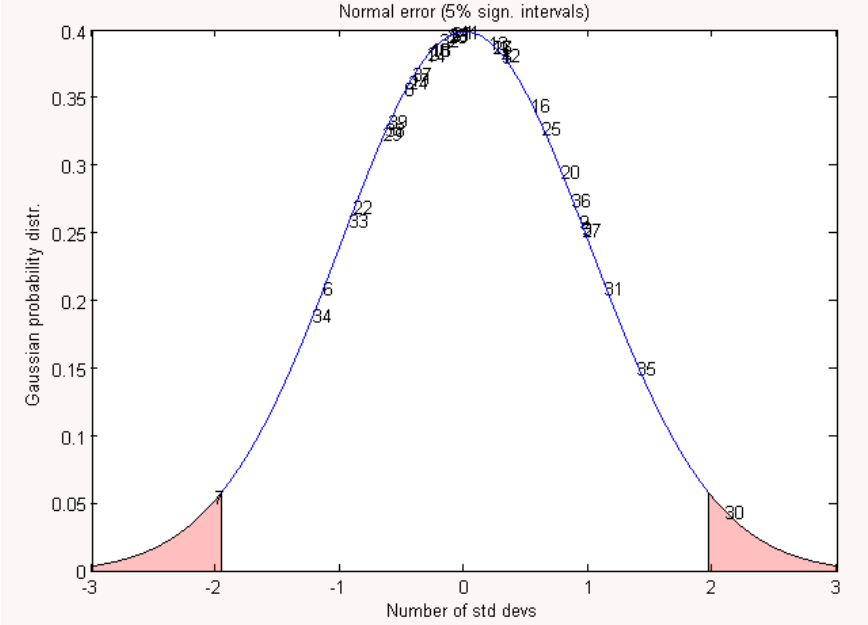

Figure 4: Gaussian probability versus standard deviation

- It provides the more relevant inputs that should be used to establish a cartography with a given output (thanks to the MAE). First, the MAE decreases when adding relevant inputs. But adding more and more inputs induces noise to the input-to-output relation which is increasing the MAE. The MAE is therefore the indicator that decides the number of input to take into account for predictive models. Figure 5 shows an example where three variables should be chosen to predict the given output (Pex, Pinj and Psu).

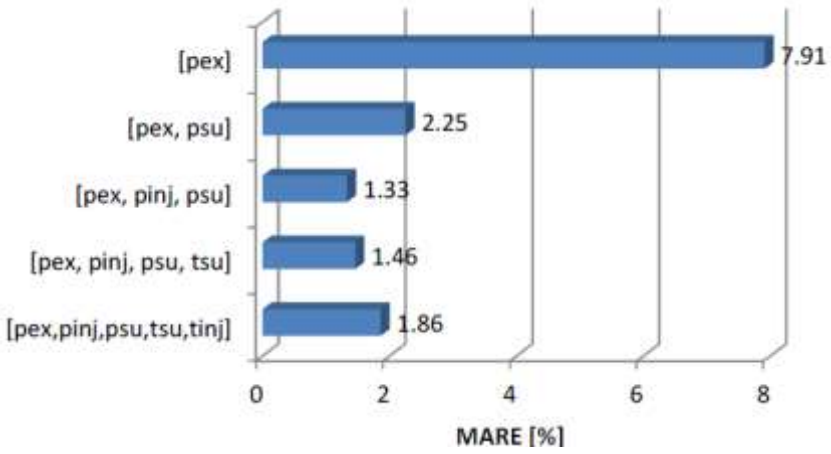

Figure 5: Example to choose the relevant inputs for a predictive model thanks to the MARE (Quoilin et al., 2014)

3.4 MEASUREMENTS VALIDATION

Experimental campaigns are often subject to measurements issues such as sensor malfunction, operator misuse or data acquisition failure. Therefore, it is of primary importance to crosscheck the experimental data for consistency using all possible redundancies in the measured data, performing heat balances on all components and checking that the measured data is self-consistent. The following verifications have been performed in the case of the reversible HP/ORC system:

- Global energy residual neglecting the heat losses in the piping (Eq. 5 (annex: Figure 33 and Figure 34)).

$$Res_{global} = \dot{Q}_{ev,w} + \dot{W}_{cmp/exp,el} - \dot{Q}_{cd,w} - \dot{Q}_{sc,r} + \dot{W}_{pp,el} \quad 5$$

- Heat balance on the condenser and evaporator (Eq. 6 appendices Figure 37-Figure 40).

$$\dot{m}_r\left(h_{r,su} - h_{r,ex}\right) + \dot{m}_{oil}.cp_{oil}.\left(t_{r,su} - t_{r,ex}\right) = \dot{m}_w.cp_w\left(t_{w,ex} - t_{w,su}\right) \quad 6$$

- Residual on the compressor and expander (Eq. 7, appendices : Figure 41 and Figure 42).

$$Res_{cmp} = \left|\dot{W}_{cmp,el} - \dot{m}_r\left(h_{r,ex} - h_{r,su}\right) - \dot{m}_{oil}.cp_{oil}.\left(t_{r,ex} - t_{r,su}\right) - \dot{V}_{oil}(P_{oil,ex} - P_{oil,su}) - \dot{Q}_{cmp,amb}\right| \quad 7$$

The verifications show that the residual of each balance is lower than the uncertainty propagation error for the different components for almost all the points. The few exceptions encountered can be explained by the solubility of oil and ambient losses not having been taken into account. Measurements are presented in two separate tables (Dumont, 2014(b)).

3.5 GLOBAL METHODOLOGY

Following the different methods described here above, a step by step global methodology can be drawn to handle experimental data efficiently (Figure 6). First, the measurements have to be validated: energy and mass balances have to be satisfied taking into account the propagation of errors due to measurement devices. This step insures the quality of the data, but is also necessary to apply correct physical constraints (Eq. 2) in the reconciliation method. Following this, the elimination of irrelevant points (outliers) is mandatory to eliminate gross error (which is mandatory for the reconciliation method). The Gaussian process is a efficient tool to perform this task. Finally, the reconciliation method can be applied and validated through the weights and confidence level (Eq. 3). Later, when an empirical or semi-empirical model is developed, the Gaussian process also helps to identify which inputs should be selected to predict a given output.

Figure 6 : Global methodology to threat experimental data.

3.6 APPLICATION OF THE METHOD TO THE CASE STUDY

The oil mass fraction is not measured despite of its strong influence on the results. The reconciliation method allows to evaluate it. The method is presented in the case of the organic Rankine cycle operation. The same approach is considered for the heat pump.

3.6.1 Model: assumptions and constraints

First, a zero pressure drop is assumed in the pipes around the condenser (Figure 1). The redundancy on pressure measurements leads to the first constraint (Eq. 8).

$$\Delta P_{cd} = P_{cd,su} - P_{cd,ex} \quad (8)$$

Also, the 1st Principle of Thermodynamics is applied to the expander (Eq. 9) with the following hypotheses: perfect mixture between oil and refrigerant, kinetic and potential energy neglected and ambient losses are evaluated with (Eq. 10). Two unmeasured variables are added (ambient temperature (T_{amb}) and heat transfer coefficient between the expander and the ambient (U)) because they play an important role in the heat balance of the expander.

$$\dot{W}_{exp,el} = \dot{m}_r\left(h_{exp,su} - h_{exp,ex}\right) + m_{oil}.c_{p,oil}.\left(t_{exp,su} - t_{exp,ex}\right) + \dot{V}_{oil}(P_{oil,ex} - P_{oil,su}) - \dot{Q}_{exp,amb} \quad (9)$$

$$\dot{Q}_{exp,amb} = AU_{exp}.\left(t_{exp,m} - t_{amb}\right) \quad (10)$$

The density measurement allows to evaluate the mass conservation at the inlet of the pump (Eq. 11).

$$\frac{1}{\rho_{meas}} = \frac{x_{oil}}{\rho_{oil}} + \frac{(1 - x_{oil})}{\rho_r} \quad (11)$$

Finally, heat balances are performed on the evaporator (Eq. 12) and on the condenser (Eq. 13) neglecting ambient heat losses and supposing a perfect mixture of oil and refrigerant.

$$m_{ev,w}.c_{p,w}.\left(t_{ev,w,su} - t_{cd,w,ex}\right) = \dot{m}_r\left(h_{ev,ex} - h_{ev,su}\right) + \dot{m}_{oil}.c_{p,oil}.\left(t_{ev,ex} - t_{ev,su}\right) \quad (12)$$

$$m_{cd,w}.c_{p,w}.(t_{cd,w,ex} - t_{cd,w,su}) = m_r\left(h_{cd,su} - h_{cd,ex}\right) + m_{oil}.c_{p,oil}.(t_{cd,su} - t_{cd,ex}) \quad (13)$$

Considering these assumptions, 5 constraints equations allow exploiting the redundancy of the measurements.

3.6.2 Optimization function and redundancy level

In this case study, the number of unknowns is equal to 24: there are 21 measurements to reconcile, plus two additional variables (expander heat transfer coefficient and ambient temperature), plus the oil mass fraction. To ease the solver, the guess of the corrected

values are imposed to be equal to measurements. The standard deviation for each sensor is computed following sensor datasheet. Finally, the maximisation of Eq. 1 is performed while respecting the 5 constraints (Eqs. 9-13) for each steady-state point. The redundancy level is simply equal to the number of constraints (5 in this case).

3.6.3 Results

41 steady-state measurements points are reconciled. The results obtained from the reconciliation method are detailed for one point in Table 3. For each measurement, the original value, the reconciled value, the weight (Eq. 3) and the confidence level are given. The ambient temperature (*t11*) and the heat exchange coefficient of the expander (*U*) are not measured but are estimated with a large standard deviation to evaluate (Eq. 10). The method applied to a typical point (Table 3) leads to an oil mass fraction of 6.2% which is a realistic value compared to the amount of oil and refrigerant injected in the system. Logically, measurements with high accuracy (i.e. low standard deviation) are very slightly (or not at all) corrected. The weighted correction is not really a reliable assessment of confidence since correction will be zero for non-redundant variables. They will not be corrected and results are therefore optimistic in Table 3. A reliable criterion is to use the value of the objective function Ψ (Eq. 1), that should follow a χ-square distribution. In this case, the confidence of the reconciliation method reaches a probability of 73%. A detailed comparison of the prediction of performance with and without this method is performed in section 5.

Table 3 : Results from reconciliation method for one point. The nomenclature is detailed in Figure 1.

Measurement	Std. deviation	Original value	Reconciled value	Weight	Confidence
t1 [°C]	0.5	16.02	16.02	0	1
t2 [°C]	0.5	17.14	17.11	0.0549	1
t3 [°C]	0.5	99.3	99.31	0.0265	1
t4 [°C]	0.5	98.5	98.38	0.2181	0.9998
t5 [°C]	0.5	63.14	63.11	0.0634	1
t6 [°C]	0.5	34.53	34.65	0.2406	0.9997
t7 [°C]	0.5	11.51	11.24	0.5438	0.9973
t8 [°C]	0.5	31.54	31.82	0.5438	0.9973
t9 [°C]	0.5	105	104.9	0.1635	0.9999
t10 [°C]	0.5	83.68	83.76	0.1635	0.9999
t11 [°C]	10	20	19.64	0.0070	1
P1 [bar]	0.0625	8.325	8.325	0.01386	1
P2 [bar]	0.1	28.45	28.56	1.075	0.9826
P3 [bar]	0.06	28.59	28.56	0.6045	0.9963
P4 [bar]	0.0625	8.608	8.599	0.1411	0.9999
DP1 [bar]	0.0012	0.2738	0.2738	0	1
DP2 [bar]	0.00075	0.06781	0.06781	0	1
M1 [g/s]	0.000235	0.235	0.235	0.0158	1
M2 [l/s]	0.02984	0.5968	0.5863	0.3521	0.9992
M3 [l/s]	0.02495	0.499	0.5255	1.062	0.9831
W1 [W]	0.25	2630	2630	0.0872	1
U [W/(m^2.K)]	2	10	10.02	0.00863	1
ρ1 [kg/m^3]	24.25	1209	1213	0.4359	0.9985

4 EXPERIMENTAL RESULTS

Measurements are performed in steady–state conditions and averaged on a five minutes basis (one second interval). All the data is presented with the reconciled dataset (not the gross measurement). Performance in both heat pump and organic Rankine cycle modes is measured.

4.1 HEAT PUMP PERFORMANCE

4.1.1 Range of operating conditions and achieved performance

Table 4 presents the variation range of the main operating conditions observed in heat pump mode for the 31 stabilized measurement points (Dumont, 2014(b)). Performance is assessed in terms of coefficient of performance (*COP*), volumetric effectiveness and isentropic efficiency, defined according to Eqs. 14-16. $\dot{m}_{tot}$ is defined as the sum of refrigerant and oil mass flow rates. Table 4 also shows the condenser thermal power on the refrigerant side ($\dot{Q}_{cd,r}$), the electrical power consumption of the compressor ($\dot{W}_{cmp,el}$), the evaporation pressure (P_{ev}) and condensation pressure (P_{cd}).

$$\eta_{cmp,is} = \frac{\dot{m}_{tot}(h_{cmp,ex,is} - h_{cmp,su})}{\dot{W}_{cmp,el}} \quad 14$$

$$\varepsilon_{cmp,vol} = \frac{\dot{V}_{cmp,su}}{\dot{V}_{cmp,th}} \quad 15$$

$$COP = \frac{\dot{Q}_{cd,r}}{\dot{W}_{cmp,el}} \quad 16$$

Table 4: Minimum and maximum values of the main parameters in HP mode

Parameter	Nom.	Minimum	Maximum
Condenser thermal power [kW]	$\dot{Q}_{cd,r}$	9	17
Evaporation pressure [bar]	P_{ev}	3	6.5
Condensation pressure [bar]	P_{cd}	6	20.5
Mass flow rate [kg/s]	$\dot{m}_{tot}$	0.049	0.113
Compressor power consumption [kW]	$\dot{W}_{cmp,el}$	1.87	4.3
Coefficient of performance [-]	COP	2.7	7.1
Compressor isentropic efficiency [%]	$\eta_{cmp,is}$	69	79
Compressor volumetric effectiveness [%]	$\varepsilon_{cmp,vol}$	95	115

4.1.2 Comparison with theoretical nominal point

In Chapter three, a nominal steady-state operating point was defined for both the HP and ORC modes. It is therefore of interest to compare the experimental data with the predicted nominal conditions. This comparison is presented in Table 5 with key performance data and in Figure 7 with the comparison of the theoretical and measured temperature-entropy diagrams. The different steps of the process are observed in Figure 7 expansion valve exhaust and evaporator supply (1), evaporator exhaust and four-way valve (Low pressure Lp) supply (2), four-way valve (Lp) exhaust and compressor supply (3), compressor exhaust and four-way valve (High pressure Hp) supply (4), four-way valve (Hp) exhaust and condenser supply (5), condenser exhaust and sub-cooler supply (6), sub-cooler exhaust and expansion valve supply (7).

Table 5: Comparison of the actual measured performance and the theoretical nominal performance (heat pump mode).

Parameter	Nom.	Theoretical nominal	Experimentation
Condenser thermal power [kW]	$\dot{Q}_{cd}$	13	11
Evaporation pressure [bar]	P_{ev}	5	4
Condensation pressure [bar]	P_{cd}	17	15.9
Mass flow rate [kg/s]	$\dot{m}_r$	0.1	0.066
Compressor power consumption [kW]	$\dot{W}_{cmp,el}$	3.09	3.5
Coefficient of performance [-]	COP	4.2	3.14
Compressor isentropic efficiency [%]	$\eta_{cmp,is}$	69	66
Compressor volumetric efficiency [%]	$\varepsilon_{cmp,vol}$	91	95

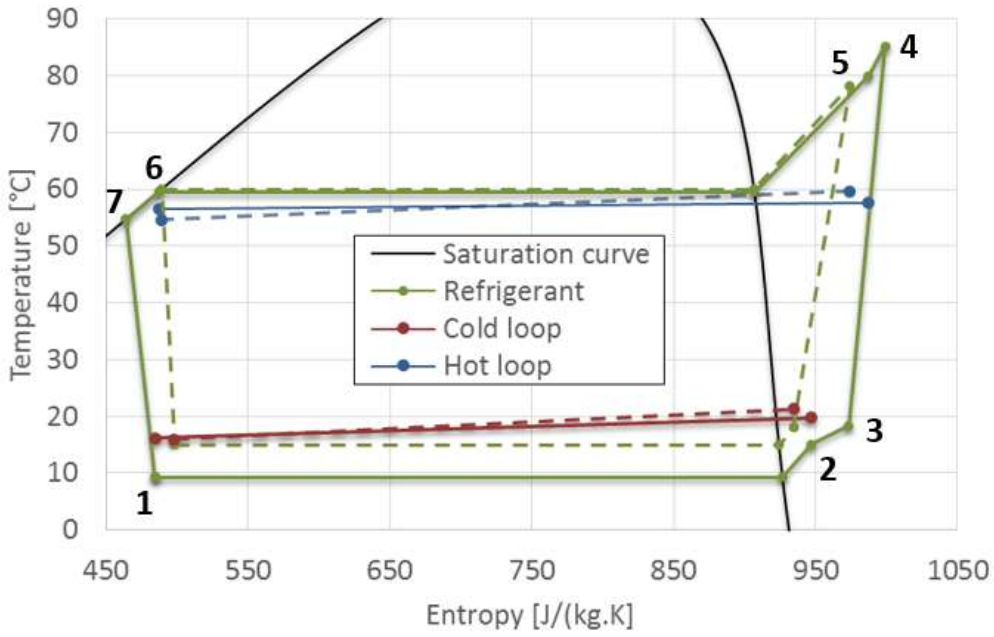

Figure 7: T-S diagram for the heat pump mode (Dashed lines = theoretical cycle, plain lines = actual cycle).

The performance of the experimental system is slightly lower than theoretical predictions for electrical power consumption and COP. This could be explained by the following elements:

- An unexpectedly high pressure drop through the four-way valve (up to 1 bar) upstream from the compressor inlet has been observed (see section 20).
- The nominal point was defined with a sub-cooling of 2K. However, in this unit, an additional sub-cooling is necessary to ensure accurate measurement in the Coriolis flowmeter (where two-phase flow is not acceptable). In Figure 7, a 6K sub-cooling is observed at the inlet of the expansion valve, 4K greater than in the theoretical model.
- Figure 7 also shows that a non-negligible heat transfer occurs between the high and low pressure sides inside the four-way valve, i.e. the refrigerant is heated before entering the compressor and the refrigerant is cooled down at the exhaust of the compressor. This heat exchange reaches a magnitude of up to 200 W depending on the data points.
- Finally, a degree of superheat higher than that assumed in the model (6K vs 3K) was imposed in the measurements. This extra superheating was necessary to avoid unsteady conditions at the compressor inlet (appendices: Figure 43)).

4.1.3 Global performance

As shown in Figure 8, and in agreement with heat pump theory, the COP decreases with an increase in the temperature lift requirement (Eq. 17). The measured COP values range between 3.1 and 3.8 around the nominal temperature lift of 45K.

$$lift = |t_{ev,sat} - t_{cd,sat}| \quad 17$$

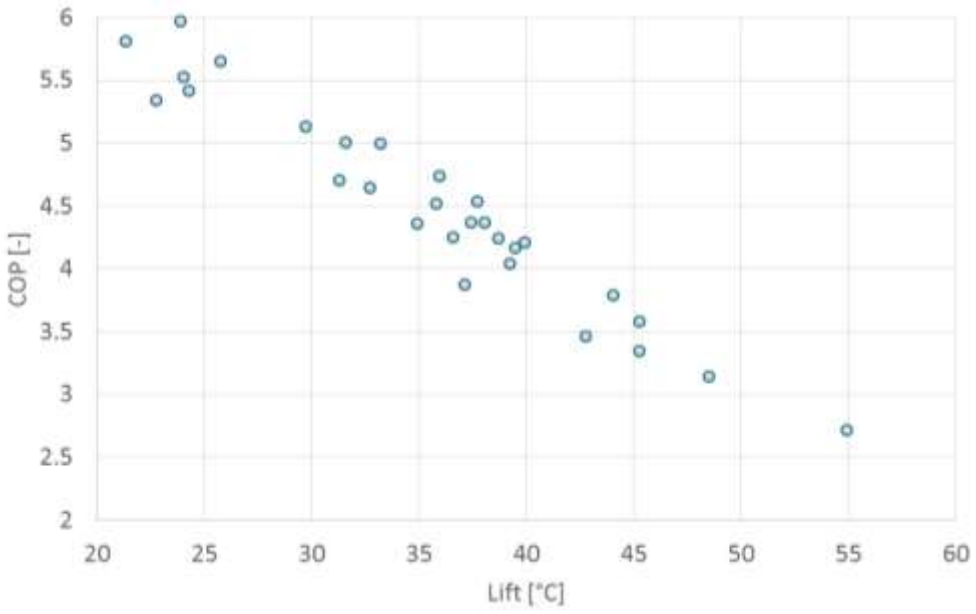

Figure 8: Evolution of the Coefficient of Performance with the temperature lift (heat pump operation).

4.1.4 Compressor performance

Figure 9 presents the isentropic and volumetric efficiencies of the compressor versus the pressure ratio. It should be noted that the evaluation of the oil mass fraction remains an unknown since there is no easy way to measure it, however, considering the amount of oil introduced in the system, the fraction is estimated to be lower than 10%. Error bars indicate its influence on the measured performance with a maximum representative 10% oil mass fraction (Eqs.18-21).

$$\dot{m}_r = (1 - x)\dot{m}_{tot} \quad (18)$$

$$\dot{m}_{oil} = x.\dot{m}_{tot} \quad (19)$$

$$\varepsilon_{cmp,vol,tot} = \frac{\dot{V}_{cmp,r,su} + \dot{V}_{cmp,su,oil}}{\dot{V}_{cmp,th}} \quad (20)$$

$$\eta_{cmp,is,oil} = \frac{\dot{m}_r(h_{cmp,ex,is} - h_{cmp,su}) + \dot{V}_{oil}(P_{cmp,ex} - P_{cmp,su})}{\dot{W}_{cmp,el}} \quad (21)$$

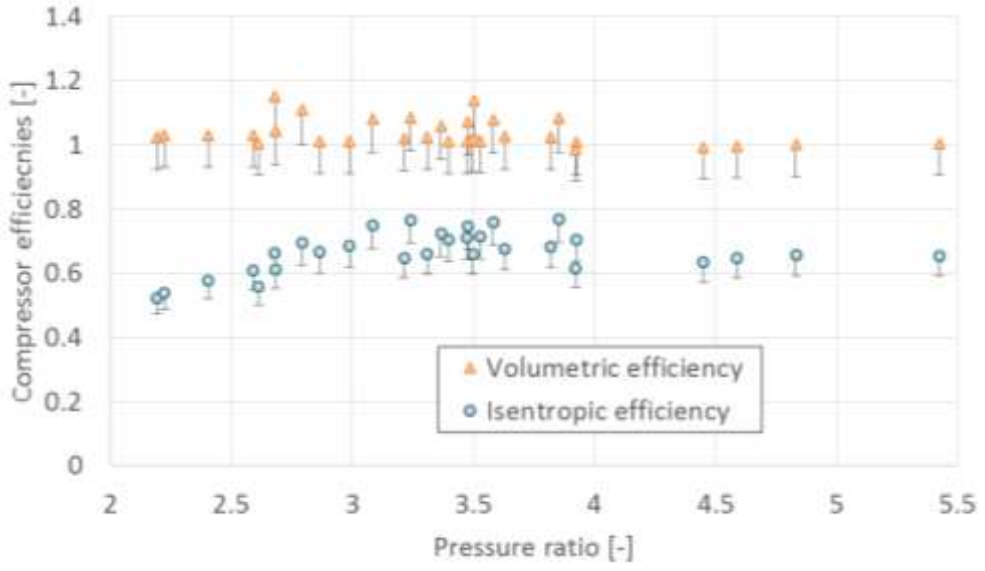

Figure 9: Evolution of the volumetric and isentropic efficiencies with the pressure ratio (heat pump mode).

The influence of the unknown oil mass fraction is greater than the influence of the sensor accuracy. The markers on the figure correspond to 0% oil mass fraction and error bars indicate the impact of a 10% oil mass fraction. Figure 9 shows that compressor volumetric effectiveness is consistently close to unity, with some relatively high values greater than 1.1. Isentropic efficiency conforms to expectations (less than 10% difference with the manufacturer data - Figure 44) and the maximum is reached at nominal volume ratio.

4.1.5 Heat exchangers

For clarity, only minimum and maximum values of the pressure drop and pinch-point in the heat exchangers are presented in Table 6. The pressure drops (Figure 10) and pinch-points are found to be small for both the evaporator and the condenser. Pressure drops are proportional to kinetic energy, presented as a function of the kinetic energy factor (Eq. 22). As the flow is always turbulent, the pressure drop is expected to be linearly proportional to the kinetic energy factor if the friction factor is considered constant.

$$\Psi = \frac{\dot{m}_r^2}{\rho} \qquad 22$$

Table 6: Exchanger performance in HP mode

Exchanger	Evaporator	Condenser
Pressure drop [bar]	[0.048:0.133]	[0.043:0.062]
Pinch-point [K]	[0.2:7.6]	[2.1:5.1]

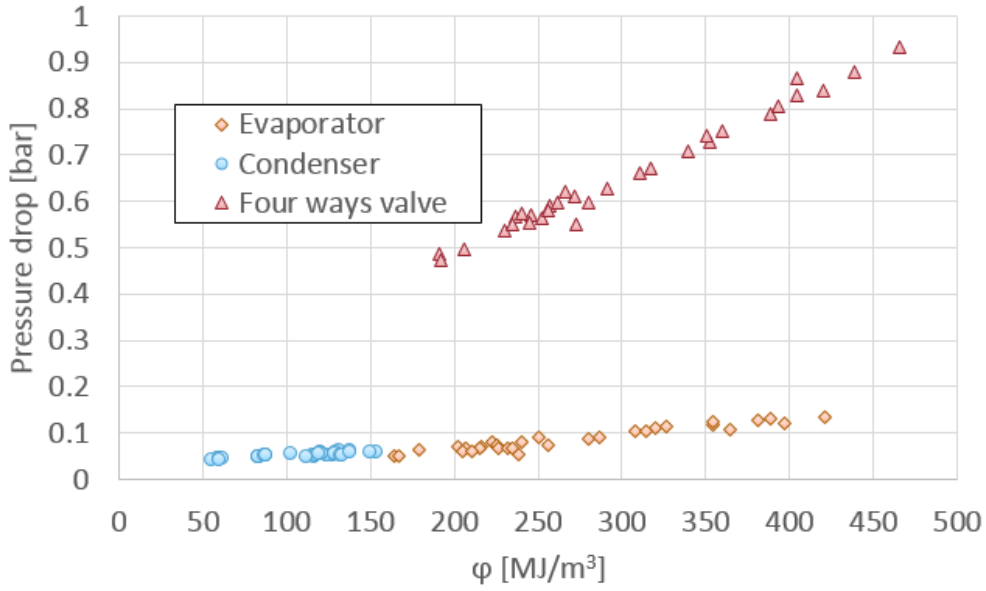

Figure 10: Evolution of the pressure drops with the kinetic energy factor (heat pump mode).

4.2 ORGANIC RANKINE CYCLE MODE

4.2.1 Range of operating conditions and achieved performance

Table 7 presents the range of the 39 stabilized measurement points in ORC mode (Dumont, 2014(b)). The performance is assessed in terms of the overall efficiency, the isentropic efficiency and the filling factor (equivalent of the volumetric efficiency for an expander) evaluated through Eqs. 21,23 and24.

$$\eta_{global} = \frac{\dot{W}_{exp,el} - \dot{W}_{pp,el}}{\dot{Q}_{ev,r}} \quad 23$$

$$\eta_{exp,is} = \frac{\dot{W}_{exp,el}}{\dot{m}_{tot}(h_{exp,su} - h_{exp,ex,is})} \quad 24$$

Table 7: Minimum and maximum values of the main operating conditions and performance in ORC mode

Parameter	Nomenclature	Minimum	Maximum
Evaporator thermal power [kW]	$\dot{Q}_{ev}$	30	65
Evaporation pressure [bar]	P_{ev}	16	32
Expander exhaust pressure [bar]	P_{cd}	5.4	10.2
Mass flow rate [kg/s]	$\dot{m}_r$	0.124	0.294
Expander electrical production [kW]	$\dot{W}_{exp,el}$	0.125	3.696
Global efficiency [%]	η_{global}	0	5.3
Expander isentropic efficiency [%]	$\varepsilon_{exp,is}$	10	63
Expander filling factor [-]	FF_{exp}	1	1.1

4.2.2 Comparison with theoretical nominal point

In the same manner as for the heat pump measurements Table 7 and Figure 11 present a comparison between the experiment and the theoretical nominal operating point. The following flow stages are presented in Figure 11: sub-cooler exhaust and pump supply (1), pump exhaust and evaporator supply (2), evaporator exhaust and four-way valve supply (high pressure side Hp) (3), four way valve exhaust (Hp) and expander supply (4), expander exhaust and four way valve (low pressure side Lp) supply (5), four way (Lp) exhaust and condenser supply (6) and, condenser exhaust and sub-cooler supply (7).

Table 8: Comparison of the results between experiments and theory (ORC)

Parameter	Nom.	Theoretical nominal	Experimentation
Evaporator thermal power [kW]	$\dot{Q}_{ev}$	62	62
Evaporation pressure [bar]	P_{ev}	33	32
Expander exhaust pressure [bar]	P_{cd}	7	10.3
Mass flow rate [kg/s]	$\dot{m}_r$	0.3	0.266
Expander electrical production [kW]	$\dot{W}_{exp,el}$	5.9	3.7
Global efficiency [%]	η_{global}	7.5	4.2
Expander isentropic efficiency [%]	$\varepsilon_{exp,is}$	68	58
Expander filling factor [-]	FF_{exp}	1.019	1.02

The performance is lower than expected by the theoretical model in terms of electrical power generation and efficiency. This could be explained by:

- A low expander isentropic efficiency (see section 4.2.4). In Figure 11, a higher entropy increase is indeed observed during the experiment (see section 4.2.4).
- In Figure 11, a significant pressure drop (up to 3.6 bar) is observed in the four-way valve at the exhaust of the expander (see section 4.2.6). This is mainly due to an unconventional way of using this component with a counter-current flow (see chapter 3 – appendices) but also to a rather large difference (ratio of 3) between the flow in heap pump mode and in ORC mode.
- A higher than expected sub-cooling is required to avoid any pump cavitation (section 4.2.5). In Figure 11, a 10K sub-cooling is observed at the exhaust of the sub-cooler.

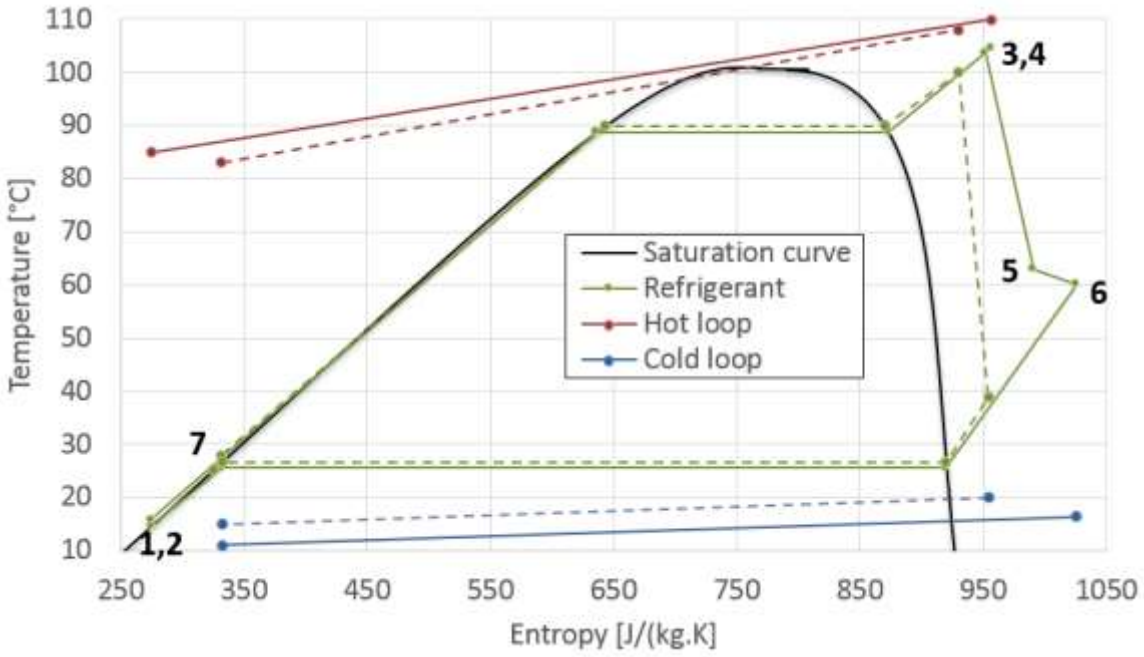

Figure 11: T-s diagram for the ORC mode (comparison between experiments and theory). Dashed lines = Theory, plain line = experiment

4.2.3 Global performance

Figure 12 shows the overall efficiency (Eq. 13) versus temperature lift (Eq. 7). The efficiency of the ORC and the power production increases with an increase in temperature lift as expected, until the efficiency reaches a maximum value of 5.2%. It should be noted that the optimal efficiency is reached at part load (i.e. with low mass flow) because it avoids the occurrence of an excessive pressure drop in the four-way valve (section 4.2.6).

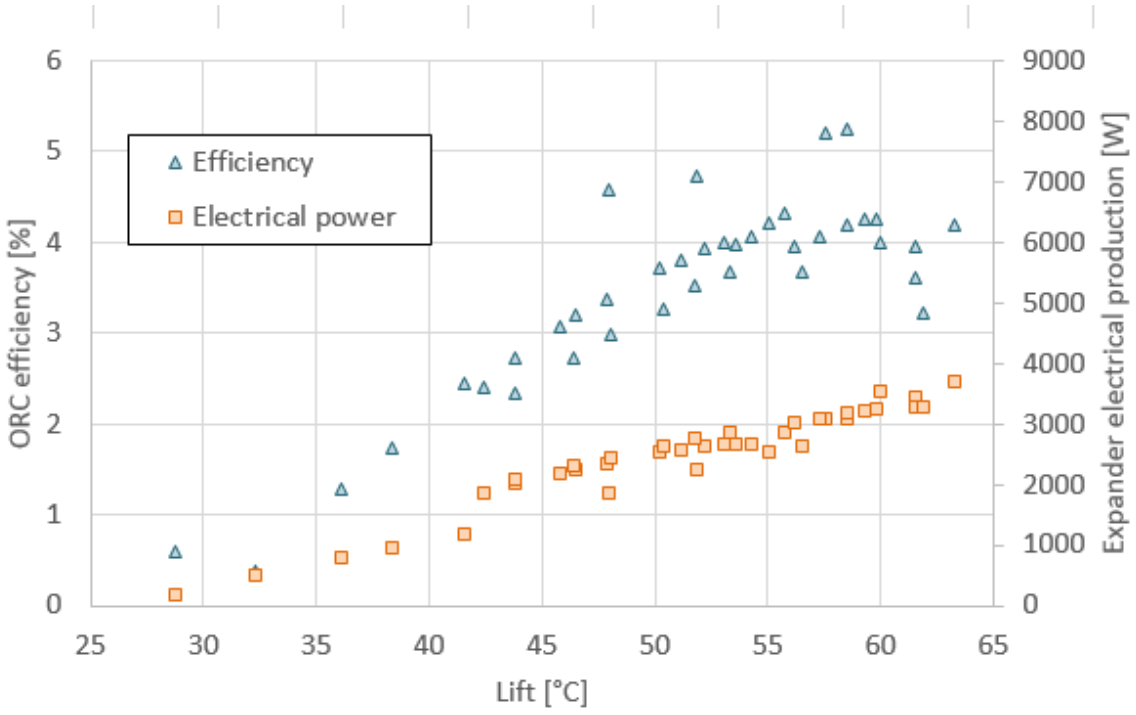

Figure 12: Evolution of the ORC efficiency and expander produced power with the temperature lift.

The pressure drop on the low pressure side of the four-way valve (see section 4.2.6) is found to reduce the overall efficiency. In the absence of such a pressure drop, the expander exhaust pressure would be significantly lower, leading to a greater pressure difference across the expander (and thus to a higher electrical production). In section 5.4, the global efficiency of the unit will be simulated without the four-way valve pressure drop.

4.2.4 Expander performance

Figure 13 presents the filling factor (as defined in Eq. 24) and the isentropic efficiency (Eq. 14) of the expander. The influence of the unknown oil mass fraction is greater than the influence of the sensor accuracy. The markers on the figure correspond to 0% oil mass fraction and error bars indicate the impact of a 10% oil mass fraction (similar to the compressor - Eqs.20-21).

The filling factor is close to unity for each point except when working at low pressure ratio (values below 2.3). This could be explained by unloading phenomenon between the two scrolls leading to larger flank leakages. The isentropic efficiency is increasing with the pressure ratio up to 0.63. This efficiency is slightly lower than the efficiency of other scroll machines reported in literature (Aoun and Clodic, 2008; Lemort et al., 2009; Quoilin, 2011, Zanelli and Favrat, 1994; Yanagisawa et al., 1990; Manzagol et al., 2002) but this could be explained by the adaptations made to the scroll unit in order to work both in compressor and in expander, and by the relatively high oil mass fraction. The use of an expander with a dedicated geometry (not a modified compressor) and a dedicated motor is expected to increase the efficiency above what is observed in this experiment.

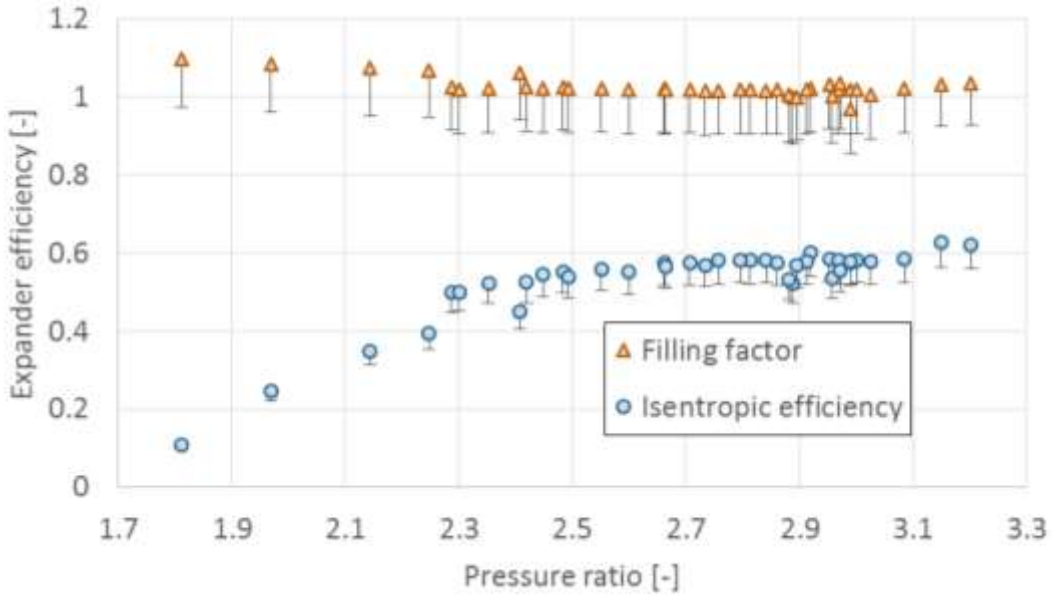

Figure 13: Evolution of the expander filling factor and isentropic efficiency with the pressure ratio

4.2.5 Pump performance

The refrigerant pump has been tested over a large range of pressure differences [8.7 bar to 25.2 bar] (Figure 14). The volumetric efficiency (Eq. 14) is found to be nearly constant and presents a slight decrease at high pressure difference, which could be explained by an increase of internal leakages. The isentropic efficiency (Eq. 15) increases with increasing pressure difference up to 50%. The main explanation is that the electrical motor efficiency is low when working at part load conditions (i.e. low pressure ratios). This isentropic efficiency is rather high for this type of applications (small power and low working fluid viscosity) compared to literature (Quoilin 2013 (b)). The pump electrical efficiency could be significantly increased with a smaller motor (i.e. 1 kW instead of 1.5 kW).

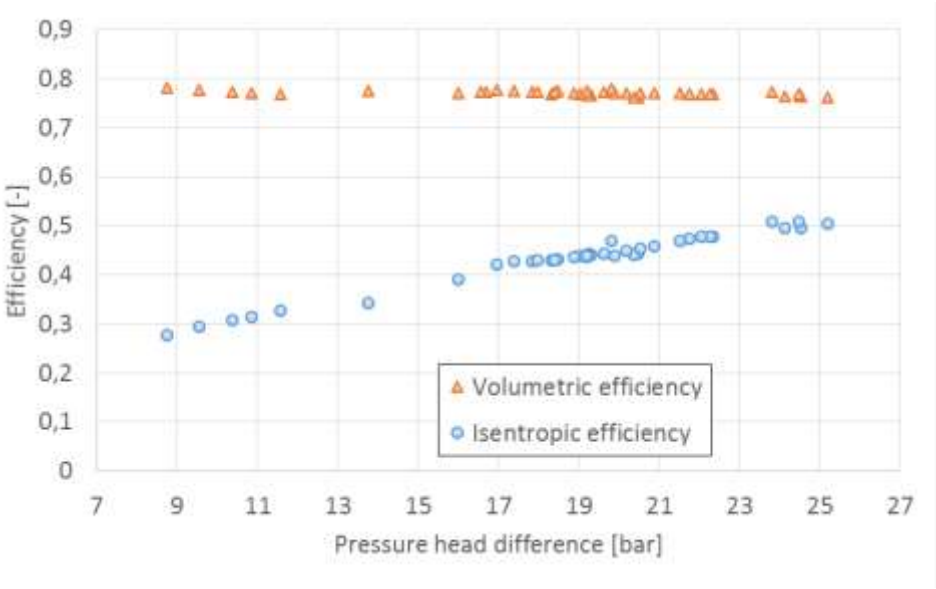

Figure 14: Evolution of the pump efficiency with the pressure head difference.

The volumetric efficiency versus the NPSH (Net Pressure Suction Head), defined by Eq. 25, is presented in Figure 15. This figure shows that this pump requires a relatively high NPSH (around 10 meters) corresponding to a minimum necessary sub-cooling of around 10K. This is necessary to avoid cavitation. One explanation for the observed spread of the measurement points is because the refrigerant level *H* above the pump is not measured, and so is assumed to be constant at 1 m.

$$NPSH = H + 10^5\left(\frac{P_{cd,ex} - P_{pp,sat}}{\rho g}\right) \qquad 25$$

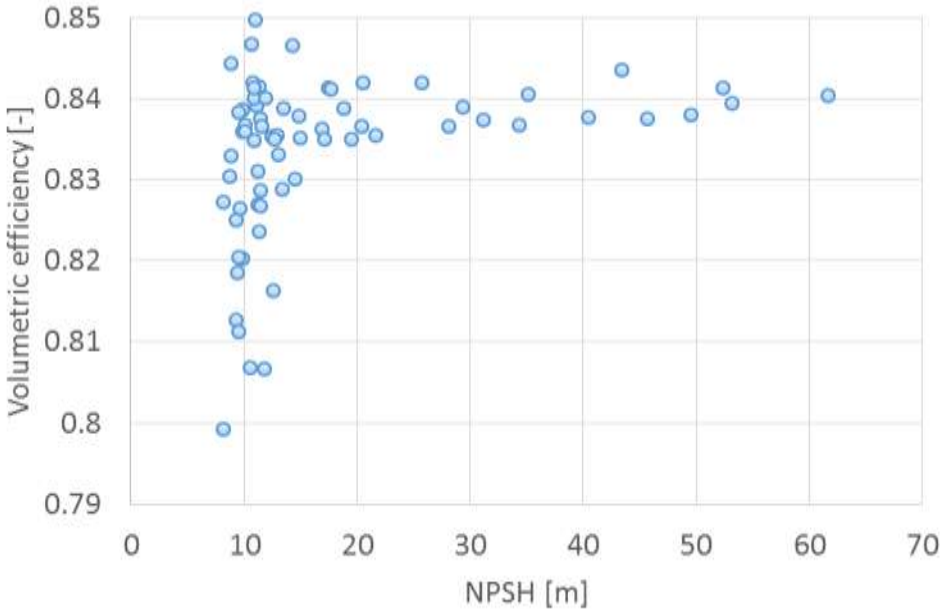

Figure 15: Evolution of the pump volumetric efficiency with the NPSH

4.2.6 Heat exchanger's performance

Similar to the heat pump operating mode, only the minimum and the maximum values of the pressure drop and the pinch-point temperature in the exchangers are presented in Table 9 for clarity. Globally, the observed pinch-points and pressure drops (Figure 16) are relatively small, indicating that the evaporator and the condenser are correctly sized for this application. The results presented show that the condenser has a non-negligible pressure drop of above 0.5 bar at high flow rates.

Table 9: Range of measured heat exchanger performance metrics in ORC mode

Exchanger	**Evaporator**	**Condenser**
Pressure drop range [bar]	[0.023:0.09]	[0.151:0.46]
Pinch-point range [K]	[0.4:8.8]	[0:13]

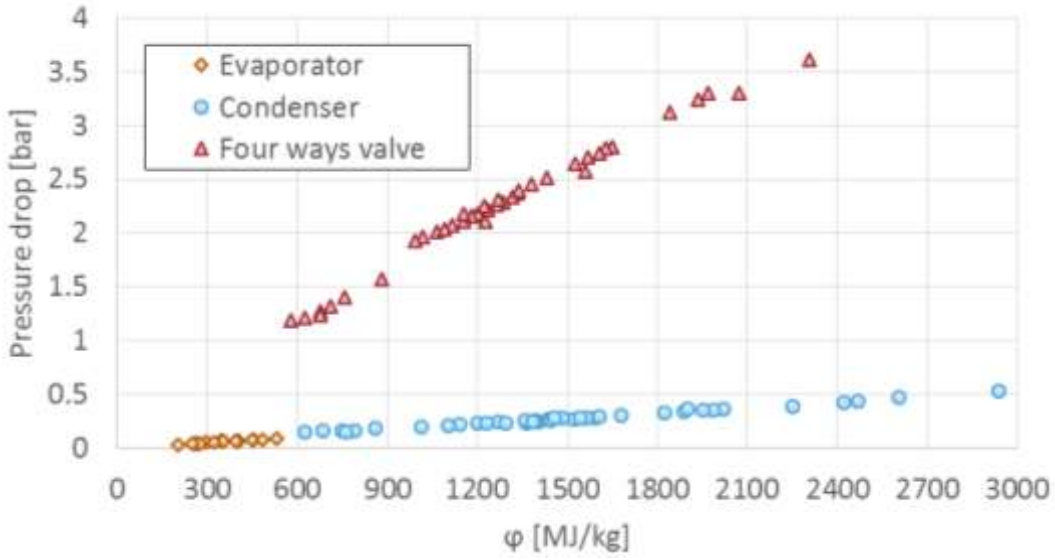

Figure 16: Evolution of the pressure drops with the kinetic energy factor (ORC mode)

5 SEMI-EMPIRICAL MODEL FOR STEADY-STATE PERFORMANCE PREDICTION

5.1 INTRODUCTION

An accurate modelling is necessary to predict the optimal performance of the HP/ORC reversible system in a wide range of conditions (extrapolation). Moreover, the impact of a design modification can be assessed. Also, this model will be coupled with other models (building, solar roof, etc.) to perform dynamic simulations for a given study case in Chapter 6. The modelling of the components can be done following three approaches: the black-box model (empirical), the grey-box model (semi-empirical) and the white box model (deterministic). The black-box model presents a very low computational time but the output prediction is not valid outside the dataset. The white box model takes the physical phenomena into account in detail but requires a long CPU time and the knowledge of the detailed geometry of the expander. Finally, the semi-empirical model is used in this section because of:

- its ability to extrapolate outside the dataset through the characterization of the most influent physical phenomena,

- its low computational time,

- its robustness.

5.2 MODELS

The expander model is fully described in Chapter two. The expansion valve is considered as adiabatic and therefore isenthalpic. Other components model are described in this section.

5.2.1 Heat exchangers

The exchanger model is detailed in Chapter three. The same modelling methodology is applied except that each relation characterising the heat exchange coefficient of each zone

is multiplied by a constant (*C*). Eq. 26 shows an example of this. Each exchanger requires as many parameters as there are zones and this for each fluid (working fluid and secondary fluid).

$$Nu = C\ Re^{0.7} Pr^{n} \quad (26)$$

5.2.2 Pump

The pump is modelled following the semi-empirical approach described by Dickes et al. (2016). This approach predicts the mass flow of the pump based on an ideal theoretical flow minus a leakage flow (Eq. 27). The power consumed by the pump is assumed to be equal to the isentropic power plus a term accounting for constant losses and a term accounting for proportional losses (Eq. 28). Heat losses in the pump are neglected (low temperature difference with the environment). Three fitting parameters are adjusted to fit the experimental data with the model prediction.

$$\dot{m}_{pp} = \rho_{pp,su} S_{pp} V_{pp,swept} - A_{leak} \sqrt{2\rho_{pp}(P_{pp,ex} - P_{pp,su})} \quad (27)$$

$$\dot{W}_{pp} = \dot{W}_0 + (1 + K_0)(\dot{V}(P_{pp,ex} - P_{pp,su})) \quad (28)$$

5.2.3 Compressor

The compressor modelling is achieved in the same way as the expander model (Chapter two). This model takes into account a supply heating up, a supply pressure drop, an adiabatic mixing between suction and leakage flows, an isentropic compression followed by an isochoric compression, an exhaust cooling down and electro-mechanical losses (Figure 17). More details are available in a former PhD thesis (Winandy et al., 2002). This model requires 7 fitting parameters: a supply diameter characterizing the supply pressure drop, three heat transfer coefficient for internal and ambient heat transfer, a leakage area, a constant and a proportional parameters characterizing the electromechanical losses.

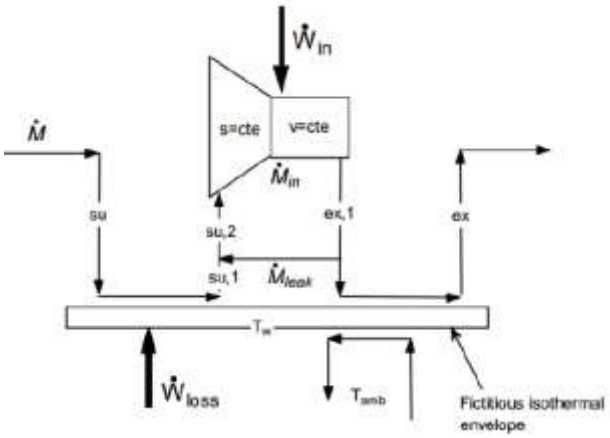

Figure 17 : Compressor semi-empirical model (Lemort, 2008).

5.2.4 Four way valve

As shown in section 4.1.5 and 4.2.6, the four-way valve presents a non-negligible pressure drop. The pressure drops are linear with the kinetic energy factor (Eq. 22). It is therefore modelled using one parameter characterising the slope of the pressure drop in function of the kinetic energy factor (section 4.1.5). The exhaust temperature is evaluated supposing an isenthalpic pressure drop.

5.3 CALIBRATION AND VALIDATION OF MODELS

5.3.1 Introduction

The measurements allow to calibrate this semi-empirical model considering only pure refrigerant (neglecting the oil influence). Three outputs (y_{pred}) are evaluated based on the calibration parameters and on the inputs. An optimization algorithm is used to calibrate the coefficients to minimize Eq. 29 using the measurements (y_{meas}).

$$Err = \sum_i \left(\left(\frac{y1_{meas,i} - y1_{pred,i}}{y1_{meas,i}} \right)^2 + \left(\frac{y2_{meas,i} - y2_{pred,i}}{y2_{meas,i}} \right)^2 + \left(\frac{y3_{meas,i} - y3_{pred,i}}{y3_{meas,i}} \right)^2 \right) \quad 29$$

The inputs and outputs for each model are listed in Table 10.

Table 10 : Inputs and outputs for the seven components

Component	Inputs	Outputs
Compressor/expander/pump	Rotational speed Supply temperature Supply pressure Exhaust pressure	Mass flow rate Electrical power Exhaust temperature
Condenser/evaporator	Working fluid mass flow rate Secondary fluid mass flow rate Supply temperature (working fluid) Supply temperature (secondary fluid) Working fluid pressure Secondary fluid pressure	Thermal power
Four-way valve (high pressure and low pressure)	Supply pressure Supply temperature Mass flow rate	Exhaust pressure Exhaust temperature

5.3.2 Compressor/expander

The fitting parameters of the expander and of the compressor have been optimised to minimise the error between the prediction of the model and the measurements. Their values are given in Table 11.

Table 11 : Calibrated parameters for the expander and the compressor

Parameter	Compressor	Expander
A_{leak}[mm^2]	1.837	6.8
AU_{amb} [W/K]	4.1	3
AU_{su} [W/K]	24.3	160
AU_{ex} [W/K]	12.6	150
α [-]	500	140
$C_{loss,0}$[W]	0.03	0.154
d_{su} [mm^2]	8.6	6.8

As an example, the predicted power consumed by the compressor and the expander power production prediction are depicted in Figure 18. Both models reproduce accurately the performance of the compressor/expander

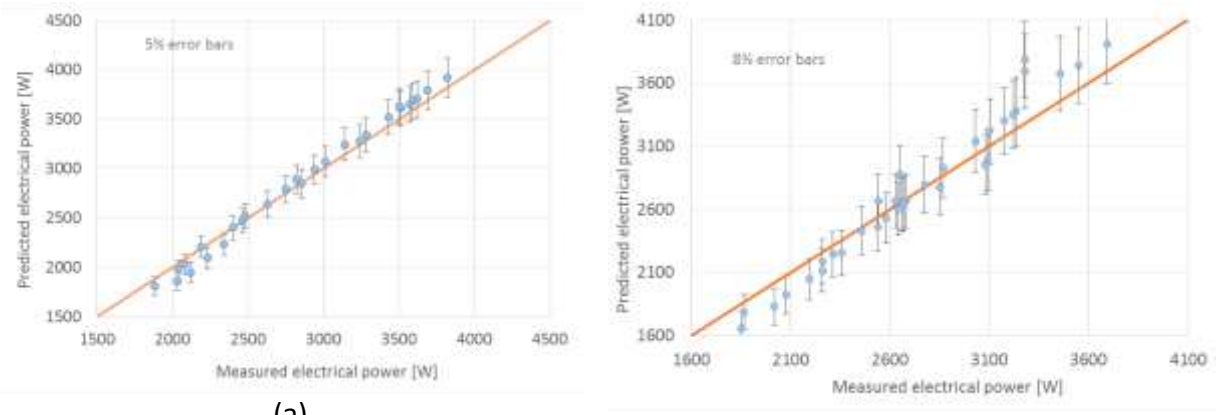

(a) (b)

Figure 18 : Prediction by the model of the electrical power. a) Compressor, b) Expander

5.3.3 Evaporator (ORC and HP)

The fitting parameters of the evaporator in HP and ORC mode have been optimised to minimise the error between the prediction of the model and the measurements. Their values are given in Table 12. No liquid phase exists in the heat pump mode since the refrigerant comes from the expansion valve in a two-phase state.

Table 12 : Calibrated parameters for the evaporator model

Parameter	HP	ORC
$C_{r,l}$ [-]	-	0.17
$C_{r,tp}$ [-]	120	0.2
$C_{r,v}$ [-]	20	0.8
$C_{w,l}$ [-]	-	35
$C_{w,tp}$ [-]	50	0.194
$C_{w,v}$ [-]	5	0.2

As an example, the predicted pinch-points in HP and ORC of the evaporator are depicted in Figure 19. The model represents accurately the pinch-point since the maximum error in HP and ORC mode is lower than 2K.

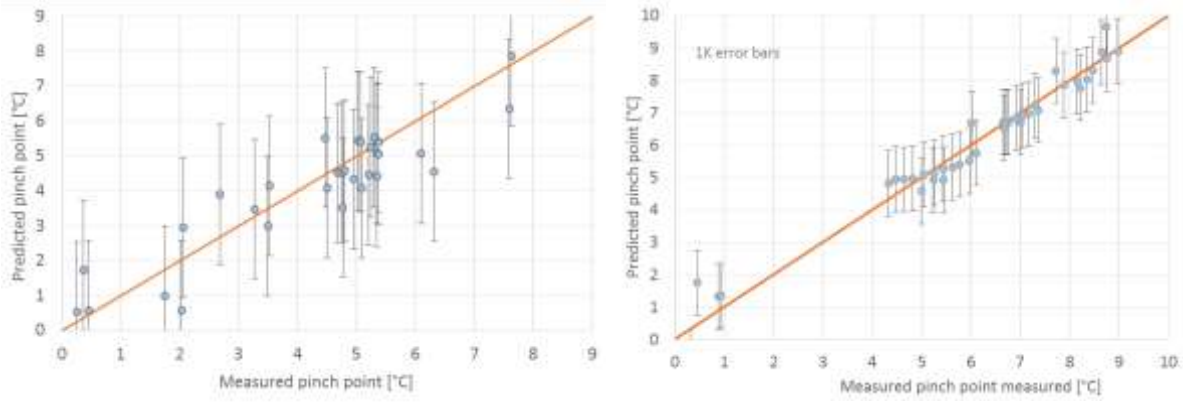

(a) (b)

Figure 19 : Prediction by the model of the evaporator pinch-point. a) HP b) ORC

5.3.4 Condenser (ORC and HP)

The fitting parameters for the condenser are given in Table 13.

Table 13 : Calibrated parameters for the condenser model

Parameter	HP	ORC
$C_{r,tp}$ [-]	120	75.8
$C_{r,v}$ [-]	20	0.2
$C_{w,tp}$ [-]	50	1.4
$C_{w,v}$ [-]	5	20

As an example, the predicted thermal power in HP and ORC of the condenser are depicted in Figure 20. The model prediction is accurate since the maximum error on the predicted thermal power fits within the 3% error bars.

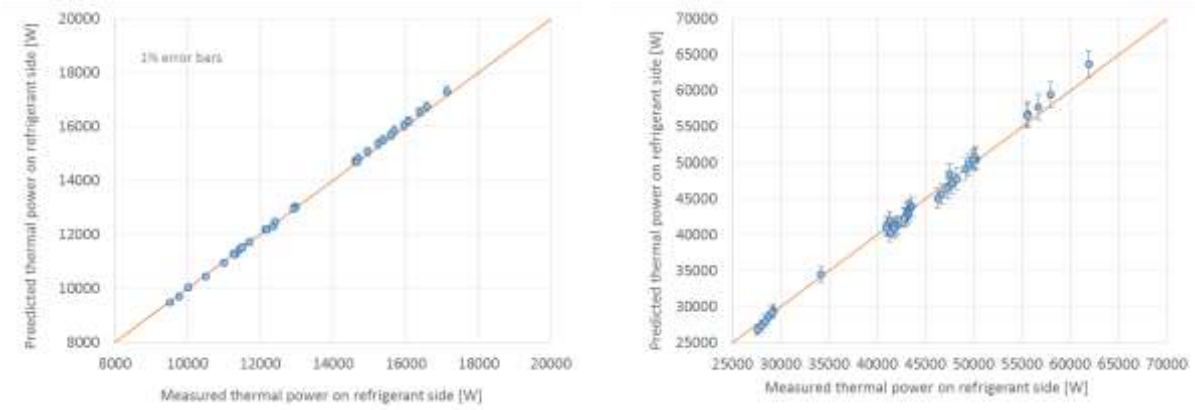

(a) (b)

Figure 20 : Prediction of the condenser thermal power. a) HP b) ORC

5.3.5 Four way valve

The fitting parameters of the four way valve in HP and ORC mode have been optimised to minimise the error between the prediction of the model and the measurements. Their values are given in Table 14. The high pressure drop is neglected.

Table 14 : Calibrated parameters for the four way valve model

Parameter	HP	ORC
$C_{,lp}$ [-]	2.15 10^8	16.2 10^9

As an example, the pressure drops in HP and ORC are depicted in Figure 21.

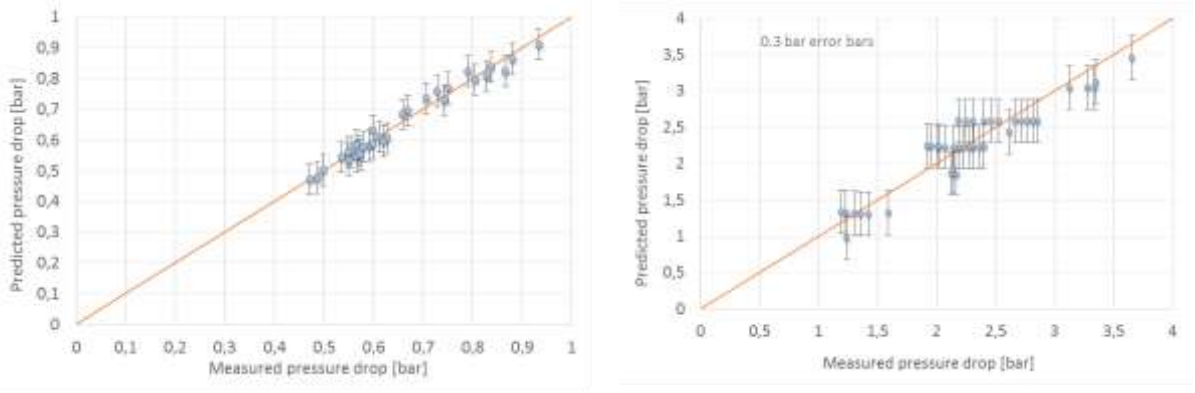

(a) (b)

Figure 21 : Prediction of the four way valve pressure drop (low pressure side). a) HP b) ORC

5.3.6 Pump

The fitting parameters of the pump are given in Table 15.

Table 15 : Pump fitting parameters

Parameter	Pump
A_{leak} [m^2]	7.7 10^{-7}
$\dot{W}_0$ [W]	158
K_0 [-]	0.74

As an example, the predicted pump power consumption is depicted in Figure 22. The error on the prediction is lower than 3% for each point.

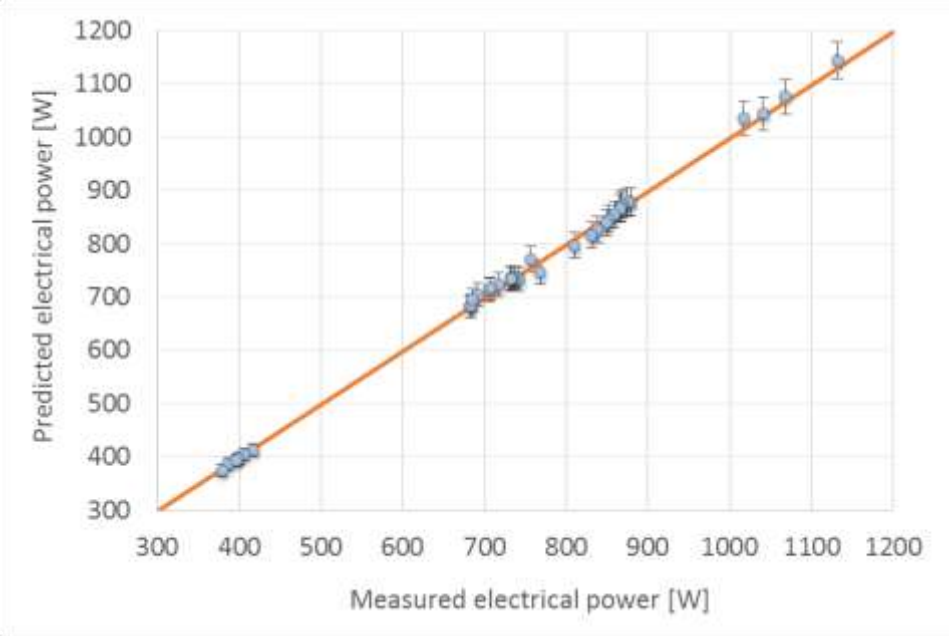

Figure 22 : Pump electrical power consumption prediction.

Globally, the value of the semi-empirical parameters for a given component are different between the ORC mode and the HP mode. This is explained by the lumped approach of the semi-empirical model and it emphasizes its limitation because of it does not take into account all the physical phenomena occurring.

5.4 GLOBAL MODELS

5.4.1 Heat pump

The global heat pump model with all sub-models connected together is shown in Figure 23.

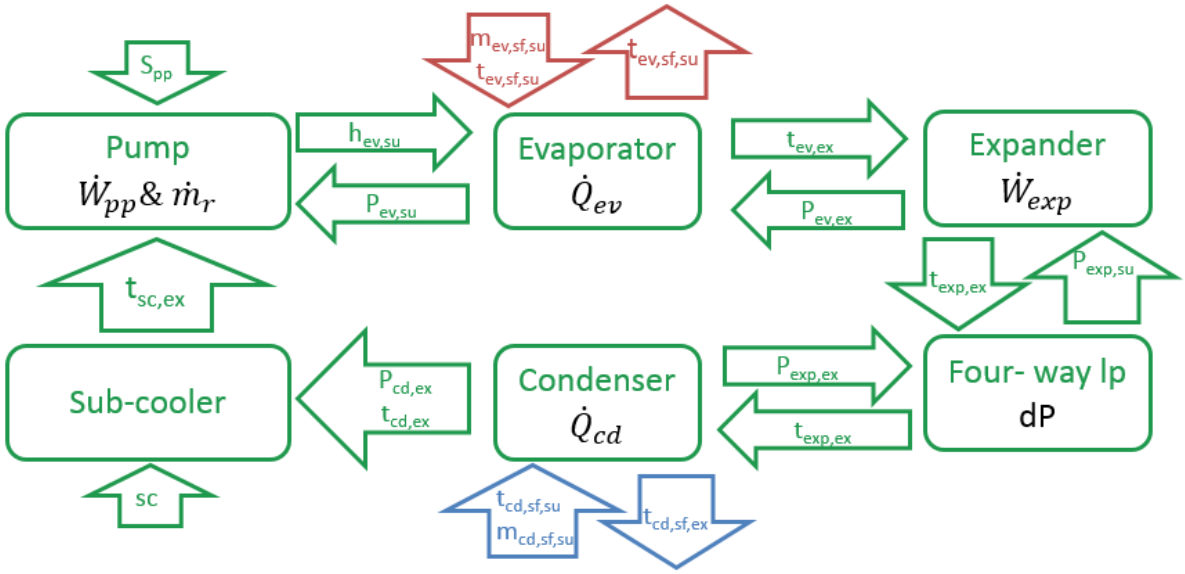

Figure 23 : Flowchart of the global model for the heat pump. Green is the refrigerant loop, red is the secondary fluid at the evaporator, blue is the secondary fluid at the condenser. The black variables are the outputs.

The cycle is implemented as follows. The compressor imposes the refrigerant flow of the cycle and the supply refrigerant temperature of the condenser. The condenser imposes the exhaust pressure of the compressor. The supply enthalpy of the evaporator is also imposed by the condenser (through the expansion valve). The evaporator imposes the supply pressure and the supply temperature of the compressor. The inputs and outputs are summarized in Table 16.

Table 16 : Inputs and outputs of the global models

	Inputs	Outputs
HP	Sub-cooling Compressor rotational speed Condenser secondary fluid supply temperature Evaporator secondary fluid supply temperature Secondary fluid flow at the condenser Secondary fluid flow at the evaporator	Over-heating Net electrical consumption Condenser secondary fluid exhaust temperature Evaporator secondary fluid exhaust temperature
ORC	Sub-cooling Pump rotational speed Expander rotational speed Condenser secondary fluid supply temperature Evaporator secondary fluid supply temperature Secondary fluid flow at the condenser Secondary fluid flow at the evaporator	Over-heating Net electrical production Condenser secondary fluid exhaust temperature Evaporator secondary fluid exhaust temperature

The prediction of COP of the global model is compared with the measurements in Figure 24 (a). The model prediction does not always fit in the 10% error bars but the results are decent regarding the error propagation occurring between all the sub-models.

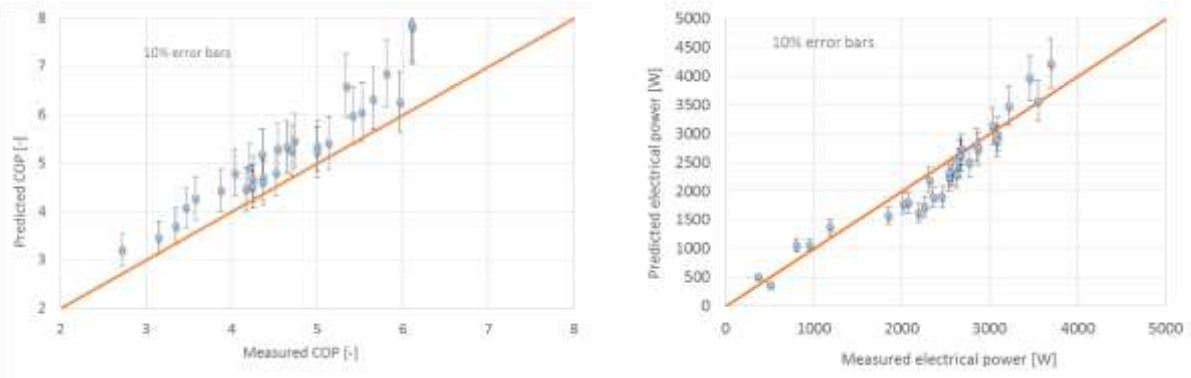

(a) (b)

Figure 24 : Prediction of performance of the global models a) COP of the heat pump, b) net power production of the ORC.

With the global model validated, it is now possible to extrapolate the performance outside of the operating range of the test-rig. An example of the exploitation of the global model is the influence of the over-heating on the COP (Figure 25 (a)). A polynomial has been fitted to predict the performance (appendices - Table 19) of the heat pump with a wide range of inputs (appendices - Table 18). This polynomial presents a very fast computational time and will be useful for the models developed in Chapter 5.

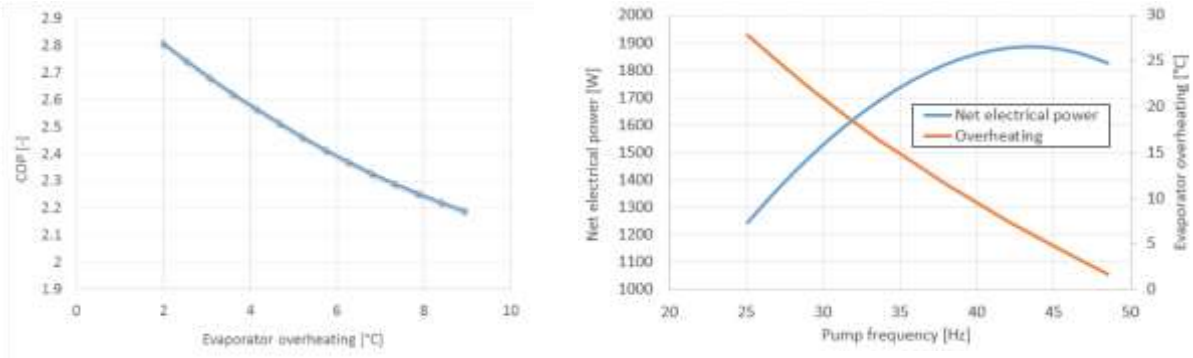

(a) (b)

Figure 25 : Performance prediction of the global model a) HP b) ORC

The analysis of the measurements clearly showed that the main weakness of the system are the pressure drops in the four way valve. This section compares the performance of the actual prototype and a virtual perfect reversible HP/ORC with a properly sized four-way valve (with negligible pressure drops). Figure 26 presents the COP of the heat pump in

function of the lift obtained with the validated global model. On average, the gain on the coefficient of performance is 19% with a properly sized four-way valve.

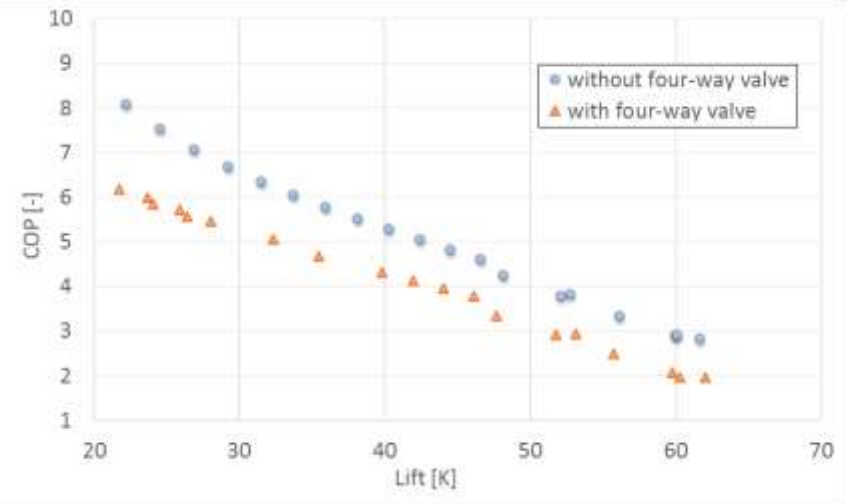

Figure 26 : Comparison of the COP of the heat pump with and without the four-way valve pressure drop

5.4.2 ORC

The ORC model with all sub-models connected together is shown in Figure 27. The cycle is implemented as follows. The expander imposes the exhaust evaporator pressure and the supply condenser temperature. The pump imposes the refrigerant flow of the cycle and the supply evaporator temperature. The evaporator imposes the supply expander temperature and the exhaust pump pressure. The condenser imposes the outlet expander pressure, the supply refrigerant temperature and the supply pressure of the pump. The inputs and outputs are summarized in Table 16.

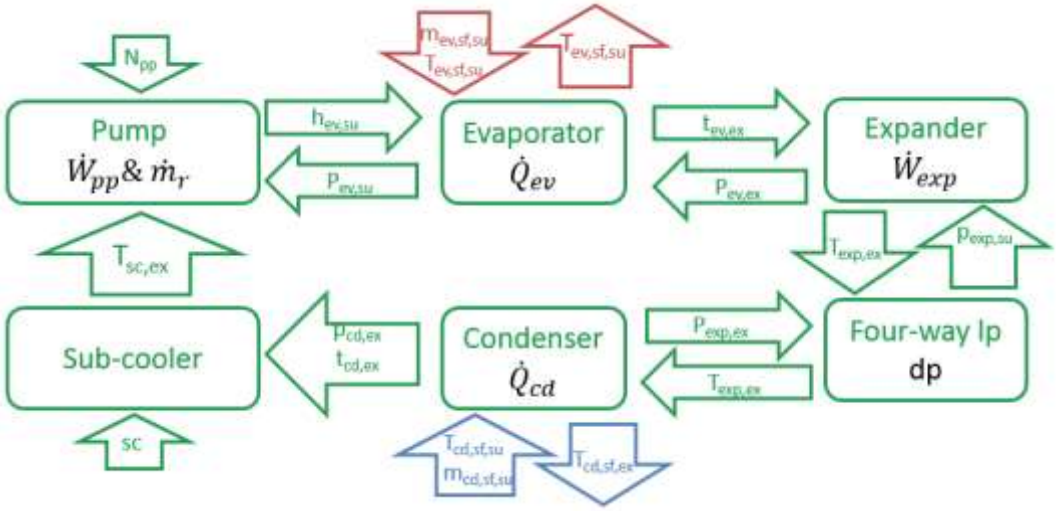

Figure 27 : Flowchart of the global model for the ORC. Green is the refrigerant loop, red is the secondary fluid at the evaporator, blue is the secondary fluid at the condenser. The black variables are the outputs.

The prediction of the net electrical power of the global model is compared with the measurements in Figure 23 (b). The model prediction does not always fit in the 10% error bars but the results are decent regarding the error propagation occurring between all the sub-models. With the global model validated, it is now possible to extrapolate the performance outside of the operating range of the test-rig. An example of the exploitation of the global model is the influence of the pump frequency on the net electrical production (Figure 25 (b)). For each set of inputs for the ORC model, there is an optimal pump speed. The optimum net electrical production (with the optimal pump speed) is computed for a wide range of inputs (appendices - Table 18). The sub-cooling is evaluated to obtain a NPSH of 10 m to avoid the cavitation of the pump (see section 4.2.5). A polynomial has been fitted to predict the performance (appendices - Table 19) of the ORC with a wide range of inputs (appendices - Table 18). This polynomial presents a very fast computational time and will be useful for the models developed in Chapter 5.

Figure 28 presents the ORC efficiency in function of the lift obtained with the global model. The cycle without the four-way valve has a gain on the global efficiency of 32% in average.

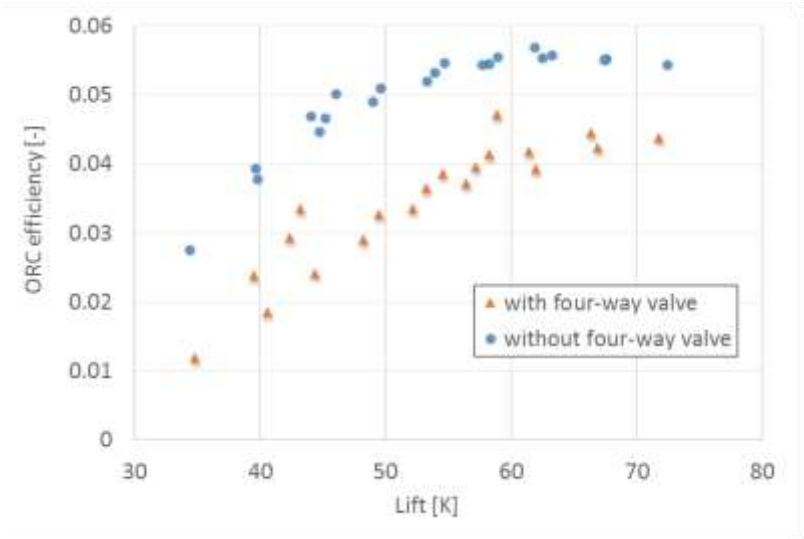

Figure 28 : Comparison of the ORC efficiency with and without the four-way valve pressure drop

5.5 IMPROVEMENT OF THE DATA QUALITY WITH THE GLOBAL METHODOLOGY TO HANDLE EXPERIMENTAL DATA

In section 3, two mathematical tools have been described. The Gaussian process allowing to reject rigorously outliers and the reconciliation method which improves the quality of the data through the redundancy of measurements. The efficiency of both methods is proven by comparing the outputs of steady-state models of the different components in the case of the ORC mode. Five main outputs are compared in this study: the expander electrical production, the pump power consumption, the thermal power at the condenser and at the evaporator and finally the net electrical power of the global model. The performance of the

models are compared (Figure 29) with the gross data (without any treatment), with the rejection of outliers (Gaussian Process), with the reconciliation method and with the combination of the two aforementioned methods (RM+GP) with the Mean Average Percentage Error (MAPE).

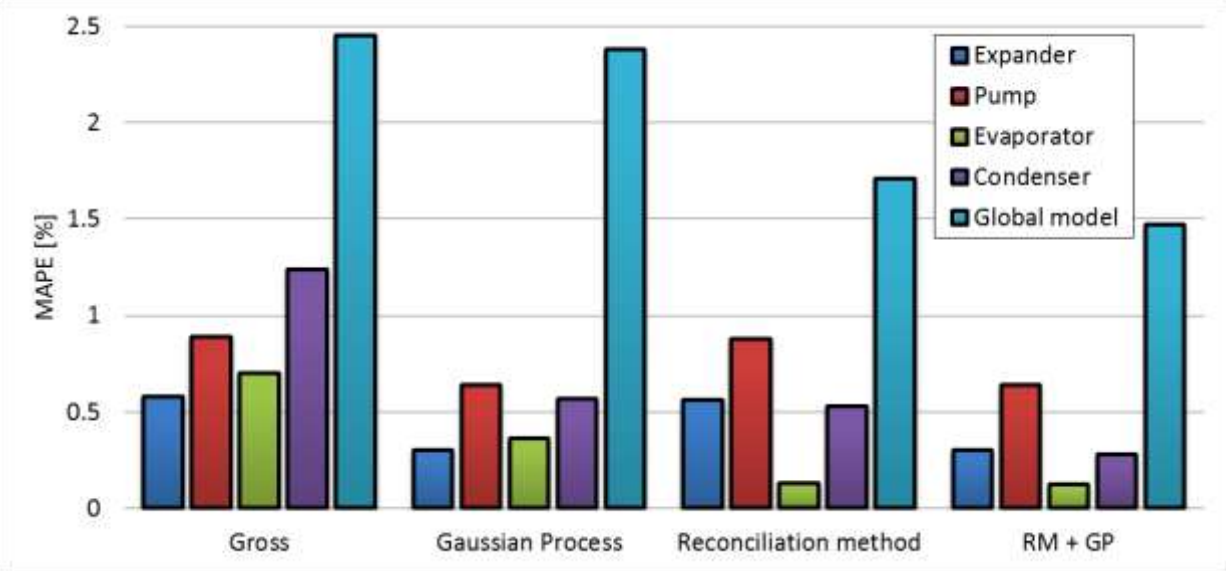

Figure 29 : Improvement of the quality of prediction of the data through the MAPE with different methods

First, the MAPE of the global model is higher than the MAPE of single models which is due to the propagation of error from one sub-model to the other. Also, the combination of the reconciliation method and of the Gaussian process always shows the best quality of prediction. This proves the efficiency of the global methodology proposed in section 3 and that it should be considered more often when dealing with experimentation. The efficiency of the method depends on the dataset. If the dataset presents a relatively high number of outliers, the GP increases significantly the quality of the data. If the redundancy of the sensors is high and their accuracy rather low, the reconciliation method increases significantly the quality of the data. That is the reason why sometimes the GP is more efficient than the RM and sometimes it is the opposite (Figure 29).

Another advantage of the reconciliation method is the determination of the oil fraction which is not directly measured. This oil fraction is plotted versus the volumetric flow at the inlet of the expander for the ORC mode and at the outlet of the compressor for the HP mode. In both cases, the oil mass fraction increases with the flow due to the higher refrigerant speed.

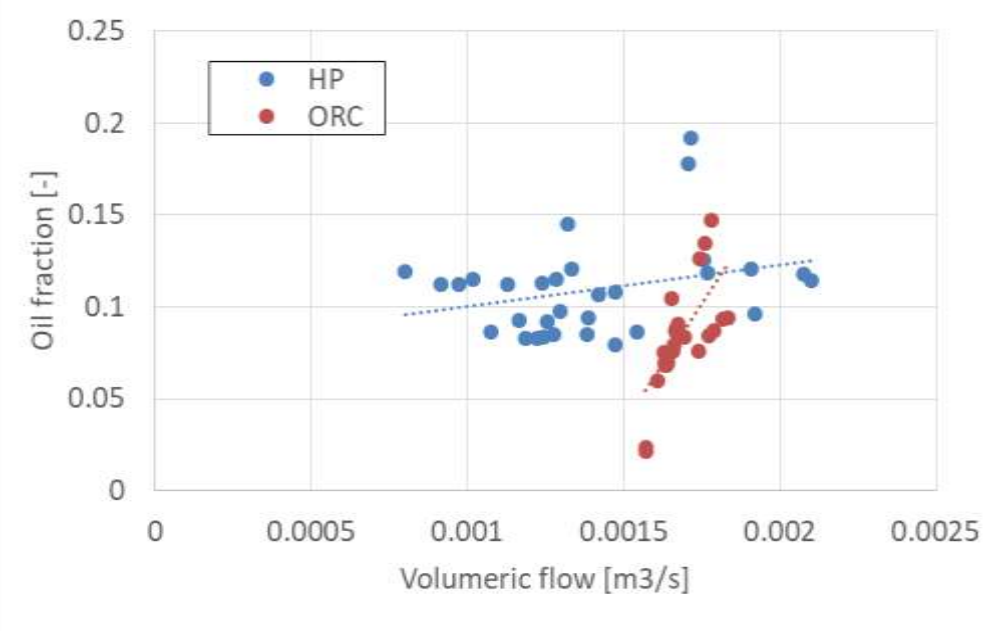

Figure 30 : Oil fraction versus the volumetric flow in HP and ORC modes.

6 CONCLUSION

Former studies in literature (Schimpf et al., 2011, Quoilin et al., 2013 (a)) have assessed the theoretical environmental and economic potential of this reversible HP/ORC unit. This chapter presents an experimental test setup, and the main results of experiments carried out in the Thermodynamics Laboratory in Liège.

The results from the experimental setup presented prove the feasibility of the HP/ORC concept, and indicate encouraging performance for the system. The heat pump provided a COP of 3.1 at the nominal point (evaporation temperature of 21°C and condensation temperature of 61°C). In ORC mode, a maximum thermal efficiency of 4.2% was measured at an evaporation temperature of 88°C and condensation temperature of 25°C with a gross power output of 3.7 kW.

Some weaknesses are identified in the experimental setup which explains its lower performance compared to theoretical predictions: the pressure drop and heat transfer occurring in the four-way valve, the lower than expected expander efficiency, the high NPSH of the pump and the lack of insulation on the test unit. The four way valve pressure drop can be reduced by using a valve with a larger cross-sectional area, or by removing this component altogether and using another system architecture. The expander efficiency could be improved by using a tailor-made expander geometry and a motor instead of an off-the-shelf compressor. Another pump design with a lower NPSH requirement could help to reduce the required sub-cooling.

A global methodology to handle the experimental data has been assessed and has proven its efficiency. These measurements can be used to calibrate semi-empirical models so as to predict the performance with a wide range of inputs. Now, the obtain correlations will allow

to simulate the performance of the reversible HP/ORC unit in a wide range of conditions (Chapter 5).

7 APPENDICES

Figure 31: Picture of the reversible HP/ORC unit

7.1 REFRIGERANT-OIL SOLUBILITY

Refrigerant-oil mixture is a zeotropic mixture which means that if oil solubility is neglected, errors could occur in the evaluation of thermodynamic properties (Barbosa et al., 2006). A certain fraction of refrigerant is trapped in liquid phase even at temperatures higher than evaporation temperatures (particularly at low overheating and/or at high oil fraction) (Youbi et al., 2002). By using equation *1*, some authors (Dirlea, 1997; Youbi et al., 2002; Cuevas, 2006) takes the effect of solubility of liquid refrigerant and oil into account to evaluate the enthalpy of the mixture.

$$h = (1 - X_v - X_{oil})h_{r,l} + X_{oil}h_{oil} + X_v h_v \qquad 1$$

This formula is based on three enthalpies: refrigerant saturated liquid enthalpy ($h_{r,l}$), refrigerant saturated vapor enthalpy (h_v) and oil enthalpy (h_{oil}). X_{oil} is the oil fraction (Eq. *2*) and X_v is the vapor mass fraction (Eq. *3*) which is estimated thanks to the liquid fraction of refrigerant in the liquid phase, ς, (Eq. *4*).

$$X_{oil} = \frac{\dot{m}_{oil}}{\dot{m}_{r,l} + \dot{m}_{oil} + \dot{m}_v} \qquad 2$$

$$X_v = \frac{\dot{m}_v}{\dot{m}_{r,l} + \dot{m}_{oil} + \dot{m}_v} \quad 3$$

$$\varsigma = \frac{\dot{m}_{r,l}}{\dot{m}_{r,l} + \dot{m}_{oil}} \quad 4$$

ς is the liquid fraction of refrigerant in the liquid mixture and is deduced from Eq. *5* with coefficient A (Eq. 6) and B (Eq. 7) given in Table 17.

$$\frac{t - t_{sat}(P)}{t_{sat}(P)} = (1 - \varsigma)\,(A(\varsigma) + B(\varsigma).P) \quad 5$$

$$A = b_1 + \frac{b_2}{\varsigma^{1/2}} \quad 6$$

$$B = b_3 + \frac{b_4}{\varsigma^{1/2}} + \frac{b_4}{\varsigma} + \frac{b_2}{\varsigma^{3/2}} + \frac{b_2}{\varsigma^{3/2}} \quad 7$$

Table 17: Coefficient for solubility equation (Dirlea, 1997)

Coefficient	R134a/oil
b_1	$-5.5x10^{-2}$
b_2	$5.19x10^{-2}$
b_3	$1.89x10^{-2}$
b_4	$-3.09x10^{-2}$
b_5	$1.64x10^{-2}$
b_6	$-3.1x10^{-3}$
b_7	$2.18x10^{-4}$

The only assumed hypothesis is that oil is perfectly miscible in the mixture and that oil always remains in the liquid form. In the case of an evaporator and a condenser, it tends to over-estimate the heat on the refrigerant side because of the overestimated latent heat (*Figure 32*). *Figure 32* shows an example of heat balance obtained with three different assumptions: no oil is taken into account, perfect mixture of oil and refrigerant without any solubility of liquid refrigerant in the oil and taking into account the refrigerant solubility. Relative differences are very high and can reach up to 17% between the basic model (no oil) and the most detailed one (oil and solubility). Furthermore, relative difference between models taking oil fraction into account with or without solubility is reaching 10% in the worst case. This graph proves that the use of a detailed model for refrigerant-oil mixture is recommended. By increasing the accuracy of the model (only R134a, R134a+Oil and R134a+Oil+Solubility), the mean heat balance error decrease respectively of 13.5%, 6.6% and 2.7%.

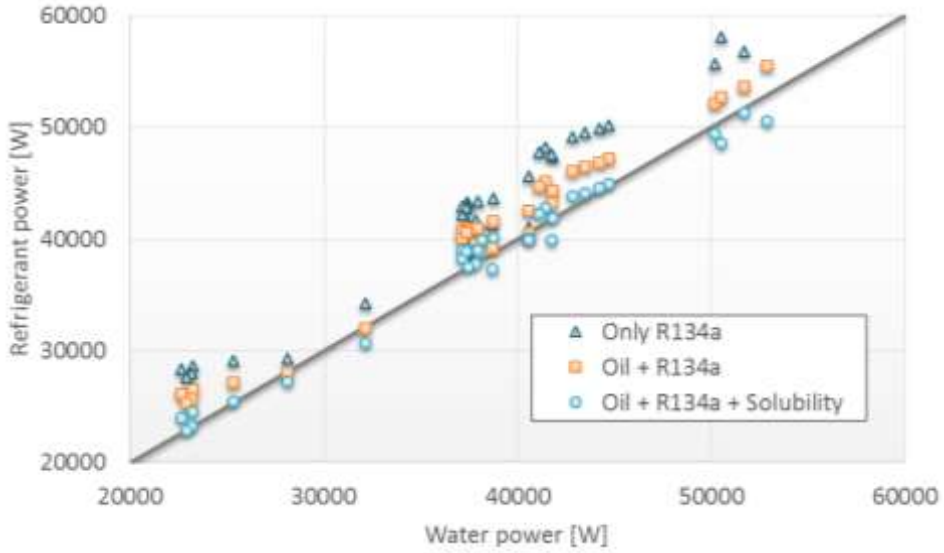

Figure 32: Comparison of the heat balance of a condenser with different assumptions. Only R134a = no oil is taken into account, Oil + R134a = perfect mixture of oil and refrigerant without any solubility of liquid refrigerant in the oil, Oil + R134a + Solubility.

However, in this thesis, the mixture between oil and refrigerant is always considered as perfect because of the high complexity to take the solubility effects into account in the model of the components.

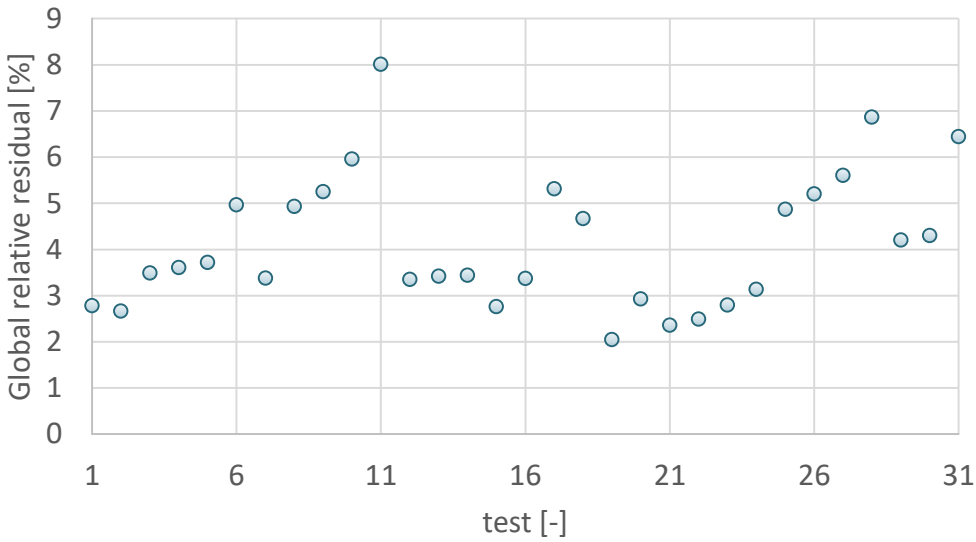

Figure 33: Global relative residual (heat pump)

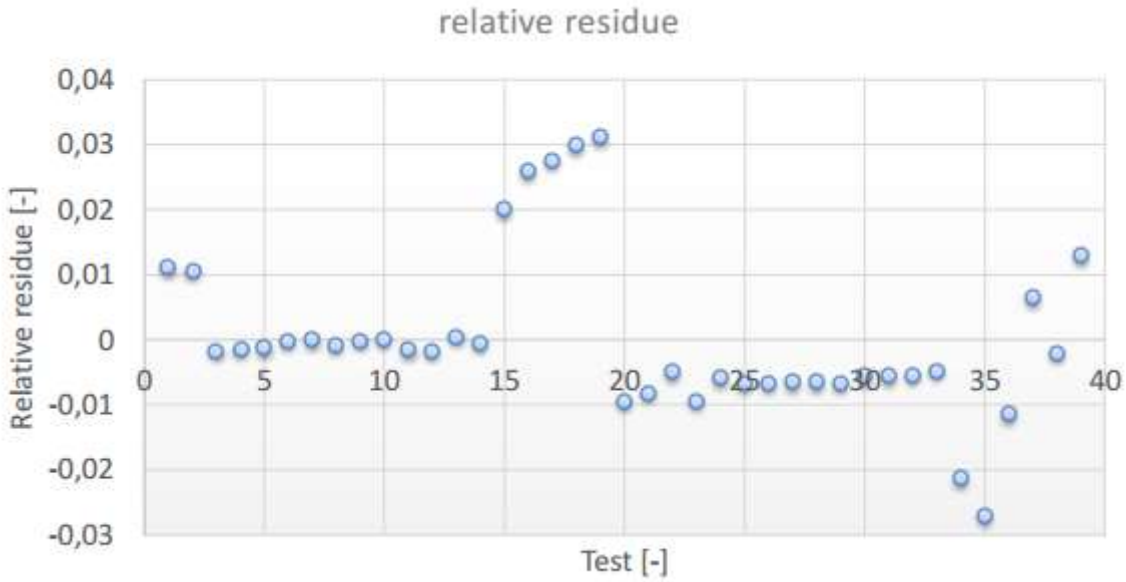

Figure 34: Global relative residual (ORC)

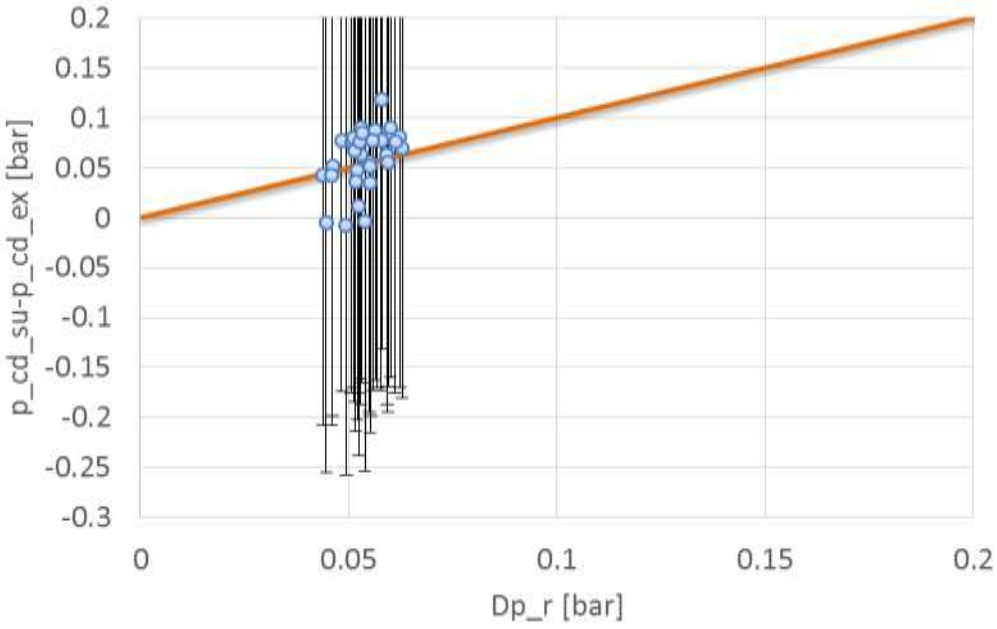

Figure 35: Cross-checking of pressure sensor of the condenser (Heat pump)

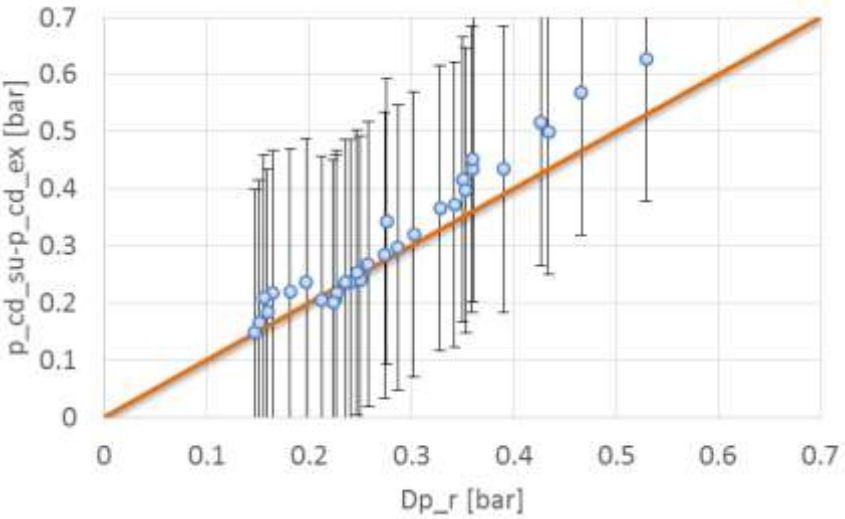

Figure 36: Cross-checking of pressure sensor of the condenser (ORC)

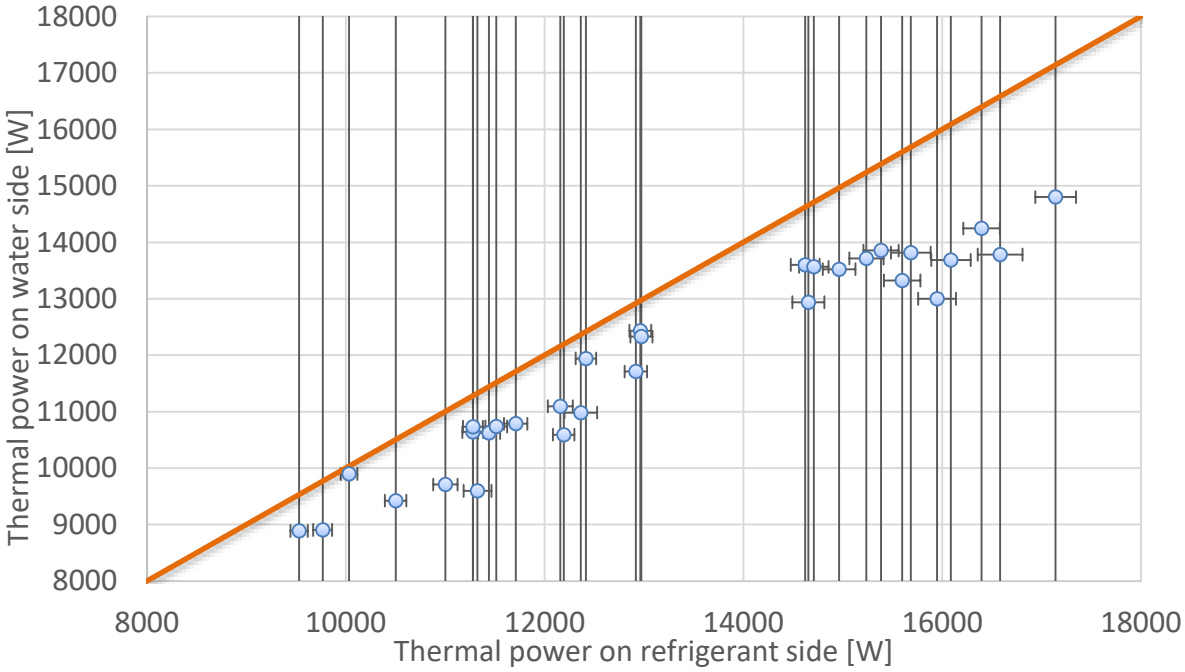

Figure 37: Heat balance on the condenser (heat pump)

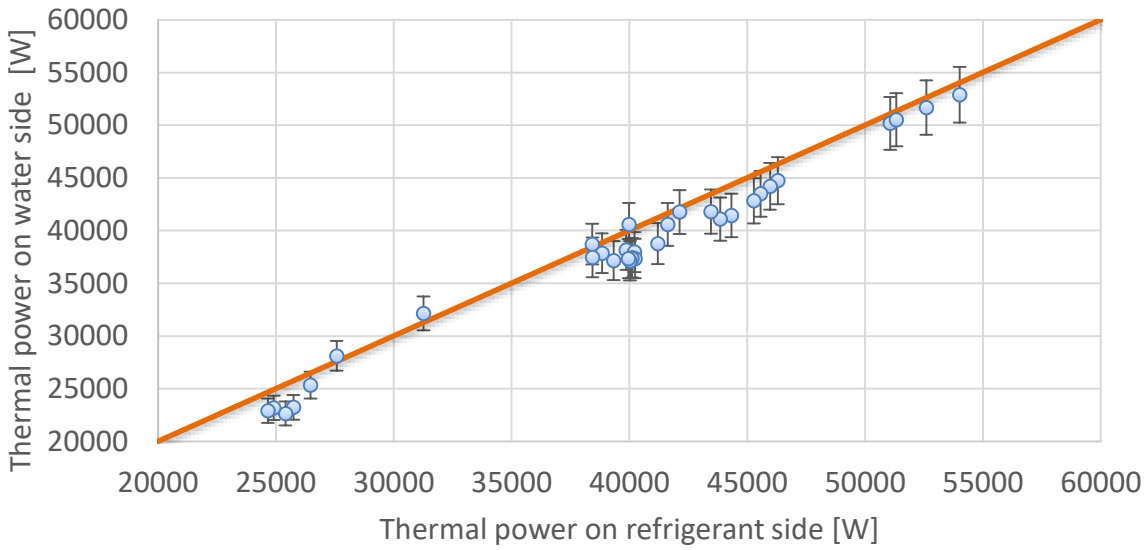

Figure 38: Heat balance on the condenser (ORC).

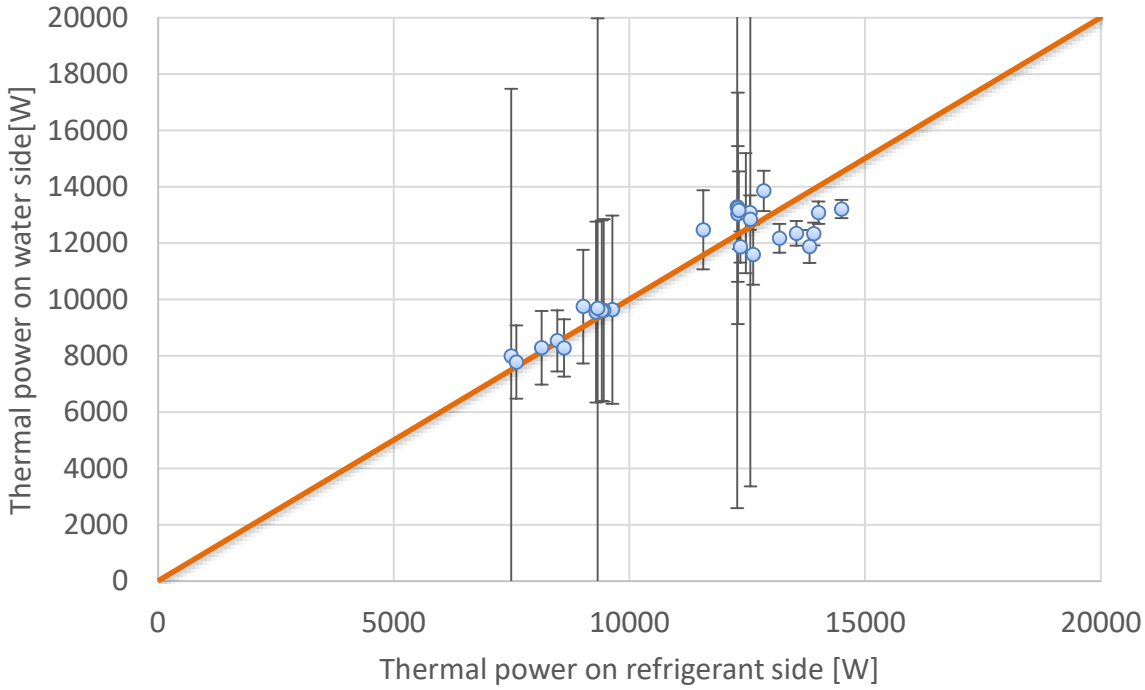

Figure 39: Evaporator heat balance (heat pump mode)

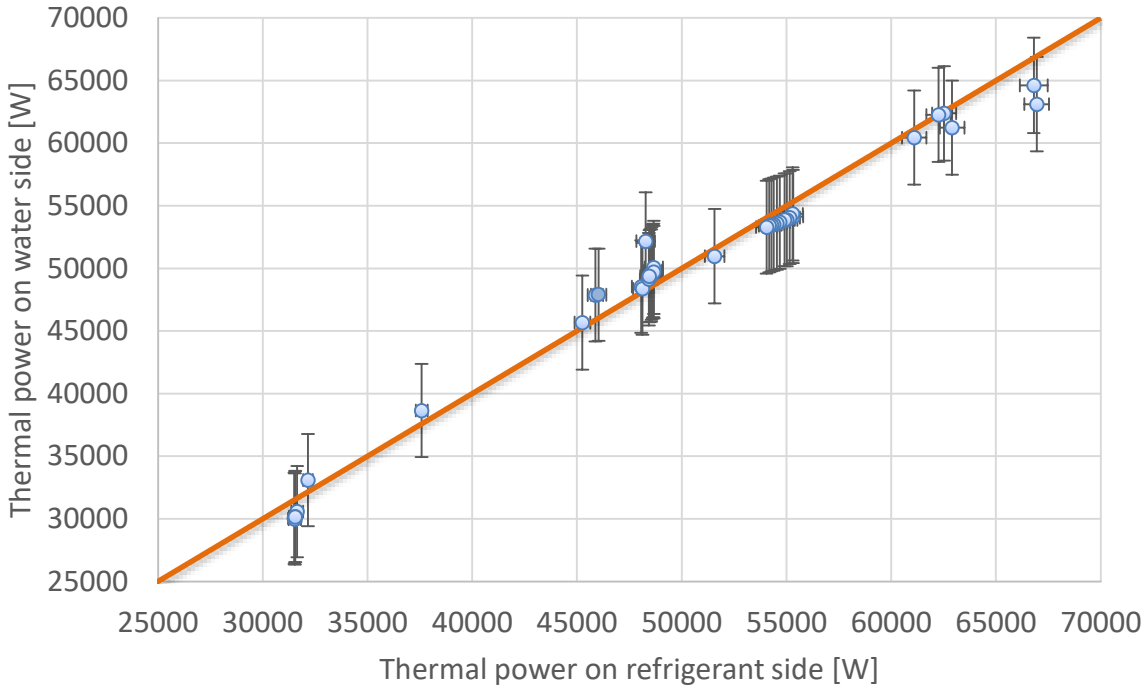

Figure 40: Evaporator heat balance (ORC generation mode)

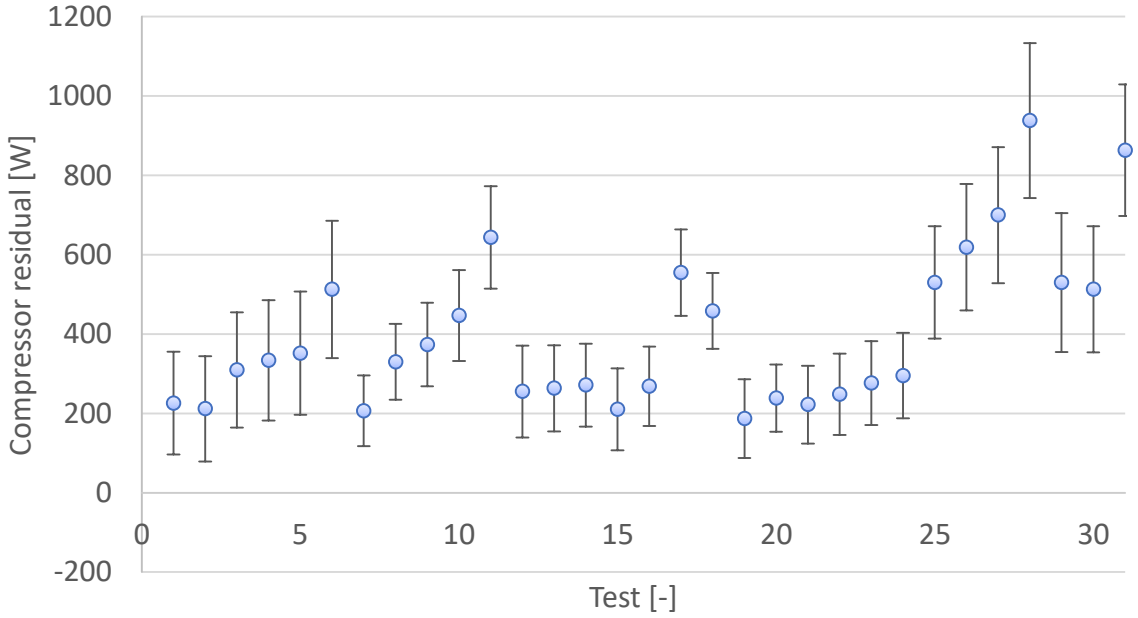

Figure 41: Compressor residual

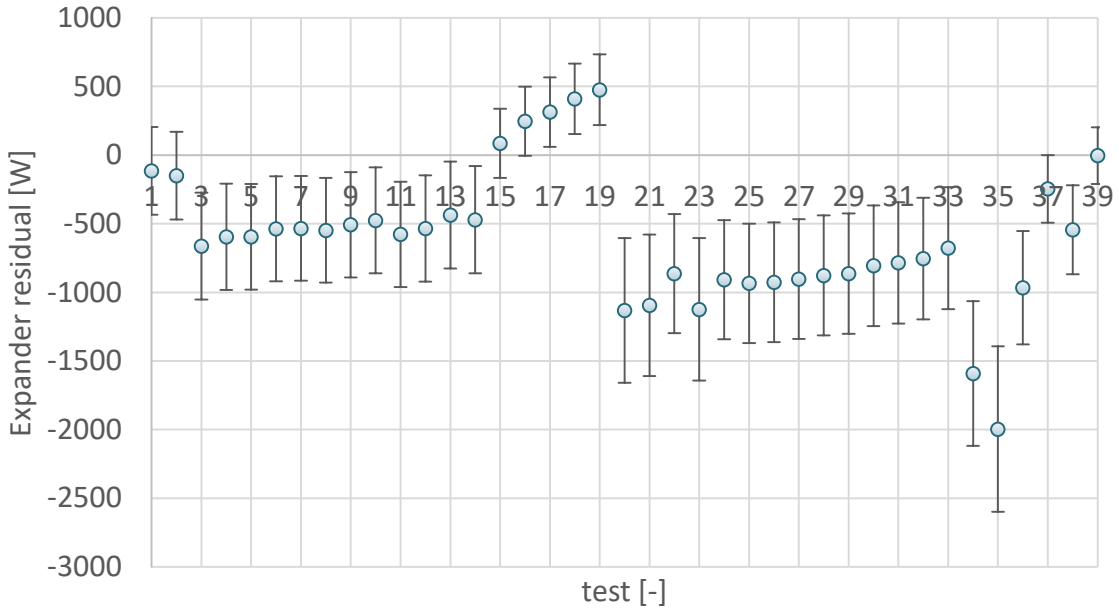

Figure 42: Expander residual

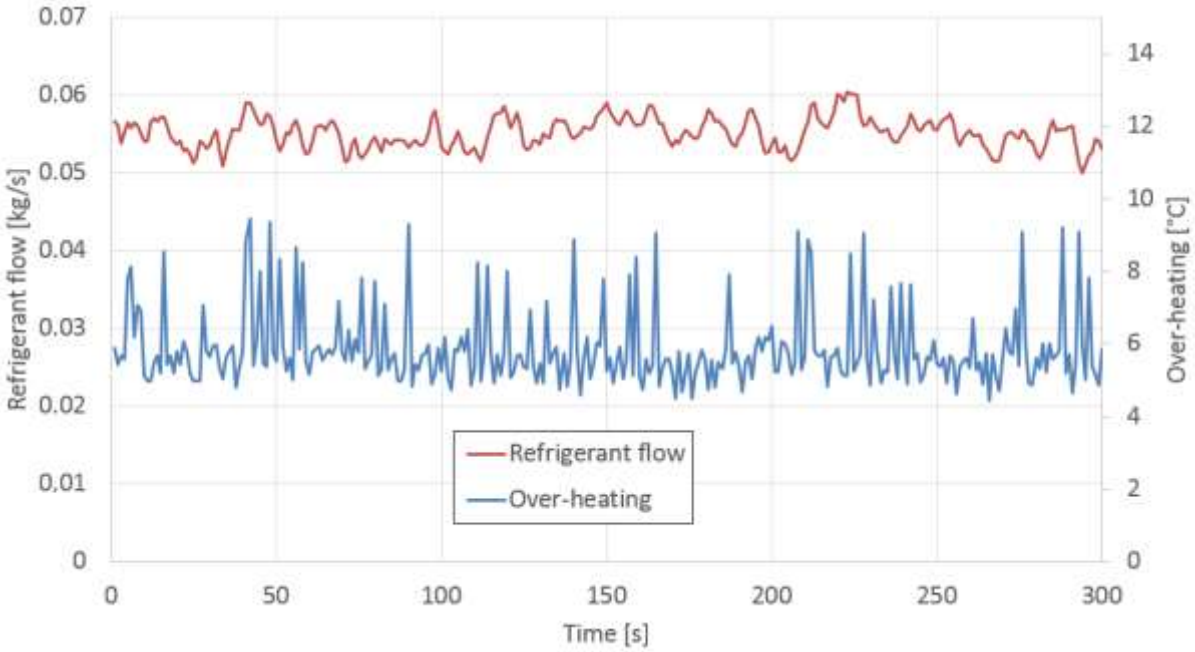

Figure 43: Oscillations of the flow due to the electronic expansion valve. This is observed when the set-point of over-heating is low

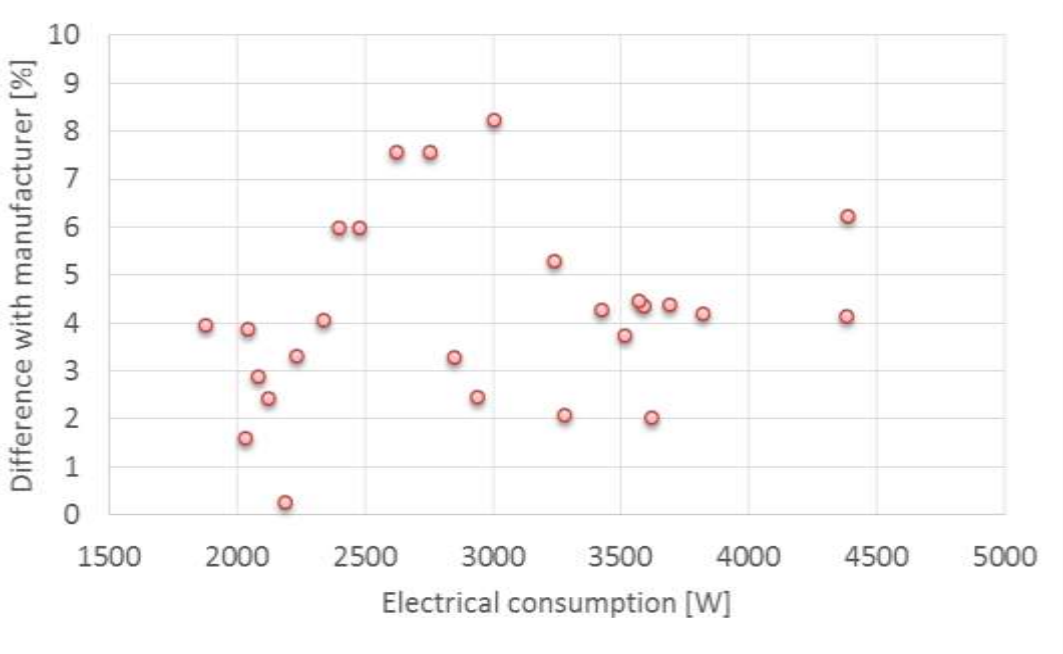

Figure 44: Difference between the experimental and manufacturer electrical consumption of the compressor.

Table 18 : Range of the inputs of the global models

Inputs	**Range**	
mode	HP	ORC
Condenser secondary fluid flow [l/s]	[0.04:1.5]	[0.5:2]
Condenser secondary fluid inlet temperature [°C]	[20:80]	[5:40]
Evaporator secondary fluid flow [l/s]	[0.05:0.5]	[0.1:0.7]
Evaporator secondary fluid inlet temperature [°C]	[-15:30]	[60:120]

Table 19 : polynomials for ORC/HP prediction of performance

$$T_{w,ev,ex,HP} = a_1 + a_2.T_{w,cd,su} + a_3.T_{w,cd,su}^{\ 2} + a_4.T_{w,ev,su} + a_5.T_{w,ev,su}^{\ 2}$$

$$\dot{W}_{el,ORC}=b_1+b_2.\dot{m}_{w,ev}+b_3.\dot{m}_{w,ev}^{\ 2}+b_4.\dot{m}_{w,cd} + b_5.\dot{m}_{w,cd}^{\ 2} + b_6.T_{w,cd,su} + b_7.T_{w,cd,su}^{\ 2}+b_8.T_{w,ev,su}\ b_9.T_{w,ev,su}^{\ 2}$$

$$T_{w,ev,ex,ORC}=c_1+c_2.\dot{m}_{w,ev} +c_3.\dot{m}_{w,ev}^{\ 2}+c_4.\dot{m}_{w,cd}+c_5.\dot{m}_{w,cd}^{\ 2}+c_6.T_{w,cd,su}+c_7 +c_8T_{w,ev,su} +c_9.T_{w,ev,su}^{\ 2}$$

$$\dot{W}_{el,HP}=d_1+d_2.\dot{m}_{w,ev}+d_3.\dot{m}_{w,ev}^{\ 2} + d_4.sc+d_5.sc\text{^}2+d_6.\dot{m}_{w,cd}+ d_7.\dot{m}_{w,cd}^{\ 2}+d_8.T_{w,cd,su}+d_9.T_{w,cd,su}^{\ 2}+d_{10}T_{w,ev,su}+d_{11}.T_{w,ev,su}^{\ 2}+d_{12}.\dot{m}_{w,ev}.sc+d_{13}.\dot{m}_{w,ev}.\dot{m}_{w,cd}+ d_{14}.\dot{m}_{w,ev}.T_{w,cd,su} + d_{15}.\dot{m}_{w,ev}.T_{w,ev,su} + d_{16}.sc.\dot{m}_{w,cd} + d_{17}.sc.T_{w,cd,su}+ d_{18}\ .sc.T_{w,ev,su}+d_{19}.\dot{m}_{w,cd}.T_{w,cd,su} + d_{20}.\dot{m}_{w,cd}.T_{w,ev,su} + d_{21}.T_{w,cd,su}.T_{w,ev,su}$$

$$\dot{Q}_{cd,HP} = e_1 +e_2.\dot{m}_{w,ev}+e_3.\dot{m}_{w,ev}^{\ 2}+e_4.sc+e_5.sc^2+e_6\ .\dot{m}_{w,cd}+e_7.\dot{m}_{w,cd}^{\ 2}+ e_8\ .T_{w,cd,su}+e_9.T_{w,cd,su}^{\ 2}+e_{10.}T_{w,ev,su}+e_{11}.T_{w,ev,su}^{\ 2}$$

Table 20 : Coefficient for the polynomial of the HP/ORC reversible unit

a_1	-9.87428468	b_1	2.71543730E+02
a_2	0.121624764	b_2	-2.18706646E+03
a_3	$-2.40859537E-04$	b_3	-6.82084229E+03
a_4	1.23728511	b_4	0.07222890E+03
a_5	$-3.96640941E$	b_5	1.65290727E+02
d_1	8.40807593E+02	b_6	-0.47805165E+01
d_2	1.89837540E+03	b_7	1.10412192E-01
d_3	-2.74503287E+03	b_8	9.48391483E+01
d_4	3.33788461E+02	b_9	-8.47467828E-02
d_5	-1.12136838E-01	c_1	-4.11634724E+00
d_6	+6.96662715E+02	c_2	3.97569704E-01
d_7	1.76531001E+02	c_3	-3.40747425E+00
d_8	4.34845595E +02	c_4	-5.07916414E-01
d_9	9.73420594E-01	c_5	1.44562242E-01*
d_{10}	6.34277013E+01	c_6	3.08137710E-02
d_{11}	9.52076505E-01	c_7	+1.47207257E-04
d_{12}	-5.46566625E+02	c_8	+1.10360430E+00
d_{13}	-2.00942356E+03	c_9	-5.81198164E-03
d_{14}	7.08494196E+02	e_1	4964
d_{15}	-9.65352859E+00	e_2	-414.2
d_{16}	-8.38139478E-01	e_3	15435
d_{17}	-1.02958290E-01	e_4	-8.24
d_{18}	2.43267726E-01	e_5	0.08991
d_{19}	-1.93089374E+00	e_6	437
d_{20}	-7.16484773E-01	e_7	-125.7805
d_{21}	-2.23569289E+00	e_8	-0.28.72
		e_9	-0.2311
		e_{10}	121.6
		e_{11}	2.993

References

- Aoun, B., Clodic, D., 2008. Theoretical and experimental study of an oil-free scroll vapor expander, International compressor engineering conference.

- Almanza, R., Lentz, A., 1998. Electricity production at low power by direct steam generation with parabolic troughs collectors, Sol. Energy, 64, 115-120.

- Bao, J., Zhao, L., Zhang, W. Z., 2011. A novel auto-cascade low-temperature solar Rankine cycle for power generation, Sol. Energy, 85, 2710-2719.

- Barbosa, R., Gessner, J., Tobias, R., 2006. Modeling absorption of pure refrigerants and refrigerants mixtures in lubricant oil, International Journal of refrigeration, vol. 29, p. 773-780, 2006.

- Bell, I., Quoilin, S., Wronski, J., Lemort, V., Coolprop: an open source reference-quality thermophysical property library, ORC 2015 conference, 2015. http://orbit.dtu.dk/ws/files/59934392/COOLPROP.pdf

- Bettgenhäuser K., Offermann M., Boermans T., Bosquet M., Grözinger J., von Manteuffel B. and Surmeli N., 2013. Heat Pump Implementation Scenarios until 2030: An analysis of the technology's potential in the building sector of Austria, Belgium, Germany, Spain, France, Italy, Sweden and the United Kingdom, ECOFYS Report, Project number: BUIDE12080.

- Bouvier, J. L., 2013. Prototype d'un micro-cogénérateur à nergie solaire : MICOSOL, Proceedings of Journées micro-cogénération CNAM Paris 2013

- Bruno, J. C., Romera, S., Figueredo, G., Coronas, A., 2007. Hybrid solar/gas Single/Double effect absorption chiller : Operational results using data reconciliation, Proceedings of the 2nd International Conference on Solar Air-conditionning, Tarragona, Spain, 244-249.

- Cuevas, C., 2006. Contribution to the modelling of refrigeration systems. PhD thesis, Liege, Belgium: University of Liege.

- Dickes, R., Dumont, O., Declaye, S., Quoilin, S., Bell, I., Lemort, V., 2014. Experimental Investigation Of An ORC System For A Micro-Solar Power Plant, Proceedings of International Compressor Engineering Conference at Purdue 2014.

- Dickes, R., Dumont, O., Daccord, R., Quoilin, S., Lemort, V., 2016. Modelling of organic Rankine cycles in off-design conditions: an experimentally-validated comparative study; Energy, Volume 123, 15 March 2017, Pages 710-727, https://doi.org/10.1016/j.energy.2017.01.130.

- Dirlea, R., 1997. Performance rating of refrigeration components, PhD thesis.

- Cuevas, C., 2006. Contribution to the modelling of refrigeration systems, PhD thesis.

- Dumont, O., Quoilin, S., Lemort, V., 2014 (a). Design, modelling and experimentation of a reversible HP/ORC prototype, Proceedings of the 11th International Energy Agency Heat Pump Conference. http://hdl.handle.net/2268/171478.

- Dumont, O., Quoilin, S., Lemort, V., 2014 (b). Design, modelling and experimentation of a reversible HP-ORC prototype, ASME TURBO EXPO 2014: Proceedings of the ASME TURBO EXPO 2014, 2014 Jun 16-20; Dusseldorf, Germany.

- Dumont, O., Quoilin, S., Lemort, V., 2015. Experimental investigation of a reversible heat pump/organic Rankine cycle unit designed to be coupled with a passive house to get a Net Zero Energy Building, Int. J. Refr. 54:190–203.

- Emerson website, 2014. www.emersonclimate.com/en-US/Pages/Home.aspx, consulted the 28th of April 2014.

- European Commission, 2012. Communication from the comission to the european parliament, the council, the european economic and social comittee and the committee of the regions, Brussel.

- European Comission, 2010. Directive 2010/31/CE of the European parliament and of the council of 19 May 2010.

- European Comission, 2011. Market observatory for energy.

- Facao, J., Palmero-Marrero, A., Oliveira, A. C., 2008. Analysis of a solar assisted micro-cogeneration ORC system, Int. J. Low-Carbon Tech., 3 (4), 254-264.

- Georges, E., Declaye, S., Dumont, O., Quoilin, S., Lemort, V., 2013. Design of a small-scale organic rankine cycle engine used in a solar power plant, Int. J. Low Carbon Tech., 8 (1), 34-41.

- Hepbasli, A., Yalinci, Y., 2009. A review of heat pump water systems, IRESR, 13, 1211-1229.

- Heyen, G., Kalitvebtzeff, B., 1997. Methodology for optimization of operation to reduce site-scale energy use in production plants, Appl. Therm. Eng. 17:1005-1014.

- Hodouin, D., Everell, M. D., 1980. A hierarchical procedure for adjustment and material balancing of mineral processed data, Int. J. Miner 7:91-116.

- Innogie ApS., 2013. Thermal solar absorber system generating heat and electricity, United States Patent Application Publication, US 2013/025778 A1.

- Innogie ApS., 2014. Innogie website, http://www.innogie.dk., Consuted 12th of January 2014.

- International Energy Agency, 2012. Technology roadmap – solar heating and cooling.

- Jagemar, L., Schmidt, M., Allard, F., Heiselberg, P., Kurnitski, J., 2011. Towards NZEB – Some example of national requirements and roadmaps, REHVA Journal, May 2011, 14-17.

- Jiang, X., Liu, P., Li, Z., A, 2014. Data reconciliation based framework for integrated sensor and equipment performance monitoring in power plants, App. En., 134:270–282.

- Kane, M., Larrain, D., Favrat D., Allani, Y., 2003. Small hybrid solar system, Energy, 28, 1427-1443.

- Kuehn, D. R., Davidson, H., 1967. Computer Control II Mathematics of control, Chem. Eng. Prog., 57:44-47.

- Kurnitski, J., Corgnati, S., Tiziana, B., Derjanecz, A., Litiu, A., 2014. NZEB definitions in Europe, REHVA Journal, March 2014, 6-9.

- Lemort, V., 2008. Contribution to the characterization of scroll machines in compressor and expander modes. PhD thesis, Liege, Belgium: University of Liege; 2008.

- Lemort, V., Quoilin, S., Cuevas, C., and Lebrun, J. 2009. Testing and modeling a scroll expander integrated into an Organic Rankine Cycle, Appl. Therm. Eng., 29/(14–15), 3094-3102.

- Lid, T., Skogestad, S., 2008. Data reconciliation and optimal operation of a catalytic naphta reformer, J. Process. Control, 18:320-331.

- Lu, Y.J., Wang, L.W., Tian, G.H., Roskilly, A.P. 2012. Study on a small scale solar powered organic Rankine cycle utilizing Scroll expander, 4th International Conference Applied Energy.

- Malavolta, M., Beyene, A., Venturini, M., 2010. Experimental implementation of a micro-scale ORC-based CHP energy system for domestic applications, proceedings of the ASME 2010 International Mechanical Engineering Congress & Exposition.

- Manzagol, J., Harboulle, P., Claudet, G., Baguer, G., 2002. Cryogenic scroll expander for claude cycle with cooling power of 10 to 100 Watts at 4.2 K, AIP Conference Proceedings, 613 (1), 267.

- Martinez-Maradiaga, D., Bruno, J. C., Coronas, C., 2013. Steady-state data reconciliation for absorption refrigeration system, App. Therm, Eng., 1170-1180.

- Oliveira, A. C., Alfonso, C., Matos, J., Riffat, S., Nguyen, M., Doherty, P., 2002. A combined heat and power system for buildings driven by solar energy and gas, Appl. Therm. Eng., 22, 587-593.

- Orosz, M., Mueller, A., Quoilin, S., Hemond, H., 2009. Small Scale Solar ORC System For Distributed Power, Solar world congress 2009.

- Oudkerk, J. F., Quoilin, S., Lemort, V., 2011. Evaluation of an ORC-based micro-CHP system involving a hermetic scroll expander, Proceedings of the ORC 2011 conference.

- Ozyurt, D. B., Pike, R. W., 2004. Theory and practice of simultaneous data reconciliation gross error detection for chemical processes, Comp. Chem. Eng., 28:381-402.

- Placido, J., Loureiro, L.V., 1998. Industrial application of data reconciliation, Comput. Chem. Eng., 22:S1035-S11038.

- Prata, D. M., Schwaab, M., Lima, E. L., Pinto, J. C., 2010. Simultaneous robust data reconciliation and gross error detection through particle swarm optimization for an industrial poplypropylene reactor, Chem. Eng. Sc., 65:4943-4964.

- Qiu, G., Liu, H., Riffat, S., 2011. Expanders for micro-CHP systems with Organic Rankine Cycle, Appl. Therm. Eng., 31, 3301-3307.

- Quoilin, S., 2011. Sustainable Energy Conversion Through the Use of Organic Rankine Cycles for Waste Heat Recovery and Solar Applications, Doctoral thesis, University of Liege, Liege.

- Quoilin, S., Schrouff, J., 2016. Assessing Steady-State, Multivariate Experimental Data Using Gaussian Processes: The GPExp Open-Source Library, Energies 2016, 9, 423; doi:10.3390/en9060423.

- Saitoh, T., Fujino, T., 2001. Advanced energy-efficient house (HARBEMAN house) with solar thermal, photovoltaic, and sky radiation energies (experimental results), Sol. Energy, 70 (1), 63-77.

- Saitoh, T., Yamada, N., Wakashima, S., 2007. Solar Rankine cycle sytem using Scroll expander, Journal of environment and engineering, 2 (4), 2007.

- Schimpf, S., Uitz, K., Span, R., 2011. Simulation of a solar assisted combined heat pump-organic Rankine cycle system, Proceedings of World renewable Energy Congress 2011 Sweden.

- Schladt, M., Hu, B., 2008. Soft sensors based on nonlinear steady-state data reconciliation in the process industry, Chem. Eng. Process. 46:320-331.

- Szega, M., Nowak, G., 2015. An optimization of redundant measurements location or thermal capacity of power unit steam boiler calculations using data reconciliation method, Energy. 92:135–141.

- Twomey, B., Jacobs, P.A., Gurgenci, H., 2013. Dynamic performance estimation of small-scale solar cogeneration with an Organic Rankine cycle using a scroll expander, Appl. Therm. Eng. 51, 1307-1316.

- Winandy, E., Lebrun, J., 2002. Scroll compressors using gas and liquid injection: Experimental analysis and modelling, Article in International Journal of Refrigeration 25(8):1143-1156, DOI: 10.1016/S0140-7007(02)00003-8

- Wolpert, J. L., Riffat, S. B., 1995. Solar-powered Rankine system for domestic application, Appl. Therm. Eng. 00032 (1), 1359-4311.

- Wang, X. D., Zhao, L., Wang, J. L., Zhang, W. Z., Zhao, X. Z., Wu, W., 2010. Performance evaluation of a low-temperature solar Rankine cycle using R245fa, Sol. Energy, 84, 353-364.

- Weiss, G. H., Romagnoli, J.A., Islam, K. A., 1996. Data reconciliation – an industrial case study, Comput. Chem. Eng., 20:1441-1449.

- Youbi-Idrissi, M., Bonjour, J., Marvillet, C., Meunier, F., 2003. Impact of refrigerant-oil solubility on an evaporator performances working with R-407C, International Journal of refrigeration, vol. 26, 284-292.

- Yanagisawa,T., Cheng, M.C., Fukuta, M., Shimizu, T., 1990. Optimum operating pressure ratio for Scroll compressor, proceeding of the International compressor engineering conference at Purdue, 425-433.

- Zanelli, R., Favrat, D., 1994. Experimental investigation of a hermetic scroll expander generator, International compressor engineering conference, 1021.

- Zhang, Z., Shao, Z., Chen, X., Wang, K., Qian, J., 2010. Quasi-weighted least squares estimator for data reconciliation, Comp. Chem. Eng., 34:154-162.

- Ziviani, D., Beyene, A, Venturini, M., 2014. Design, analysis and optimization of a micro-CHP system based on organic Rankine cycle system for ultralow grade thermal energy efficiency, Journal of energy ressources technology, 136, 011602-1.

Chapter 5:

Dynamic modelling of a reversible HP/ORC system: case of a residential heat pump coupled with solar panels

"Only when the last tree has died and the last river been poisoned and the last fish been caught will we realize we cannot eat money."
Cree Indian

Abstract

This chapter focuses on describing the dynamic model of the multi-component system followed by a techno-economic analysis of the system under different operational conditions. Sensitivity studies include: building envelope, climate, appliances, storage configuration and size, batteries, roof tilt angle, lighting and heat demand profiles. It is concluded that the HP/ORC unit can turn a single-family house into a PEB under certain weather conditions (electrical production of 3012 kWh/year and total electrical consumption of 2318 kWh/year) with a 138.8 m2 solar roof in Denmark. Also, an economic comparison with a mature technology (photovoltaic panels combined with a heat pump) is proposed. The results show that the reversible HP/ORC unit performs better in location with latitude close to Torino and in building presenting a large heat demand.

1 INTRODUCTION

This chapter studies the reversible unit in the case of a residential heat pump coupled with solar panels based on advanced dynamic models. This system has already been extensively detailed in Chapter three. A validated model of the reversible HP/ORC unit is developed and re-used here (Chapter four). The global model developed combines validated sub-models: the reversible HP/ORC unit, the solar roof, the thermal energy storage, the horizontal ground heat

exchanger and the building. An optimal strategy control is developed and presented. A parametric study is performed to observe the performance of the system in a wide range of typologies. The influence of different parameters such as lights and appliances profiles, building envelope characteristics, integration of batteries, roof tilt angles, locations and storage sizes is investigated. In this context, a decision tree is proposed to select the optimal thermal energy storage modelling approach depending on the application. Furthermore, a technical and economical comparison with a mature technology to get a positive energy building, photovoltaics panels combined with a heat pump in a passive house, is performed.

1.1 SIMULATION TOOL

Among simulation programs, some are dedicated to building performance simulation (IDA ICE, ESP-r, EnergyPlus, TRNSYS, WUFI®Plus, etc) while others are more general (Dymola/Modelica, MATLAB/ Simulink, IDA SE, etc.). Simulation tools like Matlab–Simulink need the model to be implemented, in a state-space form in which causal relations play an important role. A simulation language based on an object oriented approach and physically oriented connections – Modelica - is chosen as simulation tool to model the new system proposed in this work. Recently, Modelica has become more and more used in building performance simulation. The Lawrence Berkeley National Laboratory developed a Modelica library called "*Buildings*" that contains a large number of HVAC components models and a multi-zone building model (Wetter et al., 2011). Also, the RWTH Aachen and UdK Berlin (Nytsch-Geusen and Unger, 2009) are developing Modelica libraries for HVAC-systems and building models. Besides many models for HVAC components and different thermal zone models, the RWTH Aachen library offers a database of manufacturer's data for building technology (Muller and Badakhshani, 2010).

1.2 NON-PREDICTIVE CONTROL

It should be noted that, although an optimization has been performed, the proposed control strategy is still a myopic rule-based control strategy. A truly optimal control strategy is difficult to implement because of the high number of manipulated variables, the numerous set-points and the non-linearity of the problem. It would require a predictive non-linear optimization, based on the next 24 hours of weather forecast, user behaviour and electricity prices. Such approach would avoid, for example, starting the heat pump when the solar heat will be sufficient to cover the heat demand later in the day. Furthermore, such modulation strategies require smart-meters which are still at an early stage of practical implementation.

1.3 TIME CONSTANT

Before describing each of the different models and the control strategy, it is important to note that the dynamic modelling of a system including several sub-systems does not systematically require each model to be dynamic: components characterized by relatively low time constants

can be modelled as quasi-steady-state, since their fast dynamics are not relevant to the overall simulation and can substantially impact the computational effort (Perers, 1997, Chow, 1993, Schnieders, 1997, Fischer et al., 2004, Dumont et al., 2014a and Freeman et al., 2015). In the law of conservation of energy, if the mass and volume (or time constant) are negligible, then the equation becomes independent of time. Time constants ($\varkappa$) are evaluated experimentally or estimated with Eq. 1 and compared in Table 1.

$$\varkappa = \frac{0.63.M.\Delta t}{\dot{m}} \qquad 1$$

In this equation, M is the mass of the system, $\dot{m}$ is the typical mass flow rate and Δt (the variation of the system temperature) is taken equal to 10 K. This equation comes from an energy balance assuming that mass flow rate, specific heat and the total mass of fluid in the system are constant. The time constant is reached when the increase in temperature has reached 63% of its final value.

Table 1: Time constant of the different sub-systems

Sub-system	Method	Time constant [min]
Reversible HP/ORC unit	Experimentation	5
Solar roof	Eq. 1	18
Storage	Eq. 1	87
House	Simulation	3133 (50h)
Ground source heat exchanger	Simulation	35

The inertia of the unit is, therefore, neglected because of its very low time constant. The dynamic behaviour of the solar roof, the house, the horizontal ground heat exchanger and the storage are modelled.

2 DESCRIPTION OF THE MODEL

2.1 BUILDING MODEL

The model is based directly on the geometry and on the construction characteristics of the real Danish building where the reversible HP/ORC unit is installed. A simplified lumped parametric model is applied. The root mean square error on the yearly prediction of the inner temperature of such a model has been shown to be always lower than 1K (Masy, 2007). The

configuration of the different rooms of the building and the composition of the walls are taken into account.

Figure 1: Division of the house into 5 zones

The building is first divided into 5 zones (dining room and kitchen, main bedroom, bathroom, hall and toilet and finally guest bedrooms) with constant volume and uniform temperature in each zone. The definition of the zones is given in Figure 1 and the zone characteristics in Table 2. A PID controller controls the floor heating flow to maintain the ambient temperature inside the house close to the set point which is chosen equal to 19°C. There is no temperature constraints for the other zones. However, an a posteriori check shows a maximum deviation of 2K between zone 1 and the other ones.

Table 2: House main characteristics

	Unit	Zone 1	Zone 2	Zone 3	Zone 4	Zone 5
Floor area	m²	41.8	18.2	7.8	19.1	45.7
Volume	m³	117.2	45.5	19.5	47.8	114.3
Slab U-Value	W/m².K	0.08	0.08	0.08	0.08	0.08
Roof U-Value	W/m².K	0.09	0.09	0.09	0.09	0.09
External wall area	m²	none	20.4	4.5	24.8	41.5
External wall U-value	W/m².K	none	0.15	0.15	0.15	0.15
Window area (orientation)	m²	14.7(S)	2.4(S)	0.84(W)	0.84(W) 0.84(N)	6.7(E) 2.4(S)
Window U-value	W/m².K	0.63	0.68	0.8	0.8	0.8
Window solar factor	-	0.5	0.5	0.5	0.5	0.5
Infiltration rate	ACH	0.3	0.3	0.3	0.3	0.3
Space activity	-	Kitchen Dining	Main Bedroom	Bathroom	Hall Others	Living Bedroom
Lighting nominal power	W/m²	5	5	3	3	5
Appliances nominal power	W/m²	3	3	3	3	3
Setpoint	°C	19	None	None	None	None

The Modelica model diagram of the house is presented in Figure 2. It is composed of models developed based on the Modelica Standard Library model (version 3.2) and also use the "*MixingVolume*" and "*RadiantSlabs.SingleCircuitSlab*" models developed in the Modelica library "*Buildings*" (Wetter et al., 2013). The radiant slab (25 m^2) is connected to the only room where it provides heat in the house (zone 1). Hourly schedules are associated to the occupancy, the domestic hot water use, the lighting and appliances in each zone. The weather data used for the external temperature and the solar irradiance are provided by the DMI - Denmarks Meteorologiske Institut - (Wang et al., 2010).

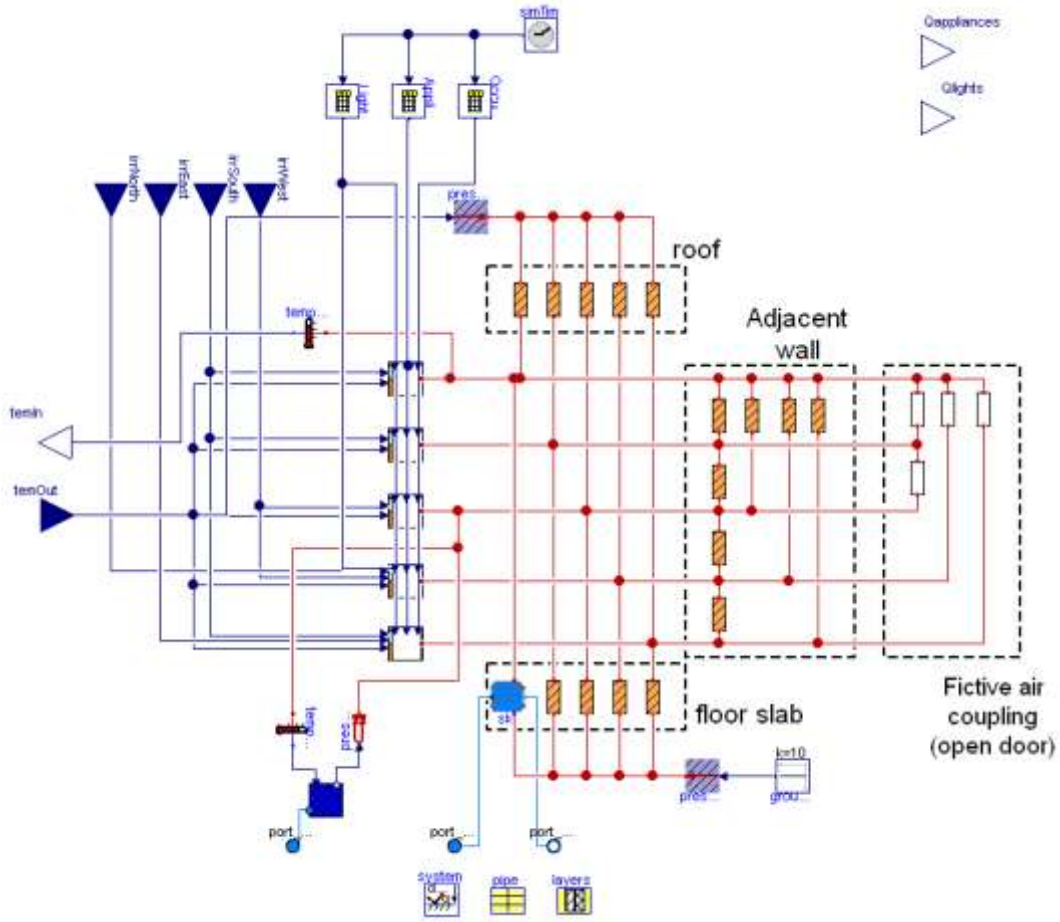

Figure 2: Modelica model diagram

The walls are modelled following Masy's PhD thesis (Masy, 2007), with four required parameters (capacity, resistance, accessibility and the proportion of the whole wall capacity accessed by a 24 h time period solicitation). Four inputs are added in each zone: lighting, appliances, occupancy and a thermal exchange with adjacent zones. Natural air circulation due to buoyancy effect (associated with the difference of temperature between the building indoor and outdoor) and wind pressure and forced air circulation due to mechanical ventilation are not modelled in order to avoid too high level of complexity and computational time.

Each zone model is based on an equivalent R-C network including 5 thermal masses (Bertagnolio et al., 2008), corresponding to one occupancy zone, surrounded by external glazed and opaque walls (Figure 3).

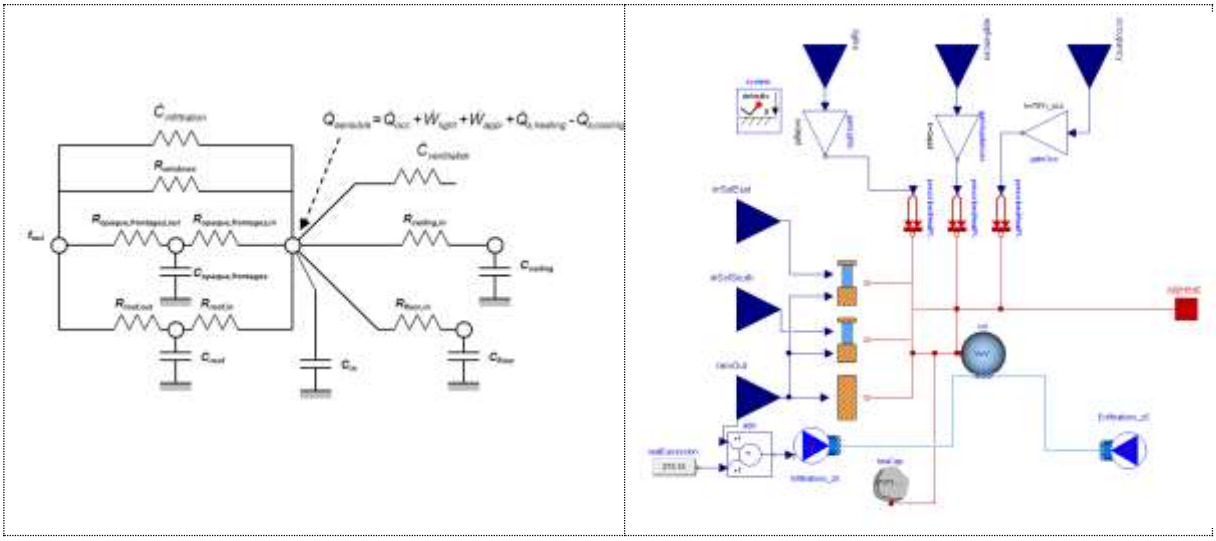

Figure 3: Zone Model – Equivalent R-C Network and Modelica Network Model

Each massive wall is represented by a first order R-C network comprising two resistances and one capacity (Figure 4). The resistance and capacity of each wall model are adjusted in order to produce wall admittance transmittance for a 24 hour period solicitation (Masy, 2006). The wall stationary U-value equals the invert of the whole two-port resistance.

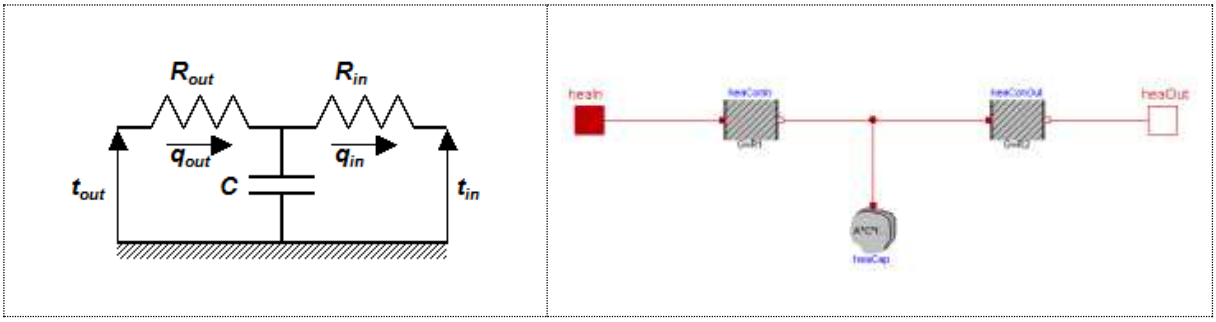

Figure 4 - Capacitive wall model diagram

Table 3 presents the inputs and outputs of the model.

Table 3: Inputs and outputs of the house model

Inputs	Outputs
Ambient temperature DNI Floor heating inlet temperature DHW inlet temperature Occupancy behaviour	House temperature Floor heating outlet temperature

In this study, only south-oriented roofs are considered to limit the number of study cases which is already high. Two different tilt angles are considered (5° and 35°). The orientation of the solar generator impacts the temporal electricity production. A horizontal solar roof orientation leads to higher summer production (while the house electrical consumption is already covered with a 35° tilt angle roof) and lower winter production and therefore to lower self-consumption of the system.

2.2 REVERSIBLE HEAT PUMP ORGANIC RANKINE CYCLE SYSTEM

The unit has been tested in a wide range of conditions experimentally (Chapter four). Following that, semi-empirical models have been calibrated to fit the measurements. The inputs and outputs of these validated models are summarized in Table 4. In heat pump mode, the sub-cooling is imposed at 2 K and the superheating at 6 K. In ORC mode, the sub-cooling is imposed by the NPSH of the pump and the over-heating is optimized (by adjusting the pump speed) to maximize the electrical power production (Chapter four). Chapter four presents the polynomials used to evaluate the outputs of the reversible unit. As mentioned in section 1.3, the thermal inertia of the machine is neglected. Hence, a steady-state model is suitable.

Table 4: Inputs and outputs of the reversible HP/ORC unit

Inputs	Outputs
Condenser water inlet temperature	Electrical consumption/production
Evaporator water inlet temperature	Condenser water outlet temperature
Condenser water flow	Evaporator water outlet temperature
Evaporator water flow	

2.3 HORIZONTAL GROUND HEAT EXCHANGER

2.3.1 Description of the case study

The ground source horizontal heat exchanger consists of three layers layout. The layers are linked in parallel and buried respectively at 0.5, 1.0 and 1.5 meters depth. Each layer consists of 24 tubes and are made in cross-linked polyethylene and are 22.89 m long with a diameter of 2.6 cm (geometry of the GHX - Figure A3). A 30% mono-ethylene glycol-water mixture is used as the heat transfer fluid. The soil is assumed to be argillaceous with a water content of 10%, which corresponds to an average soil moisture (Bircher et al., 2012).

2.3.2 Description of the model

The deep earth temperature, here considered as the temperature of the ground not affected by variation of the outside temperature, is set to 10°C. This choice is made following ground measurements conducted in Potsdam, Germany, (PICIR, 2015). The absorptance and emissivity of the soil surface are respectively set to 0.55 and 0.75. An average wind speed of 4 $m.s^{-1}$ is considered for the convective losses with ambient conditions.

A model of the ground source horizontal heat exchanger already exists (using the finite element method) in the TRNSYS simulation language (TESS, 2006). A reduced order model is

developed and calibrated based on the reference finite element model (TESS, 2006). This model is designed to be flexible and is valid for different kinds of pipes geometry and layout.

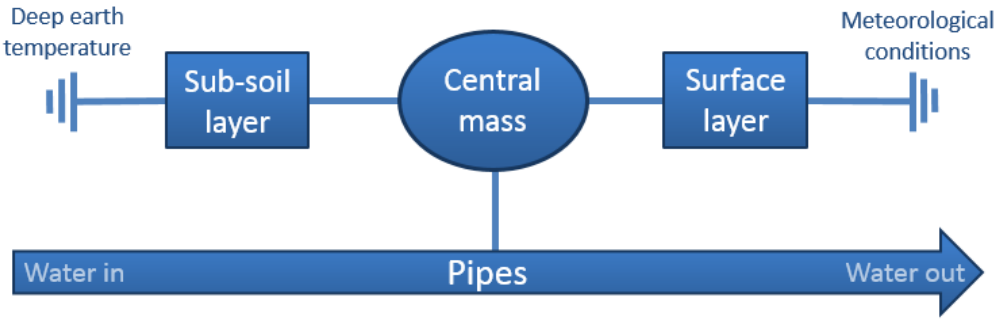

Figure 5: Layout of the reduced order model of the horizontal ground heat exchanger

The model consists in discretizing three layers of ground (Figure 5). The central element in the model is the soil central thermal mass which simulates the soil directly surrounding the GHX pipes. In addition, a surface layer which reacts rapidly to climate variations (solar irradiation, ambient temperature, sky temperature and wind) is added. Finally, a sub-soil layer presenting slow variations through the seasons is modelled and connected to the deep earth temperature. Each layer is modelled with a central capacity and two resistors. The pipes are modelled with a finite volume 1D flow model (20 cells) from the Thermocycle library (Quoilin et al., 2014). Finally, two thermal resistances are added to the pipes to account for the resistance of the tube and, for the resistance of the soil.

2.3.3 Calibration of the reduced order model

The reduced order model described here above is calibrated with the finite element model as a reference by variation of the two main inputs, which are the ambient temperature and the solar irradiation. The GHX model parameters are defined in Table A3 (in Appendices). With these parameters, results show good agreement between the two models. A maximum deviation of 0.5 K is observed for the prediction of the water outlet temperature (Figure 6).

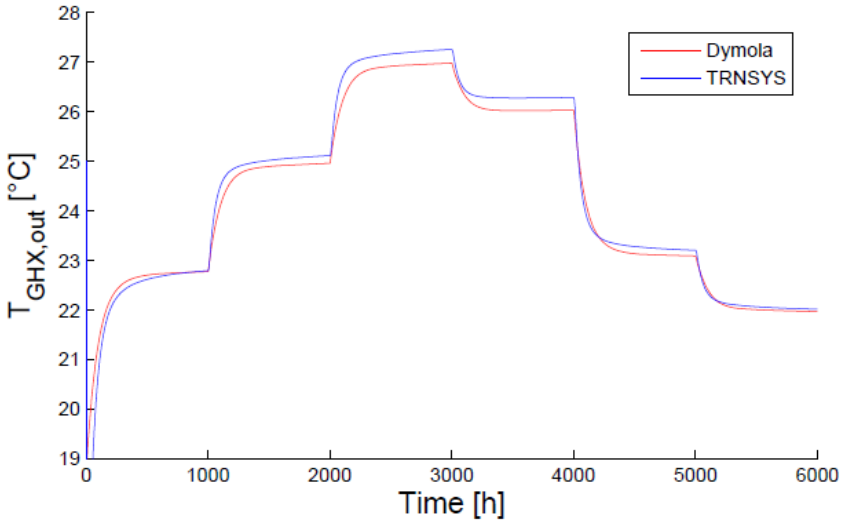

Figure 6: Water outlet temperature of the ground heat exchanger submitted to step inputs: Finite element model (Trnsys) versus reduced order model (Dymola).

2.4 THERMAL ENERGY STORAGE

2.4.1 Description

The basic type of hot water storage tank in the HP/ORC system is shown in Figure 7. It is a typical domestic hot water tank system installed in single-family houses in Denmark (500 litres). The water tank consists of a stainless steel cylinder with two built-in spiral heat exchangers (HXs) – one going from mid-height to bottom of the tank and another one going from bottom to the top of the tank. The heat transfer fluid in the HP/ORC unit is circulated through the mid-height helical heat exchanger, while the cold water from the grid is circulated through the all-through heat exchanger to supply DHW. The floor heating (FH) loop is directly passing through the tank. The technical characteristics of the storage are given in (appendices - Table 12).

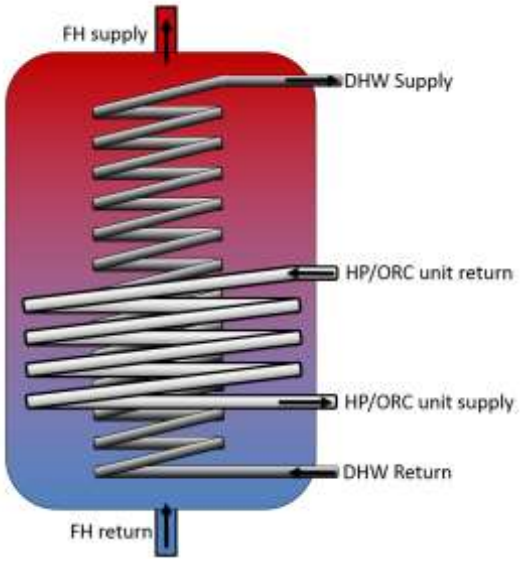

Figure 7 : Hydraulic scheme of the thermal heat storage. Unit loop is the reversible HP/ORC unit. In heat pump mode, it is connected to the condenser and in direct heating mode to the solar roof.

2.4.2 Selection of the modelling approach

A methodology to select the optimal storage modelling approach has been drawn. It allows to select the optimal modelling approach depending on the existence of a database, the accuracy required and the purpose of the model (simulation or design) (Figure 8). In our case (simulation model, experimental database and the extrapolation outside the database required), the multi-node approach with fitting parameters is recommended. More details are provided in appendices section 5.1.

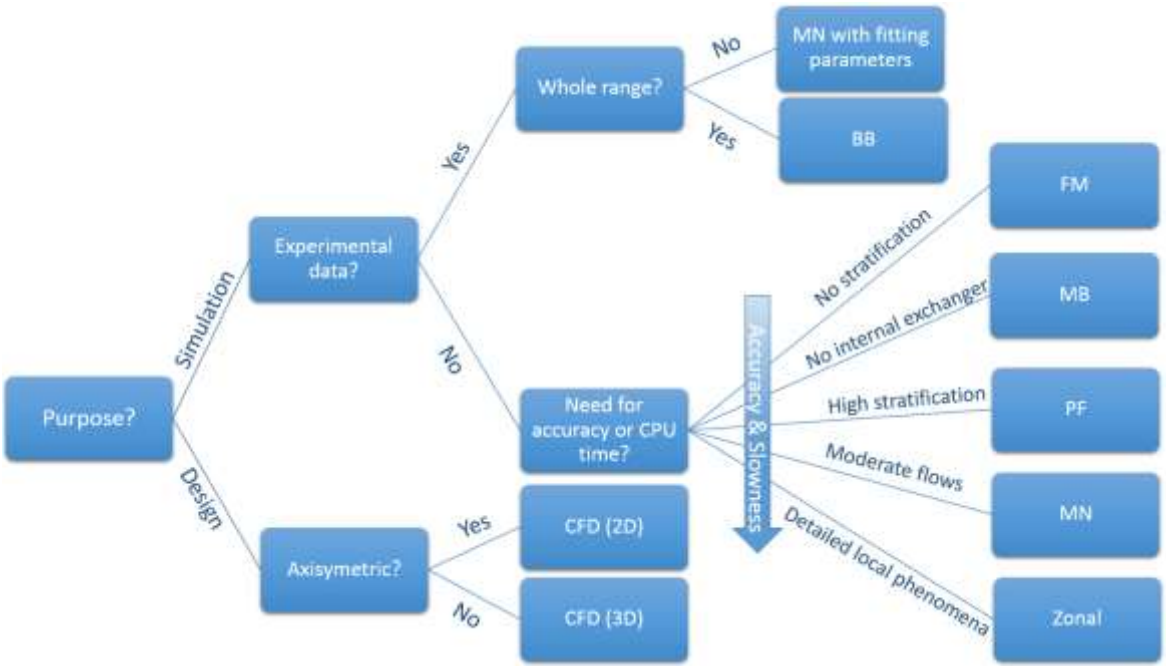

Figure 8: Decision tree to select the optimal storage modelling approach

2.4.3 Modelling

A novel 1D model for representing stratified water tank systems was developed and validated using experimental data under different charging and discharging conditions following prEN12977-3:2008 [CEN, 2008]. This work was done in collaboration with the Technical University of Denmark (Carmo et al., 2015). The aim of this work was to provide an open source water tank model which is experimentally validated and with a low computational time. The model used is based on an existing model in Thermocycle library, Heat Storage Water Heater (Quoilin et al., 2014). It is a 1-D lumped parameter model based on the finite volume discretization. This means that, in order to solve the spatial temperature dependencies, the flow is discretized into *i* interconnected cells in series. This discretization is an approximation method, in which each of the cells, is modelled by equations of energy and mass conservation and a static momentum balance. This method makes the tank model compatible with the other sub-models of the system. The original tank model was then modified to account for the two heat exchangers, heat transfer and mixing between adjacent cells, thermal losses to the ambient trough the walls (heat transfer coefficient - U_{amb}) and heat release to the floor heating. The dynamic temperature profile of the tank is represented by a set of ordinary differential equations that represent the energy balance of the tank. The dynamic temperature profile of the tank is represented by a set of *i* ordinary differential equations that represent the energy balance of the tank (Eq. 2). The first term is the thermal inertia of the cell. The second term is composed (from left to right) of the enthalpy flow rate, the thermal exchange with an eventual heat exchanger, conduction with adjacent cells and ambient losses.

$$A_i \Delta L \rho_i CP \frac{dT_i}{dt} = \dot{m}\left(h_{ex,i} - h_{su,i}\right) + A_{hx,i}\dot{Q}_{hx} + \omega_0 A_{i+1}\dot{Q}_{i+1} + \omega_1 A_{i-1}\dot{Q}_{i-1} - A_{amb,i}U(t_i - t_{amb}) \quad (2)$$

In this equation ω_0 is 0 if the i-th node is the top of the tank and 1 otherwise and ω_1 is 0 if the i-th node is the bottom node and 1 otherwise.

In addition to this equation, the model includes the mixing parameter (Ω) in order to represent the combined effect of the different mechanisms of heat transfer that can occur between tank nodes: diffusion, advection or axial mixing due to flow) as well as the mixing that occurs due to temperature inversion. This parameter is issued whenever there is temperature inversion in the tank. This parameter is estimated by minimization of errors between simulated and measured temperatures in the tank from experimental tests at operation conditions identical to the conditions in which the storage tank is operated in HP/ORC system (Carmo, 2016). Figure 9 summarizes the energy balance for each cell of the storage tank.

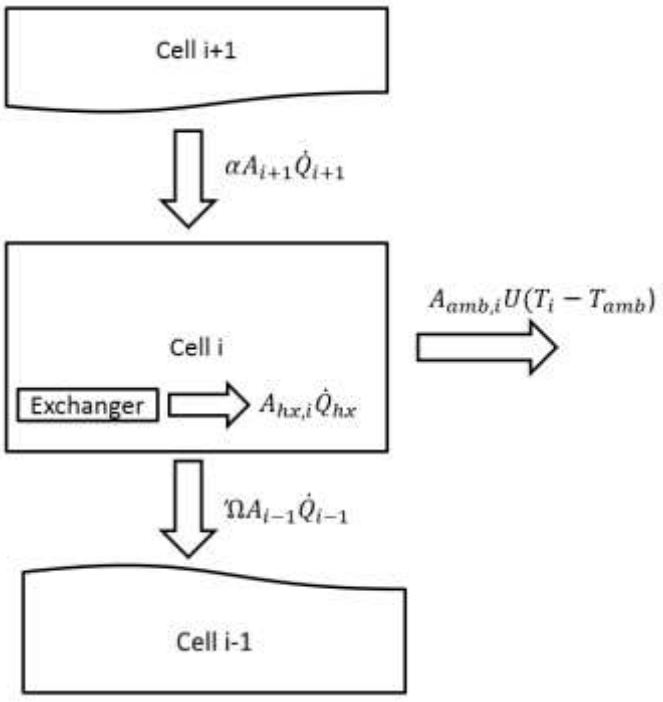

Figure 9 : Energy balance for the i-th node of the storage

Figure 10 shows the validation of the stratified hot water tank under discharging through immersed spiral conditions.

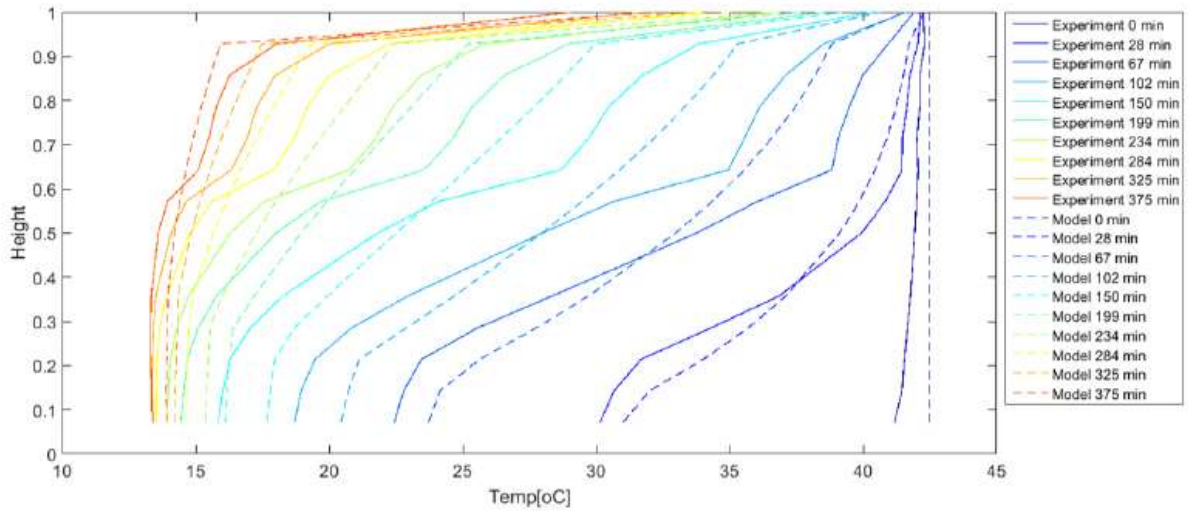

Figure 10 : Validation of the stratified hot water tank under discharging through immersed spiral conditions (Carmo et al., 2015).

There are some differences between the model and the experimentation. This is because the discretization method used, which is an approximation of the spatial partial derivatives equations (PDE) into ordinary differential equations (ODEs), exhibits a negative effect called numerical diffusion with systems with flow. This effect causes the model to exhibit higher diffusivity than the true physical system. To minimize the negative effect when using spatial discretization using a finite difference method, a different discretization scheme could be the solution to handle the convection phenomena and maintain the integrity of the results. In general, it is difficult to make a fair comparison of the simulation model's performance and this work does not intend to provide a comprehensive study of computational efficiency. However, for the purpose of the studies performed in this work, the model with 20 cells is considered to present reasonable accuracy with a maximum RMSE of 2.58 K during the entire experiment period and takes around 24 seconds to simulate 24 hours. Thus, it is considered reasonable to apply in annual simulations. The error (RMSE) was calculated as a root-mean-square of a difference of the simulation value and the experiment value at each time step of the simulation and for all cells (Carmo, 2016).

2.5 ELECTRICAL STORAGE

The battery model is based on the characteristics of domestic battery with the lowest specific selling price nowadays (Tesla, 2016). The roundtrip mean watt-hour efficiency is 92%. The maximum power (charge or discharge) is limited to 3300 W. The efficiency of the inverter is 97%. 90% of the usable battery capacity is used during the lifetime on average. The battery float charge losses (energy to maintain the battery charged when it is full), is assumed to be zero. When the total electrical load of the building is lower than the PV production, the battery is charging within its power limitation. When the load is higher than the PV production and

the battery is not empty, the battery discharges to avoid buying electricity on the grid. Considering the lifetime, the battery is guaranteed for 10 years (or 3650 cycles). An optimum battery size exists for each simulation case: a too large battery leads to high investments and poor utilization rates while a too small battery leads to insufficient load shifting capability. Due to the large number of parameters, only two different electricity prices are investigated.

2.6 PHOTOVOLTAICS

Photovoltaics panels do not make part of the reversible system but a comparison between the HP/ORC reversible unit and a classical mature alternative solution for Positive Energy Buildings which consists of photovoltaic panels combined with a water to water heat pump (HP/PV) is performed. Another alternative single-technology capable of delivering heat and electric power is PVT but it is considered out of the scope of this study (He et al., 2006, Herrando et al., 2014 and Dupeyrat et al., 2014). The efficiency of PV panels is estimated through the product of a thermal efficiency and an irradiance efficiency as detailed in Eq. 3 (De Soto et al., 2006). This formula is extracted from TRNSYS detailed model of PV – Type 194 (Trnsys 2006).

$$\eta = \eta_I . \eta_T = 0.0034 . \ln(I) . \frac{0.1592 - 0.0034 . t_{amb}}{0.1622} \qquad 3$$

The area of photovoltaic panel is fixed in a way that the electrical peak power is the same as the HP/ORC reversible unit in typical summer conditions. Outdoor temperature is fixed at 25°C, the solar irradiance is equal to 800 $W.m^{-2}$. It leads to a peak power of 5290 W and to PV area of 44 m^2.

2.7 GLOBAL MODEL

Figure 11 presents the flowchart of the global model combining the storage, the building, the roof, the reversible unit and the ground heat exchanger. Hourly schedules are associated to the occupancy, the domestic hot water use, the lighting and appliances in each zone (Georges et al., 2013). The weather data used for the outdoor temperature and the solar irradiance are provided by the DMI - Danish Meteorological Institute- (Wang et al., 2010) in the case of Denmark and by Energy Plus Energy Simulation Software (EnergyPlus, 2015) for other locations. An adaptive time step is computed by the solver, but is not allowed to exceed 900 s. A low time-step induces too much computational time and too large output file size, a time-step larger than 20 minutes could lead to errors larger than 5% (Bouvenot et al., 2015). The typical computational time is 3 hours for an annual simulation. The consumption of auxiliary pumps (except GHX pump) are neglected, they represent less than 2% of the global system power consumption.

Some parameters have to be fixed: roof water flow rate, ground heat exchanger water flow rate, and storage water flow rate and temperature set points of the storage. Practically, the following values are used for the flow rates based on real values imposed in the house:

- Roof water flow rate = 0.6 $kg.s^{-1}$,

- Ground heat exchanger water flow rate = 1.5 kg.s^{-1},

- Storage water flow rate = 0.6 kg.s^{-1}

These flow rates should be optimized in future investigations to increase the energy efficiency of the system (Burhenne et al., 2013).

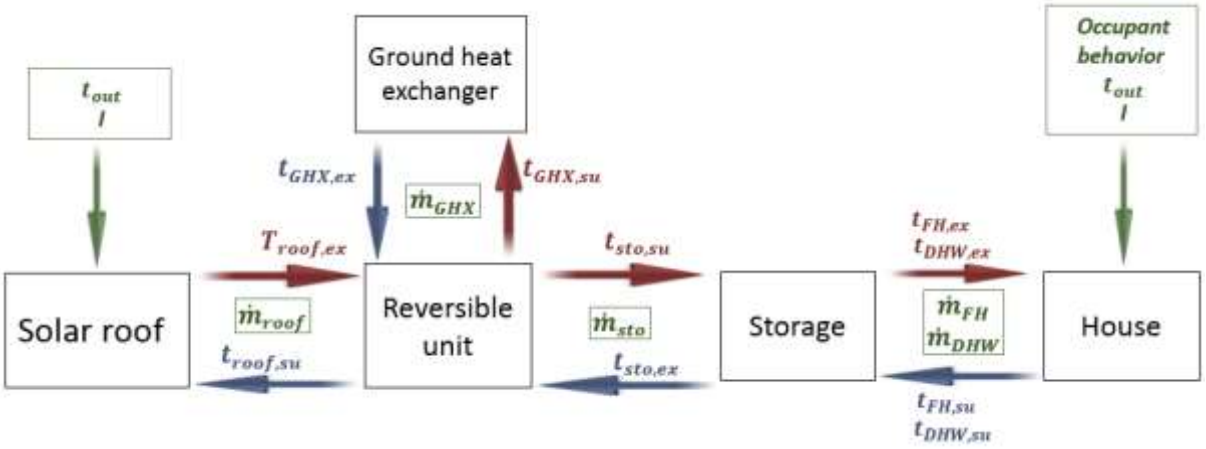

Figure 11: Global model and connections between sub-models.

2.8 CONTROL

The control strategy ensures that the heat demand is covered while electricity is produced with the surplus of heat. For this reason the first control variable used is the hot water storage tank temperature (the control temperature point is located at mid-height of the tank).

A state diagram control is implemented. The conditions governing the transitions between the three modes (HP, ORC and DH) and the stand-by mode (Bypass) are shown in Figure 12. The Bypass mode means that no HP, ORC or DH is activated, only the floor heating circuit can be activated extracting energy from the water storage, if necessary, to reach the desired indoor conditions (20°C). The principle is the following: if the storage is too cold (the control temperature of the storage is lower than the low-temperature threshold), the HP mode is activated. If the roof temperature is higher than the storage one, the DH mode is used. Finally, the ORC system produces electricity when the storage temperature has reached a given high threshold and if a stable state can be reached. This means that the ORC is only activated once it can produce a certain level of power ($\dot{W}_{ORC,min}$). The $\dot{W}_{ORC,min}$ is used to enable a smooth and efficient operation of the system in ORC mode. When a stable operation of the ORC cannot be guaranteed ($\dot{W}_{ORC} < \dot{W}_{ORC,min}$), the TES is allowed to go above the high temperature threshold. It should be noted that the HP mode is using either the roof or the horizontal ground heat exchanger depending on which one is the warmest.

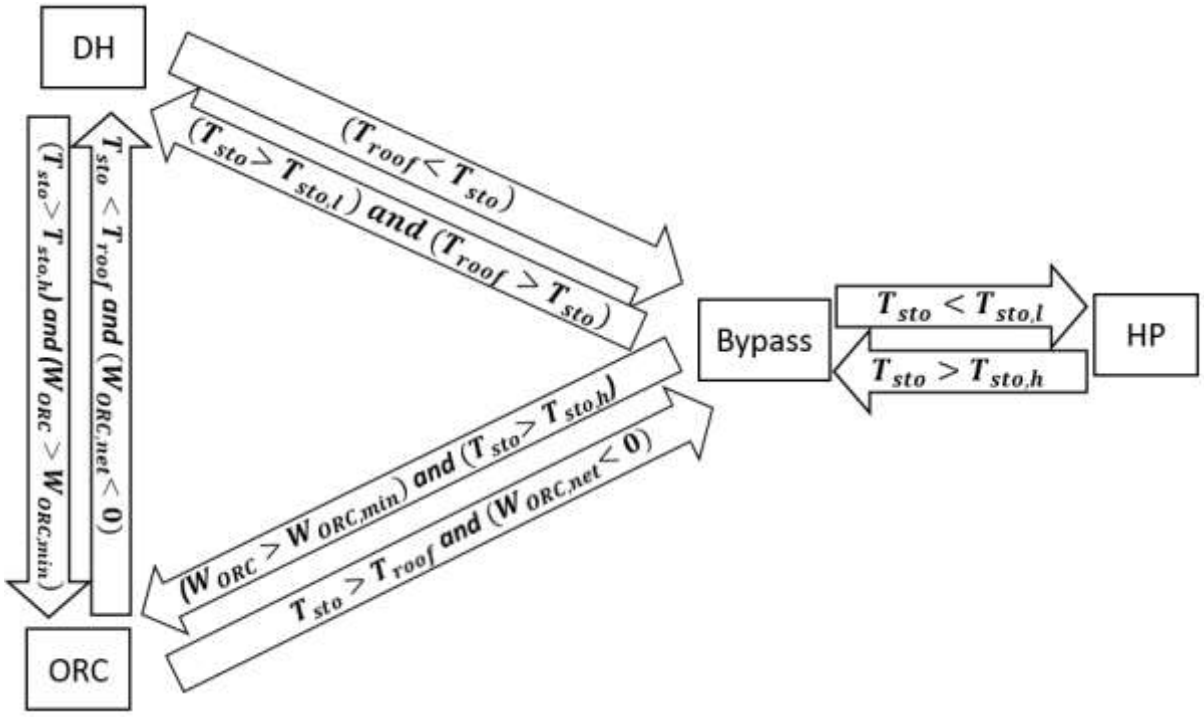

Figure 12: State diagram control. t_{roof} is the roof exhaust temperature, t_{sto} is the storage control temperature (middle height of the tank), $t_{sto,l}$ is the low temperature threshold of the storage, $t_{sto,h}$ is the high temperature threshold of the storage, $W_{ORC,min}$ is the minimum power to start the ORC system.

Table 5 summarizes the values of each threshold temperature. The threshold values were chosen to avoid chattering (too many mode changes) and to maximize the efficiency of the system in (Dumont et al., 2014a). The number of mode changes is considered high when more than one change occurs in a 15 minutes period.

Table 5: Values of the temperature thresholds

Temperature threshold	Abbreviation	Value
High temperature threshold of the storage	$t_{sto,h}$ [°C]	50
Low temperature threshold of the storage	$t_{sto,l}$ [°C]	40
Power threshold of the ORC	$\dot{W}_{ORC,min}$ [W]	2000
Indoor comfort temperature	t_{in} [°C]	20

It should be noted that, although the set points and thresholds have been optimized, the proposed control strategy is still a myopic rule-based control strategy. A truly optimal control strategy is difficult to implement because of the high number of manipulated variables, the numerous set-points and the non-linearity of the problem. Because of this, an improved myopic rule based control strategy which is robust within a wide range of parameters (building, climate…) is tricky to develop. Reaching the best performance of the system would require a predictive non-linear optimization, based on the next 24 hours of weather forecast, user behaviour and electricity prices. Such approach would avoid, for example, starting the heat pump when the solar heat will be sufficient to cover the heat demand later in the day.

2.9 PERFORMANCE CRITERIA

Yearly simulations are performed and evaluated through the following performance criteria:

- Gross electrical production [Wh]: the energy produced by the ORC (or the PV panels if specified) ($W_{el,prod}$).
- HP electrical consumption [Wh]: the electrical consumption of the HP ($W_{el,HP}$).
- Gross electrical consumption [Wh]: the sum of appliances, lighting and HP electrical consumption ($W_{el,cons,tot)}$.
- Net electrical production [Wh]: the gross electrical production minus the gross electrical consumption ($W_{el,net}$).
- The total thermal energy production of the unit, includes both thermal production from heat pump and solar thermal roof collector [Wh] ($Q_{th,prod}$).
- DH energy [Wh]: the total thermal energy gained by means of the direct heating mode (Q_{DH}).

B, annual cash-flow [€]: the income benefits evaluated following Danish law (Eq. 3). It does not take any investment into account. $\dot{W}_{HP}$ is the electrical power consumption of the heat pump. $\dot{W}_{net}$ is the net electrical power, i.e. the electrical production minus the electrical power consumption of lighting and appliances. $Price_r$ ~ 0.28 €.kW^{-1}.h^{-1} is the retail price considered when the net electrical power is negative, $P_{r,HP}$ is the retail price for the heat pump only ~ 0.22 €.kW^{-1}.h^{-1} and $Price_{bb}$ is the buy-back tariff ~ 0.17 €.W^{-1}.h^{-1} considered when the net electrical power ($\dot{W}_{net}$) is positive. Retail and buy-back tariffs are provided by real data from Denmark (Energinet, 2015). For the sake of simplicity, Eq. 1 neglects more complex tariff structures such as fixed grid costs or taxes and incentives on self-consumption, because their regulations are being implemented in very different ways in different countries (European commission, 2015). A second tariff is considered and is an extreme case where no electricity is sold on the grid (only a retail tariff of 0.28 €/kWh). Because the feed-in-tariffs are expected to decrease in the next years, the real solution should fit in between these two options.

$$\text{If } \dot{W}_{net} > 0 \; then \; B = \int_0^t \left(Price_{\text{bb}} \left(\dot{W}_{net} \right) - Price_{r,HP} . \dot{W}_{HP} \right) . dt$$
$$\text{else } B = \int_0^t \left(Price_{\text{r}} \left(\dot{W}_{net} \right) - Price_{r,HP} . \dot{W}_{HP} \right) . dt \qquad (4)$$

- Supply cover factor or self-production rate (γ_S), presents the fraction of energy production that has been consumed (Eq. 4) (Baetens et al., 2012).

$$\gamma_S = \frac{\sum \min \left(W_{cons+} , W_{prod} \right)}{\sum W_{prod}} \qquad (5)$$

- Demand cover factor or self-consumption rate (γ_d), represents the fraction of energy consumption that has been produced by the building from the grid point of view, taking the battery power into account (2). W_{cons+} is the net electrical consumption of the building including heat pump, lights and appliances consumption and battery discharging – which eventually decreases the house consumption (Eq. 5).

$$\gamma_D = \frac{\sum \min (W_{cons+}, W_{prod})}{\sum W_{cons+}} \quad 6$$

- The pay-back period, PB, for a battery is determined by equalling the battery investment, $Price_{battery}$ to the revenues related to the battery (Eq. 7). *r* is the discount rate (0.04).

$$Price_{battery} = \frac{\sum_{i=0}^{PB}(R_{bat} - R_{no\_bat})}{(1+r)^i} \quad 7$$

- The discharge depth is defined as the annual electrical stored energy divided by 365 times the usable battery capacity (Eq. 8). The average usable battery capacity is taken equal to 90% of the total battery capacity.

$$\text{DD} = \frac{W_{bat,stored}}{365.W_{bat,us}} \quad 8$$

- The number of equivalent battery cycles, *n*, is estimated by the ratio of the annual charged energy and the usable capacity of the battery (9). It is equal to the discharge depth times 365.

$$n_{cycles} = \frac{W_{bat,stored}}{W_{bat,us}} \quad 9$$

For all the simulations, the set-points temperature of the storage, the set-point in the main room of the building and the solar roof are the same.

3 RESULTS

3.1 BASIC STUDY CASE IN DENMARK

The system response is presented for three characteristic days in Denmark: a winter day (day 1), a spring day (day 62) and a summer day (day 182). Eight variables are analysed in this section: the storage control temperature (t_{sto}), the outdoor temperature (t_{out}), the house ambient temperature in zone 1 (t_{in}), the exhaust roof temperature (t_{roof}), the ground heat

exchanger exhaust temperature (t_{GHX}), the heat flow rate for floor heating ($\dot{Q}_{FH}$), the heat flow rate for Domestic Hot Water ($\dot{Q}_{DHW}$), the heat flow rate from the reversible unit or from the solar roof ($\dot{Q}_{th,prod}$) and the electrical unit power consumption (-)/production (+) ($\dot{W}_{el}$).

3.1.1 Winter - Day 1

The behaviour of the system is plotted in Figure 13 for a characteristic winter day. Slightly after 4 am, the floor heating is activated ($\dot{Q}_{FH}$) in a way to keep the indoor temperature (t_{in}) close to 20°C. This leads to a decrease of the control temperature of the storage (t_{sto}) down to the lower temperature threshold of 40°C. The heat pump mode is therefore activated to raise the control temperature of the storage up to the high temperature threshold of the storage (50°C). This phenomenon is observed three times during this day (4, 14 and 20). The heat generated in HP mode is $\dot{Q}_{HP/ORC}$ and corresponds to an electrical power of $\dot{W}_{el}$.The direct heating mode cannot be activated because of the low temperature of the water in the roof (t_{roof}). In this case, the system is acting as a classical ground source heat pump during this representative winter day.

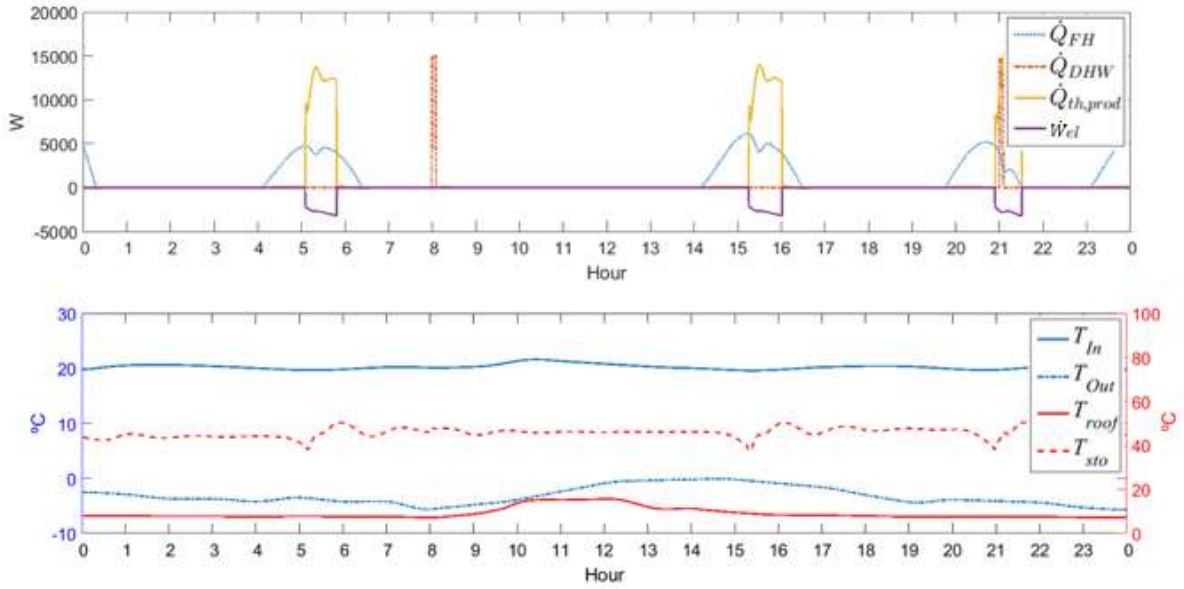

Figure 13: Dynamic simulation of the reversible unit coupled to a passive house for the 1st day of the year.

3.1.2 Spring - Day 62

A typical spring day is depicted in Figure 14. First, around 3 am, the floor heating starts, decreasing the storage control temperature. Thus, the heat pump is activated following the same scheme as for the typical winter day. The difference is that around 10:30 am, the roof exhaust temperature is higher than the storage temperature and the system can therefore benefit from direct heating until the next day. In that case, the direct heating allows to start the heat pump mode only once during day 62 to cover the heat demand of the building.

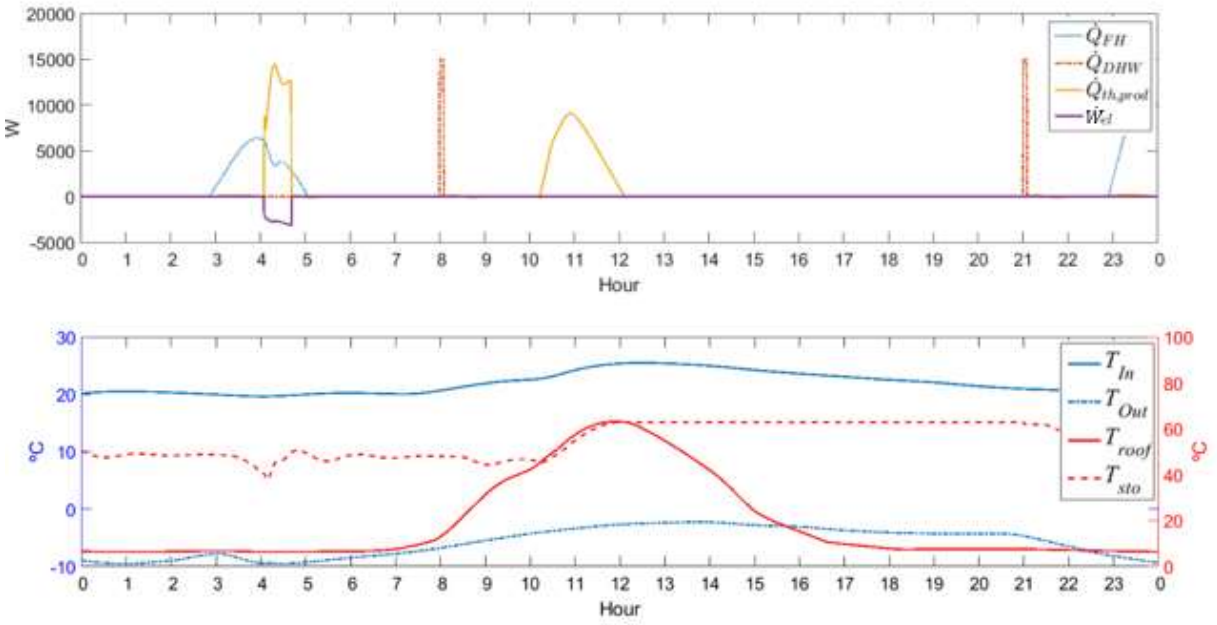

Figure 14: Dynamic simulation of the reversible unit coupled to a passive house for the 62nd day of the year.

3.1.3 Summer – Day 182

Figure 15 presents the response of the reversible unit for a characteristic summer day for the study case in Denmark. Slightly before 8 the direct heating mode is activated since the roof temperature becomes higher than the storage temperature. When the storage temperature reaches its maximum value, the ORC mode can be activated to generate electricity. The electrical production of the ORC is low (compared to the nominal power, 5290 W) due to the high temperature of the water in the GHX. Since the heat demand is rather small (no floor heating, only DHW) and the temperature of the storage is hot enough there is no need to heat the thermal energy store. The ORC mode is therefore activated as long as the electrical production is greater than zero.

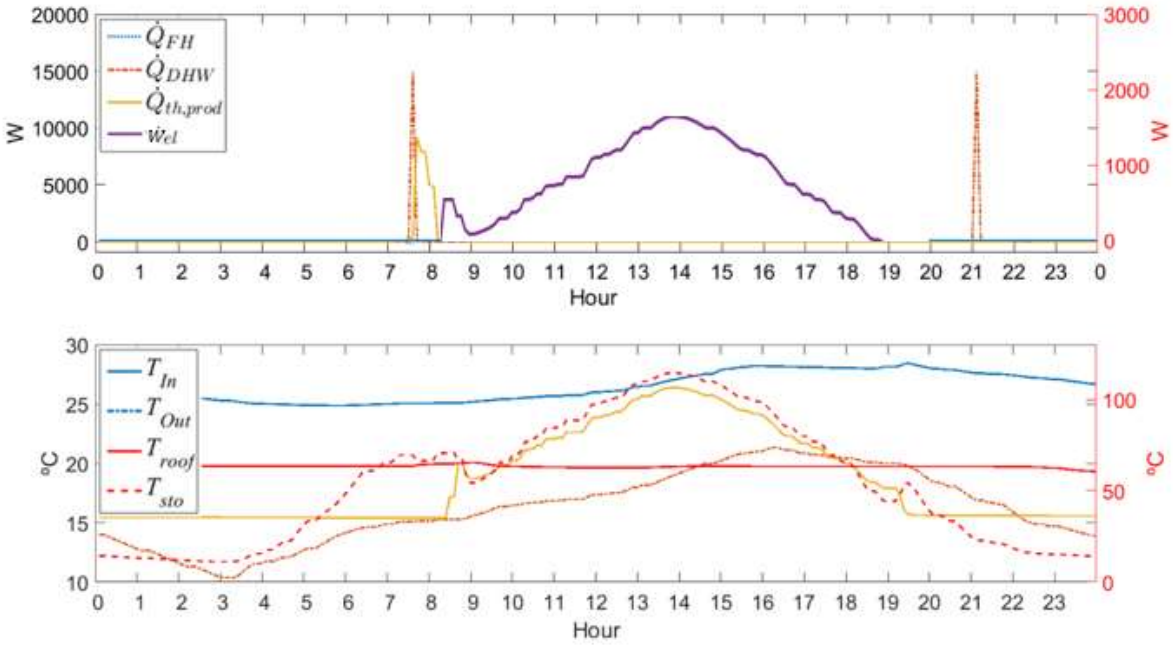

Figure 15: Dynamic simulation of the reversible unit coupled to a passive house for the 182nd day of the year.

3.2 ANNUAL PERFORMANCE IN THE REFERENCE CASE

First, before establishing a sensitivity analysis, a basic yearly simulation case corresponding to the real conditions of the house located in Herning, Denmark, is performed. In this simulation, there is one thermal storage of 500 litres for DHW and floor heating. Figure 16 presents a comparison of the electrical ORC production, heat pump electrical consumption and thermal energy provided by the direct heating mode for each month of the year. The heat pump is running during 5 months of the year, mainly in winter, leading to a total electricity consumption of 827 kWh_e and heat supply of 3082 kWh_{th}. Direct heating is used 10 months per year and produces 1207 kWth, representing 28.1 % of the total heat demand of the building during a year.

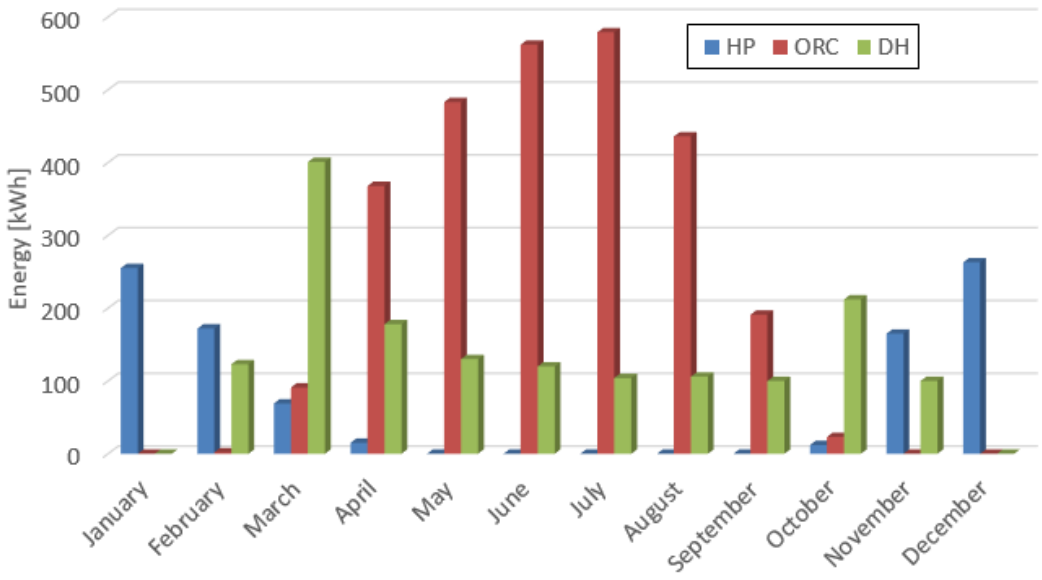

Figure 16: Comparison of the heat pump electrical consumption, electrical ORC production and thermal energy provided by the direct heating mode for each month of the year in the reference case.

The direct heating mode is less used in summer months compared to March and October because the heat demand for floor heating is significantly lower. The gross electrical ORC production is equal to 3012 kWh_e, the lighting and appliances consumption reaches 1491 kWh_e, leading to a net electrical production of 694 kWh_e on a yearly basis. This demonstrates the ability of the current technology to get a Positive Energy Building in terms of electricity use. Using Eq. 3, the annual running costs of the system in aforementioned conditions are 119€.

3.3 STUDY OF INFLUENCE

3.3.1 Climate

After considering the Danish case, it is interesting to compare the system behaviour resulting from different climates. Similarly to what was considered by Knight et al. (2010), the European climate is divided into 5 different typical zones. The system is therefore simulated for 5 cities located in each zone (from north to south): Copenhagen, Frankfurt, Torino, Rome and Palermo. For comparison purposes, the feed-in tariffs for the different locations were maintained as in the Danish case. Figure 17 presents the influence of the climate on the annual performance criteria in the case study with 3000 kWh of lights and appliances, K20 building and 5° of roof tilt.

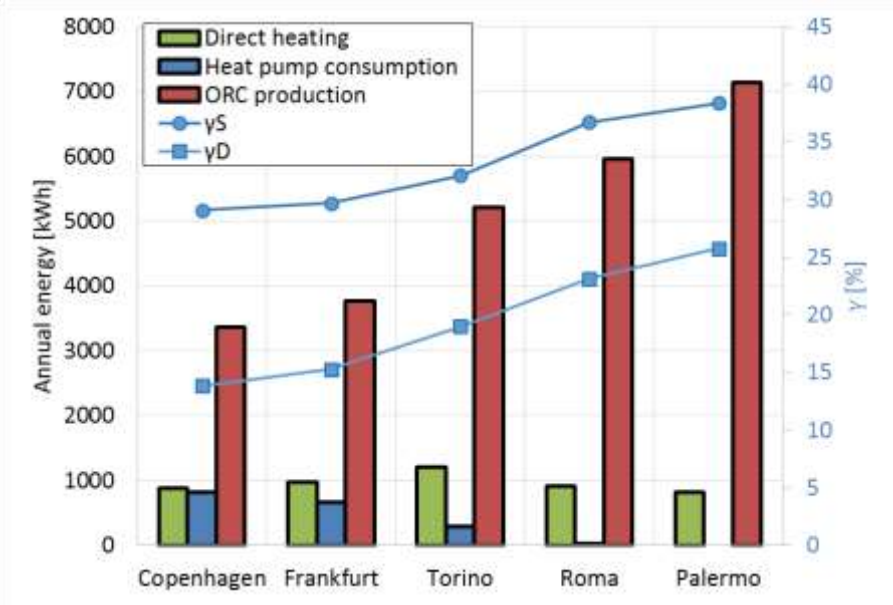

Figure 17 : Influence of the climate on the annual performance criteria in the case study with 1491 kWh of lights and appliances, K20 building and 5° of roof tilt.

It can be concluded that for any building and light and appliances demand, sunniest locations (south Europe) lead to higher power production and thus, higher self-consumption and self-production rates. On the other hand, the heat pump is almost never used in southern locations, because the heat demand is small and, therefore can benefit from the direct heating. On the contrary, northernmost locations present low heat energy provided by direct heating. There is an optimal location in latitude close to Torino that shows the best compromise to benefit optimally of the thermal energy from the DH.

3.3.2 Thermal energy storage

3.3.2.1 Layout

This section considers two different sensible energy storage configurations for the reversible heat pump/organic Rankine cycle (HP/ORC) system: a buffer tank for both space heating and domestic hot water and a hot water storage tank used exclusively for domestic hot water (Figure 18).

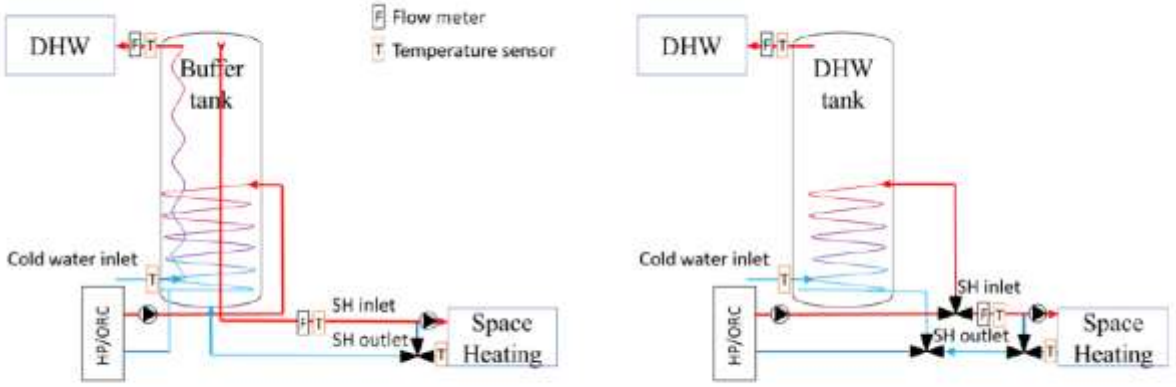

Figure 18 : Hydraulic scheme of the hot water tanks configurations studied. Configuration 1 (left) and configuration 2 (right) (Carmo et al., 2016).

The first system – on the left - consists of a hot water tank with two built-in spiral heat exchangers (HXs) – one going from mid-height to bottom of the tank and another going from bottom to the top of the tank. Solar collector fluid is circulated through the mid-height helical heat exchanger, while the cold water from the grid is circulated through the all-through heat exchanger to supply DHW. The second system – on the right of Figure 18- consists of a hot water tank with one built-in spiral heat exchanger going from the bottom to mid-height of the tank. The solar loop fluid is circulated through the heat exchanger. What makes interesting to study these configurations is that both of them are standard low costs tank configurations. They are both two standard low cost tanks readily available on the market. However, they both have advantages and disadvantages that affect the HP/ORC system performance. The advantages of configuration 1 is that it presents higher security against legionella due to the small volume of water in spiral HX that is heated for DHW use, but this represents higher heat losses (ambient) due to higher temperature set point. In addition, the disturbance of the stratification of the thermal storage is little due to the low flow (<0.2 l/min) of the floor heating loop. Configuration 2, on the other hand, presents the advantage of having very little losses due to the DHW preparation because there is no internal heat exchange between the transfer fluid and the storage medium, thus avoiding temperature losses. Plus, it presents no disturbances from the floor heating loop which is typically the larger energy demand over the year in a building. However, the high flow (9.6 l/min) at DHW supply times causes turbulence that might affect the thermal stratification of the tank, crucial for a better solar system and heat pump performance. Finally, if the solar tank is a DHW tank- as it is the case with configuration 2 - due to the risk of lime problems the controller is set to switch off the solar pump at 60°C. For configuration 1, the only limitation is the boiling temperature and the maximum temperature the material of the tank and its insulation can sustain. The characteristics of each tank configuration are described in Annex - Table 14.

Table 6 : Annual energy performance and economic results with different tank configurations

Tank	B [€]	$W_{el,HP}$ [kWh]	$W_{el,prod}$ [kWh]	Q_{DH} [kWh]	$Q_{th,prod}$ [kWh]	γ_D
Buffer	204	1512	3377	578	4271	8.1
DHW	198	1492	3371	678	3003	9.3

Table 6 shows the annual performance indicators in the case study of Denmark. The ORC production is almost not affected by the storage configuration. Due to the higher set-point required for the buffer tank configuration, the heat losses are higher. Therefore, the total heat provided, the heat pump electrical consumption and the running cost are higher. The heat pump is activated more often (preventing the electrical production), leading to lower self-sufficiency rate. The direct heating energy gains are lower in the case of the buffer tank configuration because of the higher temperature set-point (this higher set-point limits the time of use – see section 2.8). The results in this work show that for the HP/ORC unit, i.e. HP coupled with solar collectors the DHW tank configurations are preferred against buffer tank configurations. From the HP mode point of view similar, results were drawn from a monitoring programme (Carmo et al., 2016). The authors consider that further investigations with mantle tank configuration should be performed in the future. This configuration fulfills small space requirement for residential applications and has shown promising results when integrated in solar based heating systems as way to improve the thermal performance. In addition, a sensitivity analysis of different tank volumes depending on the actual daily domestic hot water consumption to further improve the overall HP/ORC system performance could also be considered.

3.3.2.2 Size

The case study of Denmark has been simulated with three different sizes of water tank (0.5 m^3, 1.5 m^3 and 3 m^3) using a buffer tank configuration. The heat pump consumption and the cash-flow have been compared (Figure 19).

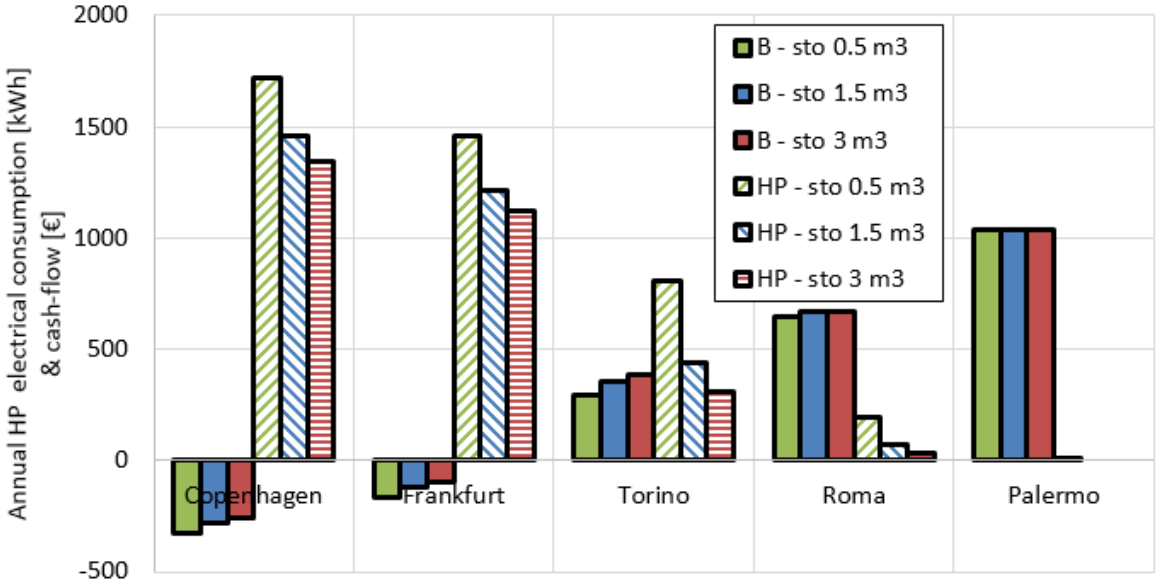

Figure 19 : Annual heat pump consumption and cash-flow for three storage sizes and five different climates.

When increasing the size of the storage, two main opposite effects appear: one the one hand, the recovery through the direct heating mode increases but on the other hand, the ambient heat losses increase. From Figure 19, the 3 m^3 tank presents the lowest HP electrical consumption through a higher direct heating energy recovered. An increase of the storage size is more influent in location close to Torino (optimum of direct heating – see section 3.3.1). The annual cash-flow is logically increased with a larger storage. However, its maximum increase is around 67 eur/year when using a 1.5 m^3 storage instead of a 0.5 m^3 in Torino. This optimum does not take into account the additional investments for a larger tank neither the difficulty to get such a volume in a residential building. The original size of the tank (500 litres) therefore appears to be a good compromise regarding those limitations. It is corroborated by a Danish study (Reshfeski, 2014) that mentions that a tank volume matching the daily DHW consumption in Danish single-family houses is typically ranging from 230 l/day to 470 l/day [13] plus 100 l/day for space heating. This section just represents one case study. Practically, each application presents an optimum storage depending on the climate, building, occupant behaviour…

3.3.3 Building envelope characteristics

The building of the basic case study in Denmark is analysed (K20 building). Secondly, two additional different building envelope characteristics –K15 and K30 (Masy et al., 2015) are studied in all climates. They differ in terms of coefficient of heat transmission and air tightness (Table 7).

Table 7 : Envelope characteristics of different typical buildings. Each building is characterized by different coefficients of heat transmission for the roof, the floor slab, the external wall and the window and a given infiltration rate coefficient.

Coefficient of heat transmission	K15	K20	K30
Roof [$W.m^{-2}.K^{-1}$]	0.093	0.09	0.228
Floor slab [$W.m^{-2}.K^{-1}$]	0.123	0.08	0.258
External wall [$W.m^{-2}.K^{-1}$]	0.102	0.15	0.245
Window [$W.m^{-2}.K^{-1}$]	0.9	0.63	1.2
Infiltration rate (50 Pa) [$m^3.h^{-1}.m^{-2}$]	0.6	2.51	2.9

Figure 20 presents the annual total heat demand of the building and direct heating energy for different buildings and climates. The three different buildings described in Table 7 allow to get a wide range of total heat demand for climates ranging from Copenhagen to Palermo (from 845 kWh to 8595 kWh). Logically, the heat demand decreases with a good insulation level of the building and with southernmost locations.

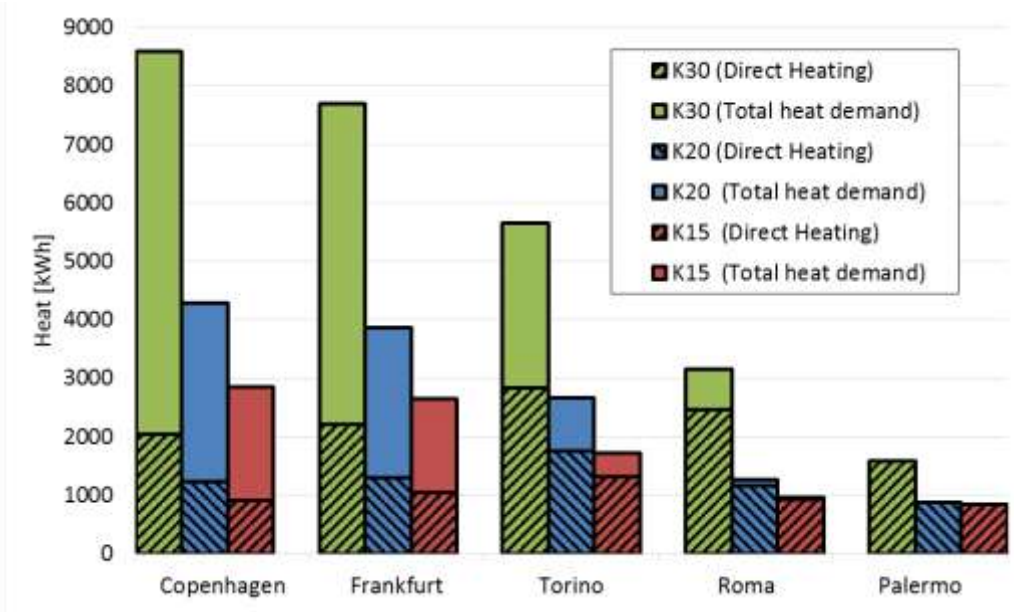

Figure 20 : Annual total heat demand of the building and direct heating energy for different buildings and climates.

On the other hand, it is shown that lower levels of insulation lead to higher heating demand covered by DH without compromising the ORC power output and the financial benefits. A maximum of direct heating energy production is observed for the case of Torino (Figure 20).

3.3.4 Light and appliances

Finally – as proposed in Georges et al. (2013), two Light and Appliances profiles (L&A) are simulated with the reference Danish building characteristics. The latter differ in the magnitude of power demand. In decreasing order of magnitude, LA3000 (3000 kWh/year) is characterized by highest demand, followed by LA2000 (2000 kWh/ year). The net annual electricity production and heat pump consumption with different lighting and appliances profiles is depicted in Figure 21 for a K20 building.

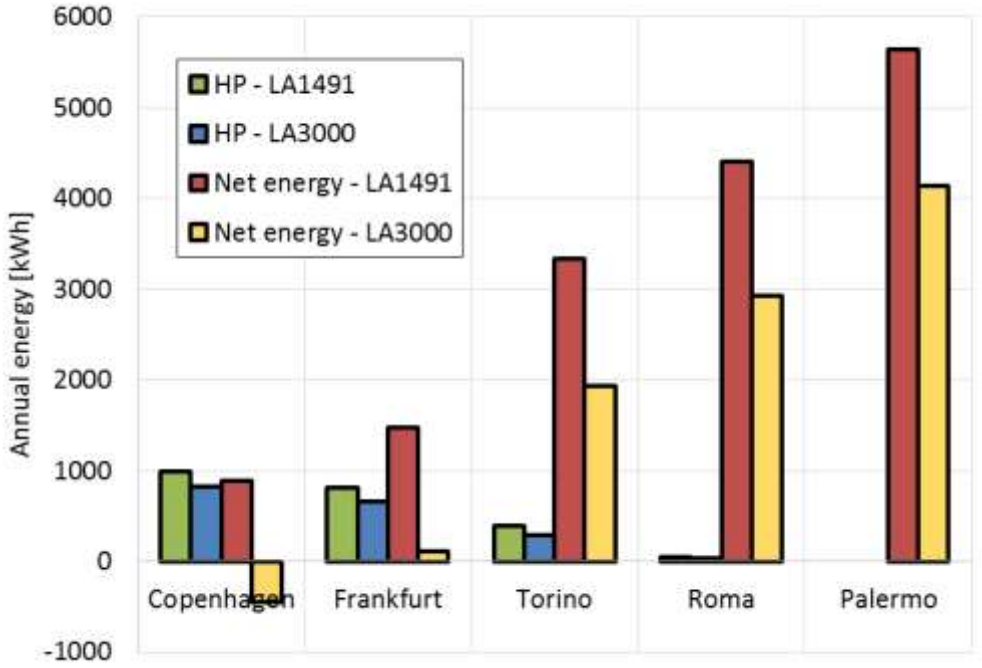

Figure 21 : Net annual electricity production and heat pump consumption with different lighting and appliances profiles.

It is interesting to note that an increase of lights and appliances demand - in all locations - decreases the net power output and benefits, but also decreases the heat pump power consumption. This is due to the internal heat gains by means of light and appliances, which decrease the heating demand.

3.3.5 Roof tilt angle

Figure 22 depicts the increase in energy (heat pump consumption and ORC production) with a 35° tilt angle roof compared to a 5° roof tilt angle.

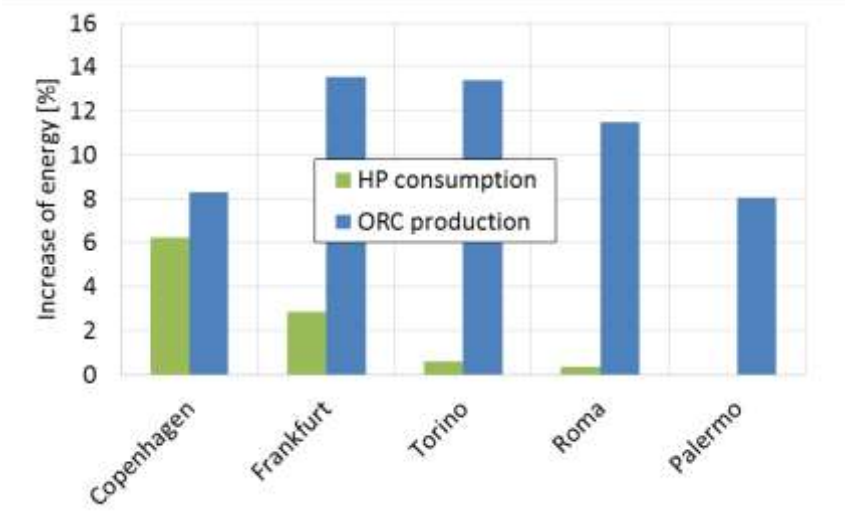

Figure 22 : Impact of the roof tilt angle on the heat pump consumption and ORC production. Case study with 3000 kWh of lights and appliances, K20 building.

In the case of a south orientation, a steeper roof leads to an increase of the electrical ORC production and to a decrease of the heat pump electrical consumption. Generally, a flatter roof leads to highest peak of thermal energy production in summer and around midday. Because of the limited thermal energy storage capacity, it is more efficient to produce thermal energy at lower level during a longer period to benefit more from direct heating and to decrease the HP consumption (see Figure 22). The ORC production is also limited with a flatter roof because peak of thermal power are transferred to the ground heat exchanger. This can lead to high ground temperature, increasing the condensation temperature and therefore decreasing the ORC production. Those results are only valid for a south-oriented roof and two tilt angles. Further simulations should be necessary to get general conclusions but are out of the scope of this study.

3.3.6 Battery for electrical production shifting

The introduction of energy storage in Positive Energy Buildings is increasingly investigated, with the objective of decreasing the dependency on the grid. In this context, electric batteries could play an important role. With decreasing feed-in tariffs, it becomes interesting to consume the electricity generated on-site (European commission, 2015). Batteries can help to increase self-consumption and also to avoid disconnecting the power system during peak power production. It also decreases the need for backup generation and the need for energy transport. The economic viability of solar production (PV panels) combined with battery storage was evaluated in 2014 in the German context (Hoppmann et al., 2014). The authors concluded that, for an economically rational household, investments in battery storage are already profitable for small residential solar systems. The cost assumption for the battery system was however notably low (171 EUR/kWh_{year} + 172 EUR/kW_{peak}). Other studies, such as (Weniger et al., 2014), found that PV is profitable in the current German regulation scheme,

but that batteries require further cost reductions to reach economic viability. In 2016, (Truong et al., 2016) the economic benefit of the Powerwall (Tesla battery) for end-users with respect to various influencing parameters was assessed. The Powerwall (~417€/kWh) (Goldie-Scott, 2016) could be a profitable investment in some, but not all scenarios investigated. Also, (Quoilin et al., 2016) showed that although decreasing at a fast pace, the cost of domestic Li-Ion storage is most likely still too high for a large-scale market uptake in Europe. The cost should be around 450 €/kWh for a battery in 2020 (Goldie-Scott, 2016). It should be noted that this hypothesis is optimistic but it can however be seen as a reasonable investment cost in a few years from now (Goldie-Scott, 2016). The installation cost plus the inverter cost are assumed equal to 890 € for all battery sizes (Goldie-Scott, 2016). Table 8 summarizes the input parameters and their investigated values. Each annual simulation requires 3 hours CPU time. The number of parameters to be tested is therefore limited. In this study, 80 annual simulations combining 20 battery sizes (leading to 1600 different cases) are analysed (appendix – Table 15). These parameters cannot capture the whole range of PEB parameters in Europe but encompass the largest number of domestic cases by testing two extreme values of each parameter with a Monte-Carlo analysis (Table 8).

Table 8 : Input parameters for the study of batteries

Parameter	Name	Value
Lighting & Appliances	LA1491	1491 kWh/year
	LA3000	3000 kWh/year
Building	K20	Global heat transfer coefficient = 0.2 W/(m^2.K)
	K30	Global heat transfer coefficient = 0.3 W/(m^2.K)
Roof tilt angle	R5	5°
	R35	35°
Battery	B1-B20	[1:20] kWh
Climate	[Copenhagen, Frankfurt, Torino, Roma, Palermo]	
Electricity price	Sell	Buy : 0.28 €/kWh & Feed-in : 0.17 € /kWh
	No_sell	Buy : 0.28 €/kWh & Feed-in : 0 € /kWh

The range of outputs given by the model is exposed in Table 3.

Table 9 : Outputs range for the study of batteries

Outputs	Nomenclature	Range
Annual electrical production [kWh]	E_{prod}	[3351:11812]
Annual heat pump consumption [kWh]	$E_{HP,cons}$	[0:2492]
Annual electrical consumption [kWh]	E_{cons}	[1491:5491]
Annual heat consumption [kWh]	Q_{cons}	[837:8679]
Payback period [years]	PB	[7.24:26.5]
Self-sufficiency rate [%]	γ_D	[8.3:81.2]
Self-consumption rate [%]	γ_S	[5.8:46.1]
Annual number of cycles [-]	N_{cycles}	[32:409]

Presenting the results of the 1600 case studies is of course not possible. Table Table 15 (appendix) shows the results for 80 simulations with optimized battery size leading to the lowest payback period.

A few examples of typical results are shown. Figure 23 presents the evolution of the electric self-consumption and production, discharge depth and payback time versus the battery size. The case study is in Copenhagen with 1491 kWh/year of lighting and appliances consumption, K20 building and a roof tilt angle of 35°.

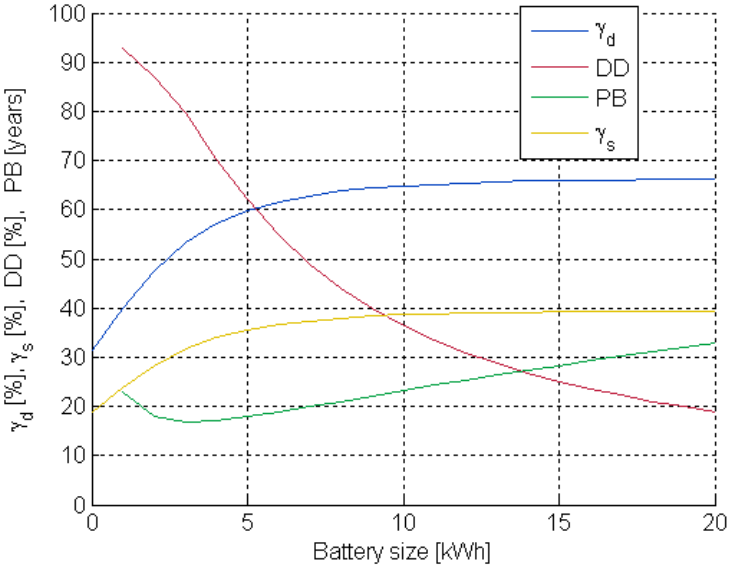

Figure 23 : Evolution of the electric self-consumption and production, discharge depth and payback time versus the battery size. Case study is in Copenhagen with 1491 kWh/year of lighting and appliances consumption, K20 building and a roof tilt angle of 35°.

The average daily discharge depth starts with high values for small batteries (higher than one in some cases) and decreases asymptotically when increasing the battery size. A trade-off between the lifetime of the battery and an optimal battery use (high discharge depth) must therefore be found. The optimum payback period results from a compromise between investment (higher for small batteries) and annual revenues (higher for large batteries). The payback period is decreasing sharply when increasing the size for small battery capacities. After the minimum of payback time is reached, the curve is increasing slowly with the battery size. It is therefore more interesting to have an over-sized battery than an undersized battery. The self-consumption and production factor are analysed more in details here under (*Figure 24*).

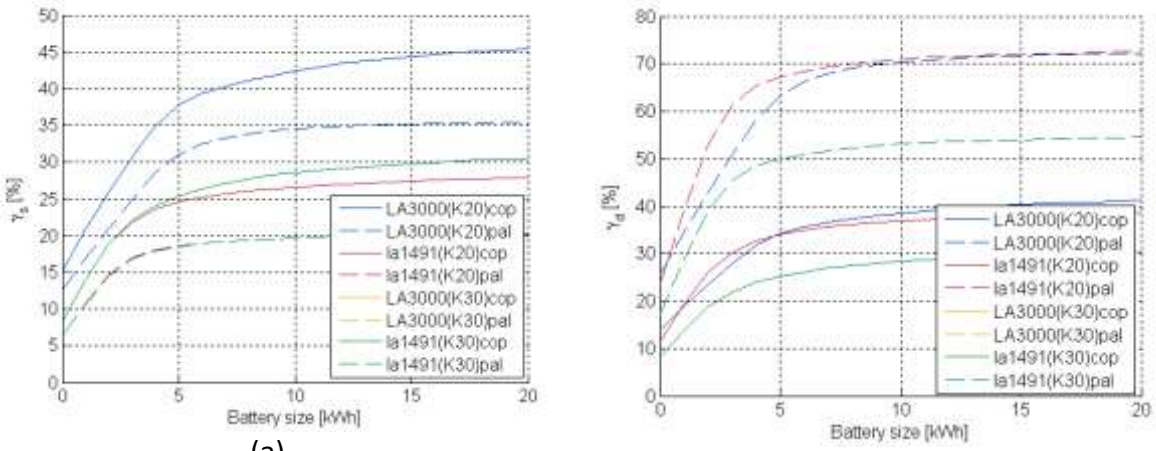

Figure 24 : a) Self-production rate. b) Self-consumption rate. In the legend, respectively K30 and K20 correspond to the building envelope characteristics presenting the higher and lower losses. The location is added at the end (cop = Copenhagen and pal = Palermo).

The self-production rate is rather low (always below 50%) mainly because the electrical production is much larger than the electrical consumption (see section 3.3). The self-consumption rate varies in a wide range (9%-80%) depending on the studied case. When increasing the battery size, the increase in self-consumption rate is relatively sharp for low battery size (up to 5 kWh). But, when the daily average electrical consumption of the building is fully covered by the power system combined with the battery, the increase in self-sufficiency rate is moderate. It can also be noted that the largest battery (20 kWh) cannot lead to a full independency of the building from the electricity grid. Batteries are well adapted to daily variations but not to longer periods of time (seasonal shift) as already shown in (Weniger et al., 2012). This conclusion applies for building electrical load representing from 12% to 97% of the annual electrical production. Globally, the self-production and self-consumption rates decrease with a poorly insulated building because the higher electrical consumption of the heat pump in winter is not covered by the solar electrical production. Lower latitudes (Palermo) show higher self-production and self-consumption rates. The average self-production and consumption rates without battery increases with the lighting and appliance consumption. The influence of the roof tilt angle is not presented here because it is almost negligible with an optimally sized battery (see Annex - Table 4).

This is only a basic approach to evaluate the economic assessment of batteries integration considering only one building. A more accurate study should take into account the network interactions and eventually the charging of hybrid (or electric vehicles) connected to the system.

Although results depend on the assumptions (electricity tariffs, investment costs, battery performance, no demand side management, etc), a varied set of parametric studies has been carried out in order to assess the performance of the system investigated in a wide range of conditions. It has been shown that the battery size leading to the minimum payback period is comprised between 2.6 kWh and 4.5 kWh (Table 15). These values are lower than the current cheapest batteries available on the market (Tesla, 2016). However, an over-sized battery will lead to a lower number of cycles leading to a higher life expectancy and a higher self-consumption. More simulations should be performed to assess the validity of the correlations in a wider range of inputs (higher roof tilt angle, other building envelope characteristics, more lighting and appliances profiles…). The economic interest has not been reached yet because of the high pay-back periods. The battery price still needs to decrease while regulatory framework should change to promote the self-consumption in buildings.

3.3.7 Thermal energy storage for electrical production shifting

A thermal energy storage to shift in time the electrical production of the ORC system is briefly investigated. A simple calculation is performed with optimistic hypotheses:

- The ORC system can operate with inlet water as low as 70°C (t_{low}).
- The storage temperature is homogenous and there is no ambient (or other) losses (maximum water temperature is 95°C (t_{high}).
- A typical nominal electrical energy to shift is 3 kWh (W_{el}).
- The efficiency of the ORC is supposed constant and equal to 5% (η_{ORC}).

Following this and neglecting dynamic effects, the electrical energy that is movable in time is equal to the thermal storage energy times the ORC efficiency (Eq. 10).

$$W_{el} = \eta_{ORC}\ M\ Cp\ (t_{high} - t_{low}) \qquad 10$$

This equation leads to a mass a 2057 kg. This value is very large and unacceptable because of the large space required and the associated costs even with those optimistic assumptions. The shift of electrical production with a thermal storage is therefore not further investigated in this work.

3.4 COMPARISON WITH PHOTOVOLTAICS PANELS COMBINED WITH A HEAT PUMP

The reversible HP/ORC unit integrated in a passive building is now compared with a classical mature technology to get a Positive Energy Building: a heat pump combined with PV (Figure 30).

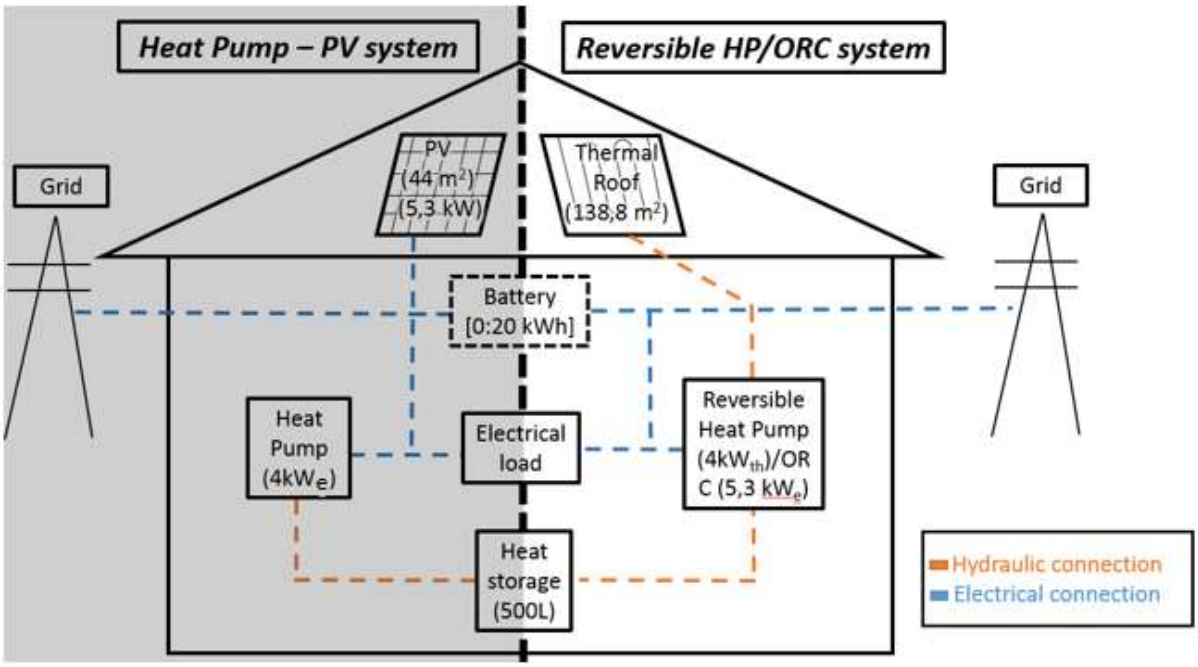

Figure 25: Layout of the heat-pump combined with PV panels (left) and of the reversible HP/ORC system.

The area of photovoltaic panels is fixed in a way that the electrical peak power is the same as the HP/ORC reversible unit in typical summer conditions. Outdoor temperature is fixed at 25°C, the solar irradiance is equal to 800 W.m^{-2}. It leads to a peak power of 5290 W and to PV area of 44 m^2. The modelling is detailed in section 2.6. Heat pump, control strategy, storage parameters, house envelope characteristics, ground temperature are all fixed in the same way as for the HP/ORC reversible unit.

The annual performance comparison is performed between the HP/ORC system and the HP/PV system in the case of the real house located in Denmark (500 L storage and 1491 kWh of lighting and appliances electrical consumption) in Table 10. First, the heat pump electrical consumption is 45% higher in the case of the HP/PV because this system does not benefit from the thermal heat furnished by the direct heating mode (1394 kWh). Also, the gross electrical production is lower in the case of the HP/ORC system. This is explained by the rather constant efficiency of the PV panels while the ORC efficiency (and solar roof efficiency) are largely affected by part load conditions (low solar irradiation, low outdoor temperature).

Table 10 : Comparison of the annual performance between the reversible heat pump/organic Rankine cycle unit (HP/ORC) and the PV panels coupled with the heat pump (PV/HP)

System	HP/ORC	HP/PV
Non HVAC electrical consumption [kWh]	1491	
Heat pump consumption [kWh]	812	1185
Gross electrical production [kWh]	2970	6511
Net electrical production [kWh]	667	3835
Thermal load (domestic hot water & floor heating) [kWh]	4403	
Thermal energy provided by direct heating [kWh]	1394	0
Cash-flow [€]	-78	494
Self-production rate [-]	12	11
Self-consumption rate [-]	8	27

Following this, it is logical that the net electrical production and the running benefits are higher in the case of the HP/PV system. Furthermore, the self-consumption and self-production rates are significantly lower in the case of the HP/ORC system. Figure 26 illustrates the underlying reason. These two systems present very different generation patterns. The reversible HP/ORC unit produces electricity mainly around midday when the electrical load of the residential building is low, while the PV system presents a better match between generation and consumption. The peak electricity demand between 6 p.m. and 7 p.m. is covered by the PV panels while the ORC stops working a little bit before 6 p.m.

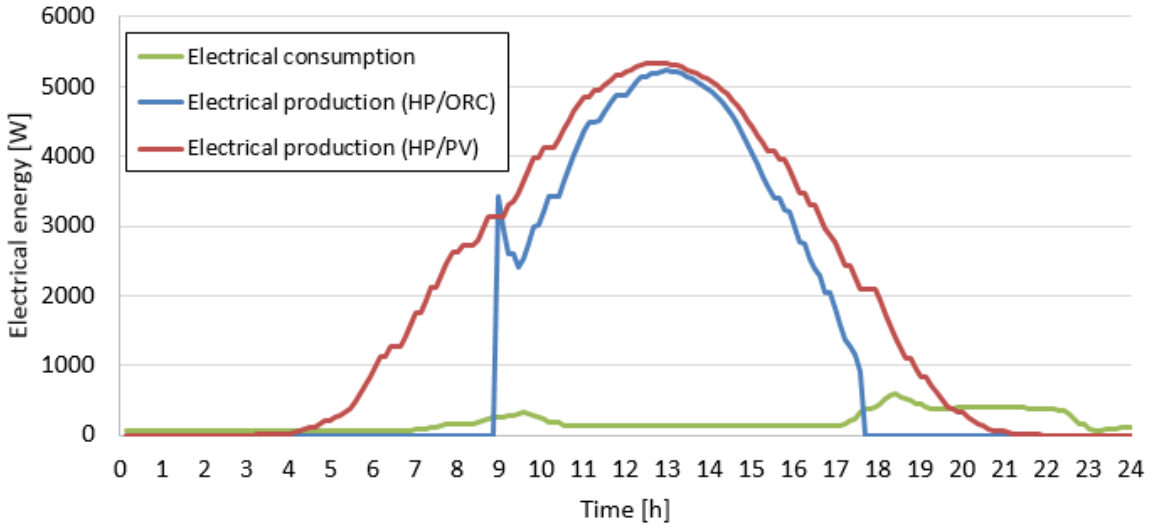

Figure 26 : Hourly electrical production and consumption for a typical summer day

The basic case has shown higher performances for the HP/PV system. It is also interesting to study the influence of the climate regarding the evolution of the performance of both systems. Figure 27 presents the gross electrical production and the heat pump electrical consumption for 5 typical climates in Europe (from North to South). First, the same conclusion as stated here above can be deduced: the heat pump consumption is significantly lower with the HP/ORC system due to the direct heating mode. In southernmost locations, the heat pump is not even necessary anymore to fulfil the heat requirements of the buildings for this system. This means that in location close to Roma and Palermo, the use of a reversible heat pump/organic Rankine cycle does not make any sense. Also, the ORC gross production increase more than the PV panels production because the ORC system works more and more often closer to nominal conditions in southernmost locations. The direct heating heat (not shown in Figure 27) presents a maximum in Torino. This is explained by the fact that if the outdoor air is too cold, the roof is not warm enough to heat the storage but if the outdoor air is too warm, the thermal load is lower.

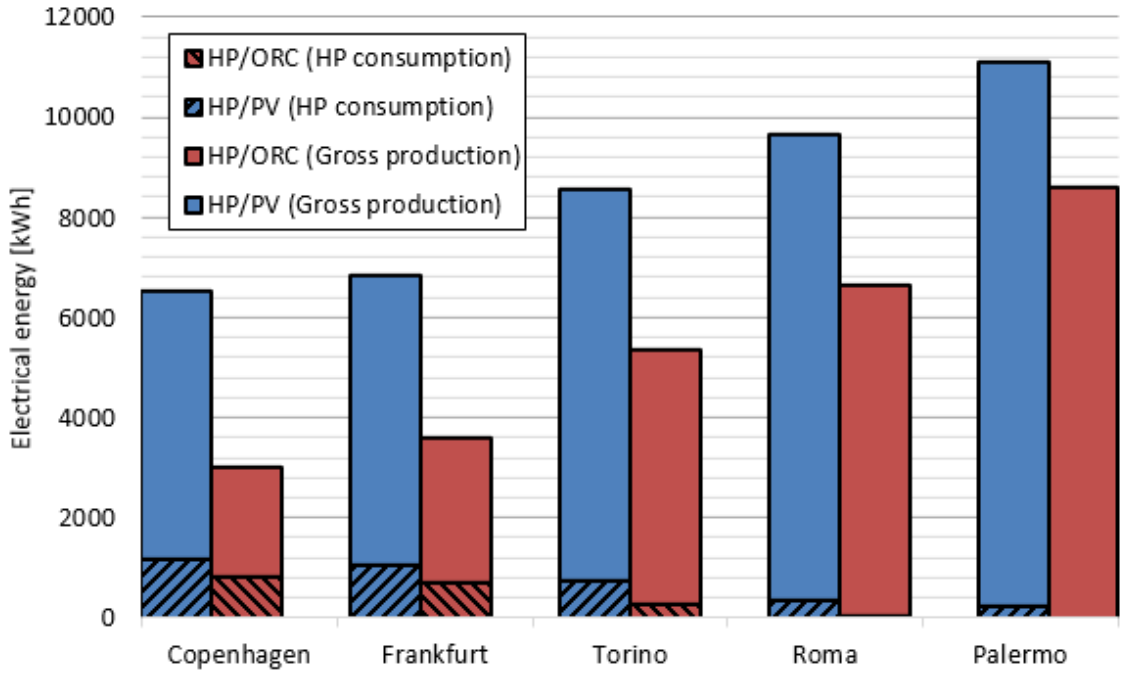

Figure 27 : Comparison of the gross electrical production and the heat pump electrical consumption for both systems (HP/ORC and HP/PV) for 5 typical climates in Europe.

Results in the basic case and with five different locations have shown that the HP/PV system presents better overall performance in terms of net electrical production, running benefits and matching of electricity demand and consumption. The HP/ORC system presents two advantages. On the one hand, the investment costs are rather low, since the cost are very close to a classical heat pump (addition of a pump and a four-way valve for the reversibility in ORC mode). On the other hand, the electrical consumption is lower for the HP/ORC system thanks to the heat provided by the roof (Direct Heating). This is a non-negligible advantage of the system since it can reduce electricity consumption during peak of electricity. This study shows that the HP/ORC system is more efficient in location close to Torino due to the direct heating mode. The direct heating mode does not reduce ORC running hour because it works at much lower roof temperatures. Therefore, cases where thermal load are higher could be very interesting and make the HP/ORC system more competitive than the HP/PV system. Some examples with high thermal load could be large buildings, buildings with poor insulation, building with high domestic hot water needs (sports hall, swimming pool,etc).

In a way to compare the two systems economically (income benefit and investment), the total cost of the HP/ORC system is compared to the cost of the HP/PV system after 25 years of operation. The total cost of the HP/ORC system is equal to the investment costs (the sum of the costs of the solar roof (*roof*), of the reversible HP/ORC unit (*HP/ORC*), of the horizontal ground heat exchanger (HGHE) and of the storage (sto) minus the income benefits generated each year and their interests (Eq. 11).

$$Price_{HP/ORC,roof,HGHE,sto} - \sum_{i=0}^{t} (B_{HP/ORC}).(1+r)^i \quad 11$$

The cost of the HP/PV solution equals to the investment costs (cost of the PV panels (PV), of the HP, of the storage, of the boreholes (BH)) minus the income benefits generated each year and their interests (Eq. 12). *r* is the interest rate and *n* is the number of year considered.

$$Price_{HP,PV,BH,sto} - \sum_{i=0}^{n} (B_{HP/PV}).(1+r)^i \quad 12$$

The equalisation of the cost of the HP/ORC (Eq. 11) and of the HP/PV (Eq. 12) leads to Eq. 13. $P_{\Delta rev,roof,\Delta HGHE}$ is the sum of the additional cost to modify a classical ground source heat pump into an ORC, plus the additional cost of HGHE compared to boreholes (usually associated with a ground source HP) and the cost of the solar roof. This term, plotted in Figure 28, is therefore the additional costs for the HP/ORC to make it as economically interesting as the HP/PV solution.

$$Price_{\Delta rev,roof,GHX} = Price_{PV} - \sum_{i=0}^{t} (B_{HP/PV} - B_{HP/ORC}).(1+r)^i \quad 13$$

$P_{\Delta rev,roof,\Delta HGHE}$ is evaluated in the case of 25 years (t=24), with a typical interest rate of 0.04 (Kost et al., 2013) and C_{PV} =8750 € (Abdul-Zahra et al., 2014) (Figure 28).

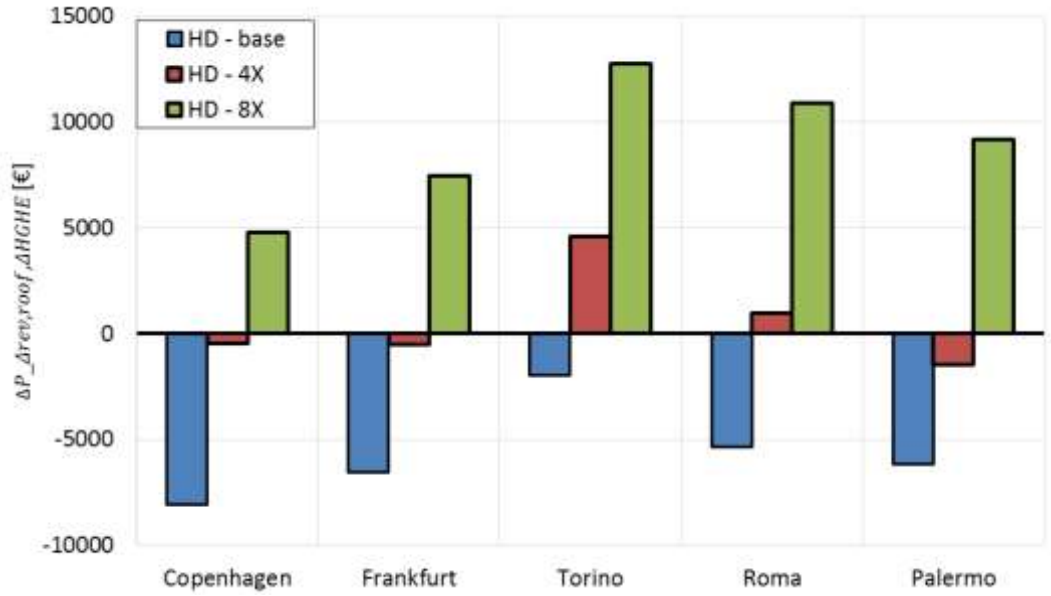

Figure 28: Comparison of the allowed additional costs for the HP/ORC system to be competitive with the HP/PV system. The different heat demands are detailed in Table 11.

The reversible system is never profitable in the base case with a heat demand corresponding to the real house (blue bars). Nevertheless, as explained in the former sections, if the heat demand is increased, the profitability of the reversible system is increased. For this reason, different heat demands (see Table 11) are simulated in the building and the results are presented in Figure 28 for 5 different locations. For the slightly higher heat demand, with four times more DHW consumption (HD – large, red bars), the system could be profitable only in Rome and Torino mainly because the direct heating is higher for these cities. Finally, if the heat demand is significantly higher, with 8 times higher DHW consumption, (HD – very large, green bars), the reversible unit is much more profitable. More generally, this means that buildings with a high heat demand, everything else being constant, are profitable for the reversible unit. A building with high heating consumption or a building with high DHW consumption could fit this constraint (office building, hospital, prison, stadium, etc.).

Table 11: Global annual heat demand for different scenarios

Heat demand [kWh/year]	HD - base	HD - large	HD – very large
Copenhagen	11320	16246	21092
Frankfurt	10029	14301	19311
Torino	7920	11620	16623
Rome	4469	7438	12440
Palermo	2194	4332	9319

The PV system presents a lower self-production rate because it generates higher power than the ORC system around midday when the electrical consumption is already covered by the

solar electrical production. On the contrary, the PV system outperforms the ORC system in terms of self-consumption rate. ORC systems (or more generally, systems presenting a low self-consumption) benefits of a higher increase in the self-consumption and self-production through the use of a battery compared to PV systems. However, in the case of smart-grid, the reversible system is thus not optimal since the self-consumption is limited.

Furthermore, the results are used to predict the optimal battery size and the optimal pay-back period in any case (see annex - Table 15)

4 CONCLUSION

The recent interest for Positive Energy Buildings (PEB) has led to development of new technologies and solutions. In this Chapter, a reversible heat pump/organic Rankine cycle coupled to a passive house is studied. This technology is a promising option to achieve a PEB. The modelling of each sub-system (ground heat exchanger, thermal energy storage, building, solar roof, reversible HP/ORC unit) and the control strategy are described extensively. Simulations show that this technology leads to a PEB on an annual basis. Moreover, a sensitivity study has led to the following conclusions:

- The HP/ORC system presents a positive net electrical production while covering the total heat demand of the building over a year, even in cold climates such as that of Denmark. The results show that, in the Danish case-study of a single family house with a 138.8 m^2 solar collector, the electrical production by the ORC system reaches 3012 kWh/year, while the total annual electrical consumption is 2318 kWh/year.
- The climate in southernmost cities is much more favourable for the ORC system because it works for longer periods and closer to its nominal conditions.
- There is an optimum location (for latitudes around Torino) where the direct heating is maximum.
- A low insulation of the building and/or a low lighting and appliances consumption profile leads to a better use of the system, benefiting from more energy from direct heating.
- When compared to a heat pump coupled with PV panels, results show that the HP/ORC unit could only be profitable in the case of a large heat demand of the building and/or restriction on buying electricity from the grid. More generally, this means that buildings with a high heat demand, everything else being constant, are profitable for the reversible unit. A large building or a building with high DHW consumption could fit this constraint (office building, hospital, prison, stadium, etc.).
- The heat pump is almost never used in southern locations, because the heat demand is small and, therefore can benefit from the direct heating. A reversible chiller/ORC would be more appropriate.
- The results in this work show that for the HP/ORC unit, i.e. HP coupled with solar collectors the DHW tank configurations are preferred against buffer tank

configurations. Further investigations with mantle tank configuration should be performed in the future

- The original size of the tank (500 litres) appears to be a good choice regarding the high cost increases and the low performance increase of larger storages.
- Although results depend on the assumptions (electricity tariffs, investment costs, battery performance, existence of a demand side management, etc.), it has been shown that the battery size leading to the minimum payback period is comprised between 2.6 kWh and 4.5 kWh (Table Table 15). These values are lower than the current cheapest batteries available on the market (Tesla, 2016). However, an over-sized battery will lead to a lower number of cycles leading to a higher life expectancy and a higher self-consumption. More simulations should be performed to assess the validity of the correlations in a wider range of inputs (higher roof tilt angle, other building envelope characteristics, more lighting and appliances profiles…).
- The economic interest of the battery integration has not been reached yet because of the high pay-back periods. The battery price still need to decrease while regulatory framework should change to promote the self-consumption in buildings.

In conclusion, after selecting one of the most promising application (building coupled with solar collectors) of the reversible HP/ORC unit (Chapter one), after an optimal design and sizing of the system (Chapters two and three) and after the calibration of model based on experimental data (Chapter four), the dynamic simulations allow to predict the performance and the economic interest of the system. Despite the proven feasibility to use this unit to get a Positive Energy Building, the combination of a heat pump coupled with PV panels is, almost always, more profitable. Other applications could therefore be studied in details to evaluate the practical feasibility (i.e. the economic feasibility).

5 APPENDICES

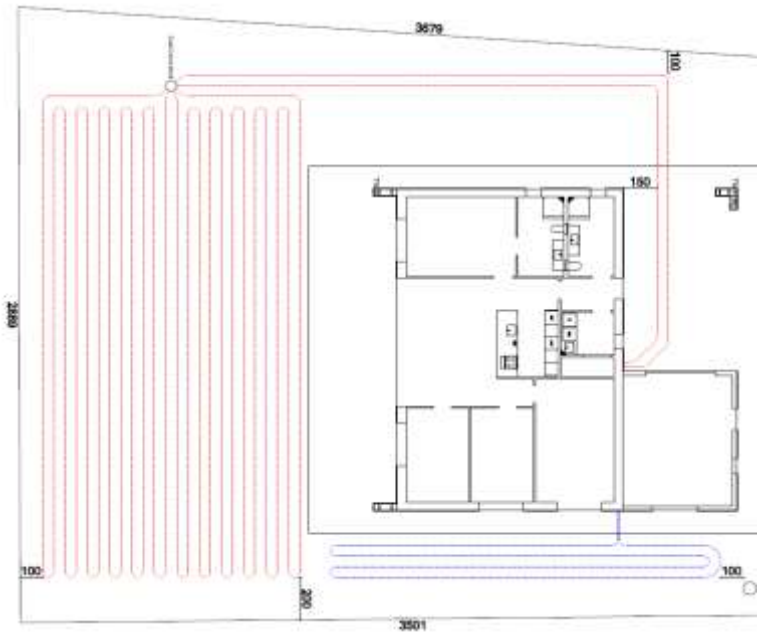

Figure A1: Layout of the GHX. Black line is the building, blue line is a cooling system and red lines are the GHX with two main hoses of connection.

	Parameter	Value	Unit
Surface	Thermal Capacity	$3E07$	J/K
	Related thickness	0.033	m
	Thermal resistance	0.0011	K/W
	Convective resistance	$1.58E-04$	K/W
Subsoil	Thermal Capacity	$4E09$	J/K
	Related thickness	4.47	m
	Thermal resistance	0.005	K/W
Central soil	Thermal Capacity	$1.2E09$	J/K
	Related thickness	2.01	m
Pipes	Convective resistance	$1.26E-04$	K/W
	Tube resistance	$4.89E-05$	K/W
	Soil resistance	$2E-04$	K/W
Contact surface	Area	299	m^2

Table A1: Validated parameters of the reduced order model

Table 12: Water tank with two heat exchangers model parameters

Parameter	Value	Parameter	Value
Tank total height [m]	1.44	Top Heat exchanger area (one side) [m^2]	2.5
Height bottom HX inlet [m]	0.54	Tank capacity [m^3]	0.5
Height bottom HX outlet [m]	0.09	Internal volume bottom HX [m^3]	0.011
Height top HX inlet [m]	0.09	Internal volume top HX [m^3]	0.025
Height top HX outlet [m]	1.225	U-value between inside of tank and ambient[W/m^2K]	2.7
Total heat exchange area of tank with ambient [m^2]	3.27	U-value of the heat exchanger[W/m^2K]	4000
Bottom Heat exchanger area [m^2]	1.8		

5.1 SELECTION OF THE OPTIMAL STORAGE MODELLING

5.1.1 Introduction

The building sector accounts for one-third of the global final energy demand (REN 21, 2015). Thermal Energy Storages (TES) play a significant role to reduce the impact of the building sector on the environment. TES have numerous advantages (Dincer, 2002):

- Enable a fundamental balance in energy supply-demand dynamics, which often do not occur at the same periods, especially in future energy systems based on renewable energy. ;
- Decrease the number of starts and stops of the heating system, thus decrease their energy losses;
- Increase deliverable capacity (heating element generation plus storage capacity);
- Shift energy purchases to lower cost periods;
- Increase system reliability.

The most important factor influencing the efficiency of hot water tanks (most widespread technology) is the vertical thermal stratification. An efficient storage conserves hot water in the upper part to limit unnecessary heating and cold water at the lower part to optimize heating system performance in the case of heat pump or solar collector. A short thermocline (layer in which temperature changes more rapidly with depth than it does in the layers above or below) allows reducing the mixing and avoids the destruction of exergy (Pizzonalto et al., 2003).

To improve the efficiency of these systems an accurate model of the hot water tank and its stratification is necessary. On the one hand, a poor tank model underestimates/overestimates the efficiency of the TES and therefore leads to over/under-sizing of the system. Sizing is crucial for different reasons. Over-sizing leads to higher investments and potential wasting of electricity if more energy is stored than is required (high losses). Under-sizing leads to more start and stops, reduced possibility of shifting production and demand, poor levels of indoor

comfort and lower solar fraction if integrated in a solar system. While, on the other hand, optimal control strategy through accurate modeling allows significant higher annual performance of the system.

In practice, modeling the behavior of hot water tanks is not trivial. A wide range of typologies (series, parallel, hybrid connections with loads and heating systems), materials (fluid, tank and insulation) and geometries (tank port type, orientation and location, internal or external heat exchangers, electrical heaters) exist. Following an introduction (section 1), this chapter briefly describes the different phenomena that take place in a sensible water storage (section 2). Thereafter, a classification of storage models and a brief description is proposed (section 3). Finally, a comparison and a decision tree is proposed (section 4).

5.1.1.1 Description of the physical processes

Different physical processes can occur in a hot water tanks:

- Heat transfer by conduction in the water due to temperature gradient;
- Ambient losses due to the temperature gradient between the storage medium and the ambiance;
- Convective currents induced by parietal heat transfer (Fan et al., 2012). The tank wall cools a thin vertical layer of water adjacent to the wall. This water layer becomes denser than its surroundings and slips towards the bottom of the tank (Fig. 1a);
- Buoyancy induced flow by temperature inversion due to loading conditions (Fig. 1b). This takes place when cold (i.e. hot) fluid enters a warm (i.e. cold) layer. This could, for example, happens when using a solar heating system in the late afternoon;
- Mixing with jets (during direct charging or discharging of the tank, the fluid entering the tank presents a certain level kinetic energy that will lead to a mixing of the temperature inside the tank);
- Quilting, which is a heat loss due to recirculation of water in the tank from hydraulic connections;
- Heat transfer through exchanger or resistor;
- Obstacles to decrease momentum driven jets (Fig. 1c).

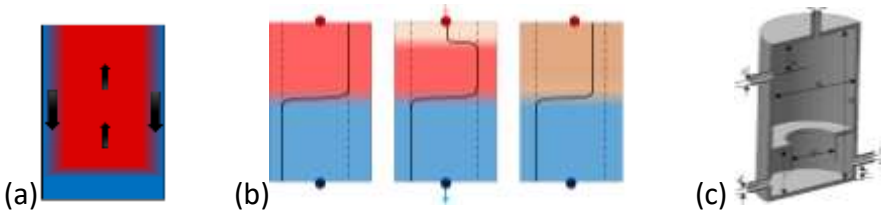

Figure 29: (a) Convective currents induced by parietal conduction. (b) Buoyancy induced flow by temperature inversion due to loading conditions (Dickes et al., 2012). (c) Obstacles to decrease momentum driven jets (Altuntop et al., 2015).

5.1.2 Description of different modelling approaches

Mathematical equations that describe the processes occurring in the storage are difficult to solve without considerable simplifying equations. That is the reason why a large number of storage models have been developed in the last decades. Some applications require fast computational time with low accuracy while other need very accurate modelling of all the phenomena occurring in the tank. The following classification is proposed to group types of

model (Fig. 2): Analytical (AN), Fully Mixed (FM), Blackbox (BB), two zone Moving Boundary (MB), Plug-Flow (PF), Multi-Node (MN), Zonal (ZN) and Computational Fluid Dynamics models (CFD).

5.1.2.1 AN - Analytical

Some authors ((Cabelli, 1977, Chung et al., 2011) among others) developed an exact analytical solution of storage modelling.

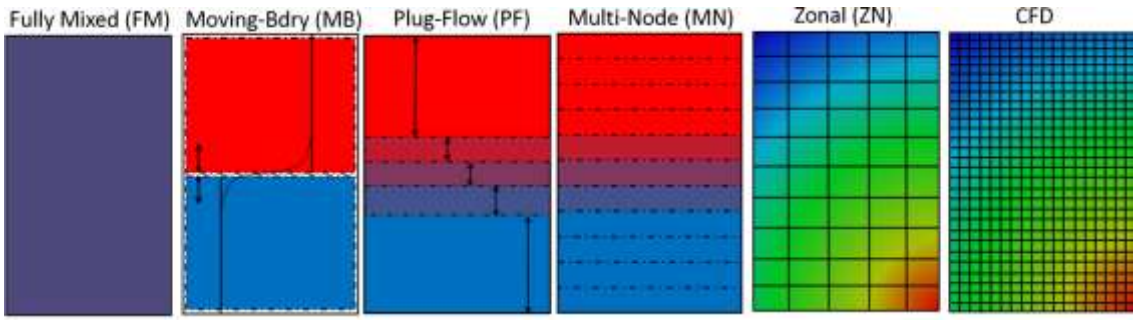

Figure 30: Different modeling approaches for a sensible thermal energy storage.

A Laplace transformation technique is used to predict the thermocline during charging. These models are based on several hypothesis. First, the tank is modelled as a one-dimensional semi-infinite body to make the problem mathematically tractable. Also, no mixing or ambient heat losses are considered. Finally, the thermo-physical properties, the inlet temperature and the mass flow rate are kept constant. This model has a narrow range of application but demonstrates to be very fast. However, this model is interesting to evaluate the upper bound achievable in terms of stratification. Also, it helps to find general correlations, (Chung et al., 2011) showed that the thermocline thickness in the case of no fluid mixing at the inlet in a charging process is proportional to the square of root time and reversely proportional to the flow rate.

5.1.2.2 FM - Fully Mixed (or one layer or thermal capacity)

The fully mixed model is the simplest and one of the fastest since the temperature is considered homogenous in the whole tank. The energy balance (Eq. 1) takes into account the inertia of the fluid, the heat input ($\dot{H}_{in}$) and output ($\dot{H}_{out}$) and eventually ambient losses ($\dot{Q}_{amb}$). m is the mass of fluid, c the specific heat capacity and T, the homogenous temperature.

$$mc\frac{dT}{dt} = \dot{H}_{in} - \dot{H}_{out} - \dot{Q}_{amb} \qquad (1)$$

Of course, no stratification is possible leading to a significant error on the estimation of ambient heat losses. Poor performance is therefore achieved for the heating system in the case of a heat pump or a solar collector. This model could be seen as a Multi-Node (MN) model with one node. But, practically, with only one node, all the physical phenomena that can be included in a MN model (convection, conduction, jets among others) cannot be included in the FM model. That is why a separate type is considered here for both models.

5.1.2.3 BB – Blackbox

Artificial neural network methods are statistical learning models that operate like a black box validated with a database (experiments or complex models). Outputs are evaluated with the inputs by means of hidden functions. This method has already been applied in the case of a TES (Kalogirou et al., 2005). These models are fast but cannot be used for extrapolation outside the calibration range. Sciacovelli (Scaciovelli, 2015)) used a proper generalized decomposition which consists in an enrichment of formula with a priori unknown functions and parameters. The model has been validated for different geometries based on CFD models. This approach allows to use BB with different geometries which is interesting. But, still, it cannot be used with other parameters (inlet and outlet position, internal heat exchanger, thermal insulation variation…), needs to run long CFD simulation several times and is very dependent of the database.

5.1.2.4 MB - Moving Boundary

In this model, an ideal thermocline (negligible thickness) is dividing the storage into two zones with fixed temperatures. The position of the thermocline (which determines the volume of each zone) is given by the energy balance including ambient losses, heat input and output. This model does not take mixing into account and there is no mass transfer between the two zones. This model presents a low CPU time (Celador, 2011). In 2015, Dickes et al. (Dickes et al., 2015) developed a two-zone moving boundary with a transition profile of the temperature. The difference with the former model is that the temperature are not fixed anymore but are evaluated with temperatures at former time step and an energy balance in each zone. A dynamic deterministic update of temperature profile (thermocline) is evaluated in function of the time and the flow. It allows to obtain a good accuracy of the stratification compared to a detailed multimode model. This upgraded model is the one which will be referred as MB in the next part of the chapter.

5.1.2.5 PF - Plug Flow

In this approach, n-variable volume isothermal disks are assumed to move through the tank without any mixing between them (Duffie et al., 2005). The modeling is quite simple: When a supply volume is inserted into the tank, a new segment with the prescribed inlet temperature is inserted. In the most common approach, the variable inlet is used (it injects the fluid in the tank in the zone where the temperature level presents the closest temperature to keep a monotonically increasing temperature with the height). If the temperature of the supply volume is close to an already existing segment (typically < 0.5 K), then the supply volume is mixed with the already existing segment. Because the tank presents a finite volume, a volume equivalent to the inlet volume is shifted out of the tank. This model is fast to be computed compared to the multimode (MN) model particularly in the case of high stratification (because of lower number of nodes required (Duffie et al., 2005)). The PF with variable inlet is interesting because it gives the upper limit of deliverable thermal energy (perfect stratification). This is almost the case practically when low mixing occurs.

5.1.2.6 MN – Multi-Node (or layer)

Other authors develop the multi-node model (one-dimensional finite-volume method). These models consider the following assumptions: uniform horizontal temperature in the horizontal layers and the flow inside the tank is one dimensional (Duffie et al., 2005). The model applies the conservation of energy for each zone (Eq. 2) taking into account the thermal inertia of the

fluid, the enthalpy flow input ($\dot{H}_{in}$), the enthalpy flow output ($\dot{H}_{out}$), the conductive losses ($\dot{Q}_{cond}$) including, or not, other effects such as induced buoyancy flows, jet mixing and plume entrainment and often ambient losses ($\dot{Q}_{amb}$) eventually including quilting losses.

$$m_i c_i \frac{dT_i}{dt} = \dot{Q}_{cond,i} + \dot{H}_{in,i} - \dot{H}_{out,i} + \dot{Q}_{amb,i} \qquad (2)$$

Furthermore, these models often require a relatively high number of cells compared to the former approaches leading to a higher computational time. The high number of cells allows avoiding artificial diffusion (i.e. the smoothing effect due to the successive ideal-mixing of the fluid in each cell (Duffie et al., 2015). Franke (1997) a variable thickness multimode model is developed and allows to use only 6 nodes instead of 15 for a constant thickness multimode model. Various number of MN models predict the temperature profile based on a few semi-empirical fitting parameters.

5.1.2.7 ZN - Zonal

The zonal model developed by Blandin (2010) is basically a 3D finite-volume method with a large mesh (division in crown and sectors) where mass and energy balance are verified. The simplification induced by the large mesh and no momentum conservation (compared to CFD models) are compensated by the introduction of laws taking into account plume entrainment, boundary layer flow, jet and quilting. This model is an intermediary between CFD models and MN models in terms of physical phenomena taken into account and CPU time (roughly seven times slower than MN model).

5.1.2.8 CFD - Computational Fluid Dynamics

Modelling tanks with Computational Fluid Dynamics is the most accurate way to model the flow field in the tank. Finite Element Method (FEM) or Finite Volume Method (FVM) can be applied but the most widespread solution in the case of water tank is the FVM because of its lower computationally expensive nature. In each volume of the mesh, Navier-Stokes equations are applied with mass, momentum and energy conservation laws. Two dimensional CFD models are suited for axisymmetric (or quasi-axisymmetric) tank configurations [16]. If not, three dimensional CFD models have to be used but can lead to much longer simulation time. These models are well suited for design optimization reducing costs that would otherwise be associated to perform experiments. Also, it allows to get useful correlation of local phenomena that can be implemented in faster models [4].

5.1.3 Comparison and selection of the optimal model

Table 1 compares the different modelling approaches in terms of the description of physical phenomena, CPU time and the need to have a database to fit parameters (not determinist). The physical phenomena are briefly described in chapter 2. The 8 modelling types considered in this study are: Analytical (AN), Fully Mixed (FM), Blackbox (BB), Moving boundary (MB), Plug Flow (PF), Multi-node (MN), Zonal (ZN) and computational fluid dynamics (CFD).

Table 13. Comparison between the modelling approaches. + is good, - is bad and o is intermediate. * means that it can be integrated in the model but not systematically.

Criterion		AN	FM	BB	MB	PF	MN	ZN	CFD
Physical phenomena	Ambient losses	-	*	-	*	*	+	+	+
	Conduction (water + wall)	-	-	-	*	-	+	+	+
	Mixing due to T° inversion	-	-	-	+	*	*	+	+
	Quilting	-	-	-	*	*	*	+	+
	Parietal induced flow	-	-	-	*	-	*	+	+
	Jets mixing	-	-	-	-	-	*	+	+
	Exchanger/resistor	-	-	-	*	*	+	+	+
	Navier-stokes + obstacles	-	-	-	-	-	-	-	+
CPU time		+	+	+	+	+	O	-	-
Determinist		+	+	-	+	+	+	+	+

Several papers compare results from different modelling approaches (Franke, 1997; Kleinbach, 1990; Allard et al., 2011; Zurigat et al., 1989; Hollands et al., 1989). It should be noted however that conclusions drawn are case dependent and should be taken with care. Also, a given type of model does not give satisfaction in every application. A decision tree is proposed to select the optimal storage model depending on the main criteria encountered: application, accuracy, computational time and availability of a database (Fig. 3). AN models are not considered here because of their very narrow range of application.

Here is the way to use the decision tree: First, if the purpose is to perform an optimal design, CFD models should be chosen because of their high capabilities to model complex flow field inside the tank with a wide range of configuration. When performing simulations of a tank, if experimental data is available, two types are possible, either AN or MN with fitting parameters. Because of their non-extrapolability, AN models would require experimentation on the whole range of inputs which is often long and costly. MN models should therefore be preferred thanks to the semi-empirical modelling assumptions. If no experimental data is available, which is often the case, a model giving the highest accuracy with acceptable CPU time should be chosen. A complexity trade-off must indeed be found for each application. The FM model should not be used because of its very poor accuracy except in the case where stratification is negligible (high flow or small storage) and in the case where a lower bound of performance is required. The MB model with temperature profile is very interesting in terms of accuracy and CPU time but needs further developments to account for internal exchanger(s) and ambient losses relevant in a wider range of applications.

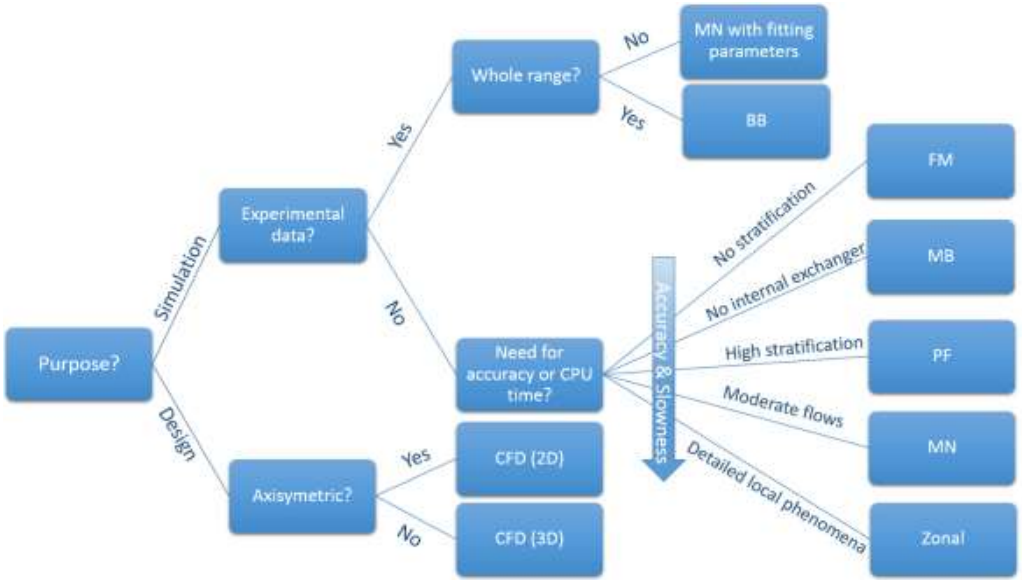

Figure 31: Decision tree to select the optimal storage modeling approach

The PF model is fast and accurate in the case of high stratification (low flow, low thermal power, large tank, efficient stratification manifold and/or diffuser) and in the case where an upper bound of performance is necessary. The PF model is fast and accurate in the case of high stratification (low flow, low thermal power, large tank, efficient stratification manifold and/or diffuser) and in the case where an upper bound of performance is necessary. The MN model is the most classical choice for annual simulation because of its decent accuracy but is too slow for optimal control (e.g. Demand Side Management). Finally, the zonal model is the most accurate model that can be used for simulation purposes. But, it requires seven times more CPU time than MN models (Blandin, 2010), which could be a rejection criterion for a lot of applications.

5.1.4 Conclusion

First, an overview of the different phenomena occurring in hot water tank is performed. Secondly, this chapter tries to determine a classification among existing simulation models through the discussion of their hypothesis and limitations. Finally, a decision tree is proposed to the analyst/designer select the optimal model depending on the given application, accuracy, computational time and availability of a database of results.

5.2 DHW AND BUFFER TANK PARAMETERS

Table 14 : Hydraulic scheme of the hot water tanks configurations studied. Configuration 1 (left) and configuration 2 (right).

				Unit Heat Exchanger				DHW Heat Exchanger			
Tank type	Amb. losses [W/m²K]	Volume [m³]	Height/ Diameter	U-value [W/m²K]	Volume [m³]	Height inlet [m]	Height outlet [m]	U-value [W/m²K]	Volume [m³]	Height inlet [m]	Height outlet [m]
Buffer	2.7	0.5	3.2	1150	0.011	0.03	0.61	1150	0.025	0.1	1.4
DHW	2.7	0.5	3.2	1150	0.011	0.03	0.61	-	-	-	-

5.3 OPTIMAL battery SIZE AND PAYBACK PERIOD

In the former section, it has been observed that each case study presents an optimal battery size corresponding to the lowest payback period. Despite the large size of battery simulated (up to 20kWh) and the large size of commercial products (up to 10 kWh), the optimal battery size for the 160 study cases only varies between 2.6 kWh and 4.5 kWh (Fig. 3a). A Gaussian Process sensitivity analysis (Knight et al., 2010) is performed to select the most relevant inputs to predict the optimal battery size with GPExp. The MARE (Quoilin et al., 2016) (Mean Average Relative Error) is used to select the optimal number of inputs (the lowest the MARE, the better the quality of prediction). From Fig. Figure 32 a), it can be seen that the electrical production and consumption are the two most relevant inputs to predict the optimal battery size.

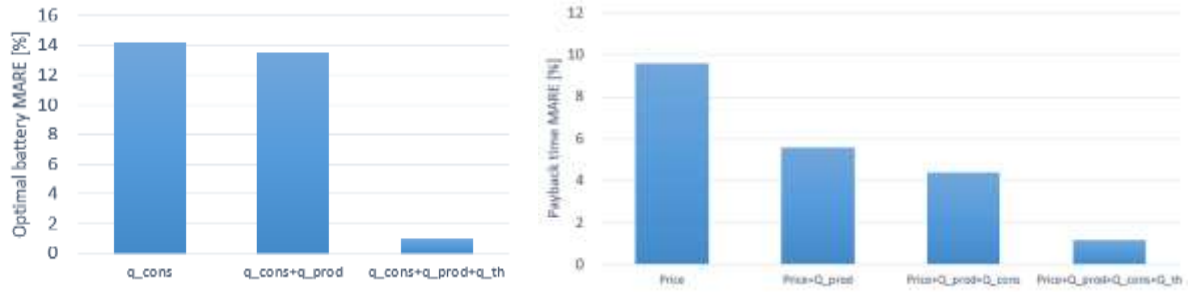

(a) (b)

Figure 32 : (a) MARE to predict the optimal battery size with optimal input. (b) MARE to predict the optimal payback time size with optimal input.

The relevance of the other simulation parameters is almost negligible (it is not the case, however for the prediction of PB): using more inputs would to a more complicated regression and to a possible over-fitting of the data. As a consequence, a correlation to predict the optimal battery size is proposed as a function of these two parameters (Eq. 14).

$$E_{bat,opt} = 3.52 - 0.1125\frac{W_{prod}}{W_{cons}} \qquad 14$$

It only considers the ratio between annual electricity production and consumption. The maximum error of prediction is 1.2 kWh which is deemed acceptable (Figure 33).

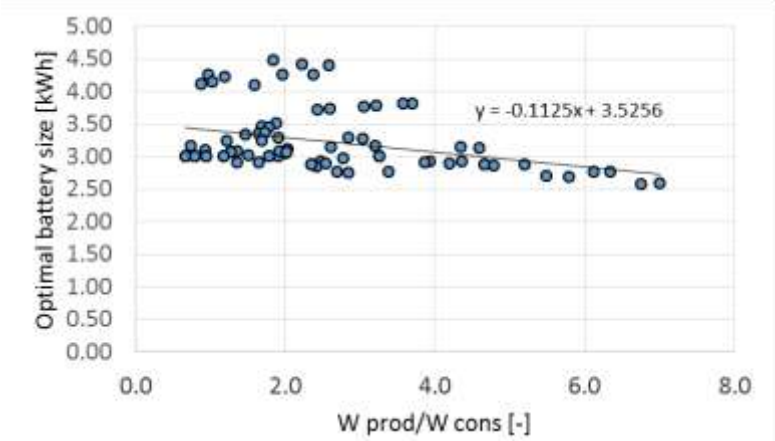

Figure 33: Optimal battery size in function of the ratio between annual electricity production and consumption.

Also, the optimal payback period (i.e. the lowest payback period simulated with the 20 battery sizes) is plotted in Fig. 6a versus the annual electrical production. The lowest payback periods, (~7 years), are reached with a well-insulated building envelope (K20), a high lighting and appliance consumption (LA3000), a low feed-in tariff (no_sell) and a 3.5 kWh battery. The payback period is very high (not actually economically feasible) in the case of the feed-in tariff of 0.17 € /kWh (blue points – sell). On the contrary, the red points (no sell – no feed-in tariff) shows low payback period which indicates that batteries could be economically viable at the considered (optimistic) investment cost. An optimum is observed: For low annual electrical production, the optimum payback period decreases sharply while for high annual electrical load, the optimal payback period slightly increases. A correlation (Eq. 15) is therefore proposed to take into account the two main relevant inputs (also selected with a Gaussian Regression – Figure 32): the electricity feed-in tariff, $Price_{bb}$, and the annual electrical production, W_{prod}.

$$PB_{opt} = 23.55 - 58.6.(price_r - price_{bb}) + 1.768.10^{-7}(W_{prod} - 9260)^2 \qquad 15$$

Figure 34 shows that the correlations predicts the optimal payback period with a decent accuracy only with two inputs.

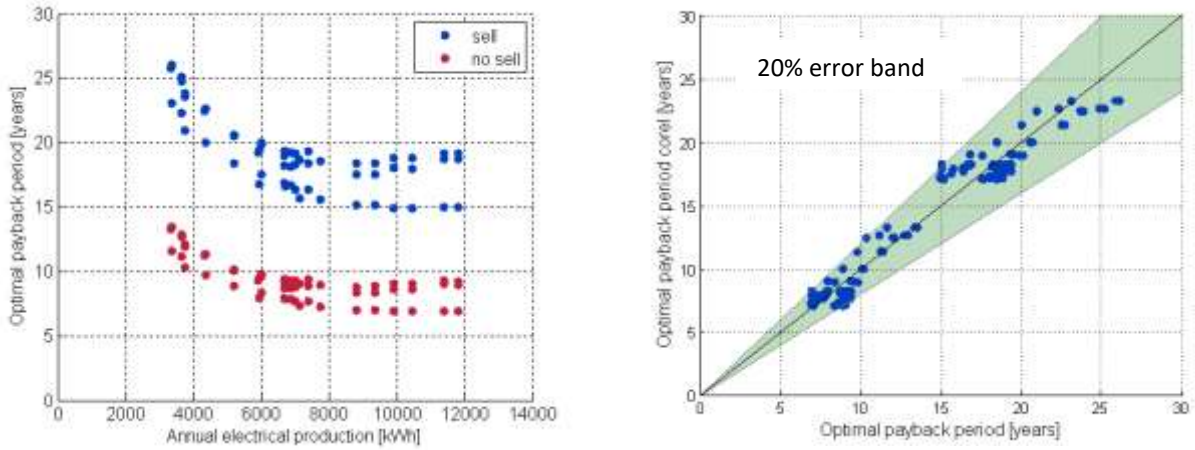

(a) (b)

Figure 34 : (a) Optimal payback period in function of annual electrical production. (b) Comparison of the optimal payback period versus the one predicted by the correlation (20% error bands).

5.4 SUMMARY OF THE YEARLY SIMULATIONS

Table 15 : Summary of results. The logic to order the data is the following : the first 5 lines corresponds to the 5 different climates, the next five lines are the same results with another roof tilt, the next ten lines are the same results with another production system, the next twenty lines correspond to another lighting and appliance consumption and finally the second last part of the table are the same results with another building.

Building	LA	System	Tilt [°C]	Lattitude [°]	Q_{cons} [kWh]	Q_{prod} [kWh]	Optim bat [kWh]	Optim bat no sell [kWh]	PB optim [years]	PB optim no sell [years]	γ_d [%]	γ_s [%]
K20	LA3000	PV	R35	56	4081	6874	3	3	17	8	31	18
K20	LA3000	PV	R35	51	3948	7404	4	4	16	8	32	17
K20	LA3000	PV	R35	45	3618	9371	4	4	15	7	34	14
K20	LA3000	PV	R35	42	3257	10466	4	4	15	7	39	13
K20	LA3000	PV	R35	38	3190	11813	4	4	15	7	38	12
K20	LA3000	PV	R5	56	4084	6701	3	3	17	8	32	19
K20	LA3000	PV	R5	51	3951	7024	3	3	16	8	32	18
K20	LA3000	PV	R5	45	3621	8818	4	4	15	7	34	15
K20	LA3000	PV	R5	42	3258	9921	4	4	15	7	38	14

K20	LA3000	PV	R5	38	3191	11396	4	4	15	7	38	13
K20	LA3000	ORC	R35	56	3767	3667	4	4	22	11	14	14
K20	LA3000	ORC	R35	51	3640	4357	4	4	20	10	16	13
K20	LA3000	ORC	R35	45	3288	6022	4	4	18	8	20	12
K20	LA3000	ORC	R35	42	3029	6727	4	4	17	8	24	12
K20	LA3000	ORC	R35	38	3000	7758	4	4	16	7	26	12
K20	LA3000	ORC	R5	56	3819	3363	4	4	23	12	14	15
K20	LA3000	ORC	R5	51	3659	3767	4	4	21	10	15	14
K20	LA3000	ORC	R5	45	3285	5214	4	4	18	9	19	13
K20	LA3000	ORC	R5	42	3029	5953	4	4	17	8	23	14
K20	LA3000	ORC	R5	38	3000	7131	4	4	16	7	26	13
K20	LA1491	PV	R35	56	2778	6874	3	3	19	9	27	11
K20	LA1491	PV	R35	51	2609	7407	3	3	19	9	28	10
K20	LA1491	PV	R35	45	2236	9371	3	3	18	9	30	8
K20	LA1491	PV	R35	42	1806	10465	3	3	19	9	35	7
K20	LA1491	PV	R35	38	1686	11812	3	3	19	9	36	7
K20	LA1491	PV	R5	56	2780	6705	3	3	19	9	27	11
K20	LA1491	PV	R5	51	2612	7024	3	3	19	9	28	11
K20	LA1491	PV	R5	45	2240	8819	3	3	18	9	30	9
K20	LA1491	PV	R5	42	1808	9919	3	3	19	9	35	8
K20	LA1491	PV	R5	38	1687	11398	3	3	19	9	36	7
K20	LA1491	ORC	R35	56	2434	3665	3	3	25	13	12	8
K20	LA1491	ORC	R35	51	2284	4356	3	3	23	11	14	7
K20	LA1491	ORC	R35	45	1881	6018	3	3	20	10	17	6
K20	LA1491	ORC	R35	42	1544	6723	3	3	19	9	21	6
K20	LA1491	ORC	R35	38	1491	7756	3	3	19	9	24	6
K20	LA1491	ORC	R5	56	2479	3360	3	3	26	13	12	8
K20	LA1491	ORC	R5	51	2295	3766	3	3	24	12	13	8
K20	LA1491	ORC	R5	45	1876	5210	3	3	21	10	17	7
K20	LA1491	ORC	R5	42	1541	5949	3	3	19	9	21	7
K20	LA1491	ORC	R5	38	1491	7129	3	3	19	9	24	7
K30	LA3000	PV	R35	56	5040	3351	3	3	26	13	8	8
K30	LA3000	PV	R35	51	4704	3755	3	3	24	12	10	8
K30	LA3000	PV	R35	45	4090	5200	3	3	20	10	12	7
K30	LA3000	PV	R35	42	3332	5932	3	3	19	9	15	7
K30	LA3000	PV	R35	38	3037	7116	3	3	19	9	17	6
K30	LA3000	PV	R5	56	5492	6702	3	3	18	9	20	11
K30	LA3000	PV	R5	51	5172	7028	3	3	18	9	21	11
K30	LA3000	PV	R5	45	4609	8821	3	3	18	8	21	9
K30	LA3000	PV	R5	42	3796	9921	3	3	18	9	26	8
K30	LA3000	PV	R5	38	3373	11395	3	3	19	9	27	7
K30	LA3000	ORC	R35	56	4996	3656	3	3	25	13	8	8
K30	LA3000	ORC	R35	51	4692	4344	3	3	22	11	10	7

K30	LA3000	ORC	R35	45	4096	6007	3	3	20	10	12	6
K30	LA3000	ORC	R35	42	3336	6704	3	3	19	9	15	6
K30	LA3000	ORC	R35	38	3040	7743	3	3	19	9	18	6
K30	LA3000	ORC	R5	56	5040	3351	3	3	26	13	8	8
K30	LA3000	ORC	R5	51	4704	3755	3	3	24	12	10	8
K30	LA3000	ORC	R5	45	4090	5200	3	3	20	10	12	7
K30	LA3000	ORC	R5	42	3332	5932	3	3	19	9	15	7
K30	LA3000	ORC	R5	38	3037	7116	3	3	19	9	17	6
K30	LA1491	PV	R35	56	3978	6873	3	3	18	9	20	11
K30	LA1491	PV	R35	51	3655	7403	3	3	18	9	21	10
K30	LA1491	PV	R35	45	3089	9374	3	3	18	8	21	8
K30	LA1491	PV	R35	42	2282	10469	3	3	18	9	26	8
K30	LA1491	PV	R35	38	1861	11809	3	3	19	9	27	7
K30	LA1491	PV	R5	56	3983	6702	3	3	18	9	20	11
K30	LA1491	PV	R5	51	3663	7028	3	3	18	9	21	11
K30	LA1491	PV	R5	45	3100	8821	3	3	18	8	21	9
K30	LA1491	PV	R5	42	2287	9921	3	3	18	9	26	8
K30	LA1491	PV	R5	38	1864	11395	3	3	19	9	27	7
K30	LA1491	ORC	R35	56	3531	3351	3	3	26	13	8	8
K30	LA1491	ORC	R35	51	3195	3755	3	3	24	12	10	8
K30	LA1491	ORC	R35	45	2581	5200	3	3	20	10	12	7
K30	LA1491	ORC	R35	42	1823	5932	3	3	19	9	15	7
K30	LA1491	ORC	R35	38	1528	7116	3	3	19	9	17	6
K30	LA1491	ORC	R5	56	3531	3351	3	3	26	13	8	8
K30	LA1491	ORC	R5	51	3195	3755	3	3	24	12	10	8
K30	LA1491	ORC	R5	45	2581	5200	3	3	20	10	12	7
K30	LA1491	ORC	R5	42	1823	5932	3	3	19	9	15	7
K30	LA1491	ORC	R5	38	1528	7116	3	3	19	9	17	6

References

- Abdul-Zahra, A., Fassnacht, T. Wagner., A., 2014. Evaluation of the combination of hybrid photovoltaic solar thermal collectors with air to water heat pumps. doi:10.1016/j.apenergy.2014.01.061

- Almeida, A., Fonseca, P., 2007. Residential monitoring to decrease energy use and carbon emissions in Europe. European council for energy efficient economy 2007, 1261-1271. http://remodece.isr.uc.pt/news/Paper_DeAlmeida.pdf

- Altuntop, M., Arslan, M., Ozceyhan, V., Kanoglu M., 2005. Effect of obstacles on thermal stratification in hot water storage tanks. Applied Thermal Engineering 25, 2285–2298.
- Baetens, R. De Coninck, R. Van Roy, J., Verbruggen, B. Driense, J. Helsen, L. Saelens, D., 2012 Assessing electrical bottlenecks at feeder level for residential net zero-buildings by integrated system simulation, Applied Energy, vol. 96, pp. 74-83.

- Bircher, S., Skou, N., Jensen, K. H., Walker, J.P., Rasmussen, L., 2012. A soil moisture and temperature network for SMOS validation in Western DK", Hydrol.Earth Syst. Sci. 16, 1445-1463.

- Blandin, D., 2010. Modélisation et validation expérimentale de nouveaux concepts de ballons solaires à forte stratification, PhD thesis.

- Bouvenot, J-B., Siroux, M., Latour, B. and Flament, B., 2015. Dwellings electrical and DHW load profiles generators development for µCHP systems using RES coupled to buildings applications. 6th International Building Physics Conference, IBPC 2015, Energy Procedia 78 (2015) 1919–1924. DOI:10.1016/j.egypro.2015.11.372

- Burhenne, S., D. Wystrcil, M. Elci, S. Narmsara, S., 2013. Building performance simulation using modelica: analysis of the current state and application areas. Proceedings of BS2013: 13th Conference of International Building Performance Simulation Association, Chambéry, France, August 26-28.

- Cabelli, A., 1977. Storage Tanks-A Numerical Experiment. Solar Energy 19, 45-54.

- Carmo, C., Dumont, O., Elmegaard, B., Nielsen, Detlefsen., 2015. Experimental validation of a domestic stratified hot water tank model in Modelica for annual performance assessmen, ORC 2015 conference.

- Carmo, 2016. Modelling and Development of an Innovative Dual-Mode Heat Pump with HP2Grid Functionality, PhD thesis.

- Carmo, C., 2016. Empirical platform data analysis to investigate how heat pumps operate in real-life conditions, in ICR2015, Yokohama, Japan.

- Castillo-Cagigal M., Caamano-Martın E., Matallanas E., Masa-Bote D., Gutierrez A., Monasterio-Huelin F., Jimenez-Leube J., 2011. PV self-consumption optimization with storage and Active DSM for the residential sector, Solar Energy;85:2338–2348.

- Celador, A., Odriozola, M., Sala, V.M., 2011. Implications of the modelling of stratified hot water storage tanks in the simulation of CHP plants. Energy conversion and management 52, 3018-3026.

- CEN, 2008. prEN12977 -3 Thermal solar systems and components - Custom built systems - Part 3: performance test methods for solar water heater stores. Technical report.

- Close, J., 1967. A Design Approach for Solar Processes. Solar Energy 11, 112-123.

- Danish Energy Agency. 2015. https://www.retsinformation.dk/forms/r0710.aspx?id=152758, accessed on the 22th of July 2015.

- Dincer, 2002. On thermal energy storage systems and applications in buildings. Energy and buildings 34, 77-388.

- Dickes, R., Desideri, A., Quoilin, S., Lemort, V., 2015. Model reduction for simulating the dynamic behavior of parabolic troughs and a thermocline energy storage in a micro-solar power unit. Proceedings of ECOS 2015 Conference.

- Dong Chung, J., Shin, Y., 2011. Integral approximate solution for the charging process in stratified thermal storage tanks. Solar Energy 85, 3010–3016.

- Duffie, J. A. and W. A. Beckham, 2006. Solar thermal engineering of thermal processes, John Wiley and sons, ISBN: 978-0-470-87366-3.

- Dumont, O., Quoilin, S., Lemort, V., 2014a. Experimental investigation of a scroll unit used as a compressor and as an expander in a reversible Heat Pump/ORC unit. Proceedings of the refrigeration conference in Purdue.

- Dumont, O., C. Carmo, F. Randaxhe, S. Quoilin and V. Lemort. 2014b. Simulation of a passive house coupled with a heat pump/organic Rankine cycle reversible unit. Proceedings of the 9th International Conference on System Simulation in Buildings (SSB2014).

- Dumont, O., Quoilin, S., Lemort, V., 2015a. Experimental investigation of a reversible heat pump / organic Rankine cycle unit designed to be coupled with a passive house (Net Zero Energy Building), International Journal of Refrigeration, http://dx.doi.org/10.1016/j.ijrefrig.2015.03.008.

- Dumont, O., Carmo, C., Randaxhe, F., Quoilin, S., Lemort, V., 2015b. Performance comparison of two types of technologies associated with a positive energy building: a reversible heat pump/ORC unit and a heat pump coupled with PV panels. Proceedings of the ISES Solar World Congress (SWC 2015). International Solar Energy Society, ISES, 2015. p. 1-6.

- Dumont O., Quoilin S., Lemort V., 2014c. Experimental investigation of a scroll unit used as a compressor and as an expander in a reversible Heat Pump/ORC unit. 2014 Purdue conferences: Proceedings of the refrigeration conference in Purdue, July 14-17 2014, Purdue, U.S.A.

- Dupeyrat P., Ménézo, P., Fortuin S., 2014. Study of the thermal and electrical performances of PVT solar hot water system. Energy and Buildings 68, 751-755.

- Energinet, 2015. http://energinet.dk/DA/El/Solceller/Har-du-solceller/Sider/Pristillaeg.aspx, accessed the 2st of January 2015.

- EnergyPlus, 2015. Available at http://apps1.eere.energy.gov/buildings/energyplus/weatherdata_about.cfm, [accessed 18.02.2015].

- European Comission, 2012. Energy markets in the European Union in 2011, ISBN: 978-92-79-25489-5, DOI: 10.2833/12806.

- European Comission, 2013. Progress by Member States towards Nearly Zero-Energy Buildings, COM (2013) 483

- European Commission, 2015. Best practices on Renewable Energy Self-consumption, COM 2015, 339, Brussels, (2015).

- EnergyPlus. 2015. http://apps1.eere.energy.gov/buildings/energyplus/weatherdata_about.cfm, Accessed the 18th of May 2015.

- EV-power, 2014. http://www.ev-power.eu/Winston-300Ah-1000Ah/, Accessed the 29th of october 2014.

- Fan, J., and Furbo, S., 2012. Thermal stratification in a hot water tank established by heat loss from the tank. Solar Energy 86, 3460–3469.

- Fischer, S.,Heidemann W., Müller-Steinhagen, H., Perers, B., , Bergquist, P., Hellströmd, B.. 2004. Collector test method under quasi-dynamic conditions according to the European Standard EN 12975-2, Solar Energy 76, 117-123.
- Franke, R., Object-oriented modeling of solar heating systems, 1997. Solar Energy 60, 171-180.

- Freeman, J., Hellgardt, K., Markides, C., 2015. An assessment of solar-powered organic Rankine cycle systems for combined heating and power in UK domestic applications, Applied Energy 138, 605-620.

- Georges, E., S. Gendebien, S. Bertagnolio, and V. Lemort. 2013a. Modeling and simulation of the domestic energy use in Belgium. Proceedings of CLIMA 2013 11th REHVA World Congress & 8th International Conference on IAQVEC.

- Georges, E., S. Gendebien, S. Bertagnolio, and V. Lemort. 2013 b. Impact of the integration of various heating technologies on the energy load profiles of the Belgian residential building stock, Proceedings of the 8th Renewable Energy Storage Conference and Exhibition (IRES 2013).

- Goldie-Scot, 2016. Cost reductions and residential energy storage drivers, Tech. rep., Bloomberg.

- He, W., Chow, T., Jianping, Lu, J., Pei, G., Chan. G., 2006. Hybrid photovoltaic and thermal solar-collector designed for natural circulation of water. Applied Energy 83, 199-210.

- Herrando, M., Markides, C., Hellgardt, K., 2014. A UK-based assessment of hybrid PV and solar-thermal systems for domestic heating and power: System performance. Applied Energy 122, 288-309.

- Hollands, K. G. T. and Lightstones, M., F., 1989. A review of low-flow, stratified-tank solar water heating systems. Solar Energy 43 (1989) 97-105.

- Hoppmann, J. Volland, J., Schmidt, T.S., Ho V., 2014. The economic viability of battery storage for residential solar photovoltaic systems A review and a simulation model, Renewable and Sustainable Energy Reviews 39 1101–1118. doi:10.1016/j.rser.2014.07.068.

- Innogie ApS. 2013. Thermal solar absorber system generating heat and electricity. United States Patent Application Publication, US 2013/025778 A1, https://patentscope.wipo.int/search/en/detail.jsf?docId=WO2012041323&recNum=27&docAn=DK2011050363&queryString=(FP/solar%20AND%20FP/thermal%20AND%20FP/electricity)%20&maxRec=107.

- Kalaiselvam, S., and R. Parameshwaran., 2014. Thermal Energy Storage Technologies for Sustainability: Systems Design, Assessment and Applications. Academic Press, Boston, Pages i-ii, ISBN 780124172913, http://dx.doi.org/10.1016/B978-0-12-417291-3.09983-7.

- Kalogirou, S. A., Tripanagnostopoulos Y., Souliotis M., 2005. Performance of solar systems employing collectors with colored absorber. Energy and Buildings 37, 824-835.

- Klein, S. A. 1975. Calculation of flat-plate loss coefficient. Solar Energy, 17, 79. http://adsabs.harvard.edu/abs/1975SoEn...17...79K.

- Kleinbach, E. M., 1990. Performance study of one-dimensional models for stratified thermal storage tank, PhD thesis, Wisconsin. Y. Allard, M. Kummert, M. Bernier, and A. Moreau. Intermodel comparison and experimental validation of electrical water heater models in TRNSYS.

- Knight I., J. Adnot J., J-L. Alexandre, P. Andre., M-N. Assimakopoulos, V. Butala, R. Hitchin, M. Masoero, C. Spitzbart and D. Wright. 2010. HARMONAC - Harmonizing Air Conditioning Inspection and Audit, procedures in the Tertiary Building Sector, energy Consumption in European Air Conditioning Systems and the Air, https://ec.europa.eu/energy/intelligent/projects/en/projects/harmonac.

- Kost, C. J., Mayer, J. Thomsen, N. Hartmann, C. Senkpiel, S. Philipps, S. Nold, S. Lude, N. Saad, and T. Schlegl. 2013. Levelized cost of electricity renewable energy technologies. Fraunhofer ISE, https://www.ise.fraunhofer.de/en/publications/veroeffentlichungen-pdf-dateien-

en/studien-und-konzeptpapiere/study-levelized-cost-of-electricity-renewable-energies.pdf

- Lund, H., A. Marszal, and P. Heiselber., 2011. Zero energy buildings and mismatch compensation factors. Energy and buildings, 43, 7, 1646-1654, doi:10.1016/j.enbuild.2011.03.006.

- Masy, G. 2007. Definition and validation of a simplified multizone dynamic building model connected to heating system and HVAC unit. PhD thesis. Liege.

- Masy, G., E. Georges, C. Verhelst, V. Lemort and P. André., 2015. Smart Grid Energy Flexible Buildings through the use of Heat Pumps and Building Thermal Mass as Energy Storage in the Belgian context. Science and Technology for the Built Environment – Ashrae, DOI:10.1080/23744731.2015.1035590.

- Marszal, A. J., P. Heiselberg, J. S., Bourrelle, E. Musall, K. Voss, I. Sartori and A. Napolitano. 2011. Zero Energy Building – A review of definitions and calculation methodologies., Energy and Buildings, Volume 43, Issue 4, Pages 971-979, ISSN 0378-7788, Zero Energy Building – A review of definitions and calculation methodologies.

- Muller, D. and A. H. Badakhshani., 2010. Gebaude und Anlagensimulati mit modelica. Proceedings of BauSIM 2010, http://info.tuwien.ac.at/bausim/conftool/mueller-2010-gekoppelte_gebaeude-_und_anlagensimulation_mit_modelica-198.pdf.

- Nytsch-Geusen, M. and S. Unger., 2009. Modelling of complex thermal energy supply systems based on the modelica-library fluidflow. Proceedings 6th International Modelica Conference, http://webcache.googleusercontent.com/search?q=cache:D2BJ4wVYr8IJ:citeseerx.ist.psu.edu/viewdoc/summary%3Fdoi%3D10.1.1.472.1996+&cd=3&hl=fr&ct=clnk&gl=be.

- Oliveski, R., Krenzinger A. and Vielmo, H.A., 2003. Comparison between models for the simulation of hot water storage tanks. Solar Energy 75, 121–134.

- Perers, B., 1997. An improved dynamic solar collector test method for determination of non-linear optical and thermal characteristics with multiple regression. Solar Energy, Volume 59, 163-178.

- PICIR (Potsdam Institute for Climate Impact Research)., 2015. www.pik-potsdam.de., accessed the 30th of July 2015.

- Pizzonalto A., Sciacovelli A., Verda V., Transient local entropy analysis for the design improvement of a thermocline thermal energy storage, Applied Thermal Eng. (2016), http://dx.doi.org/doi: 10.1016/j.applthermaleng.2015.12.072.

- Quoilin, S., O. Dumont and V. Lemort, 2013. Design, modelling and performance optimization of a reversible HP/ORC prototype. Proceedings of the ORC 2013 conference.

- Quoilin S., A. Desideri, J. Wronski and I. Bell, 2014. ThermoCycle: A Modelica library for the simulation of thermodynamic systems. Proceedings of the 10th International Modelica Conference 2014.

- Quoilin, S., O. Dumont, K. Harley, V. Lemort. 2015. Design, modeling and performance optimization of a reversible Heat Pump / Organic Rankine Cycle prototype. Journal of Engineering for Gas Turbines and Power, DOI: 10.1115/1.4031004

- Quoilin, S., Konstantinos, K., Mercier, A., Pappone, I., Zucker, A., 2016a. Quantifying self-consumption linked to solar home battery systems: statistical analysis and economic assessment, Applied Energy Applied Energy 182 58–67.10.1016/j.apenergy.2016.08.077.

- Quoilin S., Schrouff J., 2016b. Assessing steady-state, multivariate experimental data using Gaussian Processes: the GPExp open-source library, Energies, 9, 6, 1996-1073.

- REN21, 2015. Renewables 2015, Global status report.

- Reschefski, L., 2014. Vand i tal, DANVA , Skanderborg.

- Sciacovelli A., 2015. Toward efficient control of energy systems: an application of proper generalized decomposition to thermal storage. Proceedings of ECOS 2015 Conference.

- Schimpf, S., K. Uitz, and R. Span., 2011. Simulation of a solar assisted combined heat pump-organic Rankine cycle system. Proceedings of World renewable Energy Congress, 2011, Sweden.

- Schnieders, J. 1997. Comparison of the energy yield predictions of stationary and dynamic solar collector models and the models' accuracy in the description of a vacuum tube collector, Solar Energy 61, 179-190.

- Tesla motors, 2016. Available at: https://www.teslamotors.com/fr_BE/powerwall [accessed 02.02.2016].

- TESS, 2006. Standard component library overview. http://web.mit.edu/parmstr/Public/Documentation/03-ComponentLibraryOverview.pdf

- Chow, T., 2003. Performance analysis of photovoltaic-thermal collector by explicit dynamic model, Solar Energy 75, 2003, 143-152.

- Trnsys, 2015. "TESS COMPONENT LIBRARIES. http://www.trnsys.com/tess-libraries/TESSLibs17_General_Descriptions.pdf, accessed the 1st of September 2015.

- Truong, C., Naumann, M., Karl, R., Müller, M., Jossen, A., Holger, C., 2016.: Hesse, Economics of residential photovoltaic battery systems in Germany: The case of Tesla's Powerwall, Batteries, 2(2), 14, doi:10.3390/batteries2020014.

- Weniger, J. Tjaden, T. Quaschning V., 2014. Sizing of Residential PV Battery Systems, Energy Procedia 46, 78–87, 00023, doi:10.1016/j.egypro.2014.01.160.

- Wetter, M., W. Zuo, and T. S. Nouidui, 2011. Recent Developments of the Modelica Buildings, Library for Building Energy and Control Systems. Proceedings of the 8th International Modelica Conference.

- Wetter, M., W. Zou, T. S Nouidui and X. Pang., 2013. Modelica Buildings library. Journal of Building Performance Simulation, March 2013, DOI:10.1080/19401493.2013.765506.

- Wang, P.G., M. Scharling, K. P. Nielsen and C. Kern-Hansen, C., 2010."Technical Report 13-19: 2001 – 2010 Danish Design Reference Year, Climate Dataset for Technical Dimensioning in Building, construction and other Sectors. http://www.dmi.dk/fileadmin/Rapporter/TR/tr13-19.pdf, Accessed the 1st of September 2015

- Widen J., Wackelgard E., Lund D., 2009. Options for improving the load matching capability of distributed photovoltaics: methodology and application to high latitude data, Solar Energy, 83:1953-1966.

- Zurigat Y. H., Maloney K. J., and Ghajar A. J., 2011. A comparison study of one-dimensional models for stratified thermal storage tanks, transaction of ASME,

204/Vol. 111, 1989.Proceedings of Building Simulation 2011: 12th Conference of International Building Performance Simulation Association, Sydney, 14-16 November.

Chapter 6:

Conclusion

"The real misery comes when no perspectives are conceived."
Da Vinci, Leonardo

This thesis aims at investigating the concept of the reversible heat pump/ORC system. It was not trivial to study such a system since this is a totally new technology without any feed-back. To the author's knowledge, only one theoretical paper and two patents have been related to this topic until today. This thesis is divided into five main chapters: Description of the technical feasibility of a given application (Chapter one), experimental and theoretical characterization of the volumetric machines (Chapter two), optimal design and sizing for a given application (Chapter three), the demonstration of the technical feasibility and the calibration of models to predict the performance (Chapter four) and the dynamic simulation (Chapter five) with validated models for a given application (solar panels coupled with a building).

First, in **Chapter one,** a list of the possible applications of the reversible HP/ORC system is provided. Also, a tool to evaluate if a given application could be interesting is developed. Three criteria are distinguished to evaluate if a given application is promising or not based on a generic model with simple assumptions. It has been shown that the applications to a residential building with solar panels and to a truck are the most interesting on a technical point of view. The residential building coupled with solar panel is the application that is selected to apply the different methodologies proposed in this thesis.

The volumetric machine is probably the trickiest component in the concept of reversible HP/ORC. Indeed, it requires to be reversible to work as a compressor and as an expander, which has never been studied in the past following author's knowledge. The performance of four volumetric machines (scroll (constant speed and variable speed), screw and piston) are investigated experimentally in **Chapter two**. This study allows to calibrate semi-empirical models and to extrapolate the performance in optimal conditions. This modelling approach is interesting since the same formalism is considered for each technology of expander. The extrapolability of the semi-empirical outside the validation range is assessed for a given case study. Completed by a state of the art, it leads to criteria to help people choosing the optimal volumetric machine depending on the application. In summary, in the considered ranges of conditions, the scroll expander presented the best efficiency, the piston expander shows the highest shaft power through high pressure and temperature tolerance and the screw expander is very compliant with the variations of the conditions through its high shaft speed. However, the choice of the expander technology has to be conducted in parallel with the selection of the ORC architecture, range of power, operating conditions and working fluid of the selected application.

Another interesting aspect of the topic is the optimisation of the architecture and of the components (**Chapter three**). A methodology is provided to select the optimal architecture of a reversible HP/ORC system among the use of the conventional cycle or the inverted cycle (1), the choice of using only one volumetric machine acting as a compressor or as expander or two different machines (2) and the choice of having only one component acting as an expansion valve and as a pump or two components (3). The design of such a system is a challenging task since trade-offs have to be found between the two operating modes. A methodology is provided to size each component to optimise a given output (annual costs or annual net production for example) with annual simulations. An example of application of this method is provided with the application to a residential building coupled with a solar roof. Also, a simple annual steady-state model shows the theoretical interest of this application: the simulations show that the proposed system can produce up to 3500 kWh of electricity throughout the year, while also fulfilling thermal energy demand for space heating and domestic hot water.

Since the case of a residential building with a solar collector is promising because it allows to get a Positive Energy Building (even in cold climate like Denmark), a prototype is built to assess the performance (**Chapter four**). The details of the components (including the modifications required for the scroll compressor) and sensors are described. Moreover, a global methodology to handle and improve the quality of experimental data is proposed and applied to the database. This methodology includes a cross-checking of the measured data, a Gaussian process to eliminate outliers and a reconciliation method to improve the quality of data based on the redundancy and the accuracy of the sensors. This procedure shows significant improvement on the quality of data and on the prediction of models. On the test-rig, a cycle efficiency of 5.3% is achieved in ORC mode (with condensation and evaporation temperature respectively of 25°C and 88°C) and a COP of 4.21 is obtained in HP mode (with condensation

and evaporation temperature respectively of 61°C and 21°C). The performance is slightly lower than the theoretical results but the main causes of losses are identified and the way to solve them are described. Finally, semi-empirical models of each component are described, calibrated and, then, are connected together to obtain an experimentally-validated predictive model assuming an optimal control.

A dynamic model of the reversible system, coupled with the residential building and a solar roof, is also developed (**Chapter five**). This model includes validated models of all the sub-components. The thermal heat storage multi-node model is validated with a wide range of operating conditions on a dedicated test-rig (also, a decision tree is proposed in order to select the optimal storage modelling approach in function of the application). The solar roof model is modelled following a well-known validated correlation. The house model considers 5 zones based on the real investigated house. Solar gains, air infiltration, occupancy behaviour in terms of internal gain and domestic hot water consumption are taken into account. The reversible unit model is fully described (and experimentally validated in Chapter four). The horizontal ground heat exchanger semi-empirical model, specially developed for this case is validated by comparison with a finite element model. A control strategy is developed and annual simulations are performed to predict accurately the global performance of the system. A study of influence has shown the cases where the system is more profitable. Also, the integration of batteries to increase the self-consumption of the system is studied. Finally, the reversible HP/ORC unit integrated in a residential building is compared in terms of performance and economically with a mature technology: PV panels coupled with a heat pump. Despite the proven feasibility to use this reversible HP/ORC unit to get a Positive Energy Building, the combination of a heat pump coupled with PV panels is, almost always, more profitable. Other applications could therefore be studied in details to evaluate the practical feasibility (i.e. the economic feasibility).

Perspectives

1. The analysis proposed in this thesis (optimal sizing and architecture, experimentation and dynamic modelling) should be applied to the most promising applications listed in Chapter one. It would show if other applications could exhibit an economical interest and should be promoted.

2. About the testing and modelling of different volumetric machines, a lot of work remains to do:

- The performance of small scale expander technologies is difficult to predict because of the lack of literature.

- In this thesis, only the scroll, the screw and the piston expanders could be studied. Vane, trochoid and root expanders among others could also be very interesting.
- The extrapolation of the semi-empirical model remains uncertain and advanced studies could investigate and improve its performance with other fluids, size, etc.

3. The experimentation of the conventional reversible HP/ORC system has brought some interesting information since it was the first in the world to the author's knowledge. However, testing the different architectures proposed in Chapter three could also improve the knowledge of these systems.

4. In terms of components modelling, the following points could be interesting for future studies:
    - The thermal energy storage remains difficult to model. Some work could be done to be improve actual models to predict the thermal stratification accurately with a low computational time.
    - The validity of the semi-empirical model of horizontal ground heat exchanger could be confirmed with experimental data and different configurations.
    - The building model could be improved to take into account the natural air circulation due to buoyancy effect (associated with the difference of temperature between the building indoor and indoor) and wind pressure and forced air circulation due to mechanical ventilation.